

UNCLASSIFIED

| |
|--|
| |
| |
| |
| |
| AD NUMBER |
| AD839956 |
| NEW LIMITATION CHANGE |
| TO Approved for public release, distribution unlimited |
| FROM Distribution authorized to U.S. Gov't. agencies and their contractors; Administrative/Operational Use; Jul 1968. Other requests shall be referred to Air Force Materials Lab., Wright-Patterson AFB, OH 45433. |
| AUTHORITY |
| AFML/USAF ltr, 12 Jan 1972 |

THIS PAGE IS UNCLASSIFIED



AD C 99956

RESEARCH AND DEVELOPMENT OF REFRACTORY OXIDATION RESISTANT DIBORIDES

Edward V. Clougherty
David Kalish
Edward T. Peters

ManLabs, Inc.

TECHNICAL REPORT AFML-TR-68-190

July 1968

This document is subject to special export controls and each transmittal to foreign governments or foreign nationals may be made only with prior approval of the Metals and Ceramics Division, Air Force Materials Laboratory (MAMC), Wright-Patterson Air Force Base, Ohio 45433

Air Force Materials Laboratory
Air Force Systems Command
Wright-Patterson Air Force Base, Ohio

DDC
SEP 24 1968

BEST

AVAILABLE

COPY

NOTICES

When Government drawings, specifications, or other data are used for any purpose other than in connection with a definitely related Government procurement operation, the United States Government thereby incurs no responsibility nor any obligation whatsoever; and the fact that the Government may have formulated, furnished, or in any way supplied the said drawings, specifications, or other data, is not to be regarded by implication or otherwise as in any manner licensing the holder or any other person or corporation, or conveying any rights or permission to manufacture, use, or sell any patented invention that may in any way be related thereto.

This document is subject to special export controls and each transmittal to foreign governments or foreign nationals may be made only with prior approval of the Metals and Ceramics Division, Air Force Materials Laboratory (MAMC), Wright-Patterson Air Force Base, Ohio 45433.

Distribution of this report is limited for the protection of technology relating to critical materials restricted by the Export Control Act.

| | |
|---------------------------------|-----------------------|
| ACCESSION FOR | |
| CFSTI | WHITE SECTION |
| DDC | BLUE SECTION |
| UNCLASSIFIED | LI |
| JUSTIFICATION | |
| BY | |
| DISTRIBUTION AVAILABILITY CODES | |
| DISC. | AVAIL. and or SPECIAL |
| 2 | |

Copies of this report should not be returned to the Research and Technology Division unless return is required by security considerations, contractual obligations, or notice on a specific document.

**RESEARCH AND DEVELOPMENT OF REFRACTORY
OXIDATION RESISTANT DIBORIDES**

**Edward V. Clougherty
David Kalish
Edward T. Peters**

This document is subject to special export controls and each transmittal to foreign governments or foreign nationals may be made only with prior approval of the Metals and Ceramics Division, Air Force Materials Laboratory (MAMC), Wright-Patterson Air Force Base, Ohio. 45433

FOREWORD

This report was prepared by the Research Division, ManLabs, Inc., with the assistance of Avco Space Systems Division and Battelle Memorial Institute, subcontractors on this program, under U. S. Air Force Contract No. AF33(615)-3671. The contract was initiated under Project 7350, "Refractory Inorganic Nonmetallic Materials", Task 735001, "Refractory Inorganic Nonmetallic Materials: Non-Graphite." The work was administered under the direction of The Air Force Materials Laboratory with John R. Fenter acting as project engineer.

This report covers the period from 15 March 1966 to 15 September 1967.

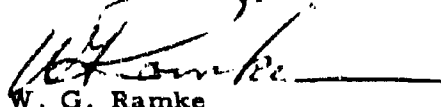
ManLabs personnel participating in this study included E. V. Clougherty, D. Kalish, E. T. Peters, R. A. Yeaton, R. D. Haviland, J. Davis, S. Wallerstein, R. Kelly, J. I. Rasmussen and J. M. Connolly.

Avco personnel included W. R. Rhodes, R. J. Hill, P. F. Jahn, A. H. Heuer and T. Vasilos. The services of the Nondestructive Testing Laboratory of Avco/SSD were also employed.

Battelle personnel included D. E. Niesz and W. Duckworth.

The manuscript of this report was released by the authors May 1968 for publication.

This technical report has been reviewed and is approved:



W. G. Ramke
Chief, Ceramics and Graphite Branch
Metals and Ceramics Division
Air Force Materials Laboratory

BLANK PAGE

ABSTRACT

The oxidation, mechanical and physical properties of zirconium diboride and hafnium diboride and composites prepared from these diborides with appropriate additives, have been determined as a function of composition, microstructure and test temperature. The composites were designed to enhance oxidation resistance, strength and thermal stress resistance without sacrificing high temperature stability; the principal additives were silicon carbide or graphite.

Several hundred diboride billets, in sizes from two inches diameter to six inches square, were fabricated by conventional hot pressing. All hot pressed billets were subjected to extensive nondestructive testing correlations and flaw identification criteria. A unique role for ceramic additives has evolved in enhancing the fabricability of diboride materials and producing fine grained crack free billets. All powder materials and hot pressed microstructures subjected to properties evaluations have undergone extensive characterization through qualitative and quantitative chemical analyses, phase analyses and grain size and density measurements.

An exploratory fabrication effort was initiated to develop alternate means to hot pressing for producing dense diboride materials; hot forging, plasma spraying and sintering are being studied. In addition, the hot pressing of diboride compositions containing additives such as SiC whiskers, carbon filaments or tungsten filaments is being studied.

Oxidation screening evaluations were performed in hot sample cold gas furnace tests in which low velocity air at a linear flow rate of 0.9 ft/sec is passed over specimens at temperatures from 1700° to 2200°C. The beneficial effect of SiC in reducing the rate of diboride oxidation and increasing the adherence characteristics of protective oxide coatings was confirmed and extended in temperature range and composition. The introduction of graphite, for improved thermal stress resistance, detracts from the oxidation resistance. Hafnium diboride compositions display superior oxidation resistance to analogous zirconium diboride compositions.

Mechanical properties screening evaluations, comprising bend strength measurements up to 1800°C and static elastic modulus measurements up to 1400°C, were performed for selected diboride compositions with variations in porosity and grain size. The fine grained fully dense diboride composite compositions possess the highest elevated temperature strengths; bend strengths of 40,000 to 60,000 psi at 1800°C are found in several compositions. Porosity and graphite substantially reduce the Young's modulus of HfB₂ and ZrB₂ from the 70 to 80 x 10⁶ psi level whereas SiC does not significantly alter the composite modulus. The temperature and strain rate dependence for the onset of plasticity are being established; all compositions have shown limited plasticity in bending at 1800°C.

Preliminary steady state thermal stress resistance measurements were performed in which hollow cylindrical specimens are heated by a concentrically

ABSTRACT (CONT)

positioned carbon rod in order to induce thermal stresses sufficient to cause brittle failure. Transient thermal stress data of materials from this program are being obtained in a variety of hot gas/cold sample arc plasma evaluations under a separate study.

The results of the current program provide an increased confidence in the choice of a diboride material as a monolithic ceramic body for applications in environments which will produce thermal stresses and surface oxidation.

Distribution of this report is limited for the protection of technology relating to critical materials restricted by the Export Control Act.

TABLE OF CONTENTS

| Section | Page |
|---|------|
| I. INTRODUCTION AND SUMMARY | 1 |
| A. Introduction | 1 |
| B. Summary | 2 |
| II. OPERATIONAL PROCEDURES AND PROGRAM MANAGEMENT | 5 |
| III. MATERIALS PROCUREMENT, CHARACTERIZATION AND IDENTIFICATION | 7 |
| A. Introduction | 7 |
| B. Material Identification | 7 |
| C. Material Characterization | 7 |
| 1. General Powder Characterization Procedures | 7 |
| 2. Diboride Materials | 8 |
| 3. Additive Materials | 9 |
| D. Procurement and Characterization of Hot Pressed Materials | 10 |
| IV. HOT PRESSING | 11 |
| A. Fabrication Conditions and Results | 11 |
| 1. Material I | 11 |
| 2. Material V | 13 |
| 3. Material VIII | 15 |
| 4. Material X | 15 |
| 5. Material XII | 16 |
| 6. Material II | 16 |
| 7. Materials III and IV | 17 |
| 8. Material VI | 17 |
| B. Furnace Variables and Process Control | 18 |
| C. Nondestructive Testing | 19 |

TABLE OF CONTENTS (CONT)

| Section | Page |
|---|------|
| V. EXPLORATORY FABRICATION | 21 |
| A. Hot Forging | 21 |
| B. Plasma Spraying | 21 |
| C. Sintering | 22 |
| D. Reinforced Diboride Composites | 22 |
| VI. THERMAL SCREENING | 25 |
| A. Introduction | 25 |
| B. Experimental Procedure | 25 |
| C. Experimental Results and Discussion of Results | 25 |
| 1. Material I (ZrB_2) | 25 |
| 2. Material VIII ($ZrB_2 + 30 \text{ v/o Graphite} + 14 \text{ v/o SiC}$) | 26 |
| 3. Material X ($ZrB_2 + SiB_6$) | 26 |
| D. Melting Points | 26 |
| VII. MECHANICAL SCREENING | 28 |
| A. Bend Testing | 28 |
| 1. Temperature Effect on Bend Strength | 28 |
| 2. Surface Finish Effect on Bend Strength | 31 |
| B. Elastic Modulus | 33 |
| C. Post-Mortem Examinations | 35 |
| 1. Visual Examinations | 35 |
| 2. Fractography | 35 |
| 3. Optical Microscopy | 36 |
| 4. Density Checks | 36 |
| VIII. OXIDATION SCREENING | 38 |
| A. Introduction | 38 |

TABLE OF CONTENTS (CONT)

| Section | Page |
|---|-----------|
| VIII. OXIDATION SCREENING (CONT) | |
| B. Experimental Procedure | 38 |
| C. Experimental Results and Discussion of Results | 39 |
| 1. Material I (ZrB_2) | 39 |
| 2. Commercial Zirconium Diboride | 41 |
| 3. Material V (ZrB_2 - 20 v/o SiC) | 41 |
| 4. Commercial Boride Z | 43 |
| 5. Material VIII (ZrB_2 + 30 v/o Graphite + 14 v/o SiC) | 43 |
| 6. Material XII (ZrB_2 + 50 v/o Graphite) | 44 |
| 7. Material X (ZrB_2 + 20 v/o SiB_6) | 45 |
| 8. Material XI (ZrB_2 + 8 v/o Cr) | 45 |
| 9. Material II (HfB_2) | 45 |
| 10. Materials III (HfB_2 + 20 v/o SiC) and IV (HfB_2 + 35 v/o SiC) | 46 |
| 11. Material VI (HfB_2 + 4 v/o Hf-27Ta) | 47 |
| 12. Effect of SiC Content on Boride Oxidation | 47 |
| 13. Occurrence of Gross Cracks in SiC Depleted Zones in Materials III, IV and V | 48 |
| D. Summary | 49 |
| IX. THERMAL STRESS RESISTANCE | 50 |
| A. Introduction | 50 |
| B. Experimental Evaluation of Steady State Thermal Stress Resistance | 50 |
| 1. Introduction | 50 |
| 2. Experimental Methods | 53 |
| 3. Experimental Apparatus and Procedure | 54 |
| 4. Experimental Results and Discussion | 56 |

TABLE OF CONTENTS (CONT)

| Section | Page |
|---|-----------|
| IX. THERMAL STRESS RESISTANCE (CONT) | |
| a. KT-SiC | 56 |
| b. 1.7 Inch Outside Diameter Diboride Samples . | 56 |
| c. 2.0 Inch Outside Diameter Diboride Sample . | 57 |
| d. Triangular Samples | 58 |
| 5. Conclusions and Future Plans | 59 |
| REFERENCES | 253 |
| APPENDIX I - CHARACTERIZATION OF DIBORIDE POWDER SHIP- MENTS | I-1 |
| APPENDIX II - PROCESSING VARIABLES FOR HOT PRESSING OF DIBORIDES | II-1 |
| A. Hot Pressing Facility | II-1 |
| B. Diffusion Barriers | II-1 |
| C. Microstructure Reproducibility | II-1 |
| APPENDIX III - OXIDATION CHARACTERISTICS OF ZIRCONIUM AND HAFNIUM DIBORIDES CONTAINING SELECTED RARE EARTH AND ALKALINE EARTH HEXABORIDE ADDITIVES | III-1 |

LIST OF ILLUSTRATIONS

| Figure | | Page |
|--------|--|------|
| 1 | Second Phase Size and Distribution in Hot Pressed Material I Billet I03A D0308 | 60 |
| 2 | Comparison of Hot Pressing Characteristics of Materials I03A and V02A | 61 |
| 3 | Comparison of Hot Pressing Characteristics of Materials I03A and V03A | 62 |
| 4 | Distribution of SiC Phase in Diboride Matrix of Material V Billet V02A D0370 | 63 |
| 5 | Location of SiC Relative to ZrB_2 Grain Boundaries in Material V Billet V02A D0370 | 63 |
| 6 | Morphology of Remaining Impurity Phases in Material V02A Demonstrating the Contact Angles Relative to the Other Phases Billet V02A D0370 | 64 |
| 7 | Morphology of Remaining Impurity Phases in Material V03A Billet V03A D0473 | 64 |
| 8 | Variation of Impurity Phase with SiC Additions in Material V . | 65 |
| 9 | Distribution of Phases in Special Material Hot Pressed with Starting Powders of ZrO_2 and SiC Billet D0624 | 66 |
| 10 | Distribution of Phases in Special Material Hot Pressed with Starting Powders of ZrB_2 , ZrO_2 and SiC Billet D0626 | 67 |
| 11 | Microstructure of Material VIII Containing Poco Graphite Billet VIII02A D0592 | 68 |
| 12 | Microstructure of Material VIII Containing Regal Carbon Billet VIII(17)(15)07 D0620 | 68 |
| 13 | Microstructure of Material X Hot Pressed at $1900^\circ C$ Billet X07 D0596 | 69 |
| 14 | Microstructure of Material X Hot Pressed at $1800^\circ C$ Billet X07 D0597 | 69 |

LIST OF ILLUSTRATIONS (CONT)

| Figure | | Page |
|--------|--|------|
| 15 | Microstructure of Material XII Containing Regal Carbon Billet XII(20)07 D0608 | 70 |
| 16 | Microstructure of Material XII Containing Poco Graphite Billet XII(15)07 D0603 | 70 |
| 17 | Microstructure of Material II Billet II05 D0316 | 71 |
| 18 | Microstructure of Material III Billet III05 D0377 | 72 |
| 19 | Microstructure of Material IV Billet IV05 D0405 | 73 |
| 20 | Comparison of Hot Pressing Characteristics of Materials II and III | 74 |
| 21 | Microstructure of Material VI Billet VI05 D0462 | 75 |
| 22 | Material Showing Cracks in the Matrix Radially Distributed Around Oxide Inclusion Billet I03A D0415 | 76 |
| 23 | Location of NDT Measurements on Diametrical Slab | 77 |
| 24 | Location of NDT Measurements on 2 Inch and 3 Inch Diameter Billets | 78 |
| 25 | Density and Sonic Velocity Variations in Billet V07 D0578 . . . | 79 |
| 26 | Variation of Electrical Conductivity for V07 D0578K | 80 |
| 27 | Material I Plasma Sprayed on Stainless Steel Billet I02A P0162F | 81 |
| 28 | Microstructure of Dense Area in Sintered Specimen I03A B0005 | 82 |
| 29 | Representative Microstructure of ZrB_2 Reinforced with Thornel 25 Carbon Fiber, Billet XII(5) D0644 | 83 |
| 30 | Photomicrographs of Material I07 D0589, As Polished, 500X . | 84 |
| 31 | Photomicrographs of Material I07 D0589, Etched, 150X | 85 |
| 32 | Photomicrographs of Material VIII, D0498, Annealed at 2200°C (Color Temperature) for 15 Minutes | 86 |
| 33 | Photomicrographs of Material VIII, D0592, Annealed at 2300°C (Color Temperature) for 15 Minutes | 87 |

LIST OF ILLUSTRATIONS (CONT)

| Figure | | Page |
|--------|---|------|
| 34 | Photographs of Material X, D0596, Annealed at 2200°C (Color Temperature) for 15 Minutes | 38 |
| 35 | Schematic of High Temperature Lever Arm Bend Test Apparatus | 89 |
| 36 | Bend Strength of Material I as a Function of Test Temperature . | 90 |
| 37 | Bend Strength of Material V as a Function of Test Temperature | 91 |
| 38 | Bend Strength of Material II as a Function of Test Temperature | 92 |
| 39 | Bend Strength of Material III05 as a Function of Test Temperature | 93 |
| 40 | Bend Strength of Material IV05 as a Function of Test Temperature | 94 |
| 41 | Bend Strength at 1800°C of ZrB ₂ -SiC and HfB ₂ -SiC Composites as Functions of SiC Content | 95 |
| 42 | Taylor Surface Contour Tracers for 200, 400 and 500 Grit Finish, Finish on Billet V07 D0576 | 96 |
| 43 | Electron Micrograph of Surface Structure from 200 Grit Finish on V07 D0576 | 97 |
| 44 | Electron Micrograph of Surface Structure from 400 Grit Finish on V0007 D0576 | 97 |
| 45 | Electron Micrograph of Surface Structure for 0.25 Micron Diamond on V07 D0576 | 98 |
| 46 | Schematic of High Temperature Apparatus used for Modulus Measurements | 99 |
| 47 | Effect of Porosity on Room Temperature Elastic Modulus for Various Diborides | 100 |
| 48 | Electron Fractograph of Material V Tested at 23°C with Bend Strengths of 50, 500 psi Billet V02A D0371 | 101 |
| 49 | Electron Fractograph of Material V Tested at 800°C with Bend Strength of 52,700 psi Billet V02A D0371 | 101 |
| 50 | Electron Fractograph of Material V Tested at 1400°C with Bend Strength of 43,000 psi Billet V02A D0371 | 102 |
| 51 | Electron Fractograph of Material V Tested at 1800°C with Bend Strength of 44,900 psi Billet V02A D0371 | 102 |
| 52 | Edge of Specimen I02A D0338 after Testing at 1800°C in Argon | 103 |
| 53 | Schematic Diagram of Air Oxidation Furnace | 104 |
| 54 | Dependency of Air Flow Rate for Hypothetical Oxidation Experiment at Constant Temperature | 105 |

LIST OF ILLUSTRATIONS (CONT)

| Figure | | Page |
|--------|---|------|
| 55 | Air Flow Rate Dependence for Material I (1800°C, 15 Minutes and Material III (2120°C, 60 Minutes) | 106 |
| 56 | Oxidation Screening: Material I (ZrB ₂) | 107 |
| 57 | Oxidation Comparison: Commercially Hot Pressed ZrB ₂ versus Material I (ZrB ₂) | 108 |
| 58 | Oxidation Screening: Material V (ZrB ₂ +20 v/o SiC) | 109 |
| 59 | Oxidation Comparison: Boride Z versus Material I (ZrB ₂) | 110 |
| 60 | Oxidation Screening: Material VIII (ZrB ₂ + 30 v/o Graphite + 14 v/o SiC), and Material XII (ZrB ₂ + 50 v/o Graphite) | 111 |
| 61 | Oxidation Screening: Material X (ZrB ₂ + 20 v/o SiB ₆) and Material XI (ZrB ₂ + 8 v/o Cr) | 112 |
| 62 | Oxidation Screening: Material II (HfB ₂) | 113 |
| 63 | Oxidation Screening: Material III (HfB ₂ +20 v/o SiC) | 114 |
| 64 | Oxidation Screening: Material IV (HfB ₂ +30 v/o SiC) | 115 |
| 65 | Oxidation Screening: Material VI (HfB ₂ +4 v/o Hf-27 Ta) | 116 |
| 66 | Oxidation Screening, Material I02A: Macrophotographs | 117 |
| 67 | Oxidation Screening, Material I03A: Macrophotographs | 118 |
| 68 | Oxidation Screening, Material I05A: Macrophotographs | 119 |
| 69 | Oxidation Screening, Material I07: Macrophotographs | 120 |
| 70 | Oxidation Screening, Material I02A: Oxide-Matrix Interfaces, 250X | 121 |
| 71 | Oxidation Screening, Material I03A: Oxide-Matrix Interfaces, 250X | 122 |
| 72 | Oxidation Screening, Materials I05A and I07: Oxide-Matrix Interfaces, 250X | 123 |
| 73 | Oxidation Screening, Material I02A: Reticule Photographs (1 div. = 4.86 mils), D0345, 1700°C | 124 |
| 74 | Oxidation Screening, Material I03A: Reticule Photographs (1 div. = 4.86 mils), D0309, 1700°C | 125 |

LIST OF ILLUSTRATIONS (CONT)

| Figure | | Page |
|--------|---|------|
| 75 | Oxidation Screening, Material I: Representative Matrix Photographs, 1700°C, 500X | 126 |
| 76 | Oxidation Screening, Material I: Representative Matrix Photographs, 1850°C (30 min.), 500X | 127 |
| 77 | Oxidation Comparison, Carborundum ZrB ₂ : Macrophotographs | 128 |
| 78 | Oxidation Comparison, Norton ZrB ₂ : Macrophotographs | 129 |
| 79 | Oxidation Comparison, Carborundum ZrB ₂ : Oxide-Matrix Interfaces, 250X | 130 |
| 80 | Oxidation Comparison, Norton ZrB ₂ : Oxide-Matrix Interfaces, 250X | 131 |
| 81 | Oxidation Screening, Material V02A: Macrophotographs | 132 |
| 82 | Oxidation Screening, Material V02A: Oxide-Matrix Interface, 250X | 133 |
| 83 | Oxidation Screening, Material V07: D0580K, OX635-2100°C | 134 |
| 84 | Oxidation Screening, Material V02A: D0372, OX343, 1960°C | 135 |
| 85 | Oxidation Screening, Material V02A: Reticule Photographs (1 div. = 4.86 mils), D0372, 1960°C | 136 |
| 86 | Oxidation Screening, Boride Z: Macrophotographs | 137 |
| 87 | Oxidation Screening, Boride Z: Oxide-Matrix Interfaces, 250X | 138 |
| 88 | Oxidation Screening, Boride Z: Reticule Photographs (1 div. = 4.86 mils), 1810°C | 139 |
| 89 | Oxidation Screening, Boride Z: Representative Matrix Photographs, 1810°C | 140 |
| 90 | Oxidation Screening, Material VIII: Macrophotographs | 141 |
| 91 | Oxidation Screening, Material VIII: Depleted Matrix-Oxide Interfaces (Left) and Matrix-Depleted Matrix Interfaces (Right), 250X | 142 |
| 92 | Oxidation Screening, Material VIII: Representative Matrix Photographs, 500X | 143 |
| 93 | Oxidation Screening, Material XII: Macrophotographs | 144 |
| 94 | Oxidation Screening, Material XII: Matrix-Oxide Interfaces, 250X | 145 |

LIST OF ILLUSTRATIONS (CONT)

| Figure | | Page |
|--------|--|------|
| 95 | Oxidation Screening, Material XII: Reticule Photographs | 146 |
| 96 | Oxidation Screening, Material XII: Representative Matrix Photographs, 500X | 147 |
| 97 | Oxidation Screening, Material X: Typical Microstructures, Pressing D0596, OX925-1700°C | 148 |
| 98 | Oxidation Screening, Material II05: Macrophotographs | 149 |
| 99 | Oxidation Screening, Material II05: Oxide-Matrix Interfaces, 250X | 150 |
| 100 | Oxidation Screening, Material II05: Reticule Photographs (1 div. = 4.86 mils), D0352, 1810°C | 151 |
| 101 | Oxidation Screening, Material II: Representative Matrix Photographs, 1800°C, 500X | 152 |
| 102 | Oxidation Screening, Material II06: OX327, D0383, 1800°C . . . | 153 |
| 103 | Oxidation Screening, Material II06: Reticule Photographs (1 div. = 4.86 mils), D0383, 1800°C | 154 |
| 104 | Oxidation Screening, Material III: Macrophotographs | 155 |
| 105 | Oxidation Screening, Material III: Oxide-Matrix Interfaces, 250X | 156 |
| 106 | Oxidation Screening, Material III: Reticule Photographs (1 div. = 4.86 mils), D0408, 1980°C | 157 |
| 107 | Oxidation Screening, Material III: D0408, OX345, 1980°C | 158 |
| 108 | Oxidation Screening, Material IV: Macrophotographs | 159 |
| 109 | Oxidation Screening, Material IV: Oxide-Matrix Interfaces, 250X | 160 |
| 110 | Oxidation Screening, Material IV: Reticule Photographs (1 div. = 4.86 mils), D0410, 1960°C | 161 |
| 111 | Oxidation Screening, Material IV: D0410, OX383, 1960°C | 162 |
| 112 | Oxidation Screening, Material VI: Macrophotographs | 163 |
| 113 | Oxidation Screening, Material VI: Oxide-Matrix Interfaces, 250X | 164 |
| 114 | Oxidation Screening, Material VI: Reticule Photographs (1 div. = 4.86 mils), D0462, 1760°C | 165 |

LIST OF ILLUSTRATIONS (CONT)

| Figure | | Page |
|------------------|---|-------|
| 115 | Oxidation Screening, Material VI: Representative Matrix Photographs, D0462, OX434, 1760°C | 166 |
| 116 | Oxidation Screening: Material III ($\text{HfB}_2 + \text{SiC}$) - Effect of SiC Content | 167 |
| 117 | Oxidation Screening: Material V ($\text{ZrB}_2 + \text{SiC}$) - Effect of SiC Content | 168 |
| 118 | Shape Factors of Circular Cylindrical Thermal Stress Specimens | 169 |
| 119 | Thermal Stress Apparatus | 170 |
| 120 | Cross Sectional Schematic of Sample Placement in Thermal Stress Testing Apparatus | 171 |
| 121 | KT SiC Sample Thermal Stress Specimen after Failure | 172 |
| 122 | Material I (I03A D0539) Thermal Stress Specimen Failed in Cooling after Test | 173 |
| 123 | Material I (I03A D0548K) Thermal Stress Specimen Failed Under Transient Heating Conditions | 174 |
| 124 | Material II (II05 D0595K) Failed Thermal Stress Specimen Before Removal from Test Apparatus | 175 |
| 125 | Material II (II05 D0595K) Thermal Stress Specimen after Failure | 176 |
| Appendix Figures | | Page |
| III-1 | Macrophotographs of $\text{ZrB}_2\text{-MeB}_6$ Hot Pressed Cylinders after Oxidation in Air for One Hour at 1700°C | III-3 |
| III-2 | Matrix Photomicrographs of Hot Pressed $\text{ZrB}_2\text{-10.5 CaB}_6$ | III-4 |
| III-3 | Reticule Photomicrographs of Hot Pressed $\text{ZrB}_2\text{-10.5 CaB}_6$, Oxidized in Air for One Hour at 1700°C (1 Div. = 4.86 mils) | III-5 |
| III-4 | Matrix Photomicrographs of Hot Pressed $\text{ZrB}_2\text{-15.5 CaB}_6$ | III-6 |
| III-5 | Reticule Photomicrographs of Hot Pressed $\text{ZrB}_2\text{-15.5 CaB}_6$; Oxidized in Air For One Hour at 1700°C (1 Div. = 4.86 mils) | III-7 |

LIST OF ILLUSTRATIONS (CONT)

| Appendix Figures (Cont) | Page |
|---|--------|
| III-6 Matrix Photomicrographs of Hot Pressed ZrB_2 -22.5 CeB_6 | III-8 |
| III-7 Reticule Photomicrographs of Hot Pressed ZrB_2 -22.5 CeB_6 ; Oxidized in Air For One Hour at 1700°C (1 Div. = 4.86 mils) | III-9 |
| III-8 Matrix Photomicrographs of Hot Pressed ZrB_2 -20.0 YB_6 | III-10 |
| III-9 Reticule Photomicrographs of Hot Pressed ZrB_2 -20.0 YB_6 ; Oxidized in Air For One Hour at 1700°C (1 Div. = 4.86 mils) | III-11 |
| III-10 Macrophotographs of HfB_2 - MeB_6 Hot Pressed Cylinders after Oxidation in Air for One Hour at 1800°C | III-12 |
| III-11 Matrix Photomicrographs of Hot Pressed HfB_2 | III-13 |
| III-12 Reticule Photomicrographs of Hot Pressed HfB_2 ; Oxidized in Air for One Hour at 1800°C (1 Div. = 4.86 mils) | III-14 |
| III-13 Matrix Photomicrographs of Hot Pressed HfB_2 -22.5 LaB_6 | III-15 |
| III-14 Reticule Photomicrographs of Hot Pressed HfB_2 -22.5 LaB_6 ; Oxidized in Air for One Hour at 1800°C (1 Div. = 4.86 mils) | III-16 |
| III-15 Matrix Photomicrographs of Hot Pressed HfB_2 -20.0 YB_6 | III-17 |
| III-16 Reticule Photomicrographs of Hot Pressed HfB_2 -20.0 YB_6 ; Oxidized in Air for One Hour at 1800°C (1 Div. = 4.86 mils) | III-18 |
| III-17 Matrix Photomicrographs of Hot Pressed HfB_2 -22.5 CeB_6 | III-19 |
| III-18 Reticule Photomicrographs of Hot Pressed HfB_2 -22.5 CeB_6 ; Oxidized in Air for One Hour at 1800°C (1 Div. = 4.86 mils) | III-20 |

LIST OF TABLES

| Table | | Page |
|-------|---|------|
| 1 | Organizational Responsibilities Breakdown | 177 |
| 2 | Diboride Material Identification: Phase Constitution and Base Composition | 178 |
| 3 | Tentative Powder Specification for Hot Pressing Grades of ZrB_2 and HfB_2 | 179 |
| 4 | Diboride Powder Procurement Schedule | 180 |
| 5 | Characterization of Zirconium Diboride Powder, I02 | 181 |
| 6 | Characterization of Zirconium Diboride Powder, I03 | 182 |
| 7 | Characterization of Zirconium Diboride Powder, I07 | 183 |
| 8 | Characterization of Zirconium Diboride Powder, I05A | 184 |
| 9 | Characterization of Hafnium Diboride Powder, II05 and II05A | 185 |
| 10 | Additive Material Procurement Schedule | 186 |
| 11 | Characterization of Silicon Carbide Additives | 187 |
| 12 | Characterization of Metals and Alloys | 188 |
| 13 | Characterization of Silicide Additives | 189 |
| 14 | Characterization of Graphite and Carbon Additives | 190 |
| 15 | Fabrication Conditions and Billet Characteristics for Resulting Densities for Custom Pressings Performed by Carborundum | 191 |
| 16 | Powder Densities and Maximum Billet Densities for Materials I to XII | 192 |
| 17 | Material I Hot Pressing Conditions and Results | 193 |
| 18 | Quantitative Metallographic Phase Analysis for Hot Pressed ZrB_2 | 196 |
| 19 | Material I with Intentional Impurity Phase Additions, Fabrication Conditions and Results | 197 |
| 20 | Material V Fabrication Conditions and Results | 198 |
| 21 | Fabrication Conditions for Special Materials Used for Material V Phase Analysis | 200 |

LIST OF TABLES (CONT)

| Table | | Page |
|-------|---|------|
| 22 | Microstructure Study of Special Materials used for Material V Analysis | 201 |
| 23 | Material VIII Fabrication Conditions and Results | 202 |
| 24 | Material X Fabrication Conditions and Results | 203 |
| 25 | Material XII Fabrication Conditions and Results | 204 |
| 26 | Material II Hot Pressing Conditions and Results | 205 |
| 27 | Phase Distributions for Hot Pressed Billets of Materials II, III and IV | 206 |
| 28 | Material III Hot Pressing Conditions and Results | 207 |
| 29 | Material IV Fabrication Conditions and Results | 208 |
| 30 | Material VI Fabrication Conditions and Results | 209 |
| 31 | Phase Distribution for Material VI Billet VI05 D0462 | 210 |
| 32 | Incidence of Billet Cracking for Materials I and II | 211 |
| 33 | Press Forging of Material I | 212 |
| 34 | Plasma Spraying of Materials I and II | 213 |
| 35 | Sintering Conditions and Results | 214 |
| 36 | Reinforced Composites Fabrication Conditions and Results | 215 |
| 37 | Possible Diboride Matrix Fiber Combinations | 216 |
| 38 | Summary of Thermal Screening | 217 |
| 39 | Melting Points of Hot Pressed Structures | 219 |
| 40 | Bend Strength as a Function of Temperature | 220 |
| 41 | Phase II Bend Strength as a Function of Temperature | 223 |
| 42 | Bend Strength Versus Test Temperature for Two Commercial Lots of Hot Pressed Zirconium Diboride | 224 |
| 43 | Bend Strengths of Preoxidized Commercial Hot Pressed Zirconium Diboride | 225 |

LIST OF TABLES (CONT)

| Table | | Page |
|-------|--|------|
| 44 | Effect of Surface Finish on Bend Strength of Billet V07 D0576K at 23°C | 226 |
| 45 | Dynamic Elastic Modulus Measurements | 227 |
| 46 | Elastic Modulus as a Function of Temperature | 228 |
| 47 | Static And Dynamic Modulus Values for Hot Pressed ZrB_2 | 230 |
| 48 | Comparison of Post - 1800°C - Test Fracture Grain Size With As Hot Pressed Grain Size | 231 |
| 49 | Density Measurements on Bend Specimens Tested at 23°C | 232 |
| 50 | Air Flow Rate Dependence for Material III | 233 |
| 51 | Oxidation Screening: Material I (ZrB_2) | 234 |
| 52 | Oxidation of Commercial Hot Pressed Zirconium Diboride | 236 |
| 53 | Oxidation Screening: Material V ($ZrB_2 + 20$ v/o SiC) | 237 |
| 54 | Oxidation of Commercial Hot Pressed Boride Z | 239 |
| 55 | Oxidation Screening: Material VIII ($ZrB_2 + 30$ v/o Graphite + 14 v/o SiC) | 240 |
| 56 | Oxidation Screening: Material XII ($ZrB_2 + 50$ v/o Graphite) | 241 |
| 57 | Oxidation Screening: Material X ($ZrB_2 + 20$ v/o SiB_6) | 242 |
| 58 | Oxidation: High Pressure Hot Pressed Materials | 243 |
| 59 | Oxidation Screening: Material II (HfB_2) | 244 |
| 60 | Oxidation Screening: Material III ($HfB_2 + 30$ v/o SiC) | 245 |
| 61 | Oxidation Screening: Material IV ($HfB_2 + 30$ v/o SiC) | 246 |
| 62 | Oxidation Screening: Material VI ($HfB_2 + 4$ v/o Hf-27Ta) | 247 |
| 63 | Effect of SiC Content on the Oxidation Behavior of Materials III and V | 248 |
| 64 | Summary of Average Oxide Recessions of Oxidation Screening Materials and of Selected Commercial Materials as a Function of Temperature | 249 |
| 65 | Experimental Verification of Product Relation $R_2 = W_{max}/S$. . . | 250 |

LIST OF TABLES (CONT)

| Table | | Page |
|-------|--|------|
| 66 | Summary of Preliminary Results of Thermal Stress Evaluations . . | 251 |

| Appendix Tables | | Page |
|-----------------|--|--------|
| I-1 | Characterization of Zirconium Diboride Powder, I04 . . | I-2 |
| I-2 | Characterization of Zirconium Diboride Powder, I05 . . | I-3 |
| I-3 | Characterization of Zirconium Diboride Powder, I06 . . | I-4 |
| I-4 | Characterization of Hafnium Diboride Powder, II06 . . . | I-5 |
| I-5 | Characterization of Hafnium Diboride Powder, II07 . . . | I-6 |
| I-6 | Characterization of Hafnium Diboride Powder, II08 . . . | I-7 |
| II-1 | Hot Pressings of Various Diboride Compositions Showing Degree of Process Control | II-3 |
| II-2 | Effect of Pressure on Hot Pressing Material II at 2200°C | II-4 |
| II-3 | Billet Densities of Material I03A Hot Pressed at 2000°C, 4000 psi for 75 minutes | II-4 |
| III-1 | Compositions and Densities of Hot Pressed Diboride + Hexaboride Specimens | III-21 |
| III-2 | Oxidation of Hot Pressed Diboride + Hexaboride Materials | III-22 |

I. INTRODUCTION AND SUMMARY

A. Introduction

The diborides of zirconium and hafnium have been identified as excellent candidate materials for applications involving exposure to oxidizing environments at elevated temperatures. A previous investigation of diboride materials showed that the oxidation resistance of the refractory diborides decreased in the order $\text{HfB}_2 < \text{ZrB}_2 < \text{TiB}_2 < \text{TaB}_2 < \text{NbB}_2$; extensive thermodynamic data were presented and reviewed (1^{*}). Subsequently, extensive oxidation evaluations confirmed the superior oxidation resistance of HfB_2 over ZrB_2 and demonstrated that metal rich compositions of HfB_2 or ZrB_2 were more oxidation resistant and possessed higher thermal stability than boron rich compositions of the same diboride (2). More recently, the oxidation characteristics of polycrystalline microstructures of ZrB_2 and HfB_2 containing various additives were investigated; the oxidation behavior was studied in hot sample/cold gas furnace tests in which air was passed over the sample at low velocities (3). The addition of SiC as a second phase constituent substantially improved the oxidation resistance of ZrB_2 and HfB_2 . Additional oxidation characteristics were obtained from a limited number of hot gas/cold sample, arc plasma tests in which hot air was passed over the sample at subsonic and supersonic velocities. In these arc plasma evaluations, the HfB_2 was again more oxidation resistant than the ZrB_2 . No thermal stress failures were encountered in forty arc plasma tests. Bend strength data were also obtained for ZrB_2 and HfB_2 from room temperature to 1400°C.

The present program was undertaken to prepare a number of diboride materials containing either ZrB_2 or HfB_2 as the principal component with selected additives designed to enhance one or more of the following: oxidation resistance, mechanical properties and thermal stress resistance. Diboride materials, including ZrB_2 and HfB_2 with no additive, are being fabricated with microstructural variations of grain size and porosity. Billets are prepared by conventional hot pressing procedures suitable for the production of components such as nose caps, leading edges, vanes and similar objects anticipated for use in high velocity flight or re-entry conditions. The program is broadly divided into three phases: (1) composition and microstructure screening, (2) extensive properties testing and (3) simulated application evaluations and verification of properties in scaled-up fabrication. In Phase One, oxidation, mechanical and thermal screening tests of a wide range of compositions and microstructures are being used to select a limited number of particularly attractive diboride materials. In Phase Two, the selected compositions and microstructures are being fully characterized over a wide temperature range in terms of oxidation resistance, strength, elastic modulus, linear expansion, thermal conductivity and steady state thermal stress resistance. Finally, in Phase Three these properties will be redetermined for materials prepared in scaled up billet sizes and a leading edge configuration will be subjected to simulated hypersonic flight heating conditions of varying severity.

* Underscored numbers in parentheses designate References given at end of report.

It is anticipated that at the completion of the program, sufficient powder material procurement and characterization information, fabrication technology, physical, mechanical and oxidation property data and thermal stress resistance performance data will be available so that future utilization of diboride materials for a particular application can be readily achieved with a minimum of additional required data. Appropriate information is being generated to ascertain property trade off consequences which may be utilized in developing optimized materials for specific applications, or which may be necessary if other fabrication techniques must be employed.

B. Summary

Zirconium and hafnium diboride powders were procured in several lots ranging from fifty to three hundred pounds. Additive material procurements included silicon carbide powders and fibers, hafnium silicide and boron silicide powders, hafnium metal, hafnium-tantalum alloy and chromium metal powders, tungsten filament, Poco graphite and Cabot Regal carbon powder and Thorne 25 graphite fibers.

Several hundred diboride billets were fabricated with and without one or more of the above additives by conventional hot pressing procedures. The diboride materials fabricated include the following basic compositions which are identified by roman numerals: Material I, ZrB_2 with no additive; Material II, HfB_2 with no additive; Material III, HfB_2 with 20 v/o SiC; Material IV, HfB_2 with 30 v/o SiC; Material V, ZrB_2 with 20 v/o SiC; Material VI, HfB_2 with 4 v/o Hf-Ta alloy; Material VIII, ZrB_2 with 14 v/o SiC and 30 v/o C; Material X, ZrB_2 with 20 v/o SiB_6 ; and Material XII, ZrB_2 with 50 v/o C. Additional billets having variations from the basic compositions were also fabricated. The majority of the billets were 2.0 inch diameter by 0.7 inch high, although several dozen 3.0 inch diameter x 1.0 inch high and about a dozen 5.75 inch square by 0.75 to 1.5 inch high billets were also prepared. All hot pressed billets were subjected to extensive non-destructive testing evaluations to provide sufficient data for subsequent development of property correlations and flaw identification criteria. These evaluations are being performed under a separate program (4).

Considerable difficulty was encountered in the fabrication of crack free billets of Materials I and II, which do not contain intentional additives. Furthermore, fully dense billets of Materials I and II could not be prepared without significant grain growth. A unique role for ceramic additives in enhancing densification by hot pressing, heretofore not fully understood nor exploited, was found. The incidence of cracking was virtually eliminated for composite compositions based on either ZrB_2 or HfB_2 ; this effect is particularly well documented for additions of SiC, C or both SiC + C. High density fine grained diboride microstructures were hot pressed and characterized in terms of chemistry, density, grain size and phase analysis. The various intentional additives to the diborides also resulted in apparent reductions of the impurity phases found in the as-received diboride powders.

An exploratory fabrication effort was undertaken to develop alternate means to hot pressing for producing dense diboride materials; hot forging, plasma spraying and sintering are being studied. In addition, the hot pressing of composite

compositions containing additives not in powder form has been attempted; the materials that were prepared include Material V with SiC whiskers, Material XII with Thornel 25 yarn and a Material XIII containing ZrB₂ with W filaments.

Phase One screening evaluations were performed on diboride compositions representing variations in porosity, grain size and chemical composition. Specimens were subjected to thermal, oxidation and mechanical tests in order to select a limited number of microstructures for more extensive properties measurements in Phase Two.

Thermal screening evaluations were performed in argon and at 10⁻⁵ torr vacuum at temperatures up to 2300°C. Screening evaluations at 2300°C for 15 minutes in argon revealed no change in the initial microstructures of Materials I, II, III, IV, V and XII. Surface depletion zones of additive phases at depths of 15 to 50 mils were found for Material VIII and second phase melting was observed in Material X. Melting data obtained on hot pressed samples from several different lots of ZrB₂ and HfB₂ powders indicated incipient melting temperatures consistent with identified oxide and carbide impurity phases. Complete melting was observed at 3075° to 3095°C for three different high purity ZrB₂ materials and at 3345°C for one high purity HfB₂ material.

Oxidation screening evaluations are performed in hot sample/cold gas furnace tests in which low velocity air at a linear flow rate of 0.9 ft/sec STP is passed over the specimen (0.35 inch diameter by 0.35 inch high) at temperatures from 1700° to 2200°C for 30 or 60 minutes. Oxidation characteristics are determined by post oxidation metallographic analysis which yields measurement of the depth of conversion of diboride to oxide, observation of adherence characteristics of oxide coatings and determination of high temperature limit for the formation and retention of a protective oxide for 30 to 60 minutes. Hafnium diboride displayed better oxidation resistance than zirconium diboride at all temperatures in agreement with earlier results (2); the high temperature limit for protective oxide formation was 1875°C for ZrB₂ and 2050°C for HfB₂. Previously reported (3) enhancement of diboride oxidation resistant characteristics by the introduction of SiC were confirmed and extended in Materials III, IV and V. The adherence characteristics of the oxide produced in the latter materials is improved relative to ZrB₂ and HfB₂ with no additive and protective oxide formation is extended to a temperature limit of 2000°C for Material V and was observed up to 2100°C for Materials III and IV. Preferential oxidation of SiC was observed at all temperatures; this phenomenon leads to the occurrence of three discreet zones in an oxidized specimen: the outer oxide, the diboride plus void zone and the unaltered diboride plus SiC matrix. The introduction of C detracts from oxidation resistance, as in Materials VIII and XII, which were formulated to maximize thermal stress resistance. Material VIII with 14 v/o SiC and 30 v/o C is more oxidation resistant than Material I but less than Material V. Material XII with 50 v/o C is substantially less oxidation resistant than Material I; reduction of C to 20 and 5 v/o renders Material XII competitive with Material I. Addition of SiB₆ to ZrB₂, Material X, extended the range of protective oxide formation to 1925°C but did not improve oxidation resistance at lower temperatures; addition of Cr to ZrB₂, Material XI, lowered the oxidation resistance of ZrB₂. Addition of Hf-27Ta to HfB₂, Material VI, showed no appreciable effect on the oxidation resistance of HfB₂.

Mechanical screening evaluations, comprising transverse bend strength measurements from room temperature to 1800°C and static elastic modulus measurements from room temperature to 1400°C, are being performed for selected diboride compositions of several microstructural variations in grain size and porosity in Phase One. The effects of grain size ranges of 6 to 40 microns, for Materials I and II, and 5 to 10 microns for Materials III, IV and V and porosities from 0 to 15 per cent have been evaluated. Materials I and II display peak strengths at 800°C; Materials III, IV and V show relatively flat temperature bend strength curves up to 1800°C. Bend strengths of 40,000 to 55,000 psi have been obtained with the fully dense fine grained compositions of Materials III, IV and V. These strengths are substantially higher than those of Materials I and II at 1400°C and 1800°C. Young's modulus values of 70 to 80 x 10⁶ psi were obtained for the fully dense diboride materials. Porosity substantially reduces the elastic modulus, whereas additions of SiC do not significantly alter the diboride modulus. Currently, the temperature and strain rate dependence for the onset of plasticity are being established; all compositions have shown limited plasticity in bending at 1800°C.

Preliminary steady state thermal stress resistance measurements were initiated to obtain experimental data on the response of several of the diboride materials to the selected evaluation technique in which hollow cylindrical specimens are heated by a concentrically positioned carbon rod to induce thermal stresses sufficient to cause brittle fracture. The initial results suggest that sufficient plastic strain occurs during the slow heating cycle at temperatures as low as 1275°C to prevent fracture due to the thermal stresses. Transient thermal stress data for many high temperature materials including the diborides developed in this study are being obtained in a variety of hot gas/cold sample arc plasma evaluations under a separate investigation (5).

The combined results of the current program strongly suggest increased confidence in the choice of diboride material as a monolithic ceramic body for applications in environments which will produce thermal stresses and surface oxidation. Such materials can be recommended for aerospace applications, particularly when the application requires retaining a specific geometry such as the radius of leading edge or nose tip for long periods of time. Diboride materials can now be considered for nonaerospace applications for which oxides, boron carbide and silicon carbide have been the leading candidates. Such applications include extrusion dies and liners for working of aerospace alloys and stainless steel, drawing dies, turbine engine parts or other components subject to combinations of abrasive wear, thermal stress and elevated temperature. The success of the ceramic additive approach has eliminated the need for the consideration of low melting metal additives as a means of enhancing consolidation; material fabricated with metallic binders would of course have limited high temperature properties and be less oxidation resistant than the base diborides. Ceramic additives can now be considered for other ceramic systems to enhance fabricability, improve properties and adjust chemical composition.

II. OPERATIONAL PROCEDURES AND PROGRAM MANAGEMENT

This program is a materials research, development and evaluation effort directed and co-ordinated by a prime contract to ManLabs, Inc., Dr. Edward V. Clougherty, Principal Investigator. ManLabs, Inc. provides technical and administrative management and is also responsible for materials procurement and several experimental tasks. Subcontracting services and evaluations are being obtained, or planned, from Avco Space Systems Division, Battelle Memorial Institute, Bell Aerosystems Company, Atomic International Division of North American-Rockwell Corp., The Carborundum Company and the Raytheon Research Division.

Technical management responsibilities at ManLabs are provided by Drs. Edward V. Clougherty and David Kalish. This task includes direction of materials procurement, initiation and supervision of subcontracting efforts and co-ordination and integration of program results with other directly related current Air Force programs. A breakdown of organizational responsibilities is provided in Table 1.

Individual responsibilities for specific tasks and subcontract descriptions are as follows:

Dr. Edward T. Peters of ManLabs supervises materials characterization, thermal and oxidation evaluations and complementary service support for the entire program which includes among other things chemical analyses, X-ray diffraction and electron microprobe analyses.

Avco/Space Systems Division subcontract is directed by Dr. Russell J. Hill and William H. Rhodes; Dr. Thomas Vasilos provides technical consultation. An extensive fabrication effort is being expended which includes hot pressing as the principal method and several other methods including plasma spraying, hot forging and sintering. Avco performs complete metallographic analysis of all billets fabricated. Nondestructive testing services are also provided by Avco under AF33(615)-3942, "Nondestructive Methods for the Evaluation of Graphite and Ceramic Type Materials", Russell C. Stinebring, Supervisor. Mechanical property measurements and emittance determinations are also performed. Dr. David Kalish of ManLabs provides technical liason for the Avco subcontract.

Pyrolytic deposition procedures for boride materials will be pursued in a subcontract to the Raytheon Research Division under the direction of Dr. James Pappis.

Thermal diffusivity data will be obtained in a subcontract to Atomic International under the supervision of Dr. C. A. Smith.

Steady state thermal stress resistance evaluations are being performed at Battelle Memorial Institute under Dr. Dale E. Niesz.

Transient thermal stress behavior are being obtained from dynamic air oxidation evaluations performed in arc plasma tests under a concurrent

ManLabs' program, AF33(615)-3859, "Stability Characterization of Refractory Materials Under High Velocity Atmospheric Flight Conditions", Dr. Larry Kaufman, Principal Investigator.

Simulated leading edge evaluations will be performed in a subcontract to Bell Aerosystems Co. under the direction of Mr. Frank Anthony.

III. MATERIALS PROCUREMENT, CHARACTERIZATION AND IDENTIFICATION

A. Introduction

The zirconium and hafnium diboride materials for this program were generally procured as powder in fifty to several hundred pound lots with realistic purity specifications set in accordance with the required quantities, the anticipated contaminant materials, the state of the art of diboride powder production and cost factors. Powder production processes employ the metal oxide as a starting material and boron carbide, crystalline boron, or a combination of boron oxide and carbon as the source of boron. Accordingly, the price and availability of hafnium diboride are determined by availability of and requirements for hafnium oxide for preparing this and other hafnium-base materials such as hafnium metal alloys. In general, one hundred pound lots were purchased at prices from \$75 to \$120 per pound for hafnium diboride and \$8 to \$10 per pound for zirconium diboride. The latter is readily available and has been prepared in larger batches than hafnium diboride. Considerable variation was found in different lots from the same manufacturer allegedly following the same production process. Some powder variations were found to influence certain material properties including thermal stability and hot pressing characteristics.

A limited number of diboride materials were procured as hot pressed billets to provide a comparison for materials fabricated in the program. Diboride powders for these pressings were either taken from the fabricator's stock or supplied by ManLabs.

B. Material Identification

A number of diboride compositions based on zirconium and hafnium diboride were designed with various additives to improve one or more of the following properties or characteristics: oxidation resistance, mechanical properties, thermal stress resistance. Compositions selected for evaluation in the Phase One screening are provided in Table 2. Roman numerals are used to identify phase constitution and a base composition. The latter was changed for some materials as the program developed.

C. Material Characterization

1. General Powder Characterization Procedures

Physical and chemical characterizations specifically obtained for zirconium and hafnium diboride, but generally applicable in entirety or in part to other refractory materials include the following:

(a) Emission spectrographic analyses are obtained to check qualitatively the presence of metallic impurities which can in turn be related to raw materials, powder processing or particle size reduction. The presence of hafnium in zirconium compounds and particularly, of zirconium in hafnium compounds is generally expected as 1 to 3 per cent; careful interpretation of emission spectra is needed to distinguish these very similar metals and estimate their relative contents.

(b) Quantitative chemical analyses are obtained for the principal metal (Hf or Zr), boron, oxygen and carbon. In addition, quantitative analyses are also obtained for any impurity qualitatively indicated at 0.1 per cent or higher by the emission spectra. A phase assay is calculated for the powder on the basis of the chemical analyses and other characterization results.

(c) X-ray diffraction analyses are used to identify the diboride phase and major impurity phases such as metal oxides and metal carbide. Light element-containing phases such as boron carbide, although possibly present in relative large amounts, are difficult to identify in the presence of metal borides, carbides and oxides.

(d) Powder density determinations are generally performed with an air pycnometer. The powder density of relative high density materials such as hafnium compounds is a sensitive measure of low density impurities, but is a less sensitive measure of metal oxide and carbide impurities in a metal boride powder, as such impurities have similar densities. The powder density is also important for comparison with the measured density of billets fabricated from these powders.

(e) Powder particle size analyses are determined for as-received and milled materials. The principal particle size reduction method used thus far is fluid energy milling in air. The particle size distribution is determined with U. S. Standard Series Screens and with a Rollar Particle Size Analyzer. The latter is used for the range 40 to 1μ .

(f) Hot pressing characteristics and metallographic analysis of resulting consolidated billets are obtained. The minimum conditions of time and temperature (and to a lesser extent pressure) in the range 1,000 to 4,000 psi reflect the presence of various impurities which are known to enhance the densification processes. The metallographic phase assay interpreted in the light of possible reactions between the consolidation powders and the hot pressing atmosphere and container material provide a comparison to the phase assay of the starting powders. Quantitative chemical analyses for metal (zirconium or hafnium) boron, carbon and oxygen and X-ray phase identification of the hot pressed billet provide an indication of any reactions which occurred during consolidation. High pressure hot pressing can be employed to provide dense billets for metallographic phase assay and X-ray analysis for direct comparison with powder characteristics.

(g) Melting point and solidus temperatures and/or impurity phase melting temperatures for samples obtained from the hot pressed billets are determined by a direct observation method. The solidus temperature and/or the melting temperature of the impurity phase is a particularly good technique to confirm minor phase identification. The melting point of the matrix phase provides an indication of composition.

2. Diboride Materials

Zirconium and hafnium diboride powders have been obtained from several supplier-producer companies in fifty to several hundred pound lots to provide an adequate supply of a given lot for a series of fabrication

experiments. Several sources were considered for both ZrB_2 and HfB_2 in order to both select the most suitable powder and to gain information about the relative capabilities of these producers. Capabilities of particular interest include, but are not limited to, adherence of produced materials to purchase order specifications, maintenance to delivery schedules and reproducibility of production runs.

Request for quotations for 100 pound lots of ZrB_2 and HfB_2 were issued to U. S. Borax Research Corp., The Carborundum Company, Wah Chang Corp. and Shieldalloy Corp (U. S. distributor for H. C. Starck Berlin). Powder procurements were initiated with 100 pound orders of ZrB_2 to U. S. Borax Research Corp. and Shieldalloy Corp., 100 pounds of HfB_2 to Wah Chang Corp. and 50 pounds of HfB_2 to Shieldalloy. In addition, samples weighing less than 10 pounds were ordered for special lots of ZrB_2 and for production runs of HfB_2 from U. S. Borax Research Corp. Subsequently, a second 100 pound lot of ZrB_2 and a 400 pound lot of ZrB_2 were procured from U. S. Borax Research Corp. A three hundred pound lot of HfB_2 was ordered from Wah Chang Corp. Extensive delays in the delivery of latter has required that the order to the Wah Chang Corp. be changed to 100 pounds and another 100 pound order has been placed with The Carborundum Company. Some delays have also been encountered in the preparation of acceptable ZrB_2 and HfB_2 by H. C. Starck. These delays were caused in part by the attempts of this producer to rigidly follow an early set of diboride powder specifications which restricted the boron to metal ratio to the range 1.7 to 1.9. The initial materials produced did in fact have a boron to metal ratio of 1.6 but such material could not be synthesized without considerable amounts of cubic phase boride. After this specification was relaxed, an acceptable shipment of ZrB_2 was prepared and delivered. The original 50 pound order of HfB_2 is now being reprocessed. A tentative powder specification is illustrated in Table 3. A complete powder identification chart and a summary of procurement status are provided in Table 4.

Detailed characterization results are presented in Tables 5 through 9 for the four lots of ZrB_2 and one lot of HfB_2 which have been used extensively in the program. Appendix I contains a summary of characterization results for the lots of diboride powders which were obtained in sample quantities, but not used extensively in the program; appropriate discussion of the results and the reasons for rejecting the extensive use of these materials are presented therein. Inspection of the results in Tables 5 through 9 reveals that oxygen and carbon are the principal impurities in the diboride powders. The oxygen is present in the metal oxide, and the carbon is present as metal carbide for metal rich, over-all composition or as boron carbide for boron rich, over-all composition. The ZrB_2 obtained from U. S. Borax Research Corp. contained only minor quantities of hafnium; the material from Shieldalloy contained a normal amount of hafnium (1 to 3 per cent) for a relatively high purity powder. All the hafnium diboride material examined contained 1 to 3 per cent zirconium. Other metallic impurities generally conformed to the powder specification, viz., less than 0.1 per cent.

3. Additive Materials

The additives required to formulate the compositions shown in Table 2 include silicon carbide powder and fibers, hafnium metal powder,

hafnium-tantalum alloy powder, hafnium silicide powder, boron silicide powder, Poco graphite powder and Thorne 25 graphite fibers, amorphous submicron carbon powder, chromium powder and tungsten filament. Procurement information for the additive materials is presented in Table 10. Characterization results are provided in Tables 11 through 14.

D. Procurement and Characterization of Hot Pressed Materials

The procurement of hot pressed billets independent of those prepared in the research and development program at Avco, originally planned for a later stage of the program, was initiated in order to gain earlier assessment of the commercially available material fabricated from a particular supplier's diboride powder. In addition, the relatively high incidence of cracking in unalloyed hot pressed ZrB_2 and HfB_2 experienced in the present program (see Section IV) dictated an investigation of the hot pressing characteristics of the same powders in another hot pressing apparatus. Accordingly, two six inch diameter billets of ZrB_2 were ordered from U. S. Borax Research Corp. and twelve two inch diameter billets of ZrB_2 were ordered from The Carborundum Company. The diboride powder materials for these billets were specified as high purity materials to be supplied by the respective fabricator. In addition, The Carborundum Company agreed to hot press powder from the I02 and I03 lots of ZrB_2 powder according to specified conditions of pressure, time and temperature (optical).

One hot pressed billet of ZrB_2 , six inch diameter by two inch high, was received from U. S. Borax Research Corp. and forwarded to Avco for NDT confirmation of the visually observed crack-free surface and for radiographic inspection. The latter evaluations confirmed the absence of surface cracks and showed no indication of gross density variations. Subsequently, the NDT measuring techniques were refined and re-examination failed to show any irregularities.

The conditions employed by Carborundum for the fabrication of the two inch diameter billets are presented in Table 15. Characterization results for the billets are also provided. The results of the NDT evaluations show no incidence of cracking for the first group of billets prepared from the I02 and I03 powders; circumferential cracks were observed in two of 92% dense billets prepared from the Carborundum powder. Both single billet and triplicate billet pressings were performed by Carborundum. The six billets prepared from the Carborundum powder were fabricated in two triplicate pressings; the six billets prepared from I02 and I03 were fabricated by individual pressings. Two final triplicate pressings were performed using conditions to produce fully dense billets of I02 and I03 material. All six billets contained radial cracks of varying severity; two billets showed cracks running across the entire diameter. The significance of these results is discussed in Section IV.

IV. HOT PRESSING

A. Fabrication Conditions and Results

Diboride specimens for Materials I through VI, VIII, X and XII were fabricated using graphite die hot pressing techniques described in Appendix II. The hot pressing conditions and results for each material are discussed below.

Air pycnometric powder densities were measured on all as-received powders; these values were used as the theoretical densities or as a basis for calculating theoretical densities for powder mixtures. However, for certain compositions, the powder theoretical density was not equivalent to the observed maximum billet density apparently due to phase changes during hot pressing. In those cases where densities higher than the powder theoretical density were observed in fabricated billets, the maximum experimental density was employed for calculating relative densities. Table 16 presents a summary of powder densities, calculated densities for Materials III through VI, VIII, X and XII and maximum densities obtained to date for all materials examined.

1. Material I

Table 17 lists the fabrication conditions and results for billets fabricated from six different ZrB_2 powders.

The microstructure of Material I fabricated from the 03A powder exhibits a marked difference from that fabricated from 02A powder. The hot pressing characteristics of the two powders are also different. The dominant impurity phase in billets of the 03A powder is a dark gray zirconium dioxide with a reflectivity similar to that shown by the 5 v/o ZrO_2 additive in billet I02A D0302. The oxide impurity phase in I03A billets is distributed in two ways: small 1 to 5 micron singularities and large grains closely approaching the grain size of the ZrB_2 matrix, Figure 1. An orange zirconium carbide phase is observed in both the I02A and I03A materials. This carbide phase is distributed as isolated patches in billets of either powder.

A quantitative metallographic phase distribution was conducted on sample I03A D0308. The gray and black phases were counted together because of the tendency for the gray oxide phase to pull out during polishing; it is difficult to metallographically distinguish between residual porosity and pulled out impurity phases. The bulk density of this sample was 6.05 gm/cc which was slightly greater than the pycnometric density for I03A powder (6.038 gm/cc). Accordingly, it was assumed that essentially zero pore phase was present. The combined concentration of the ZrO_2 and ZrC phases are higher by approximately 2% in billet I03A D0308 than in billet I02A D0283, Table 18.

A number of fabrication runs with roughly equivalent time cycles at temperature and pressure are compared in terms of relative density as a function of temperature for Materials I02A and V02A, Figure 2 and Materials I03A and V03A, Figure 3. The fabrication time for the I03A and I02A pressings was 60 minutes at each indicated temperature. The data in these figures show that the

I03A powder densifies more rapidly than the I02A powder; this behavior may be attributed to the higher impurity phase content. The impurity phases could act as a high diffusivity or plastic phases for enhanced densification by either of the two most probable pressure sintering mechanisms; stress directed diffusion or plastic flow. (The densification of Material V will be discussed in a subsequent section.)

Four additional experiments were conducted to verify the effect of second phases on the densification behavior of Material I, Table 19. Billets I02A D0302 and I02A D0303 containing intentional 5 w/o additions of ZrO_2 and ZrC , respectively, were consolidated to essentially theoretical density under conditions which resulted in 90% relative density for the as-received I02A powder (cf., I02A D0613). It appears that increased oxide or carbide content in ZrB_2 powder facilitates consolidation by hot pressing.

Two pressings of Material I02A were made with ZrO_2 additions as a means of assessing the possible effects of the crystal structure of the ZrO_2 phase which is often present in Material I compositions. Pure ZrO_2 undergoes a monoclinic to tetragonal phase inversion at approximately $1000^\circ C$ which is accompanied by a large volume change. The occurrence of this inversion within a diboride matrix could be the source of cracking or high residual stresses. Stabilization of cubic ZrO_2 can be effected by additions of 6 to 12 mole per cent of certain materials of which Y_2O_3 is one of the more common. Stabilized ZrO_2 - Y_2O_3 was added to pressing I02A D0504 while pure ZrO_2 was used in I02A D0505. By a visual inspection both billets appeared uncracked after processing, but during the course of the NDT inspection, the billets were heated in an oven at $200^\circ C$ to drive off some cleaning solvent. At this time billet I02A D0505 crack 1 which indicates that high residual stresses were present. These limited experiments suggest that the crystal form of the ZrO_2 phase could be an important factor in controlling the incidence of cracking and possibly even the strength of the fabricated billets. It is important to note that the HfO_2 phase undergoes an analogous transformation. Accordingly, the impurity phase structure could also be a source of residual stresses in HfB_2 base materials.

Several other Material I powders were employed to a limited extent in Phase One of the program. Billets using powders I04 from U. S. Borax, I05 from Shieldalloy, I06 from U. S. Borax and I07 from U. S. Borax were hot pressed and are included in Table 17. The I07 powder is being used as the major source of zirconium diboride for Phases Two and Three. The effect of fluid energy milling is demonstrated by comparing billets I07 D0628F and I07 D0589; the particle size reduction effected through the milling led to enhanced densification. The fluid energy milled I07 powder achieved 100% density at a lower temperature and shorter time than the unmilled powder. Similar effects of particle size reduction were noted for fluid energy milled I02A and I03A powders, e.g., billets I02A D0345F and I03A D0314F. It is not clear whether the milling fractures single crystal diboride grains or breaks up polycrystalline agglomerates in the as-received powders.

Metallographic phase analyses were performed on the additional material microstructures. Material I04 contains the smallest amount of second phase of all the ZrB_2 fabricated; about 7 volume per cent of a light gray

phase. Material I05 contains two impurity phases, between 3 to 9 volume per cent gray ZrO_2 and 11 to 14 volume per cent orange phase; these phases appear as well dispersed grains smaller than the boride grains. The I05 powder was reprocessed by Shieldalloy with the result that I05A material has no measurable second phase. Material I06 exhibited a gray second phase which was distributed as in the I03A microstructure. Hot pressed Material I07 often shows a grain orientation such that the length of the tabular grain is orthogonal to the direction of pressing. Otherwise, Material I07 appears similar to I03A, but contains a little more of the orange phase and less gray phase. In terms of the hot pressing behavior the I07 is easily densified to 100% density at conditions comparable to those employed with the I03A powder.

2. Material V

Billets of Material V ($ZrB_2 + SiC$) were fabricated with the conditions and results listed in Table 20. The ZrB_2 and SiC powders were dry mixed in a shaker mill.

Typical microstructures developed by hot pressing are shown in Figures 4, 5, 6 and 7. Figure 4 illustrates the extent of mixing of the SiC phase. In general, the phases are well dispersed, but several small patches rich in SiC or ZrB_2 are apparent. Figure 5 demonstrates that very few SiC particles are trapped within the ZrB_2 grains. Some SiC agglomerates are apparent, but it is doubtful that this feature could be avoided at this high level of additive concentration (20 v/o). Figures 6 and 7 show the reduced amount of the impurity phases in Material V relative to the amounts observed in the unalloyed Material I. It is thought that the impurities are 'gettered' by the SiC phase; a similar result was found for the HfB_2 -SiC system as is discussed in Section IV.A7. There was little tendency for radial cracking in the pressed billets of this material.

The base composition studied in Material V contains 20 v/o SiC. However, a series of billets were fabricated where the composition of the silicon carbide was varied from 5 to 50 v/o in a mixture with the I02A ZrB_2 powder. The amount of impurity phases present after hot pressing was determined metallographically. The 9 to 10 v/o impurity phases in the I02A powder were reduced to less than 2 v/o by hot pressing the diboride powder with SiC additions. The quantity of diboride impurity phase remaining as a function of the volume per cent SiC is given in Figure 8; a minimum is observed at 10 to 15 v/o SiC.

The impurity phases remaining in Material V do not appear to wet the SiC, but are generally observed as partially penetrating the diboride grain boundaries, Figure 6. Since the impurity phases are nonwetting with respect to the SiC it is assumed that the reduction in the impurity phase content is due to a chemical reaction (gettering) rather than a physical change such as the formation of a thin film surrounding the SiC grains. A higher per cent of impurity phases is found in V03A, Figure 7, as compared to V02A, Figure 5, due to the higher impurity content of I03A compared with I02A. A special series of billets were hot pressed containing large amounts of the presumed impurity phases, ZrO_2 and ZrC, in an effort to understand the phase changes occurring during the fabrication of Material V. The compositions and pressing conditions of these billets are

given in Table 21. The two component mixtures of SiC-20 v/o ZrC and SiC-20 v/o ZrO₂ were hot pressed to study possible analogous impurity phase-SiC carbide reactions in Material V compositions. X-ray diffraction patterns confirmed the absence of extraneous impurities in the powder mixtures in Table 21. After hot pressing, the zirconia phase was not detected by X-ray analysis. However, ZrSi₂ and ZrC phases were identified in billet D0624; this billet did not contain these phases in the starting powders.

The microstructures of the hot pressed billets listed in Table 21 were analyzed by microhardness measurements and metallographic techniques and the results are given in Table 22. Billet D0624 prepared from ZrO₂ and SiC powders contains three distinct phases identified as ZrSi₂, ZrC and SiC. A dark gray high hardness phase present as the major phase is SiC. The hardness values on the two other phases indicate that the white phase is ZrSi₂, but the value for the third phase of gray color does not agree well with the accepted values for ZrC. Etching helped to confirm the identification since ZrSi₂ and SiC do not react in concentrated nitric acid whereas ZrC is etched. Similar results were obtained with concentrated sulphuric acid as the etchant. When a mixture of hydrofluoric and nitric acid was used on billet D0624, both the ZrC and SiC phases were etched leaving the ZrSi₂ still unaffected.

Billet D0626 prepared from the high purity 05A ZrB₂, ZrO₂ and SiC produced the same type of reactions as billet D0624 during hot pressing. The resulting microstructure contains four phases, ZrC, ZrSi₂ and SiC with ZrB₂. The microstructures of billets D0624 and D0626 are shown in Figures 9 and 10. The ZrSi₂ phase morphology suggests molten phase formation during fabrication.

Billet V03A D0473 was examined for the silicide phases by electron diffraction using an extraction replication technique. Two phases were identified, Zr₂Si and a Zr-B-Si ternary D8₈ phase as reported by Brukl (6). The lower silicide could be expected to form in the CO reducing atmosphere of hot pressing in the presence of SiC with a small concentration of ZrO₂. Furthermore, it is reasonable that a ternary could be formed when ZrB₂ is present. These compounds with ZrB₂ have minimum incipient melting temperatures of 2312°C (6). The ternary silicide may be the phase which is found when billets have 'reacted' during hot pressing due to exceeding the temperature of 2312°C. In addition to the silicides, ZrC should be formed due to the CO rich hot pressing atmosphere; the special compositions substantiate this supposition.

The orange phase often found in Material I was never observed in any of the special materials, D0623 through D0627. This orange phase is believed to be a zirconium carbide containing some boron. The lack of consistency in observing the orange phase may be attributed to a high dependence of color on stoichiometry. It has also been suggested that the orange phase is a complex zirconium boride with oxygen (7). The electron beam microprobe analyses performed by ManLabs contradict this latter assumption, but supports the monocarbide containing boron theory.

The influence of the 20 v/o addition of SiC on the hot pressing characteristics of ZrB_2 is illustrated in Figures 2 and 3. The relative densities of hot pressed 02A and 03A powders with and without SiC additions are compared for similar fabrication conditions. The data demonstrate that the addition of SiC enhances the densification of zirconium diboride during hot pressing.

Several problems were encountered during the early fabrication of the large plates (5-3/4 inch squares) of Material V; billet V02A Q2206 cracked during extraction from the die although the billet is fully dense and the SiC phase is uniformly dispersed; billet V02A Q2221 is less dense than was desired, 92.5% and contains a low density 2 inch diameter central core; the edge of the billet V02A Q2225 was contaminated by the BN mold wash. In this last case, the BN wash must have scraped off the die wall during the initial compaction and mixed with the loosely packed V02A powder. These early problems have been overcome and fully dense large plates of Material V are now made reproducibly, Table 20.

3. Material VIII

The Material VIII hot pressing conditions and results are listed in Table 23. Two lots of ZrB_2 were used, the 02A and the 07 powder and the graphite was introduced in one of three forms, Poco graphite, Regal carbon or Aquadag carbon. In many instances the billet density exceeds the theoretical density for the powder mixture indicating that a change in the chemistry has occurred. However, no attempt has been made to determine the identity of the phases in the hot pressed microstructure, Figure 11. The small grain size, about 4μ and the relatively poor mixing of the SiC with the ZrB_2 , shown in Figure 11 is typical of Material VIII. Figure 12 shows the microstructure of Material VIII containing Regal graphite; an impurity phase reminiscent of that found in Material V03A, Figure 8 is observed.

Billets 3 inches diameter and 5-3/4 inches square were fabricated from this material. A variable density in the large plate VIII07 Q2301L was indicated radiometrically suggesting that there is a segregation of the phases during handling as powders.

4. Material X

The hot pressing conditions and results for the four billets of Material X are listed in Table 24. The limited availability of suitable SiB_6 powder required for this material has precluded further fabrication. As in the case of Material VIII the high density of billet X07 D0635 indicates that the SiB_6 has reacted with the ZrB_2 ; theoretical density of Material X is 5.25 gm/cc. The microstructure of billet X07 D0596, Figure 13 shows a third phase present which appears to have been liquid during hot pressing; a homogeneous distribution of phases was developed in this billet. However, the microstructure of billet X07 D0597, Figure 14 contains large aggregates of both the matrix and additive phases. Additional billets are scheduled to be hot pressed and phase analyses of Material X will be performed.

5. Material XII

The Material XII hot pressing conditions and results are listed in Table 25. It was found that the Poco graphite powder could be mixed more easily than the Regal grade. The microstructure of billet XII(20)07 D0608, Figure 15 with segregation of the phases is typical of a billet made with Regal carbon. In comparison, Figure 16 indicates how the Poco powder mixes well to form evenly distributed phases throughout the material. At 2100°C, the powder mixture was found to react forming a liquid phase clearly visible in the resulting microstructure as a gray third phase. After hot pressing at 2050°C only a few areas can be found containing a gray phase. It has been reported (8) that ZrB_2 forms eutectic type, pseudo binary with graphite at 2390°C. A fine grain material is produced at 2050°C, the smallest obtained for any material in the program. Comparatively longer pressing times are required for complete densification. The material containing Poco graphite is more difficult to densify than the Regal carbon material.

6. Material II

The Material II hot pressing conditions and results are listed in Table 26. Several hafnium diboride powders were employed for hot pressing experiments; powder lot II05, from Wah Chang, has been the principal source of powder for Material II fabrications. Pressing II05 D0316, 99.3% dense, contains at least one and possibly two impurity phases shown in Figure 17. The major gray impurity phase which tended to pull out during metallographic polishing, occurred in both irregular and spherical shaped grains between 2 and 30 microns in size. A minor grain boundary impurity phase, which was apparently liquid during fabrication was observed in billets fabricated at 2200°C. The quantitative metallographic phase analysis of billet II05 D0316 is presented in Table 27. The hot pressed microstructure contains about 8 v/o of impurity phases principally consisting of a cubic hafnium borocarbide.

The II06 powder, from Shieldalloy, had a high impurity content which was manifested by approximately 31 v/o impurity phases in the hot pressed billet. A finely divided gray phase (17 v/o) and large areas of a very dark gray to black phase (14 v/o) which had a grain size of the same order as the boride phase was observed. The high level of impurities in the II06 powder aided the densification of the material; full density could be obtained at 1950°C compared with 2160° to 2200°C required for the II05 powder. The high impurity phase content correlates with the high carbon and oxygen levels in both the II06 powder and the fabricated billets.

The II07 powder, from U. S. Borax, was used for one hot pressing and there were indications that a reaction occurred during the fabrication. The microstructure was examined and the billet contained approximately 15 v/o of a nonwetting grain boundary phase.

The HfO₂ powder, also from U.S. Borax, gave a microstructure with approximately 5 v/o second phase located at the grain boundaries. This powder was hot pressed to high density under comparable conditions to those employed with the HfO₂ powder.

7. Materials III and IV

The hot pressing conditions and results for the HfB₂-SiC compositions, Materials III and IV are presented in Tables 28 and 29 respectively. These powders were dry mixed in a shaker mill.

The microstructures produced for fully dense billets of Materials III and IV are shown in Figures 18 and 19. The impurity phases in Materials III and IV have decreased from the 8 v/o level present in the HfO₂ billets. This phenomenon is verified in the quantitative metallographic data reported in Table 27. The impurity phase still remaining, occupies a position adjacent to the SiC phase, and from the apparent contact angle ($>90^\circ$), it appears to be nonwetting. There is further evidence that the impurity phases are gettered by the SiC rather than occupying some other position such as surrounding the SiC in a thin film which would require a contact angle of $<90^\circ$. Similar to the observations on Material V, this gettering of the oxide and carbide impurity phases by the silicon carbide addition may be significant in enhancing the mechanical properties. The SiC phase in Material IV is well dispersed, but because of the high percentage of additive involved there are many aggregates containing several SiC grains.

It is possible to determine the effect of the SiC on the hot pressing characteristics of HfB₂ by comparing hot pressing results for Materials II and III. The relative densities of these materials hot pressed at equivalent temperatures and pressure and similar times are presented in Figure 20. The SiC significantly aids the densification of HfB₂ as well as acting as a getter for the impurities. One striking feature of microstructures of the SiC alloys of both ZrB₂ and HfB₂, that may account for the enhanced densification behavior over the unalloyed materials, is their much smaller grain size. Diffusion models for densification during hot pressing (including Nabarro-Herring creep) are favored by a small particle size. The SiC phase may serve to restrict grain growth and thereby promote densification.

Finally, it is interesting to note that the decrease of the impurities in Materials III, IV and V is accompanied by enhanced densification whereas in Materials I and II impurity phases appear to enhance densification. There are evidently several factors which affect the rate of densification and the addition of SiC to the base materials may serve to influence more than one of these factors.

8. Material VI

The first hot pressings of Material VI were performed with a powder mixture of 96 v/o HfB₂ and 4 v/o of an Hf-27Ta alloy, Table 30. The component powders were dry mixed in a tungsten carbide ball mill at ManLabs. The air pycnometric density of this composition is 10.89 gm/cc. However, one of the first three hot pressings prepared had a density of 10.97 gm/cc. The three

pressings of Material VI gave relative densities of 100, 91 and 82%. Similar fabrication conditions, produce equivalent densities for Material II. The 4 v/o addition of the hafnium-tantalum alloy does not improve the hot pressing characteristics of hafnium diboride, HfB₂. Billet VI05 D0462 (fully dense) contains three phases as shown in Figure 21. The major gray impurity phase normally found in Material II05 is present, although the minor grain boundary phase is not observed. A quantitative metallographic phase determination for sample VI05 D0462 is given in Table 31. The hafnium-tantalum alloy addition lowered the gray phase concentration from 7.8 to 1.7 v/o; this is similar to the effects of the SiC additions to ZrB₂ and HfB₂. Billets VI05 D0461 and VI05 D0462 exhibited different hafnium-tantalum alloy phase morphology. In billet VI05 D0462 the Hf-Ta phase was located as isolated widely spaced grains of about the same size as the matrix, whereas in specimen VI05 D0461, this phase possessed a similar spacing and size, but contained fine precipitates. Knoop microhardness values (100 gram load) of the HfB₂ matrix phase and the gray Hf-Ta phase (no apparent precipitates) were measured in billet VI05 D0462 with resultant values of 2380 and 2650 Kg/mm², respectively. The high hardness of the phase produced by the additive indicates that the Hf-Ta has undergone a chemical conversion during fabrication, probably to a boride or a borocarbide of these metals.

B. Furnace Variables and Process Control

The hot pressing furnace used for the fabrication of the 2 and 3 inches diameter billets is described in detail in Appendix II. The fabrication of larger billets in the program is conducted on a scaled-up version of the same apparatus.

Below about 2000°C the operating parameters, including temperature, pressure, and rate of densification can be controlled adequately so that reproducible materials can be obtained. However, when 2000°C is exceeded, the lowering of the creep resistance of graphite now makes close control more difficult to obtain. It is precisely within this range of temperature (above 2000°C) where borides can be successfully hot pressed; this explains why some specimens are not reproducibly densified even within a series of seemingly identical hot pressings. To add to the difficulty, the temperature of the material being hot pressed cannot be measured directly and optical sightings are made on a point within the graphite mold away from the sample. Temperature is measured continuously, however, to monitor power input. It is important to note therefore that the temperatures recorded for hot pressing can only be used for comparisons between the hot pressing characteristics of various materials. Even this relationship is in question when different furnace configurations have been used. However, the hot pressing temperature must be regarded as only an approximation when compared to the true temperature of the billet, or the temperatures measured in the various tests performed in the program.

Finally, it has been found that in a typical graphite hot pressing assembly the atmosphere found in the region of the billet is reducing above 1000°C and consists of a CO rich CO/CO₂ mixture. Carbon rich phases are likely, therefore, to predominate in an equilibrium environment.

C. Nondestructive Testing

Billets fabricated in the first 45 hot pressings of Materials I and II showed a high incidence (15%) of cracking. Consequently, a crack detection screening program was initiated through the Avco Nondestructive Testing Section under a separate program (4). The primary purpose of this NDT program is to identify the presence of cracks in the hot pressed billets in order to allow particular materials and billets to be chosen for the mechanical and oxidation screening programs. Approximately 90% of the billets fabricated were tested in the following manner:

1. fluorescent dye penetrant for crack detection and surface inhomogeneities;
2. ultrasonic freon bath cleaning for removal of dye penetrant to check for open porosity and
3. radiography for density gradients (with either the Avco 150 KV machine or the A. Green Company 1 MEV machine).

Almost without exception, the compositions containing SiC for both ZrB_2 and HfB_2 base materials exhibit no cracking. The graphite die wall/diboride and BN wash/diboride reactions that often occur appear to be associated with the high density rim detected by radiography.

Information concerning the source of cracks was obtained by making correlations with Materials I and II. The parameters considered and the corresponding incidences of cracking are given in Table 32. Certain powders show a greater incidence of cracking, namely, the I03A and the II06 pressings. This indicated that within each material category the powder with the most impurities has the higher tendency for billet cracking. An etched microstructure of I03A D0415, Figure 22, exhibits cracks radiating from an oxide inclusion. The strong indications of the importance of powder chemistry on the tendency for cracking is supported by the results in Materials III, IV and V. The addition of SiC reduces the volume of impurity phases to less than 2% and virtually eliminates the cracking.

It was not possible to make any other correlations between processing parameters or microstructure and the incidence of cracking; primarily due to the small sampling within each powder lot. The data for the different powder lots could not be combined (for example, to study the effect of billet density on cracking) due to the complicating effects of powder chemistry.

The nondestructive testing program was extended on billets examined after number D0599 in the following ways. A small ground V-mark notch was ground on one edge of each billet and all subsequent tests were referred to this datum mark. If an area of anomalous density showed during radiography, the billet could be cut accurately to show what caused the discrepancy. During the machining for metallography, another cut was added to the billet so that a bar is

cut across the diameter and a view through the billet can be made radiographically as shown in Figure 23. In addition to the radiography and die penetrant, each billet is examined by conductometric, radiometric and ultrasonic velocity measurements to assess variations in these parameters at different locations within each billet. A fixed array of points shown in Figure 24 was oriented with respect to the notch datum point for each billet and the measurements were taken for each indicated point. The array of points used was taken along four diameters spaced at regular intervals of 45° . This fine structure in density, velocity and conductivity was plotted for all billets subsequent to D0597 as indicated in Figures 25 and 26. These results were used in the analysis of a particular billet and will not be reported in detail here.

V. EXPLORATORY FABRICATION

Hot forging, plasma spraying, sintering and the fabrication of filament composite studies were initiated in order to explore the utility of these methods for consolidating diboride materials.

A. Hot Forging

Two hot forgings were conducted in a hot pressing furnace identical to that utilized for billet fabrication except that Poco graphite pistons were used. A previously hot pressed specimen was core drilled to 1.5 inches diameter and forged with the conditions and results listed in Table 33.

The first experiment, billet I05 D0463, was not a true forging because the starting billet was only 79% dense, thus, much of the forging reduction may be attributed to further densification. However, billet I03A D0466 was fully dense and subsequent forging resulted in a 16% height reduction. This height reduction did not show any microstructural texturing and probably would not effect properties; additional hot forging work has been scheduled for several diboride compositions.

B. Plasma Spraying

Preliminary plasma spraying of diborides was accomplished using an Avco Model PG-100 spray gun. Argon carrier gas was used and a variety of substrates were employed. Nine sprayings of Material I and one spraying of Material II were performed with the conditions and results given in Table 34.

The metal substrate surfaces were prepared for plasma spraying by grit blasting with 0.062 inch steel shot. The bonding between coating and substrate remained intact for all runs except I02A P0162 where the coating readily peeled off the substrate. Poor surface cleaning could give rise to a low joining efficiency. The stainless steel substrates were cylindrical and were rotated at approximately 300 rpm during spraying. The other substrates were flat and the gun was traversed during the operation.

The coatings made with a 5 inch gun distance exhibited poor self bonding as demonstrated by a qualitative abrasion test. The shorter gun to substrate distance greatly improved the self bonding and this was apparent in the metallographic examination. Many of the specimens were extremely porous and they all exhibited an impurity phase, presumably an oxide, which was present in a larger volume percentage than in the hot pressed billets of the same material. The microstructure in Figure 27 is a typical dry plasma sprayed layered structure of Material I and contains a high quantity of second phase.

Further plasma work is scheduled and will involve spraying in an argon atmosphere to reduce the impurity level in the coating. Measurements will be made of the bond strength of the coating to substrate and the strength of the sprayed diboride.

C. Sintering

A sintering program was initiated with the objective of producing diboride specimens with a minimum density of 90%, which could be characterized and tested for comparison with hot pressed material. Initial sintering runs were conducted in a tungsten mesh element vacuum furnace. Temperature was read optically by sighting directly on the sample and correcting for absorption through the sight windows. The processing conditions and results are summarized in Table 35.

The 1/2 inch diameter samples were cold pressed without a binder whereas the 1 inch diameter samples required a polyvinyl alcohol binder to promote adequate green strength for die extraction and handling. Several pre-sintering experiments were conducted to find the correct temperature for binder removal; 400°C for two hours in air was chosen.

The vacuum sintering resulted in significant weight loss, so subsequent experiments were conducted in argon. Sample I03A B005 was quite dense in areas, Figure 28 and had an over-all density of 89%. This structure demonstrates a marked anisotropy of grain size. Small regions of high porosity were macroscopically apparent which may have originated from the accompanying evaporation. Laminations were encountered in specimens B0001 to 5 which were thought to be caused by excess cold pressing pressures. Green densities measured for ZrB_2 pressed at 10,000 and 20,000 psi, were 56.1 and 56.9 per cent. These green densities were considered adequate for sintering to high density. Consequently, the 1 inch diameter specimens were pressed at less than 20,000 psi and with one exception this avoided further cracking.

In general, argon sintering resulted in low density specimens for conditions where 90% relative density was previously attained (2). This could be due to either the chemistry of the ZrB_2 (relative to that previously used) or oxygen contamination and oxide formation from the argon. A purer argon source and lower flow rate will be used to reduce the oxygen content in the chamber.

D. Reinforced Diboride Composites

The use of fiber reinforcing procedures are often considered to enhance the ability of brittle ceramic materials to sustain stresses induced by mechanical and thermal environments which would be produced in various applications. Ceramic bodies reinforced with metal fibers should display improved mechanical properties and thermal stress resistance. Krochmal's review of fiber reinforced ceramics and summary of possible matrix fiber combinations (9) shows that present technology has been unable to capitalize on this approach to achieve improved thermal stress resistant ceramic materials with predictable mechanical integrity. Among other things, thermochemical interaction, matrix cracking and preferential reinforcement oxidation have prohibited the application of this concept to technologically interesting materials.

Earlier work under Tinklepaugh at Alfred University which is summarized in Krochmals review (9) showed that suitably prepared metal reinforced oxide composites failed in bending only after the outer fiber stress was increased several hundred per cent over that of specimens without reinforcement. Deviations from linear stress strain behavior were noted for these ceramic matrix composites where the onset of the deviation was coincident with the stress required to fracture the unreinforced ceramic. The ceramic matrix actually fractured at this stress, but the specimen was held together by the reinforcing metal fibers. The stress applied after the noncatastrophic matrix fracture effected a gradual removal of the fibers across the fracture and eventually complete failure ensued.

Three types of reinforcing agents were employed in an attempt to prepare reinforced diboride composites for evaluation in the Phase One screening tests. Composite compositions are identified and designated as follows: (1) Material V, ZrB_2 with five and twenty volume per cent SiC whiskers, Vf(5) and Vf(20) respectively; (2) Material XII, ZrB_2 with five volume per cent Thornel 25 carbon filaments, XII(5) and (3) Material XIII, ZrB_2 with 5 volume per cent W filaments. These composites represent three different approaches to the utilization of reinforcing agents to effect improvement over the inherently brittle behavior of diboride materials. The Material V composition is a ceramic whisker reinforced ceramic matrix which would not be subject to failure by oxidation of the reinforcement material. The over-all mechanical property enhancement and the improvements in fabricability of the diboride base materials derived from the addition of SiC powder in Material V compositions suggested the examination of the SiC whiskers as a reinforcing agent for ZrB_2 . Thornel 25 was chosen as a reinforcing agent in Material XII to provide crack arresting particles and to improve mechanical properties. Polycrystalline compositions of Material XII with particulate graphite additions were designed to enhance thermal stress resistance by increasing the strength to modulus ratio, σ/E . However, the relatively high modulus of Thornel 25 carbon, $E \sim 20 \times 10^6$ psi, coupled with the low percentage addition is not expected to provide any significant reduction in σ/E for Material XII(5). Tungsten filament was selected as a reinforcing agent in Material XIII on the basis of its thermochemical compatibility with ZrB_2 and HfB_2 and its availability. This composite is representative of the conventional metal reinforced ceramics. Successful fabrication of this material would provide improved mechanical behavior and thermal stress resistance at the expense of decreased oxidation resistance. The characterization of the selected reinforcing agents was presented in Section III.

Conventional hot pressing procedures were employed to attempt to prepare the chosen composite compositions. The fabricating conditions and results are summarized in Table 36. The preliminary experiments appear to be characterized by experimental difficulties common to reinforced composite fabrications. Mechanical difficulties were encountered with the SiC whiskers while thermochemical instability was observed with the Thornel 25 carbon. The behavior of the latter is probably associated with interaction of the additive with the oxide impurity in ZrB_2 . Mechanical difficulties and chemical reaction with the hot pressing atmosphere were observed for the W filament - ZrB_2 system. Partial success in fabricating Material XII(5) was obtained in billet XII(5) D0644 by winding the continuous yarn on a mandrel and cutting round mats of the windings. Each mat was held together at its ends with

Duco cement to facilitate handling. Mats were loaded consecutively with layers of boride resulting in continuous aligned layers of Thornel yarn in the pressing. Reaction was reduced at least in the center of the Thornel yarn by not separating the yarn into its constituent filaments. A representative microstructure is provided in Figure 29. The average room temperature bend strength measured from three specimens of billet D0644 was 30,000 psi indicating no improvement in properties as compared to 100% dense Material I07 which has a bend strength of 40,000 psi.

Full co-operative effects typical of functional composites was not realized almost certainly due to the stresses not being transferred fully to the graphite filaments. This is because each filament of the yarn is not in contact with the boride. This would only be possible if the yarn were separated into its filament constituents. However, under such circumstances the filaments are degraded under the hot pressing conditions. Thus, the principal problem in forming filament boride composites revolves around chemical compatibility of the filament material and the diboride during hot pressing. It is clear that processes employing lower fabricating temperatures must be developed.

A summary of possible diboride matrix fiber reinforced composite systems taken from Krochmal's review (9) is presented in Table 37; thermal stability and other pertinent remarks are included. The results obtained to date and the information in Table 37 will be used as a basis for the continuing effort on fiber reinforced diborides in the current program.

VI. THERMAL SCREENING

A. Introduction

Thermal screening procedures have been carried out on representative structures of each material prepared during Phase One. Cylindrical specimens (about 0.35 inch diameter by 0.35 inch high) of the hot pressed material are initially subjected to metallographic examination to characterize grain size and shape, phase distribution and porosity. The specimens are then subjected to high temperature anneals in argon after which they are re-examined to determine changes in both gross and microscopic features.

B. Experimental Procedure

Screening runs at temperatures up to 2200°C (optical pyrometer) were carried out in a belljar with a resistance heated tantalum tube furnace. A series of tantalum radiation shields were employed to maintain a uniform hot zone of 2.5 inches diameter by 5 inches long. The specimens were contained in tantalum wire baskets for screening at 1800° to 2000°C. In operation the furnace was twice evacuated to ~ 1 torr and back filled with argon; specimen degassing was promoted by initially heating the specimens to ~ 1000°C in a vacuum of 10^{-5} torr followed by cooling to room temperature. After introducing argon to provide an operating pressure of ~ 650 torr, the furnace was heated to temperature by a manually controlled power supply at a rate of 5 to 10°C per minute. Temperature was measured periodically with a micro-optical pyrometer, accurate to $\pm 10^\circ\text{C}$. After the test, the specimens were slowly cooled to room temperature.

For temperatures above 2000°C, where the diborides alloy with tantalum to form a liquid phase, the specimens were placed on a HfB₂ plate supported on a ZrO₂ pedestal. Temperatures in excess of 2200°C (optical) could not be obtained because of contamination of the heating element by vapor transport from the specimens. To overcome this difficulty, thermal screening anneals were carried out in flowing argon at 2300°C (color temperature) in the oxidation furnaces (Section VIII).

C. Experimental Results and Discussion of Results

A summary of the thermal screening experiments is given in Table 38. Except where noted by a remark, there was no evidence for any localized melting or for second phase coalescence, redistribution or dissolution. Line intercept analyses of initial and annealed structure photomicrographs yielded on the average, a small increase in grain size. The following microstructural features were observed.

1. Material I (ZrB₂)

Specimens of pressing I07 D0589 were observed to have a number of microstructural variations in both the as-pressed and annealed conditions.

Figures 30(a) and 30(b) present photomicrographs of two areas within the hot pressed billet; the variations in microstructure are clearly evident. Both sections contain a gray phase and pores, some of which appear as having previously contained a secondary phase which was pulled out during metallographic preparation. In contrast, a section of the specimen screened at 2200°C (optical) contains a different porosity distribution and contains large amounts of an orange second phase, Figure 30(c).

Structural variations in the specimens thermally screened at 2200°C (optical) and 2300°C (color) are depicted in Figure 31; the structures include a) large, elongated grains with a considerable amount of grain boundary precipitation and porosity, b) large pores, c) small pores and d) small pores and large amounts of an orange precipitate. Complete evaluation of the specimens indicates that the structural variations that have been noted are characteristic of the billet and have not been affected by the annealing treatments.

2. Material VIII ($\text{ZrB}_2 + 30 \text{ v/o Graphite} + 14 \text{ v/o SiC}$)

Two formulations of Material VIII were thermally screened, including preparations from Regal 330R carbon powder (D0498) and Poco graphite powder (D0592); microstructures of these billets are presented in Figures 11 and 12. After thermal screening treatments, transverse section microstructures of both pressings exhibited a peripheral ring depleted of additive phase. Pressing D0498, treated at 2200°C (color temperature) for 15 minutes exhibited an average additive phase depletion of 50 mils, whereas pressing D0592, treated at 2300°C (color temperature) for 15 minutes exhibited an average depletion of about 10 mils. Photomicrographs of both specimens, including an over-all view of the transverse section and microstructures of both the depleted and matrix zones, are presented in Figures 32 and 33. In both cases, the matrix zone structures are identical to those of the original materials. It is of interest to note that heat treatment in argon at about 2200°C produces about five times greater additive phase depletion in the material prepared from Regal 330R carbon compared to preparation from Poco graphite.

3. Material X ($\text{ZrB}_2 + \text{SiB}_6$)

Exposure at 2200°C (color temperature) for 15 minutes resulted in SiB_6 -phase melting in specimen D0596. The original and heat treated microstructures are presented in Figure 34. The SiB_6 phase, which originally is quite uniformly dispersed, is observed to be present as a grain boundary phase. The rounding of the ZrB_2 grains is characteristic of the past presence of a liquid grain boundary phase. As one traverses from the center to the surface of the sample, the extent of porosity and ZrB_2 grain size is observed to increase and the amount of SiB_6 phase is observed to decrease. Further experiments are planned to determine the necessary conditions (temperature, time and atmosphere) for SiB_6 -phase melting.

D. Melting Points

In addition to the foregoing, melting point measurements have been carried out on six hot pressed specimens by E. Rudy, Aerojet General Corporation.

The specimens, in the shape of right cylinder dumbbells, were melted under a positive helium pressure of 2 atm. Apparent temperatures were corrected for the black body sighting hole configuration and for transmission through a quartz furnace window. Incipient melting is generally associated with a visual observation of liquid infiltration by melting of secondary phases. The observed results are presented in Table 39.

The melting results of the Carborundum, 102A and 103A structures are consistent with the X-ray finding that the major impurity phase is ZrO_2 (melting point $\sim 2600^\circ C$). The diboride melting at $\sim 3085^\circ C$ is in reasonable agreement with the melting point of ZrB_2 (1). The Norton ZrB_2 , containing ZrC as the major impurity phase, yields incipient melting at a higher temperature than zirconium borides containing ZrO_2 as the impurity phase.

The melting behavior of the Material II (HfB_2) samples are also consistent with second phase impurities. The II05 material, containing very little second phase impurity, shows no evidence of melting to $3235^\circ C$; complete melting was observed at $3345^\circ C$. The II06 material, which contains large amounts of HfO_2 and HfC , showed incipient melting at $2697^\circ C$ and complete melting at $3085^\circ C$, considerably lower than the II05 material.

Additional melting point evaluations are scheduled for specimens prepared from Materials III, V, VI and VIII.

VII. MECHANICAL SCREENING

A. Bend Testing

Bend tests at Avco were conducted within an inductively heated graphite four point bending cell, Figure 35. The load was applied at a constant rate (24 lb/min) from a constant head water tank and the loading was terminated by a microswitch operated selenoid water valve at the instant of fracture. A W-5% Re vs. W-26% Re thermocouple was located directly under the specimen. This couple was checked against a Pt-5% Rh vs. Pt-20% Rh thermocouple for accuracy. The specimen was allowed to thermally equilibrate several minutes prior to the application of load. The graphite cell was constructed so that alignment of the specimen throughout assembly and testing was assured. Specimens were 0.875 inches long by 0.150 inches wide by 0.050 inches thick and the moment arm was 0.187 inches giving a span to height (1/2 thickness) ratio of 7.5. Three tests per temperature were performed for each microstructure.

1. Temperature Effect on Bend Strength

The results of the bend test measurements at Avco which were performed at temperatures from 23°C to 1800°C are given in Table 40 for Phase I structures and Table 41 for Phase II structures. The average results for Materials I to V are plotted as a function of test temperature in Figures 36 to 40. Several microstructures are not represented graphically as only limited comparative data were available.

Almost all Material I microstructures tested display a strength peak at 800°C with the strength falling sharply at 1400°C, Figure 36. This agrees with previous results on high pressure hot pressing ZrB_2 and HfB_2 (3). At 1800°C, the maximum average strength for one microstructure was 31,000 psi and this occurred for a 90% dense billet. An increase in porosity does not appear to decrease bend strength of the material at any temperature. However, it was not possible to independently vary the porosity and grain size of Material I microstructures. Consequently, the dense Material I microstructures generally have a larger grain size than the more porous ones. The beneficial effect of the smaller grain size of the less dense microstructures may compensate for the detrimental effect of the porosity producing the somewhat ambiguous results in Figure 35. This suggests that it would be desirable to fabricate fine grained dense materials, but this was difficult with the 102A powder. Relatively fine grained materials could be made from 03A powder at the 95% and 100% density levels, but these samples were not appreciably stronger than coarser grained 02A materials of equivalent density. The fact that a strength increase was expected from the finer grain size, but was not observed may be attributed to impurity phase differences between the two powders.

The role of grain size and porosity in determining the strength of ZrB_2 may be clarified by comparing the results for Material I with the bend strengths of two additional lots of ZrB_2 material. The strength properties as a function of test temperature for ZrB_2 materials supplied by the Norton and Carborundum Companies were determined for temperatures from -196°C to 1800°C, Table 42. The testing at temperatures up to 1400°C was performed at ManLabs

using a three point bending apparatus. Tests at 1400°C and 1800°C were performed at Avco with the four point apparatus being employed in mechanical screening studies of the other boride materials. The strengths measured on the Norton material were comparable to those determined in the previous boride program (3). However, the new results for the Carborundum ZrB₂ show higher strengths than the earlier measurements. The discrepancy may be due to the different sample preparation technique; the earlier specimens were cut by electrical discharge machining whereas the recent material was cut by diamond tools. Other work has shown that EDM of TiC was detrimental to the bend strength due to the creation of microcracks (10).

The Carborundum ZrB₂, low in metallic impurities behaves similarly to the Avco microstructures of Material I. The major decrease in strength occurs between 1200°C and 1400°C. The Norton material shows an unusual behavior in that the strength declines gradually up to 1400°C and then at 1800°C drops to the lowest value observed for any of the diboride material. The unusually low strength at 1800°C is attributed to the combination of a relatively large grain size and the high porosity which is unlike the Material I microstructures where the 90% dense materials are all fine grained.

Specifically, the Norton material with a porosity of 11% and grain size of 18μ has a bend strength at 1800°C of 5,000 psi; Carborundum's ZrB₂ was 95% dense with a grain size of 16μ and had a strength at 1800°C of 15,000 psi. These lower strengths as compared with other Material I microstructures may again be due to impurity differences. However, at their respective porosity levels, these data support a grain size dependence in the bend strength. If the data for the Norton and Carborundum materials are compared with the data in Figure 36 for 90% and 95% dense materials, respectively, a trend for decreasing strength with increasing grain size emerges.

Consequently, within a given powder lot, the fine grained dense microstructure will display the highest strength, but among powders of different chemistry the impurity phase content and morphology may be the dominating factor in determining the strength.

It should be mentioned that the limited number of tests per microstructure and temperature also complicates the problem of determining the role of microstructure and chemistry on the strength of Material I. This factor may be most important in the brittle fracture range at temperatures up to 800°C as opposed to conditions where limited plasticity is observed at 1400° to 1800°C.

A preliminary series of experiments were performed on the Norton ZrB₂ and Carborundum ZrB₂ where an oxide layer was developed prior to bend testing at 23°C and 1000°C. The specimens were preoxidized at 1600°C for 30 minutes; this temperature is in the region where the oxide is coherent to the diboride matrix. The oxide layer produced was about 0.007 inch thick. Examination of the oxide boride interface at high magnifications revealed that the oxide preferentially penetrated the diboride grain boundaries to a depth of 1/2 to 1 grain beyond the general interface. However, at no point was a diboride grain completely surrounded by grain boundary oxide nor were any microcracks found to be generated from the penetrating oxide. The bend test results were analyzed from two

standpoints: first, it was assumed that the diboride matrix supported the entire load; second, it was assumed that the matrix plus the oxide supported the load. These calculated stresses are compared to the range of strengths measured on the unoxidized matrix for each material in Table 43.

The results indicate that the oxide layers do not detract from the strengths of the ZrB_2 matrices. However, the oxide does not appear to have the strength of the diboride matrix. Future plans include preoxidizing structures of all the materials and using preoxidization conditions in the different regions of oxide formation (coherent, semicoherent, incoherent). In addition, the studies will be extended to include the effect of SiC depletion on the strength of the alloyed materials.

Fully dense Material V microstructures were fabricated with 02A, 03A and 07 ZrB_2 powders. In both Materials V and I the chemistry effects seem to be most important at low test temperatures, 25° and 800°C, whereas at 1400° and 1800°C the grain size dominates. In Material V, for fully dense and comparable grain size microstructures, there is essentially no difference among the three base powders in the bend strength at 1800°C. Residual stresses introduced by impurity phases in the base materials due to thermal contraction differences may influence the strength at the lower test temperatures. At the higher test temperatures these stresses could be relieved thus minimizing the effect of powder chemistry.

Comparison of Material V with Material I, Figures 36 and 37 indicates that the SiC addition suppresses the strength maxima at 800°C and increases the strength at 1800°C. The strengthening effect of SiC for the 02A ZrB_2 and 05 HfB_2 base materials at 1800°C is shown in Figure 41, only data for billets 98-100% dense are plotted. The 1800°C data for both ZrB_2 and HfB_2 base materials suggests a significant increase in strength with the addition of SiC. There is a substantial difference in grain size for the microstructures with and without SiC and this must be kept in mind when comparing strength values. The morphology of the SiC does not allow for strengthening by dispersion hardening since the SiC grains are of the same order of size as the matrix. However, the two phase aggregate may be more resistant to deformation than the boride alone and thereby contribute to the elevated temperature strengthening. The ZrB_2 base compositions do not show any dependence on SiC content for compositions between 10 and 35 v/o SiC. Alternately, the HfB_2 -SiC composite strength continues to increase with increasing SiC content. This discrepancy is not understood at this time, but may be due the chemistry changes induced by the additions of SiC. This problem will receive further consideration from the standpoints of phase analyses and strength measurements; the latter will include the definition of the stress strain curves for samples tested at 1800° and 2200°C.

The limited bend strength data for Material II, Figure 38 indicates that a fine grain size is more important than low porosity for obtaining a high strength. The addition of SiC to HfB_2 greatly facilitated the densification of Material III and allowed fine grained microstructures to be produced at all porosity levels, Section IV. The bend strengths as functions of test temperature for Materials III and IV, Figures 39 and 40 demonstrate that porosity is detrimental to the strength although this effect does not persist at all test

temperatures, Figure 39. The general effects of the SiC additions are believed to be similar to those for ZrB_2 base materials as discussed in the previous paragraphs. The strength level at 1800°C, 59,600 psi, is thought to be the highest strength ever reported for an oxidation resistant material.

Limited testing was performed on Materials VI, VIII and XII. Material VI exhibited strength values at 23°C and 1800°C comparable to those of an equivalent density Material III. Material VIII possessed moderate strength values at 23°C, but excellent elevated temperature strength was attained in a similar manner to other SiC containing diboride compositions. Material XII, with 20 v/o C high temperature values no better than Material I.

An additional point of interest with respect to Materials III, IV and V was revealed in the etched microstructures. Fine linear features are observed within the matrix grains; these facets being as much as half a grain diameter in length. It is unknown at this time whether these features are microcracks or a precipitate. However, it should be noted that even the highest strength microstructures of these materials contained these hairline features, Figures 18 and 19.

2. Surface Finish Effect on Bend Strength

Surface finish could be important in determining the level of fracture stress in brittle materials because fracture is thought to often originate from pre-existing flaws. The surface placed in tension in a bend test would be most critical and thereby control the fracture stress. In the case of catastrophic brittle fracture, the crack length and fracture stress are related by the Griffith relation

$$\sigma_f^2 = \frac{2\gamma_f E}{\pi C} \quad (1)$$

where σ_f = the fracture stress, γ_f = fracture surface energy, E = elastic modulus and C = crack length. If the fracture surface energy is the true chemical surface energy, which would be about 1 to 2×10^3 ergs/cm², then the critical crack length would be of the order of 1 to 5 microns (using $E = 51.7 \times 10^{11}$ dynes/cm² and $\sigma_f = 44.8 \times 10^8$ dynes/cm²). Bend tests on a series of surface finishes were conducted to test the importance of the starting surface on determining fracture stress.

A number of bend specimens were machined from the 100% dense billet V07 D0576; the NDT report indicated that this billet was uniform in density and was uncracked. Various surface finishes were prepared by grinding the tensile surface with 220, 400 and 500 grit wheels. A fourth surface condition was prepared by obtaining essentially a metallurgical finish with a final 0.25 micron diamond polish. The structure of the surfaces was characterized in two ways; Talysurf (Taylor-Hobson) surface contour traces and electron microscope surface replica examination.

Sections of the Taylorsurf traces are shown in Figure 42 for the four surfaces tested. Associated with each tracing is the vertical magnification and the C.L.A. (integrated average deviation of the ridges and grooves from the centerline). As can be noted, many grooves have total depths much deeper than twice the C.L.A.; 180 μ inch in the case of the 220 grit finish, 100 μ inch for the 400 grit finish, 100 μ inch for the 500 grit finish and 3 μ inches for the polished surface. The 400 and 500 grit finishes appear very similar.

The electron microscope examination showed surface structures represented by Figures 43 to 45. The 400 and 500 grit finishes appeared quite similar, so the structure for only the 400 grit is shown, Figure 44. The 220 grit finish reveals the microstructure since many grains were completely pulled out. Evidence for possible intergranular surface cracking is also shown in Figure 43. The 400 grit surface has resulted in a greatly increased surface cutting although some grain pull out also took place. Possible surface cracks are shown in Figure 44 for this finish. The finely polished surface shown in Figure 45 reveals very little structure or scratches. The pits that are present show no well defined structure at higher magnification; they are apparently areas where polishing did not completely remove the results of rough grinding. However, no cracks were observed on the polished surface.

The room temperature strength data for the four surface finishes are reported in Table 44. There was a trend for increased mean strength with the finer surface finishes; however, the standard deviation for each population was large, except for the 500 grit finish. The "Student's T" test was utilized to investigate the significance of the variation between the mean strength of the 220 grit and the polished surface. The probability of significance was 38.9% and this shows that from statistical considerations they essentially belong to one strength group.

The insensitivity of the fracture strength to the surface condition may be attributed to slow growth of the existing flaws by localized plastic flow processes at stresses below that for catastrophic failure. Room temperature slip in polycrystalline TiB_2 has been observed (11). All the surface finishes produced cracks and could be subcritical up to stress levels where slow crack growth initiates. An alternate mechanism for slow crack growth could involve stress corrosion of the diboride, both static and dynamic stress corrosion effects have been reported for alumina (12). In either case pre-existing cracks could grow under increasing stress until the Griffith-Orowan criteria for fracture is reached and then rapid crack propagation ensues. Independent measurements at ManLabs of fracture energies on conventionally hot pressed ZrB_2 and obtained values of 71,000 and 134,000 $ergs/cm^2$ for two different grades of material. (The materials studied were the Norton and Carborundum grades.) Using these numbers for twice the surface fracture energy in the Griffith-Orowan equation, crack lengths of greater than 90 microns could be tolerated without initiating fracture at the observed fracture stresses. Fracture stress insensitivity to surface condition coupled with the fracture energy measurements lends considerable support to the prospect that localized plastic deformation processes are involved in the fracture of the diborides.

There are two alternatives to the assumption that slow crack growth occurs prior to fracture. First, other defects may be present in the material from the fabrication and these defects are larger than any flaw created by the rough surface finishes. Metallographic studies do not support this assumption; cracks of several grain diameters would easily be detected by light microscopy. Second, the flaws introduced by the surface finish techniques do not have a morphology that creates a critical stress concentration. For example, pre-existing atomically sharp cracks of less than a grain diameter may provide a more severe condition than deep, but relatively blunt grinding grooves. Microstructural features have been observed in Materials III, IV and V that could be transgranular cracks although they have not been positively identified as cracks. However, the surface grinding in these brittle materials does not create blunt grooves, but removes material by chipping and pulling out grains thereby providing high stress concentrations.

B. Elastic Modulus

Dynamic measurements of Young's Modulus (E) were made by the sound velocity technique at 23°C. High density half billets of Materials I to V were employed in order to measure both the compressional pulse velocity (V_L) and the transverse pulse velocity (V_T). The results of these measurements on seven billets are listed in Table 45. Considerable disagreement is found among the calculated values of Poisson's Ratio. It is believed that the primary source of error in the calculations is in the measurement of V_T . Therefore, a value of $\nu = 0.145$, as previously used (3) will be adopted in future calculations of Young's Modulus until accurate determinations can be made for each material in this program.

Static measurements of Young's Modulus were made using a four point bending and a single point probe strain measuring apparatus, Figure 46. At present, the measurements are being conducted in argon, so the spring support of the load cell cage is unnecessary. The schematic also shows three tungsten probes positioned against the sample. This design was intended to bring the strain reference point directly to the sample. This would eliminate errors due to knife edge interactions, etc. However, the early work with this design has been inaccurate, so at present, the outer two probes are fixed to the lower knife edge block. A W-5% Rp vs. W-26% Ro thermocouple is placed next to the lower graphite pedestal and is positioned directly under the sample. A Mo furnace is being used. As extremely small strains are measured ($4-9 \times 10^{-4}$ inches) for the specimens which are the same size as used for bend tests, the LVDT was calibrated with a series of four gage blocks having height differences of 25×10^{-6} inches, as well as a micrometer reading to 1×10^{-4} inches. Also three standard modulus materials were used to check the accuracy of the apparatus; they were 9Ni-4Co-0.45C steel (28.5×10^6 psi), 99.5% dense alumina (58×10^6 psi) and WC-5.75% Co ($88-92 \times 10^6$ psi).

The static Young's Modulus measurements are summarized in Table 46. Also included in this table are a limited number of dynamic modulus measurements and static measurements conducted at ManLabs. The different measurements served as further checks on the accuracy of the equipment. Furthermore, data

are included which were collected both prior to and after several equipment modifications, so varying levels of accuracy are represented.

It will be necessary to collect additional self-consistent data in order to separate the effects of composition on the elastic properties; however, at this time it is possible to relate porosity to Young's Modulus in the diborides.

MacKenzie (13) analyzed the effect of small amounts of porosity on elastic moduli in an isotropic body. This relation is given as

$$1 - \frac{G}{G_0} = \frac{5(1-\rho)(3K_0 + 4G_0)}{(9K_0 + 8G_0)} + A(1-\rho)^2 \quad (2)$$

where G = modulus of rigidity, ρ = relative density, K_0 = bulk modulus, A = constant and the zero subscript refers to the full density value. Cable et al., (14) calculated the constant A by setting $G/G_0 = 1$ at $\rho = 0$ and found this equation accurate for several materials. For Poisson's ratio $\nu = 0.145$ for ZrB_2 and $G/G_0 = 1$, $K_0 = 1.08$ and $A = 1.04$. The curve for Eq. (2) is plotted in Figure 47 along with Young's Modulus data for Materials I through V at various porosity levels. The data plotted is thought to be self-consistent in that apparatus design and calibration was constant throughout the measurements. Several interesting features emerge; the SiC alloys of the diborides fall on the same curve as their respective base materials, the ZrB_2 base materials agree with the predicted relation and Young's Modulus for the HfB_2 base materials is much more sensitive to porosity than predicted. Rossi et al. (15) have shown that anisotropic geometry for porosity or second phase inclusions can account for marked deviations from predicted behavior. The ZrB_2 and HfB_2 base materials must be carefully re-examined for differences in these microstructural features which may be responsible for the behavior shown in Figure 47.

In order to determine the accuracy of the elastic modulus measurements at Avco, a sample exchange study with ManLabs, Inc. was instituted. The room temperature Young's Modulus values obtained at Avco (four point bending - single deflection probe) were approximately 7 to 10 per cent lower than those obtained at ManLabs, Inc. (three point bending - single deflection probe). Both laboratories also tested a series of standard materials (steel, Al_2O_3 and WC-5.75Co) with the same discrepancy between test techniques. A comparison of the measurements on the standards with published values revealed that the ManLabs, Inc. measurements were within 5 per cent of the absolute values. It was concluded that the static Young's Modulus measurements on the diborides at Avco obtained as of this report are up to 10 per cent lower than the ManLabs numbers. The measurements at 800° and 1400°C at Avco have the same accuracy as those obtained at 23°C.

The elastic moduli of the Norton and Carborundum lots of hot pressed zirconium diborides were determined by a three-point bending, single-point deflection probe technique at ManLabs, Inc. The results are presented in Table 47 with some dynamic measurements for another hot pressed ZrB_2 (16).

There is excellent agreement between the static and dynamic measurements and the 5 data points for modulus vs. density form a curve which extrapolates to a value of about 7 to 79×10^6 psi for fully dense ZrB_2 .

C. Post-Mortem Examinations

1. Visual Examinations

All specimens were examined after testing with respect to the location of the fracture. Single and double asterisks appear after certain specimens in Tables 40 and 41 and these denote primary and secondary* knife edge fractures, respectively. The incidence of such knife edge fractures is common in transverse rupture tests utilizing four-point bending; the origin of this phenomena is still a matter of some controversy (17). Compressive stresses are anticipated in the areas under the knife edge, hence, tensile failures should be prevented in these regions. However, there has been at least one investigation (18) in which knife edge failures did originate in tension surfaces, so that the actual stress distribution under a knife edge is probably far more complicated than previously supposed. In addition, the incidence of knife edge failures could be correlated in one case (18) with absorbed surface moisture, the frequency of such failure increasing on dry surfaces and this is also a factor which has not previously been recognized.

It was not possible in this study to correlate the incidence of knife edge fractures with any microstructural or testing parameters, although the frequency of such failures was much higher in certain materials. Similar information will be recorded in the future and trends may become apparent when more data are available.

Plastic bending was observed in many of the samples tested at 1800°C as evidenced by curvature on the fragments when placed against a flat plate. In all cases, however, the amount of plastic bending was estimated to be less than 1%. The notations N.B., S.B. and B in Tables 40 and 41 denote no plastic bending, slight plastic bending and plastic bending of less than 1%, respectively. Again, it was not possible to correlate these observations with either microstructural parameters or strengths. Much more information will be forthcoming when high temperature stress strain curves are generated.

2. Fractography

Replicas were taken from a selected number of fractured samples, for Materials I to V and examined in the electron microscope. The fracture mode was predominantly transgranular in samples tested at room temperature, while the percentage of intergranular fracture increased with increasing test temperature. Figures 48 to 51 show fractographs of a Material V microstructure tested at four different temperatures. It can be seen that a limited amount of transgranular fracture occurred even at 1800°C .

* The main fracture in these cases was within the gage length, but an additional fracture occurred at one of the loading points, resulting in three fragments.

It is difficult to differentiate between the ZrB_2 matrix and the SiC addition, as the fracture mode was similar for both phases. However, light microscopy of polished surfaces shows that the SiC phase is generally smaller than the ZrB_2 matrix. The smaller grains visible in Figures 48 to 51 are almost certainly the SiC phase. The terraces visible in the 1800°C fractograph are probably due to thermal etching.

The increase in the amount of intergranular fracture with increasing temperature occurred even when the fracture strength increased. Previous observations on fine grained ZrB_2 and HfB_2 showed that the percentage of transgranular fracture paralleled the strength peak (9). This difference in behavior is not understood.

3. Optical Microscopy

One aspect of the post-mortem studies is to determine the relative stability of the microstructure to the testing environment. The grain sizes for specimens tested at 1800°C are given in Table 48 and reveal that significant grain growth only occurred in one ZrB_2 structure. The I02A D0338 specimen shows an apparent anomaly, undoubtedly due to grain size variability within the billet itself. The unalloyed HfB_2 , Material II and the diboride-SiC mixtures, Materials III, IV and V show little or no grain growth during the 1800°C test (at temperature approximately 5 minutes). The SiC second phase evidently inhibits movement of the diboride grain boundaries as it does during fabrication. The thermal stability of impurity phases in the HfB_2 (solidus 3235°C) relative to those in the ZrB_2 (solidus 2560-2630°C) may also contribute to the observed increased grain size stability for HfB_2 . The grain sizes determined from the electron fractographs agreed with the grain size measurements by light microscopy.

The specimen from billet I02A D0305 showed an increased concentration of orange carbide phase relative to the gray oxide impurity phase, compared with the starting billet, but the over-all second phase content remained constant. All other specimens examined possessed structures that appeared identical to the as-fabricated material. The edge of specimen I02A D0338, Figure 52 (tested at 1800°C) shows no evidence for oxidation during testing in argon.

In several cases, anomalously weak specimens were encountered and examined. There was nothing unusual in the fractographs which could explain the low strengths at room temperature and the fracture mode was still predominantly transgranular.

Although plastic deformation occurred at 1800°C as manifested by permanent specimen curvature there were no details on the fractographs which could be correlated with the limited amount of macroscopic plasticity.

4. Density Checks

Post-testing density checks on bend specimens fractured at room temperature are shown in Table 49.

In order to measure the geometric density, the fracture face of the test fragment was squared off and the radius on the tension face was removed by grinding. When a discrepancy between the air density and the water displacement density occurred, the geometric density was always lower.

It was also possible to correlate the differences between original billet density and the true (water displacement) specimen density. X-radiographs were available for billets I02A D0345, III05 D0386 and IV05 D0410. Billet D0386 had a high density rim and this was the reason for the higher density of the billet compared to the bend specimen. Billets I02A D0345 and IV05 D0410 had low density areas on the edge, therefore, the higher density of the bend specimens is to be expected. The density variations on the exterior of certain billets is attributed to the chemical reaction of the billet with the BN mold wash or the graphite liner. Clear examples of reaction zones were visible metallographically in several billets.

VIII. OXIDATION SCREENING

A. Introduction

Furnace oxidation screening experiments have been carried out on hot pressed specimens of Materials I through VI, VIII, X and XII and on high pressure hot pressed (HPHP) specimens of Materials VI, X and XI. In addition, oxidation comparisons have been made between commercially hot pressed ZrB_2 (obtained from two sources) and Material I and also between Boride Z (Carborundum Corporation) and Materials I, V and VIII. The oxidation characteristics of selected diboride compositions containing rare earth and alkaline earth additives were also determined. These materials were fabricated under a separate Air Force program investigating boride coating compatibility for graphite. The results are summarized in Appendix III.

B. Experimental Procedure

The oxidation exposures are carried out in a furnace depicted schematically in Figure 53. Cylindrical specimens, which are generally 0.35 inch diameter by 0.35 inch high, are placed coaxial with the furnace tube and are mounted on zirconia knife edge supports. The specimens are heated by radiation from a zirconia liner which in turn is heated by a carbon tube resistance furnace. Four identical furnaces, each having an inside tube diameter of 0.75 inch, are being used.

The specimens are heated to the desired test temperature in argon having an effective flow rate of 0.9 ft/sec STP; heating times are generally 30 to 40 minutes. After the desired temperature is stabilized, air is admitted for a fixed time interval, usually one hour. Then argon is readmitted to displace the air and the specimen is cooled; 60 to 90 minutes are required to reach room temperature.

Several experiments were carried out to determine satisfactory air flow rates to sustain reaction (or diffusion) controlled oxidation. Figure 54 presents a hypothetical oxidation experiment in which a protective oxide is formed. The amount of oxygen required to sustain equilibrium oxidation as a function of time is indicated by line 1. The amount of oxygen supplied to the specimen is linear with time; two air flow rates are represented with $v_2 > v_1$. For any given time, the supply of oxygen (v) must exceed the oxygen requirement (line 1). Thus, a 60 minute experiment requires an amount of oxygen corresponding to point (a); either air flow rate would be satisfactory. For a 30 minute experiment, however, flow rate v_1 would supply an amount of oxygen corresponding to point (c), whereas a quantity corresponding to point (b) is required; a 30 minute experiment employing flow rate v_1 would be oxygen supply limited. For a given specimen material, temperature and time, the critical flow rate v_c corresponds to the rate which supplies just the amount of oxygen required for specimen oxidation.

Flow rate dependencies have been determined experimentally for Material I (ZrB_2 , 1800°C , 15 minutes) and Material III ($\text{HfB}_2 + 20 \text{ v/o SiC}$, 2120°C , 60 minutes); pertinent data are presented in Table 50 and Figure 55. In both cases which represent the severe extremes of short time and high temperature, the critical flow rates were determined to be 0.4 ft/sec STP. The oxidation experiments reported upon were all carried out at an air flow rate of 0.9 ft/sec STP.

The specimen surface temperature is measured and recorded continuously by means of a two color pyrometer. The pyrometer is calibrated weekly against an NBS certified tungsten filament to detect and correct for calibration changes. The temperatures reported in this section are color temperatures which, for tungsten are 20° and 50°C higher than true temperatures at 1500° and 2000°C , respectively.

After oxidation, a quantitative metallographic procedure is employed to measure the extent of material recession; post-mortem metallographic inspection also provides morphological information about the diboride matrix, the oxide and the matrix oxide interface region. Initially, a low magnification photograph of the specimens obtained to provide a record of the shape of the specimen and of the physical condition of the outer oxide layer. The specimen is mounted longitudinally and is polished to reveal the oxide diboride interface; the final specimen height (and height of undepleted additive phase zone, if present) is measured on a traveling stage microscope. A reticule photograph of the longitudinal section is taken for future reference. The specimen is then re-mounted and polished in the transverse direction to provide a measure of final diameter. Reference photomicrographs are obtained of the transverse section, the diboride matrix and the matrix oxide interface. The conversion of diboride (and additive phase) to oxide is calculated from the difference between initial and final dimensions.

C. Experimental Results and Discussion of Results

The experimental results of oxidation screening are presented in Tables 51 to 62 and are shown graphically in Figures 56 to 65. A discussion of the results for each of the materials is given below.

1. Material I (ZrB_2)

The oxidation screening results for zirconium diboride over the temperature range 1550° to 1850°C are provided in Table 51 and are shown graphically in Figure 56. All of the selected specimen structures were subjected to one hour screening runs at 1700° and 1800°C and to 30 minute runs at 1850°C ; additional data were collected on representative structures between 1550° to 1650°C and at 1770°C .

The data presented in Figure 56 yield a logarithmic variation of the one hour recession values with temperature for the range 1550° to 1800°C ; average one hour boride recessions are 8, 13 and 22 mils at 1550° , 1700° and

1800°C, respectively. These data are consistent with previous findings (3) and are comparable with results obtained in another study (2) for the temperature range 1550° to 1850°C. Above 1800°C, the rate of oxidation was found to increase substantially so that it was necessary to reduce oxidation times to 30 minutes. By assuming a parabolic dependence for oxidation kinetics, the one hour boride recessions at 1850°C are within the range 25 to 75 mils and average 50 mils.

The ten selected screening structures of zirconium diboride, representing I02A, I03A, I05A and I07 powders exhibiting variations in grain intercept of 6 to 40 microns and relative densities of 89 to 100 per cent, yield equivalent oxide conversions to within +2 mils at 1700°C and +4 mils at 1800°C. Furthermore, there is no particular trend in the 1850°C data. Consequently, the selected structures cannot be rated by means of the oxidation screening tests. Representative photographs of the oxidized specimens are presented in Figures 66 through 76. The photographed specimens are fully dense structures prepared from the four ZrB₂ powders having grain intercepts of 20 microns (I02A D0345 and I03A D0309), 40 microns (I02A D0326 and I05A D0590) and 70 microns (I07 D0589). The outer oxide of these specimens, Figures 66 to 69, is dense and adherent after one hour exposures at 1550°, 1700° and 1770°C, but becomes somewhat puckered at 1800°C; a very porous outer oxide is observed after a 30 minute exposure at 1850°C*. Oxide matrix interface pictures at several temperatures are presented in Figures 70 to 72. The oxide formed at 1550°C is characterized by columnar grains whereas oxides formed at higher temperatures have an equiaxial grain morphology. The oxides are adherent to the matrix after one hour exposures for all temperatures up to 1800°C**. The grain size of the oxide is smaller than that of the diboride at 1700°C, but becomes larger than that of the diboride at 1800°C. Oxide porosity is observed to increase at higher temperatures.

Longitudinal and transverse section reticule photographs of specimens oxidized at 1700°C are shown in Figures 73 and 74; the uniformity of the boride recession is clearly evident. Matrix photographs of I02A and I03A structures after one hour oxidation exposures at 1700°C are presented in Figure 75. Similar photographs of I05A and I07 structures after 30 minute exposures at 1850°C are presented in Figure 76. The chemical characterizations of these structures were presented in Sections III and IV.

* The letter F appearing in the macrophotographs indicates the leading face exposed to the air stream; in addition, several of the macrophotographs (including Plates 1-3042, Figure 66 and 1-2074, Figure 67) include the zirconia mount which has fused to the specimen.

** The oxide layer on OX335, Figure 70 was inadvertently broken off during metallographic preparation.

2. Commercial Zirconium Diboride

Oxidation data have been obtained for hot pressed billets of zirconium diboride obtained from the Norton and Carborundum Companies in order to compare the oxidation behavior of commercially available material to that prepared in this program. The results of oxidation tests over the range 1550° to 1900°C are presented in Table 52 and Figure 57.

The particular lot of Carborundum ZrB_2 that has been tested possesses oxidation behavior comparable to that of Material I. On the other hand, the Norton ZrB_2 exhibits a somewhat higher and more random rate of oxidation for temperatures up to 1800°C. It was noted that a black or dark gray oxide formed on those specimens of the Norton material which yield the greatest oxidation. For example, the uppermost point at 1700°C, Figure 57, was obtained for a specimen having a very dark gray oxide. X-ray diffraction analysis of the black oxides yields monoclinic ZrO_2 ; no additional phases could be detected. Electron probe microanalysis was carried out for a representative black oxide from a Norton ZrB_2 sample oxidized at 1700°C for 60 minutes, OX272. In addition to Zr, trace quantities of Cr and Ti were detected in the matrix and metallic particles rich in Fe, Cr and Ti were observed in the oxide. A few isolated positions in the diboride matrix were found to yield very high chromium contents; these areas were not metallographically distinguishable from the diboride matrix. It is concluded that the enhanced and variable oxidation behavior of Norton ZrB_2 is related to rather high impurity levels of iron and chromium.

Typical microstructures of oxidized Norton and Carborundum ZrB_2 are presented in Figures 77 through 80. The outer oxides of the commercial materials, Figures 77 and 78, are observed to become porous at lower temperatures than for the Material I screening structures, Figures 66 to 69; above 1800°C, the commercial materials are very porous and quite distorted. The boride oxide interface pictures of the Carborundum ZrB_2 , Figure 79, reveal structures that are comparable to the screening materials. The Norton ZrB_2 , however, is characterized by considerable porosity which results in the formation of a boride oxide band at the higher temperatures; this behavior is exhibited in Figure 80. Complete characterization data for the commercially hot pressed ZrB_2 materials has previously been presented (3).

3. Material V ($ZrB_2 + 20 \text{ v/o SiC}$)

The effectiveness of silicon carbide additions in promoting the oxidation resistance of the diborides was first reported in an earlier study (3). Boride compositions containing a SiC additive undergo preferential oxidation of the additive phase at elevated temperatures leading to zones of outer oxide, boride plus voids (formed by preferential oxidation of SiC) and a core of boride plus SiC. The results of oxidation screening experiments carried out for six structures of Material V for the temperature range 1800° to 2100°C are presented in Table 53 and Figure 58. The structures represent pressings prepared from 102A, 103A and 107 powders. The results presented in Figure 58 show a larger spread in the

recession values as compared to Material I; it should be noted, however, that a higher than average boride recession for a given temperature is accompanied by a lower than average SiC recession and vice versa. No particular distinction can be made between the screening structures in regards to the level of protection afforded.

The oxide recession results are somewhat lower than those obtained in the previous boride program (3). The addition of 20 v/o SiC is found to increase the oxidation resistance of ZrB_2 about 20 times for one hour exposures at 1800°C. Average one hour diboride to oxide conversions are 2.5, 6, 20 and 60 mils at 1800°, 1900°, 2000° and 2100°C, respectively. Typical post oxidation microstructures are presented in Figures 81 to 85. The outer oxide, Figure 81, is smooth and glassy after a one hour exposure at 1800°C, becomes roughened and less glassy after one hour at 1960°C and is very rough and porous after one hour at 2100°C. The macrophotograph of the 2100°C specimen reveals several blow holes which presumably are the result of silica loss from the oxide during the exposure.

Oxide matrix interface pictures are presented in Figure 82. The oxide is adherent after exposures up to 1960°C and exhibits a grain size and porosity distribution comparable to the silicon carbide depleted matrix. The oxide is nonadherent at room temperature after oxidation at 2100°C; it is probable that oxide separation occurred during cooling as a result of differences in the thermal expansion coefficients between the oxide and the depleted diboride. In one case, after oxidation at 2100°C, the voids near the surface (caused by the preferential oxidation of SiC) were observed to be partly filled with oxide. Photomicrographs of this oxide intrusion are presented in Figure 83.

The 1800°C interface picture, Figure 82, clearly defines three zones; these are (1) the oxide, consisting of ZrO_2 and probably SiO_2 , (2) the diboride matrix, where SiC has been preferentially oxidized, leaving voids and (3) the original diboride SiC matrix. The corresponding zones in a specimen oxidized for one hour at 1960°C are presented in Figure 84 which also presents the specimen microstructure consisting of essentially discontinuous grains of SiC within a ZrB_2 matrix.

Reticule photographs of the 1960°C exposure specimen are presented in Figure 85. The longitudinal section reveals a dark outer band corresponding to the oxide, a light intermediate band corresponding to the SiC depleted matrix and a central core of the ZrB_2 + SiC matrix. The oxide has become detached during preparation of the transverse section; the two matrix zones are apparent. Several radial cracks are observed within the SiC depleted zone of the transverse section. It is suggested that the ZrB_2 -SiC composite matrix might have a lower coefficient of thermal expansion than does the ZrB_2 matrix which is depleted in SiC, resulting in circumferential tensile stresses within the depleted band; stress relief would occur by the formation of radial cracks within the SiC depleted zone.

4. Commercial Boride Z

The oxidation of samples of Boride Z, a commercial ZrB_2 MoSi_2 composite which contains SiC and Mo dissolved in the ZrB_2 lattice, was evaluated over the temperature range 1550° to 1950°C for comparison to Material V. The oxidation data are presented in Table 54 and Figure 59. The commercial material is found to have oxide recessions of 3, 6, 12, 25 and 32 mils after one hour exposures at 1600° , 1700° , 1800° , 1900° and 1950°C , respectively. These values are about half as large as for Material I (ZrB_2) and 5 to 10 times larger than for Material V (ZrB_2 - 20 v/o SiC).

Typical photographs and microstructures of the oxidized Boride Z specimens are given in Figures 86 to 89. The macrophotographs are generally comparable to those of Material V; there is less evidence for the formation of a glassy oxide phase and the outer oxide is observed to become very porous at 1950°C .

Microstructures of the oxide matrix interface are given in Figure 87; the oxides are adherent after exposures up to 1900°C . Some difficulty was encountered in the metallographic preparation of the interface region, accounting for the apparent oxide detachment from the matrix. Representative reticulate and matrix photomicrographs are shown in Figures 88 and 89, respectively.

5. Material VIII (ZrB_2 + 30 v/o Graphite + 14 v/o SiC)

Oxidation screening has been carried out on two pressings of Material VIII. The first (D0498) employed Regal 330R carbon having a particle size of 200\AA . The second (D0592) employed Poco graphite milled to 325 mesh; microstructures of this pressing reveal a graphite particle size of 5 to 20 microns. The screening results are given in Table 55 and Figure 60; the latter also contains oxidation data for Material XII to be discussed in the following section.

The pressing prepared with Regal carbon exhibits recessions considerably lower than Material I and corresponding to 8 mils per hour at 1800°C and 12 mils per hour at 1980°C . The latter value is comparable to those obtained for Material V. A specimen run at 2180°C was completely oxidized. Further oxidation screening runs have been scheduled to provide a more complete evaluation of this material.

In contrast, the pressing prepared from Poco graphite yields oxidation data comparable to Material I up to 1800°C . Some improvement over Material I is observed at higher temperatures where a one hour recession of 75 mils is obtained at 1970°C ; this is about six times greater than for the pressing containing Regal graphite. A specimen run for one hour at 2000°C was completely oxidized.

Representative post oxidation microstructures of the two pressings are given in Figures 90 to 92. The Regal graphite containing material yields a

glassy outer oxide at 1820°C, Figure 90 and a tight, uniform oxide at 1980°C. The Poco graphite containing material yields a slightly puckered outer oxide at 1900°C and a distorted porous oxide at 1970°C. The interface pictures presented in Figure 91 depict a very porous depletion zone (between the original matrix and the oxide) in the Regal graphite material and a uniform depletion (much like observed for Material V in Figure 82) in the Poco graphite material. Representative matrix photographs of the two screening materials are presented in Figure 92.

6. Material XII (ZrB_2 + X v/o Graphite)

Three pressings of Material XII have been screened. The oxidation results are given in Table 56 and Figure 60. The pressings represent the following formulations:

D0561 - ZrB_2 (I02A) + 50 v/o Poco graphite

D0572 - ZrB_2 (I03A) + 5 v/o Thornel 25 graphite yarn

D0585 - ZrB_2 (I07) + 20 v/o Poco graphite

In the ensuing discussion, these will be referred to as the 50, 20 and 5% mixtures. The 50% mixture yields very high oxidation rates at all temperatures over the range 1600°C to 2000°C. It is likely that the oxidation experiments carried out were either air supply or diffusion limited; the data points presented in Figure 60 therefore represent minimum values. The 20% and 5% mixtures yield oxidation data which is essentially the same as Material I. The presence of graphite in these specimens does not appear to have an effect on oxidation behavior.

Representative photomicrographs of the various oxidized specimens are presented in Figures 93 to 96. The macrophotograph of the 50% mixture after exposure at 1800°C, Figure 93, shows a uniform outer oxide containing numerous pits or blow holes. This oxide proved to be very fragile and could easily be crumbled away from the matrix core. The outer oxides of the 20% and 5% mixtures are similar in appearance and exhibit a somewhat flakey oxide; in addition, that corresponding to the 5% mixture contains some large blow holes. The interface photographs of the 20% mixture, presented in Figure 94 show a tight adherent oxide matrix interface. The specimen treated at 1860°C for 30 minutes exhibits a much larger oxide grain size with considerably more porosity than does the specimen treated at 1800°C for one hour. In both cases, the matrix exhibits a band adjacent to the oxide which is depleted in graphite. The oxide is detached from the 5% mixture specimen and is definitely nonadherent in the case of the 50% mixture.

The extent of oxidation at 1800°C for the 50% and 20% mixtures is shown in the longitudinal reticule photographs presented in Figure 95. The zone depleted in graphite is clearly evident in the 20% mixture photograph. Representative matrix photographs of the three pressings are presented in Figure 96. The second phase observed in the 5% mixture specimen (Plate 1-5962) is believed to be an impurity phase present in the ZrB_2 powder.

7. Material X ($\text{ZrB}_2 + 20 \text{ v/o SiB}_6$)

Oxidation screening of ZrB_2 with a SiB_6 additive phase expected to improve oxidation resistance was screened over the temperature range 1700° to 1900°C . The results are given in Table 57 and Figure 61; the latter also includes data obtained for selected high pressure hot pressed specimens of Material X and for Material XI to be described later. The oxidation data for the high pressure hot pressed materials is given in Table 58.

The oxidation behavior of the conventionally hot pressed material is essentially the same as for Material I. The high pressure hot pressed material presents a slightly lower level of oxidation and also exhibits preferential oxidation of the additive phase resulting in a depleted band between the oxide and the matrix.

Typical microstructures of the oxidized specimens are given in Figure 97. The outer oxide is dense and uniform. The oxide forms an adherent interface with the matrix. The grain size and distribution of the additive phase is shown in the matrix photograph.

8. Material XI ($\text{ZrB}_2 + 8 \text{ v/o Cr}$)

A limited amount of oxidation data was collected on high pressure hot pressed specimens of Material XI, in which the chromium was expected to act as a grain boundary binder phase. The oxidation results are given in Table 58 and Figure 61. At 1700°C , the one hour oxidation of Material XI is twice that of ZrB_2 ; the two materials have approximately equivalent oxide recessions at 1850°C . It was determined that the oxidation behavior of Material XI did not fulfill original expectations and no further screening was carried out.

9. Material II (HfB_2)

Specimens of hafnium diboride prepared from three separate powders were tested over the range 1600° to 2050°C ; the experimental results are presented in Table 59 and Figure 62. Samples from the three powders (II05, II06 and II07) all yielded equivalent oxidation results; furthermore, the various screening structures prepared from II05 powders all yielded comparable behavior, precluding a ranking in order of oxidation resistance.

The data yield a logarithmic variation of the one hour recession values with temperature over the entire range of testing. One hour boride recessions of 5, 12, 28 and 70 mils were observed at 1700° , 1800° , 1900° and 2020°C , respectively. These values are very similar to data obtained in another current study for the entire temperature range investigated (5). Two experiments carried out near 2000°C involved air flow rates of 0.2 and 0.5 ft/sec STP. The boride recessions were lower than average in both cases, indicative of air supply limited oxidation behavior. For comparable temperature ranges (1550° to 1800°C), the oxidation resistance of HfB_2 is about twice that of ZrB_2 .

Representative photomicrographs of the oxidized specimens are presented in Figures 98 through 103. The outer oxides shown in Figure 98 are tight, dense and adherent for exposures up to 1800°C; at 1900°C, the oxide becomes very porous. The interface pictures in Figure 99 show adherent oxides for specimen exposures up to 1800°C; the oxide consists of equiaxial grains at all temperatures with a grain size comparable to that of the diboride matrix. Oxide porosity increases with temperature and is especially pronounced after 1900°C. Reticule pictures of a specimen oxidized at 1810°C are shown in Figure 100; diboride conversion to oxide is very uniform. The matrix structure of the same specimen is shown in Figure 101. For comparison, various pictures of an oxidized specimen prepared from the evaluation lot of HfB₂ powder are given in Figures 102 and 103. The latter specimen exhibits smaller matrix and oxide grain sizes than does the equivalently screened specimen prepared from HfB₂ powders. Other metallographic features of the two materials are comparable.

10. Materials III (HfB₂ + 20 v/o SiC) and IV (HfB₂ + 35 v/o SiC)

The oxidation screening results for the temperature range 1800° to 2100°C are presented for formulations of HfB₂ and SiC in Tables 60 and 61, Figures 63 and 64. These data show a 15 to 20 times improvement of oxidation resistance over that of unalloyed HfB₂. On the average, the oxidation data for Material III show a slightly lower recession than was obtained in studies carried out in a concurrent program (5). This slight difference is not considered to be significant. A limited number of tests carried out for Material IV show an increased protection above 2000°C relative to Material III. The HfB₂ + SiC materials are about twice as protective as previously reported (3) and exhibit 3 to 4 times the protection that is afforded by Material V (ZrB₂ + SiC). Silicon carbide recessions of Material III and IV as well as V are equivalent. As with the previous materials, it is not possible to rate the effectiveness of protection for the selected screening structures.

Representative microstructures of the oxidized specimens are presented in Figures 104 to 111. The outer oxides, Figures 104 and 108 are dense and adherent at all temperatures examined; the oxides are definitely glassy at the lower temperatures but lose this characteristic and become somewhat roughened at 2100°C. In contrast, Material V loses the glass forming property and becomes roughened at 1960°C, Figure 81. The interface pictures show good adhesion between the oxide and the matrix, which in all cases is depleted of SiC. The oxide is detached from the matrix in the case of Material IV at 2100°C, Figure 109. This separation probably occurred as a result of differences in thermal expansion between the oxide and matrix. The matrices of Material IV show more porosity than can be accounted for by SiC depletion alone; the additional porosity is a result of grain pullout during metallographic preparation.

Reticule photographs of the longitudinal and transverse sections of specimens oxidized at 1950°C are presented in Figures 106 and 110. Radial type cracks are observed in the photographs of the Material III specimens which, as described previously, are attributed to circumferential stresses developed in the SiC depleted matrix zone during specimen cooling. Matrix photomicrographs of the same specimens are shown in Figures 107 and 111. The excessive grain pullout

within the depleted zone of Material IV, which is believed to occur during metallographic preparation, is clearly evident in the low magnification interface picture presented in Figure 111. Since Material IV contains 35 v/o SiC, it is likely that there are localized interconnections of SiC grains enhancing the likelihood of grain pullout.

11. Material VI ($\text{HfB}_2 + 4 \text{ v/o Hf-27Ta}$)

Oxidation screening was carried out over the temperature range 1750°C to 1950°C ; the results are presented in Table 62 and Figure 65. The oxidation results yield slightly higher conversion values than for unalloyed HfB_2 . For comparison, a few additional oxidation runs were carried out on high pressure hot pressed specimens. The results, which are given in Table 58 and Figure 65 are exactly comparable to the conventionally hot pressed material.

The characteristics of the outer oxide shown in Figure 112 are very similar to those observed for unalloyed HfB_2 at equivalent temperatures. Selected microstructures of the oxidized specimens are shown in Figures 113 to 115. Oxide adherency to the matrix is maintained at room temperature in specimens exposed at temperatures up to 1875°C ; the oxides of the 1875° and 1960°C test specimens are very porous. The distribution of the additive phase, believed to be a carbo-boride of the original Hf-27Ta alloy phase, is shown in the matrix photographs, Figure 115. No evidence was found for preferential oxidation of the converted additive phase.

12. Effect of SiC Content on Boride Oxidation

To determine the effect of silicon carbide content on boride oxidation, a series of oxidation experiments have been carried out at 1800° , 1950° and 2100°C on Material III specimens containing 10 v/o SiC and Material V specimens containing 5, 10, 15, 35 and 50 v/o SiC. The results are presented in Table 63.

The boride and SiC depletions of Material III specimens containing 10 v/o SiC are two times greater than for specimens containing 20 v/o SiC at 1800°C and are approximately the same at 2100°C ; these data are presented in Figure 116. In the case of Material V, Figure 117 the one hour boride recession is lowest in specimens containing 35 v/o SiC; observed recessions are 2, 3 and 33 after one hour exposures in air at 1800° , 1950° and 2100°C , respectively. The specimens containing 50 v/o SiC yield low one hour recessions (3 and 6 mils) at 1800° and 1950°C , but are completely oxidized at 2100°C . Addition of 15 v/o SiC show behavior comparable to the data presented for Material V while the 5 and v/o additions are less oxidation resistant.

It is concluded that additions of 35 v/o SiC to both ZrB_2 and HfB_2 provides the greatest protection for the temperature range 1800° to 2100°C while reasonable good protection can be maintained with SiC contents as low as 15 v/o for ZrB_2 and 10 v/o for HfB_2 .

13. Occurrence of Gross Cracks in SiC Depleted Zones in Materials III, IV and V

Several of the reticule section photographs of Materials III, IV and V (for example, Figures 85 and 106) exhibit cracks within the SiC depleted matrix zone; the cracks are generally normal to the oxide matrix and SiC depleted - undepleted matrix interfaces. It has been suggested that the cracks form as a result of circumferential tensile stresses within the depleted matrix which are generated during the specimen cooldown after an oxidation exposure due to differences in thermal expansion between the depleted and normal matrices. In this event, cracking would be expected only for the cases where a diboride plus SiC core is still present in the oxidized specimens.

The interpretation is supported in part by an examination of the longitudinal and transverse section photographs of all oxidation specimens of Materials III, IV and V for the presence of cracks. Pictures requiring a marginal judgement were disregarded. The following results were obtained.

a. Specimens Partially Depleted in Silicon Carbide

| | <u>Material</u> | | |
|--------------------|-----------------|-----------|----------|
| | <u>III</u> | <u>IV</u> | <u>V</u> |
| Total Number | 29 | 4 | 28 |
| Number Cracked | 15 | 8 | 14 |
| Frequency of Crack | | | |
| Formation - % | 52 | 50 | 50 |

b. Specimens Completely Depleted in Silicon Carbide

| | <u>Material</u> | | |
|--------------------|-----------------|-----------|----------|
| | <u>III</u> | <u>IV</u> | <u>V</u> |
| Total Number | 15 | 2 | 4 |
| Number Cracked | 3 | 0 | 0 |
| Frequency of Crack | | | |
| Formation - % | 20 | 0 | 0 |

Half of the specimens of each material were found to have cracks in the depleted matrix zone when a diboride SiC core is present, but only 3 of 21 specimen sections were found to have cracks when SiC depletion was complete.

D. Summary

A summary of the observed screening material recessions after one hour exposures in flowing air is given in Table 64 . Three distinct levels of oxidation resistance are represented. The first, including Materials I, VIII (Poco graphite) X, XI, XII and the commercial zirconium diborides have good resistance in comparison to other refractory materials and are useful for one hour exposures to 1800°C. A second level is represented by Materials II, VI, VIII (Regal graphite) and by commercial Boride Z which are twice as protective as ZrB_2 and can be employed up to temperatures of about 2000°C. Finally, ZrB_2 and HfB_2 containing SiC present in amounts of 20 to 35 v/o (Materials V, III and IV) provide an order of magnitude reduction in oxide conversion compared to HfB_2 . These materials can be used for one hour exposures at temperatures up to 2100°C or higher for shorter times.

IX. THERMAL STRESS RESISTANCE

A. Introduction

The failure of ceramic materials under stresses induced by thermal gradients is well known. One of the objectives of the present investigation of diboride materials is to develop a thermal stress resistant material without significant loss of high temperature thermal and mechanical stability and oxidation resistance.

Laboratory thermal stress resistance measurements under steady state heat flow conditions are being performed to provide an experimental relative rating of the materials and microstructures under evaluation in Phase Two of this program. Such data will be used to assist in the selection of the microstructures which will be fabricated as six inch diameter discs in the final phase of the program. The thermal stress resistance data will also be useful in the selection of the materials to be evaluated in transient heating conditions of simulated hypersonic flight leading edge specimens (19).

Additional dynamic thermal stress resistance data for materials developed in this investigation are being generated under a concurrent Air Force program at ManLabs, Inc. (5). A variety of candidate high temperature materials are being characterized by performance in hot gas/cold sample arc plasma evaluations over a wide range of stream conditions and time exposures. Extensive background information is needed to fully understand the significance of these evaluations; consequently, the results are not presented herein, but are described in detail in the reports of the other program.

B. Experimental Evaluation of Steady State Thermal Stress Resistance

1. Introduction

A primary consideration in the use of brittle materials in high temperature applications is the resistance of the material to thermal stress fracture. These stresses arise from the requirement for displacement accommodation of body elements when they undergo different thermal dilations due to temperature variations in the body. In a ductile material, accommodation of thermal stresses result from a combination of plastic and elastic strain; fracture does not usually occur since the induced plastic strain is normally only a small percentage of that needed for fracture. On the other hand, in brittle materials, the accommodation can only result from elastic strain and catastrophic failure will result when strains of the order of 0.01 to 1 per cent develop, depending on the mechanical properties of the material. However, as temperature is increased, a point is reached where formerly brittle materials will exhibit enough plastic flow to significantly increase their ability to accommodate thermal strain. This tendency will first appear under slow heating or low strain rates and as temperature is further increased, it appears at increasingly higher strain rates (20).

When significant plastic flow does occur, simple thermoelastic theory will underestimate the thermal stress resistance of the material. In order to completely define the potential of a material under conditions where such stress relaxation occurs, the stress strain behavior of the material as a function of temperature and strain rate must be known. Although such an approach is desirable, its use in a materials development program is usually prohibited by the time and cost involved in obtaining the property data required. For materials that behave elastically, the resistance of a material to thermal stress can be calculated much more readily from the thermal and mechanical properties of the material, but measurement of the thermal stress resistance greatly reduces the number of measurements that must be made and gives a more reliable result.

Two general types of tests for the resistance of materials to thermal stress are commonly used. In one, the extent of damage (e.g., spalling or strength loss) is measured after application of thermal exposures standardized as to severity and number. These tests provide a measure of the characteristic referred to as "thermal-shock-damage resistance" (21). In the other type of test, the exposure conditions necessary to initiate fracture are measured directly. This type of test yields data on a characteristic referred to as the "thermal-shock-fracture resistance" or thermal stress resistance (21). The first type of test involves the tacit assumption that fracture may occur. However, the extent of damage measured is governed by those physical properties of the material which affect the propagation of cracks once nucleated. Such a test is limited in value to specific applications and is quite unsuited for general evaluations of structural materials in which even a small crack can act as a stress concentrator and must be avoided. Thus, a thermal stress test which is to provide quantitative data for structural materials must be one that measures the conditions for crack initiation. This type of test can have broad utility and can provide data having clear significance.

By considering simple shapes in a variety of thermal stressing situations, analytical descriptions have been developed for the conditions to initiate fracture of a brittle material. These descriptions show that no single parameter or test value is a suitable index to rate a materials resistance for all conditions of thermal stressing. Material properties that affect thermal stress resistance are thermal expansion coefficient, Young's modulus, strength and, depending on the situation, Poisson's ratio, thermal conductivity, diffusivity and emissivity and where plastic strain occurs, the stress strain behavior as a function of temperature and strain rate. The shape and sometimes the size of the specimen also have significant effects.

Analyses for different conditions result in the following three parameters that can be used to rate the thermal stress resistance of material under conditions where plastic strain is insignificant:

$$R_1 = \frac{\sigma_f}{E\alpha} \quad (1)$$

$$R_2 = \frac{\sigma_{fk}}{E\alpha} \quad (2)$$

$$R_3 = \frac{\sigma_{fa}}{E\alpha} \quad (3)$$

where

- σ_f = fracture stress
- E = Young's modulus
- α = linear coefficient of thermal expansion
- k = coefficient of thermal conductivity
- $a = \frac{k}{\rho c_p}$ = thermal diffusivity
- ρ = density
- c_p = specific heat

Conceptually, the critical conditions for fracture f is defined by the simple product relation, $f = P \cdot S$, where R is the appropriate material parameter, R_1 , R_2 or R_3 and S is a corresponding parameter dependent only on specimen geometry or size. R_1 applies when fracture results from an extreme thermal shock, in which case f is the instantaneous surface temperature change, ΔT_f , of an object initially at uniform temperature and suddenly immersed in a medium at a different temperature. R_2 is the proportionality factor for the steady heat flow, W_{\max} , that will cause a sufficient temperature gradient to induce fracture. R_3 applies to the minimum constant rate of surface temperature changes, $\dot{\phi}_f$, that will cause fracture.

These relations only apply when plastic strain does not occur and they do not cover all possible conditions. For example, in the case of a shape at a uniform temperature immersed suddenly in a medium at a lower temperature, the relation $\Delta T_f = R_1 S$ holds only when Biot's modulus* is greater than about 20 (22). If Biot's modulus is very small $\Delta T_f = R_2 S$ is applicable, but for intermediate values of β , ΔT_f is not directly proportional to any of the three material parameters. Manson (23) has developed an expression, however, for ΔT_f in terms of R_1 , R_2 and $r_m h$ for all values of β .

* Biot's modulus is the surface heat transfer ratio defined by:

$$\beta = \frac{r_m h}{k}$$

where

- r_m = normal distance from center, midplane or axis to surface of specimen
- h = coefficient of heat transfer between surroundings and surface
- k = coefficient of thermal conductivity

Poisson's ratio has not been included in the material parameters R_1 , R_2 and R_3 even though it is a material property that can affect thermal stress resistance. The analyses indicate that the nature and extent of the influence of Poisson's ratio depends solely on the shape under consideration. Therefore, it has been considered as a property of the shape rather than of the material and is included in the shape parameter, S . This requires an assumption that Poisson's ratio does not vary significantly, which is a good approximation in the case of dense ceramic materials.

2. Experimental Methods

A simple experimental technique has been developed for quantitatively measuring the R_2 parameter directly; this method does not require prior knowledge of the thermal and mechanical properties of the test material (24-26). R_1 and R_3 values can be determined readily from R_2 from the following relations:

$$R_1 = R_2/k \quad (4)$$

$$R_3 = R_2/\rho c_p \quad (5)$$

Under conditions of steady radial heat flow through the wall of a hollow cylinder, the heat flow per unit length at fracture, W_{\max} , is the product of the separable parameters R_2 (defined by properties of the material) and S (defined by the specimen shape) where:

$$W_{\max} = R_2 \cdot S \quad (6)$$

$$R_2 = \frac{\sigma_f k}{E \alpha}, \text{ as defined above}$$

S = a dimensionless parameter describing the shape of the specimen

For a hollow circular cylinder with radii b and a and height h , S depends on b/a , h/a and in some cases also on Poisson's ratio.

The use of this relationship to assess quantitatively the thermal stress resistance of different ceramic materials, i.e., to measure values of R_2 requires the following:

- (a) an apparatus in which hollow cylindrical specimens can be fractured under a condition of radial steady heat flow and in which heat flow per unit length at fracture, W_{\max} , can be measured accurately;
- (b) a separate evaluation of the shape factor, S , for the specimens so that the desired material factor, R_2 can be obtained from the relationship:

$$R_2 = W_{\max}/S \quad (7)$$

Past work at Battelle (24-26) has established the validity of the above product relationship and developed an apparatus to provide the required heat flow conditions and values of shape factors for a range of specimen shapes.

In order to experimentally establish the validity of the product relation given by Eq. (6), groups of well controlled ceramic specimens of two different types (SiC and Al_2O_3) with significantly different shape factors were tested. One group of specimens had a circular inner boundary and a square outer boundary and samples in the other group were hollow cylinders. In both groups of samples, the ratio of the area between boundaries to that enclosed by the outer boundary was about 60 per cent. Some results obtained with specimens having lengths five times their inner radii are shown in Table 65. Failure was always marked by the appearance of a longitudinal crack, which was located at one of the places of minimum wall thickness in the square tubes.

The product relation is tested by computing the SiC to Al_2O_3 ratio for each geometry. If the product relation is valid, the two ratios should be equal. The ratios and their probable errors in the above case are listed in the final column of Table 65. Since the ratios are nearly equal, the results tend to support the theoretically derived product relation given by Eq. (6).

To obtain values of R_2 , the material factor of the ceramic, it is necessary that the shape factor, S , of the specimen be known. Theoretical and experimental analyses at Battelle have yielded values of S for a range of specimen shapes.

Figure 118 gives shape factor values for hollow circular cylinders having radius ratios of 1.5 and 1.7 and of any length. Similar data are available for circular cylinders having a radius ratio of 1.3. Although experimental data are not available for hollow circular cylinders having radius ratios of 2.0, calculation of the shape factor for a thin washer along with extrapolation of the experimental data for thinner walled cylinders gave the data shown for a radius ratio of 2.0. The curve for cylinders having a triangular (equilateral) outer boundary, a one inch diameter circular inner boundary and a solidity* of 70 per cent was obtained by extrapolation between the theoretical (26) and photoelastic (27) results for a thin washer and the experimental results for two inch long triangular samples of 60 per cent solidity with a 1 inch diameter inner boundary (26).

3. Experimental Apparatus and Procedure

A view of the experimental apparatus used to measure the material parameter, R_2 , is shown in Figure 119. A cross sectional view of the arrangement of the sample and guard rings around the graphite heater element are provided in Figure 120. This apparatus has been designed to provide a controlled, measurable radial heat flow through the wall of a hollow, cylindrical specimen.

*Solidity is the solid cross sectional area divided by the area defined by the outer boundary.

The specimen is aligned concentrically on the heater rod between one or more upper and lower guard tubes. Upon applying power to the heating rod, heat flows radially through the specimen, producing a radial temperature drop and resultant thermal stresses. As the power delivered to the heater rod is increased, the critical tensile stress in the wall becomes greater. In testing, the stress is increased by increasing the power until fracture occurs. The temperature is measured by sighting an optical pyrometer on the outer surface of the specimen and by placing thermocouples near the inner and outer surfaces of the sample. The thermocouple outputs are fed into a two point recorder to obtain a record of the thermal history of the sample and to indicate when steady state conditions are established.

To obtain fracture under steady state conditions, the power to the heater rod is increased in small increments and it is retained after each increment until the outer wall temperature becomes constant. The heat flow (power) per unit length at which fracture occurs (W_{max}) is recorded. This value divided by the appropriate shape factor gives the R_2 parameter which quantitatively describes the resistance of the material to fracture due to thermal stress. No difficulty had been experienced in determining fracture; an axial crack opens which can be readily discerned because of the bright heater rod background. For circular cylinders, the maximum tensile stress occurs at the outer diameter. For a triangular sample, the maximum tensile stress occurs at the outer boundary at the center of the sides of the triangle.

For power measurements, small holes are drilled in the heater rod at points approximately opposite the ends of the specimen and the distance between these holes is measured accurately. A 4 mil tungsten wire is forced into each hole and passed through a small hole drilled in a guard tube. A connection is then made through the base to a Model 300G Ballantine electronic voltmeter which has an accuracy of 1 per cent and is relatively unaffected by high resistance in the measuring circuit. The heater current is passed through the primary of a type RT Westinghouse current transformer with a calibrated primary/secondary current ratio of approximately 800/5. A Model 1954 Weston ammeter with an accuracy of 1/2 per cent is used to measure the secondary current. The power (heat) dissipated per unit length at the gage section of the heater element is the product of the transformer ratio times the current reading times the voltage reading divided by the distance between the voltage leads.

In past work, a major concern was whether the necessary conditions of radial steady heat flow could be met adequately in the apparatus. As a result, the heater element was made long compared with the specimen length so that the temperature of the center section of the heater rod shows little variation in the axial direction. This feature also minimizes axial conduction in the heater rod and axial heat flow by radiation. Axial conduction in through the guard rings was also found to be insignificant so long as the heat transfer characteristics of the guard ring are similar to those of the test specimen. If the tests are run in an inert atmosphere rather than in vacuum, axial heat flow by convection can also occur. However, heat loss is considered insignificant in the closed space between the heater rod and the sample.

4. Experimental Results and Discussion

The experimental work thus far has consisted of preliminary evaluations to determine the behavior of refractory diborides to thermal stresses resulting from steady state temperature gradients. The objective of these determinations is to define the sample geometry and test conditions necessary to cause brittle failure without appreciable plastic strain. Under these conditions, quantitative thermal stress resistance data can be obtained with measuring the materials properties which fix thermal stress resistance. For comparison purposes, KT-SiC has also been evaluated. The results of the preliminary evaluations are summarized in Table 66.

a. KT-SiC

The KT-SiC samples evaluated for comparison purposes were 1.7 inches outside diameter and 1.0 inch long. Calculation of the factor R_2 from the best available property data (28) yielded a value of 4.87 cal/cm sec. Property data at 1315°C were used for this calculation, since strength and modulus data are not available at 1350°C. The range shown in Table 66 for the experimental values of R_2 is due to the size of the incremental increases in heat flux. In each case, the lower value represents the highest R_2 value at which the sample did not fail and the higher value represents the R_2 value to which the sample was exposed when failure occurred. Thus, the actual experimental value of R_2 lies somewhere between these values. As shown by the data in Table 66, the calculated and experimental values agree quite well for this material. Figure 121 shows one of the KT-SiC samples after thermal stress failure. The failure was catastrophic, as evidenced by the separation of the broken pieces by the kinetic energy imparted to them when failure occurred. It should also be noted in Figure 121 that some of the free silicon in KT-SiC has beaded on the inside diameter where the temperature was above the melting point of silicon, 1410°C.

b. 1.7 Inch Outside Diameter Diboride Samples

The samples in the first group of diboride samples evaluated were 1.7 inches outside diameter, 1.0 inch inside diameter and approximately 0.75 inches long. Evaluation of Material I, I02 D0364 revealed that the temperature at the inner wall of the sample at the heat flux required to cause failure was between 1700° and 1800°C. Since macroscopic plastic flow has been observed in mechanical tests conducted in this temperature range, it was apparent that lower sample temperatures would be required in order to produce brittle failure under the slow heating (strain) rates used in evaluating the materials under steady state conditions. Several techniques for lowering the sample temperature by increasing the rate of heat transfer away from the outer surface were evaluated. These included (1) coating the outer surface of the sample with colloidal carbon to improve its emissivity, (2) conducting the test in a helium atmosphere to get conductive and convective transfer away from the surface and (3) conducting the tests in a helium atmosphere with a water cooled, carbon coated cylinder near the outer surface to get increased conduction through the helium. The specimen temperature was lowered 100°, 75° and 150°C, respectively, for Techniques 1, 2 and 3 listed above. However, a greater temperature reduction was considered necessary to prevent stress relief due to plastic flow.

c. 2.0 Inch Outside Diameter Diboride Sample

The most convenient way to lower the specimen temperature is to use a geometry that gives a lower shape factor. Since lowering the shape factor lowers the heat flux required to create a critical stress, the specimen temperature is lowered. Therefore, a group of samples 2 inches outside diameter, 1 inch inside diameter and 1 inch high was evaluated. Since the shape factor for this size sample is 20, the heat flux required to create a critical stress is 33 per cent lower than for the first group of samples which had a shape factor of 26. Material I, I03A D0539 was evaluated in a helium atmosphere up to an R_2 value of 15.0 cal/cm sec using the standard test procedure as described above. This R_2 value is about twice the value calculated from thermoelastic theory, but no failure occurred. The sample must have experienced considerable plastic strain. However, the sample did fail while cooling after completion of the test. Since the sample experiences a much lower temperature gradient during cooling than during evaluation, failure probably did not occur as a result of thermal stress caused by a temperature gradient. Rather, failure must have occurred as a result of a stress reversal on cooling caused by plastic strain which occurred during the evaluation followed by elastic behavior on cooling. Such behavior would create a residual tensile stress at the inner wall and apparently this stress exceeded the fracture stress of the material. Since the outer wall temperature at the heat flux required to obtain the calculated R_2 value was approximately 1330°C and that of the inner wall approximately 1500°C; significant plastic strain must have occurred at temperatures of 1500°C and below. Figure 122 shows the sample after failure. As in the case of KT-SiC the pieces of the fractured specimen were displaced as a result of catastrophic failure.

In order to determine whether the creep rate was in a range where, because of strain rate sensitivity, failure could be induced by more rapid heating, sample I03A D0548K (2.0 inch o.d.) was heated at a faster rate. In this evaluation, the specimen was exposed to the heat flux necessary to obtain a material factor of 7.18 cal/cm sec (i.e., 143 cal/cm sec) instantaneously. Under this heating rate, failure occurred in just over 3-1/2 minutes at an outer wall temperature of approximately 1315°C which is approximately the equilibrium temperature for the heat flux employed. Figure 123 shows the sample after thermal stress failure. Failure was catastrophic as in the case of the KT-SiC sample. Although this sample was heated under transient conditions, the temperature gradient established was nearly the same as the one established in steady state heat flow, because of the high thermal conductivity of the sample. The fact that failure occurred on rapid heating is a further indication that significant stress relief due to plastic strain can occur at temperatures as low as 1400°-1500°C under the heating (strain) rates normally used in the steady state test. Since sample I03A D0548K (2 inch outside diameter) failed when rapidly heated with the approximate heat flux calculated to cause failure under steady state conditions, the creep rate of this sample was considered insignificant for the resulting heating (strain) rate. A slight modification of this technique was employed in an effort to obtain some quantitative data. The modified technique involved slowly increasing the heat flux until a material factor of one half that calculated to cause failure was attained and then allowing equilibrium to be established. The heat flux was then increased in one increment to that required to give a material factor around three quarters of that calculated to cause failure. After establishing equilibrium, the heat flux was again reduced to the one half level and allowed to

equilibrate. In the absence of plastic strain, repeating this procedure at successively higher heat fluxes (material factors) would serve to bracket the material factor.

In order to evaluate this technique, a 2.0 inch o.d. specimen of Material V, V07 D0571K was tested in a helium atmosphere. The time allowed for equilibrium to be established was 2 minutes for the heating cycle and 2-1/2 to 3 minutes for the cooling cycle. The material factors evaluated and the corresponding temperatures are shown in Table 66. The heat flux was reduced to give a material factor of 3.5 cal/cm sec between each of the levels shown. Failure did not occur during the test nor did failure occur on cooling as a result of residual stress caused by plastic flow during the test. The fact that failure did not occur on heating indicates that significant plastic strain took place during the test and these conditions cannot be used for quantitative evaluation.

d. Triangular Samples

In order to further lower the testing temperature, equilateral triangular specimens with an outer boundary 2.5 inches on a side, 1.0 inch diameter circular inner boundary and 1.0 inch high were evaluated. This geometry reduces the shape factor to 15 which lowers the required heat flux 25 per cent of that for the above 2.0 inch outer diameter samples.

Material V07 D0582K was evaluated in vacuum under steady state conditions. Incremental heat flux increases were made every two minutes which represented a change of approximately 0.50 cal/cm sec in the material factor (R_2) up to 9.5 cal/cm sec; this value is approximately 125 per cent of the material factor where failure would be expected based on available property data and elastic theory. The heat flux was then increased in one increment to change the material factor from 9.5 to 11.1 cal/cm sec and, after 5 minutes, from 11.1 to 12.8 cal/cm sec. No failure occurred during this test, probably because of plastic strain. The sample temperatures at the outer boundary and at the center of the triangular sides were 1240°, 1330°, 1365° and 1475°C for material factors of 7.75, 9.5, 11.1 and 12.8 cal/cm sec, respectively. Since failure should occur at a material factor of approximately 7.75 cal/cm sec, significant stress relief due to creep must have occurred when the outer wall temperature was as low as 1240°C during the time the material was under stress in the experimental run. However, this temperature represents a considerable reduction from the outer wall temperatures of 1650° and 1325°C required to attain the same material factor for the 1.7 inch O.D. and 2.0 O.D. samples, respectively.

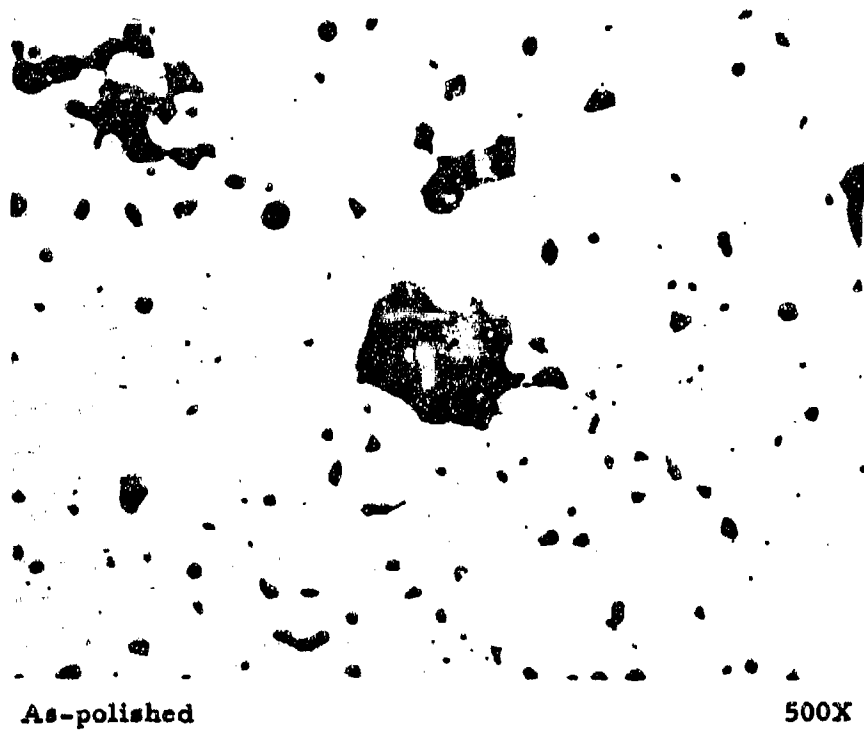
In order to further lower the testing temperature, Material V07 D0586K was evaluated under steady state conditions in a helium atmosphere. In this evaluation, the same procedure was used as for sample V07 D0582K except that the incremental increases in the heat flux were such that the change in the material factor was only 0.25 cal/cm sec. In this test, the sample temperatures were 1175°, 1235°, 1320°, 1385°C at material factors of 7.75, 9.5, 11.1 and 12.8, respectively. No failure occurred, probably as a result of plastic strain. At a material factor of 7.75 which is near the value where failure would be predicted based on elastic theory, the inner wall temperature was approximately 1275°C.

Material II05 D595K was also evaluated under steady state conditions in a helium atmosphere. In this evaluation, the same procedure was used as for sample V07 D0586K except that the incremental heat flux increases were made every minute. One other difference in this experiment was the use of samples V07 D0586K and V07 D0582K for guard rings instead of graphite. Since graphite has somewhat different heat transfer characteristics, this difference is probably significant. This sample failed when the material factor was increased from 11.1 to 12.8 cal/cm sec after a 2 minute hold at 11.1 cal/cm sec. Figure 124 shows this sample after catastrophic thermal stress failure and before removal from the test apparatus. Note the relative displacement of the pieces of the sample. The fractured specimen is shown in Figure 125. Since this failure occurred at about 1.5 times the heat flux where failure would be expected based on available property data and elastic theory, significant plastic strain probably took place before failure. However, the creep rate was too slow to prevent the build up of a critical fracture stress for the heating (strain) rate employed.

5. Conclusions and Future Plans

Analysis of KT-SiC confirmed that steady state thermal stress failure occurs at a material factor near that calculated from property data providing the material behaves elastically while under test. However, preliminary evaluations of several diboride materials having several different shape factors revealed that significant plastic strain occurred at temperatures as low as 1275°C for heating (strain) rates normally used in the steady state technique, which prevented fracture due to thermal stress. This ability to relieve thermal stress by plastic rather than elastic strain is quite significant for these materials, as evidenced by the fact that some samples have withstood twice the heat flux calculated to cause failure in steady state (slow heating rate) evaluations.

In order to obtain thermal stress failure, lower sample temperatures or faster heating rates will be required to cause fracture of simple shapes of the materials to be evaluated. Of these alternatives, lower temperature tests where plastic strain is negligible for the times involved in making a run under essentially steady state conditions is more desirable for making quantitative evaluations of thermal stress resistance. The technique to be used for making lower temperature evaluations is as follows. A thin walled, tight fitting, rubber tube will be placed around the sample and guard rings. The rubber tube will be connected to a concentric brass cylinder and water will be passed between the brass and rubber cylinders to remove the heat conducted through the sample and guard rings. By this technique, outer wall temperatures below 200°C could be attained for the steady state heat flux required to cause failure due to thermal stress. Thus, the probability of brittle failure would be maximized. Aside from a minor change in the attachment of the voltage leads, the only experimental difficulty will be in detecting fracture, which should be detectable with an audio pick up placed on the guard ring below the water cooling jacket.



Avco Plate No.
4189C

Figure 1. Second Phase Size and Distribution in Hot Pressed Material
I. Billet I03A D0308.

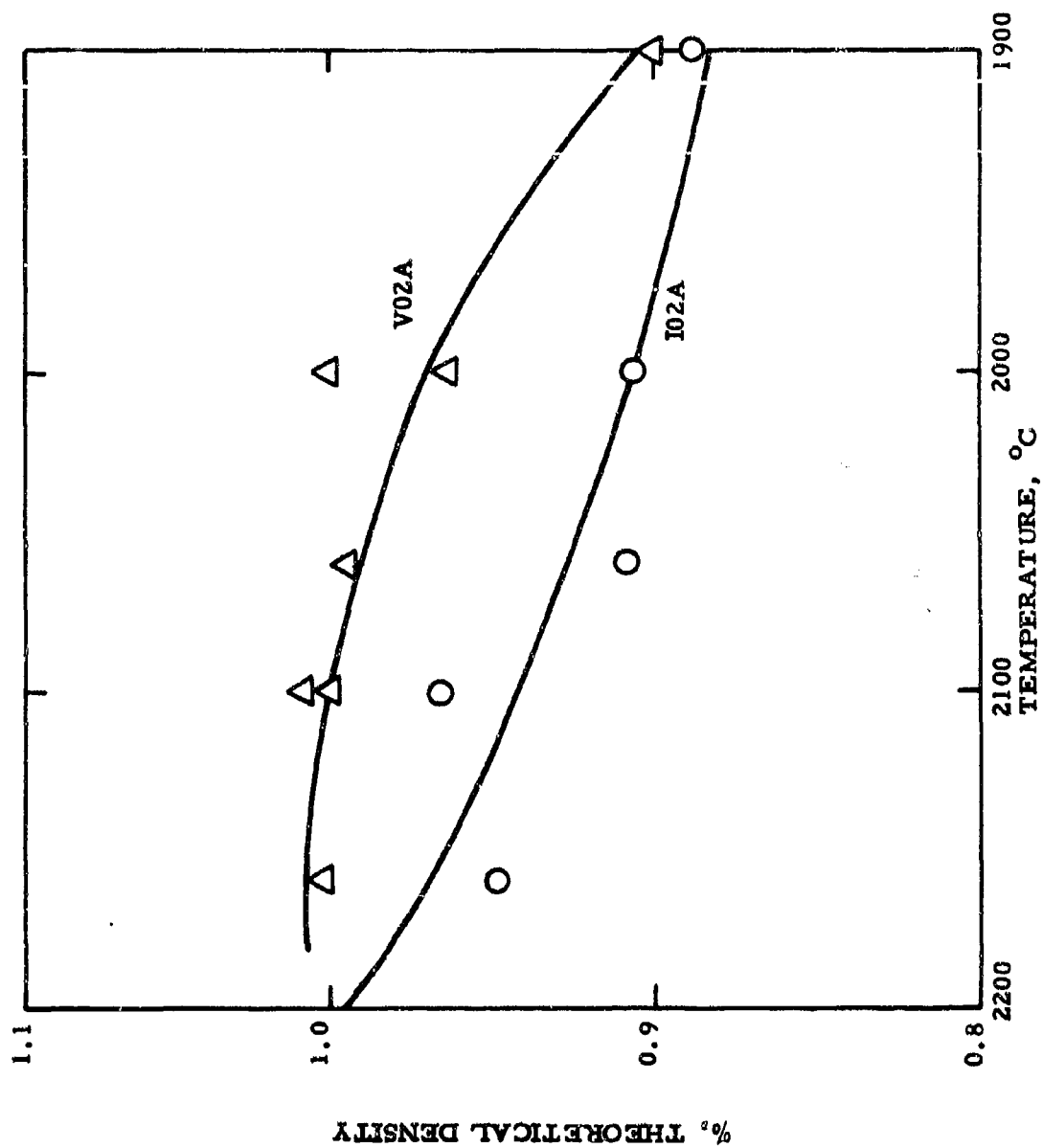


Figure 2. Comparison of Hot Pressing Characteristics of Materials I02A and V02A.

% THEORETICAL DENSITY

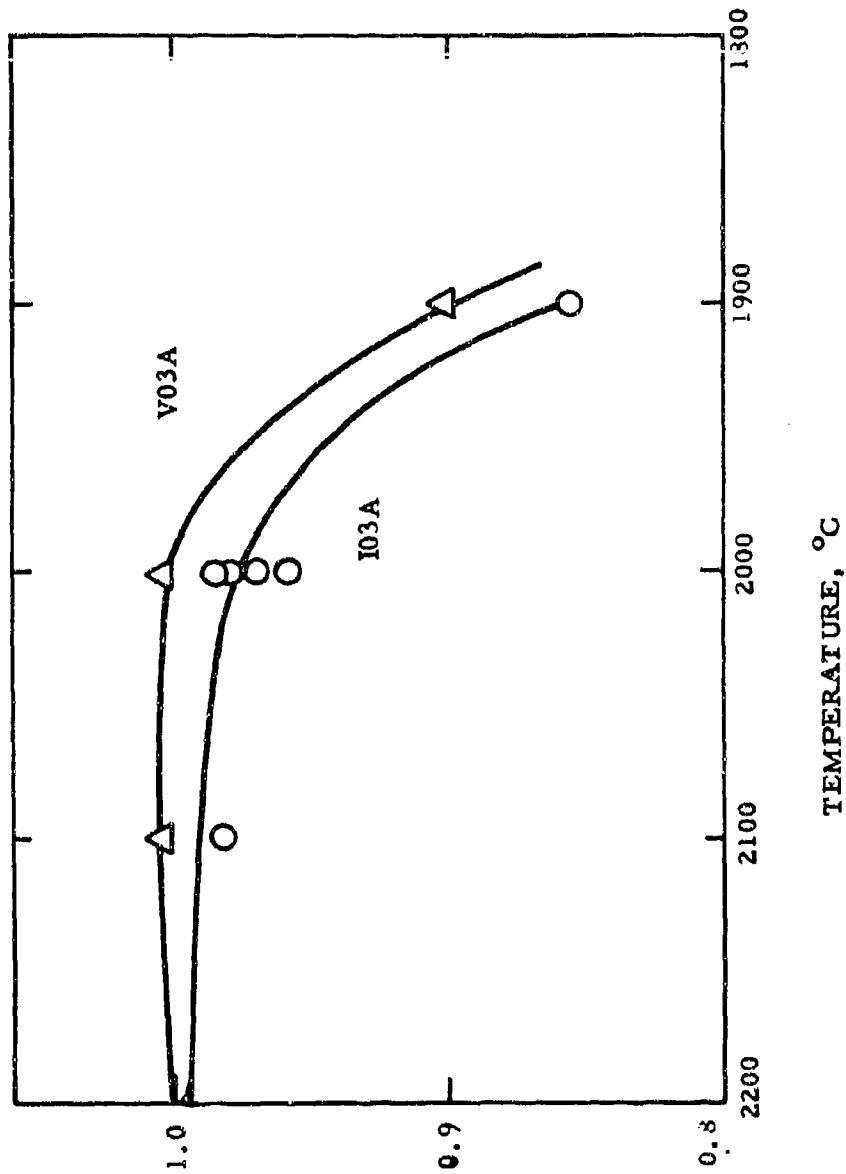
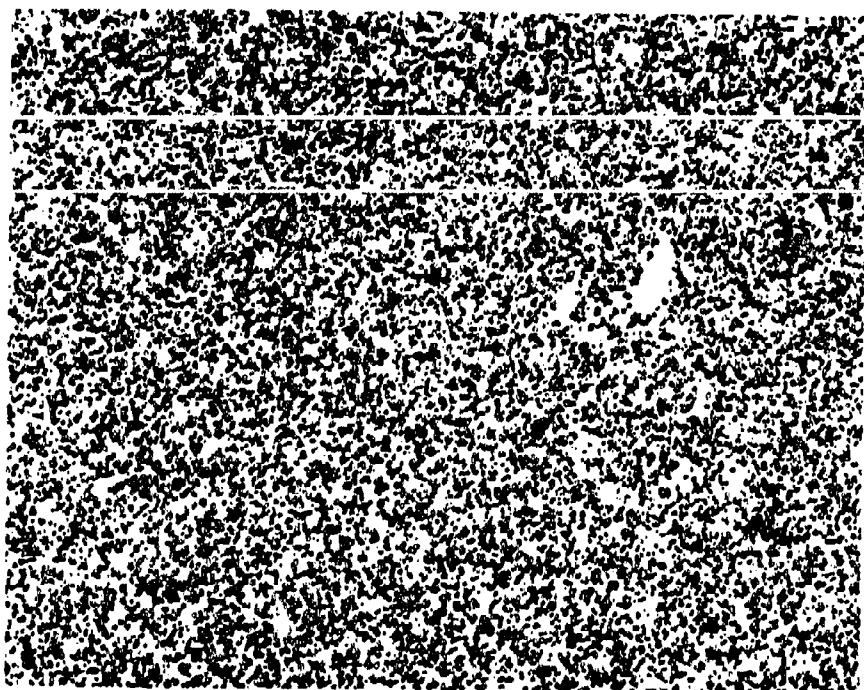


Figure 3. Comparison of Hot Pressing Characteristics of Materials I03A And V03A.

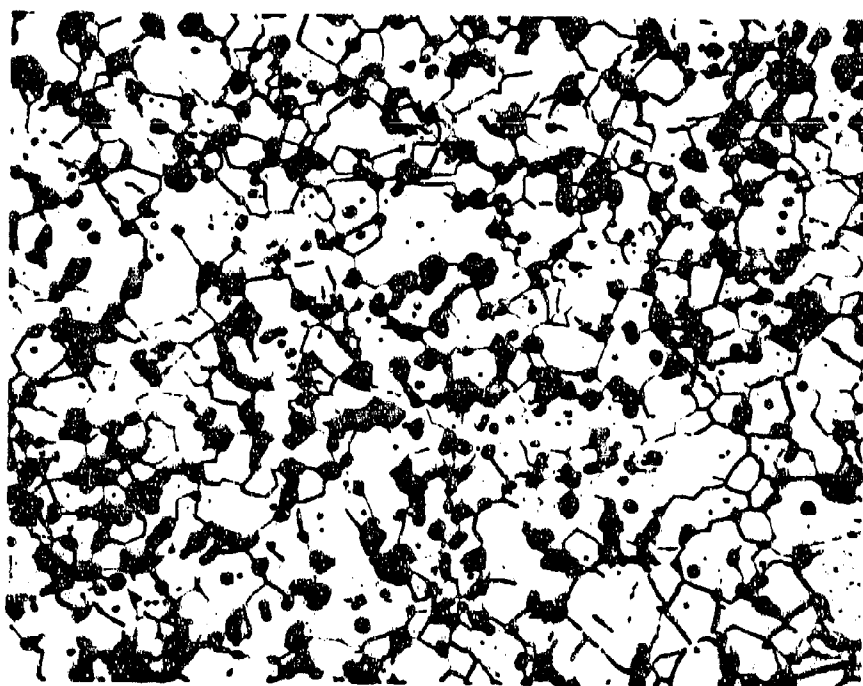


Avco Plate No.
4235C

As-polished

100X

Figure 4. Distribution of SiC Phase in Diboride Matrix of Material V.
Billet V02A D0370.



Avco Plate No.
4235F

Etched

500X

Figure 5. Location of SiC Relative to ZrB_2 Grain Boundaries in Material V.
Billet V02A D0370.

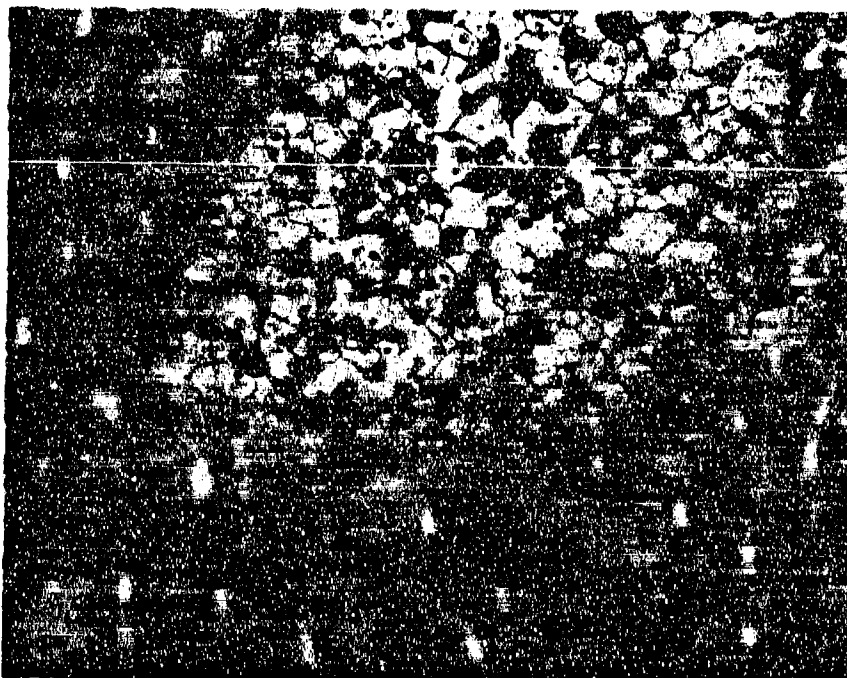


Avco Plate No.
4235E

As-polished

1000X

Figure 6. Morphology of Remaining Impurity Phases in Material V02A
Demonstrating the Contact Angles Relative to the Other Phases.
Billet V02A D0370



Avco Plate No.
4371C

Etched

500X

Figure 7. Morphology of Remaining Impurity Phases in Material V03A.
Billet V03A D0473.

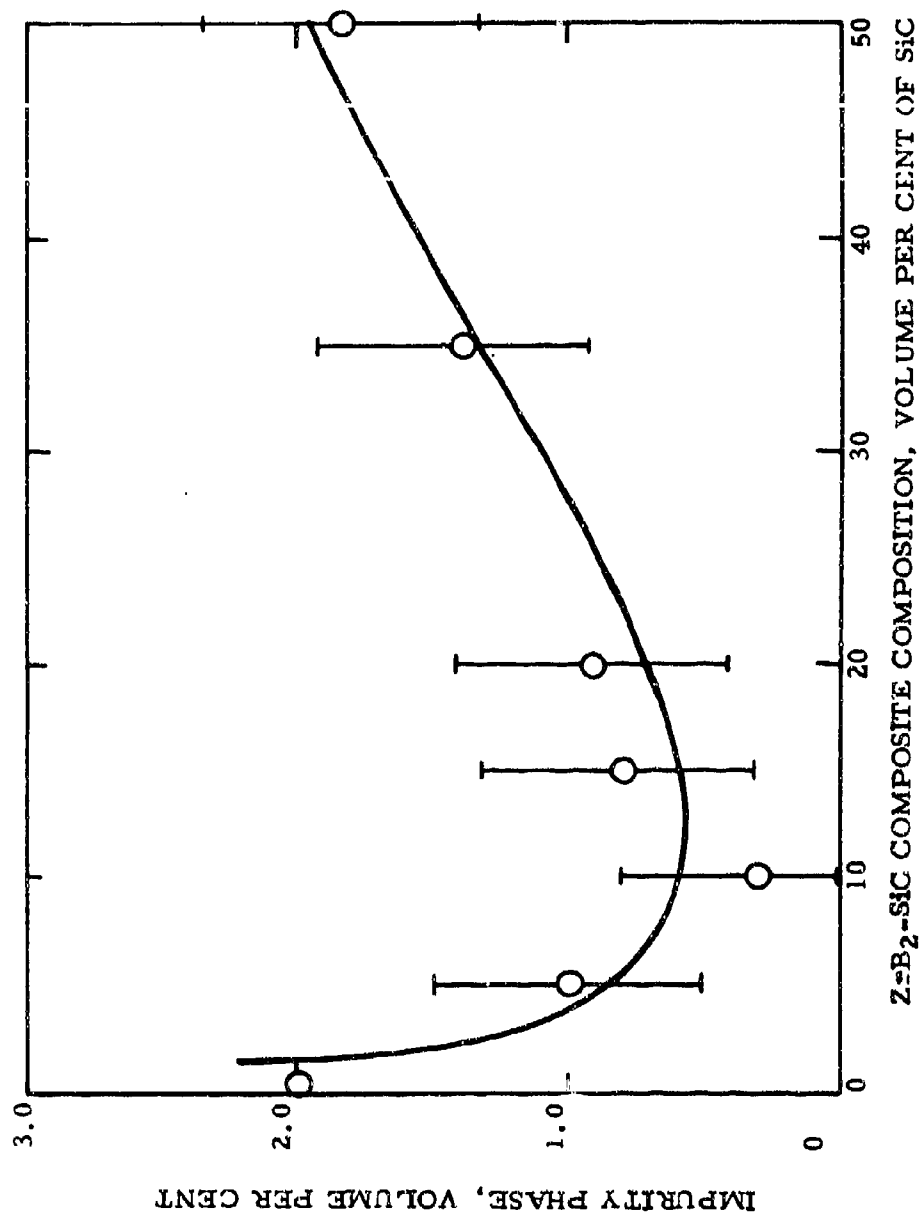
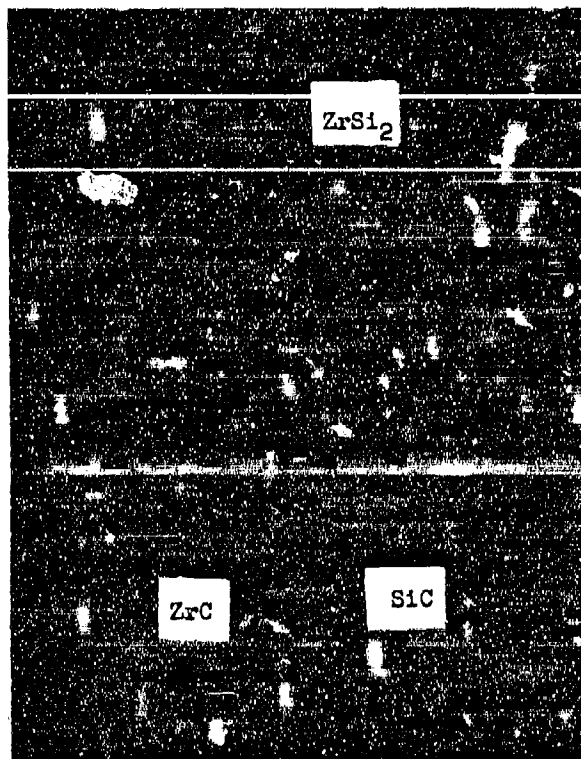


Figure 8. Variation of Impurity Phase with SiC Additions in Material V.

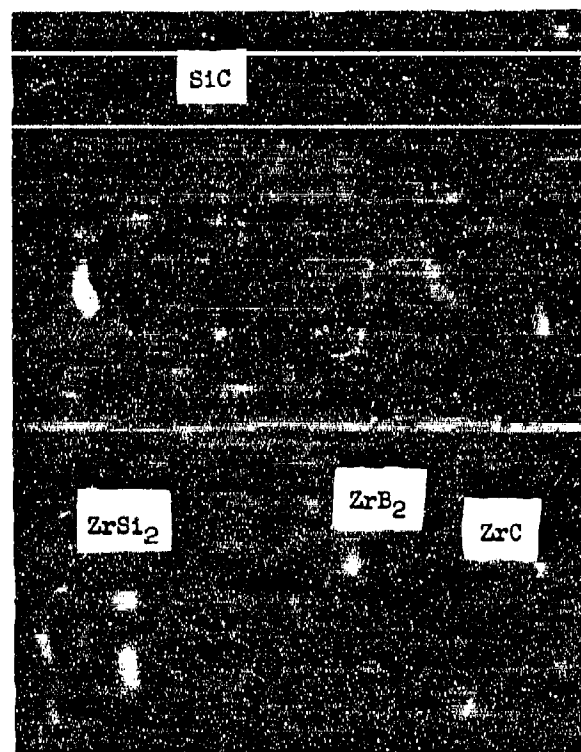


Avco Plate No.
4555B

As-polished

500X

Figure 9. Distribution of Phases in Special Material Hot Pressed with Starting Powders of ZrO_2 and SiC . Billet D0624.

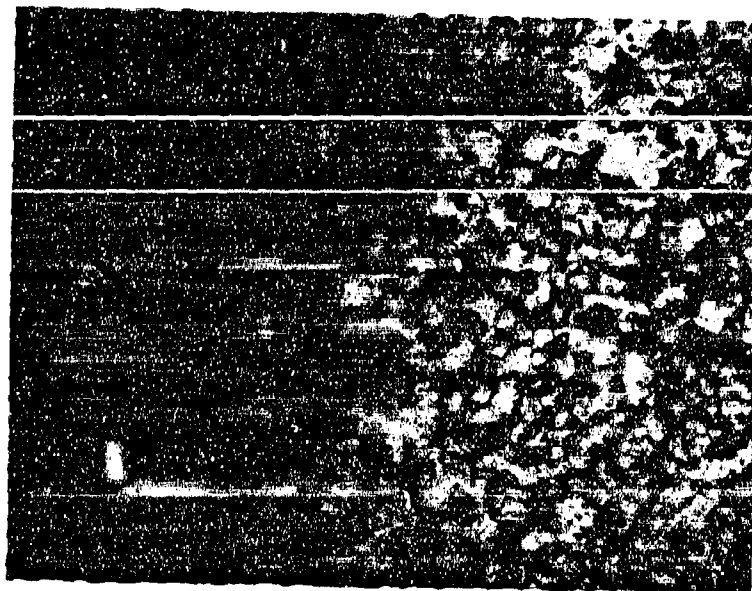


Avco Plate No.
4555D

Unetched

500X

Figure 10. Distribution of Phases in Special Material Hot Pressed With Starting Powders of ZrB₂, ZrO₂ and SiC. Billet D0626.

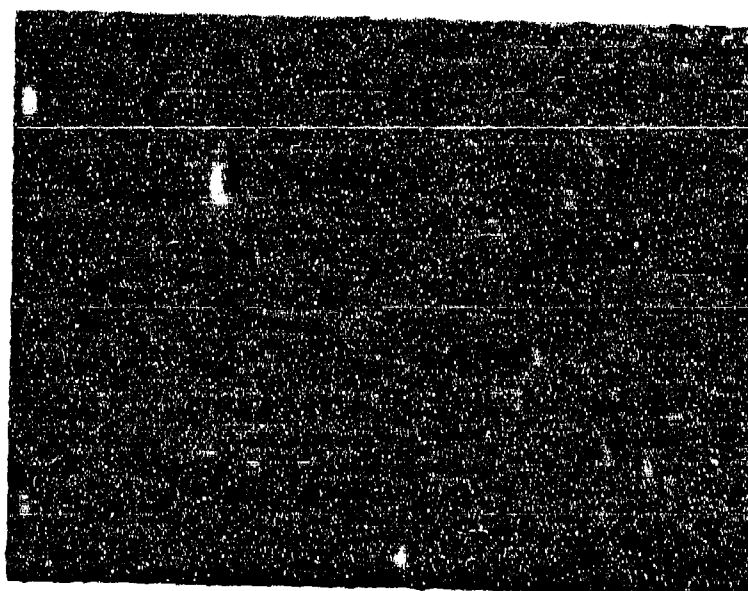


Avco Plate No.
4539Q

Etched

500X

Figure 11. Microstructure of Material VIII Containing Poco Graphite.
Billet VIII02A D0592.

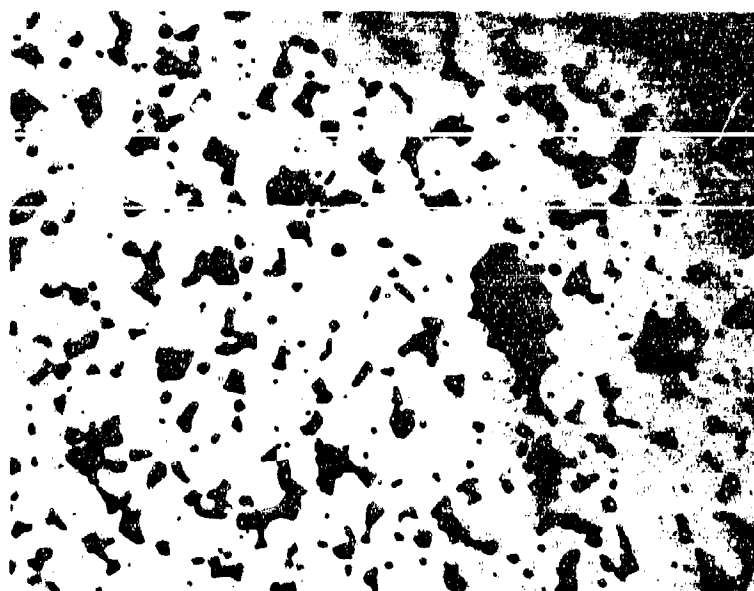


Avco Plate No.
4584Y

As-polished

500X

Figure 12. Microstructure of Material VIII Containing Regal Carbon.
Billet VIII(17)(15)07 D0620.

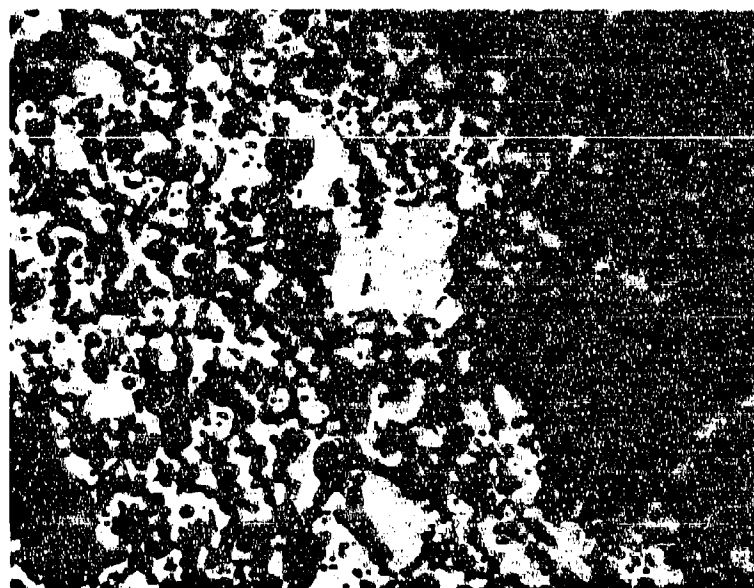


Avco Plate No.
4539T

As-polished

500X

Figure 13. Microstructure of Material X Hot Pressed at 1900°C.
Billet X07 D0596.

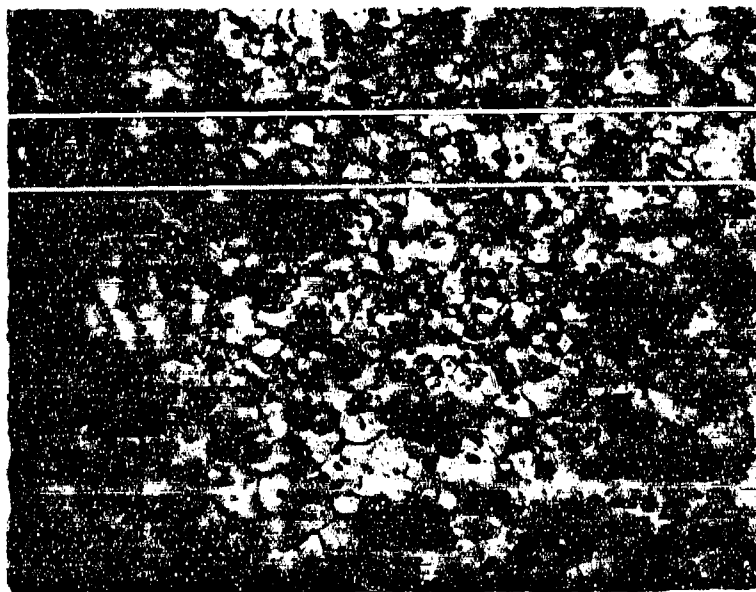


Avco Plate No.
4539V

As-polished

500X

Figure 14. Microstructure of Material X Hot Pressed at 1800°C.
Billet X07 D0597.

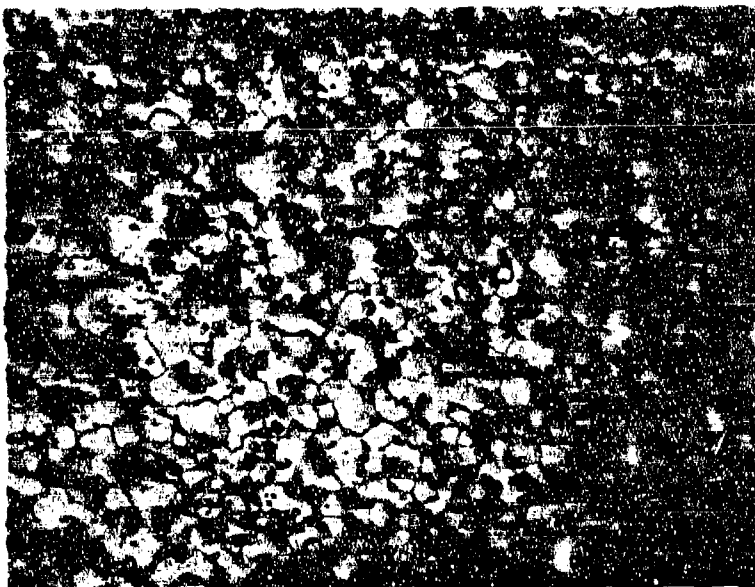


Avco Plate No.
4584L

Etched

500X

Figure 15. Microstructure of Material XII Containing Regal Carbon.
Billet XII(20)07 D0608.



Avco Plate No.
4584D

Etched

500X

Figure 16. Microstructure of Material XII Containing Poco Graphite.
Billet XII(15)07 D0603.

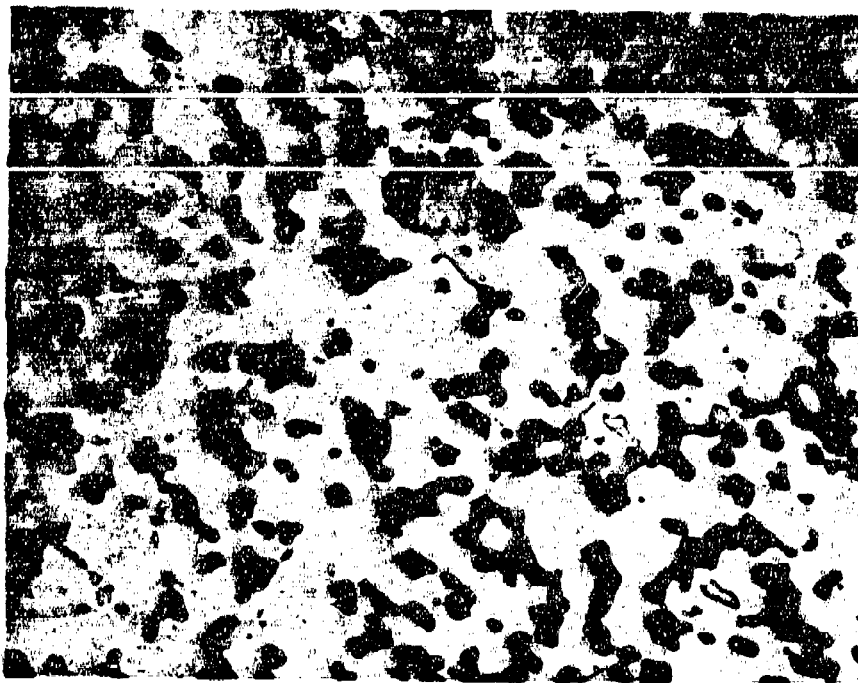


Avco Plate No.
4203I

As-polished

500X

Figure 17. Microstructure of Material II. Billet H05 D0316.

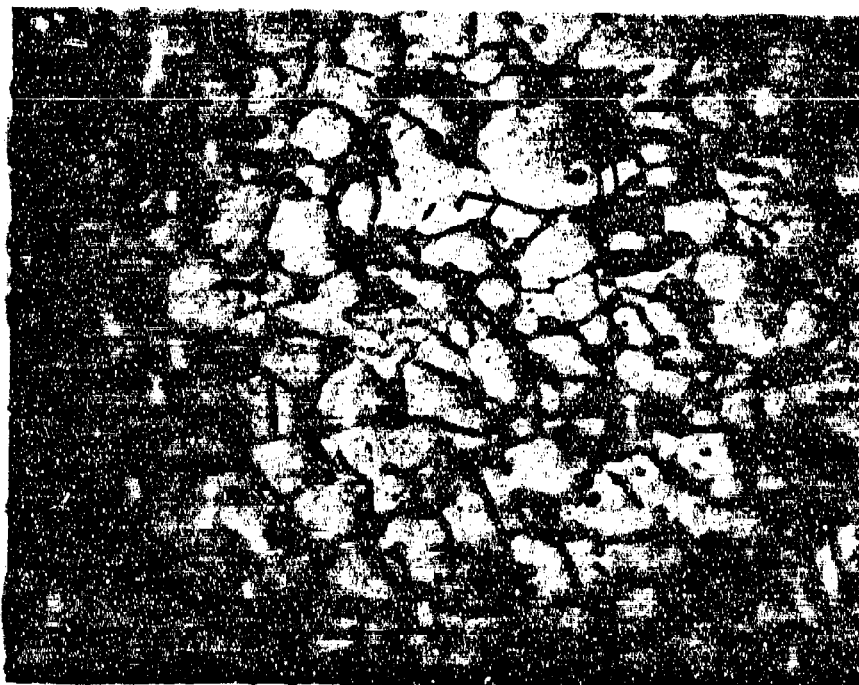


As-polished

(a)

500X

Avco Plate No.
4296B



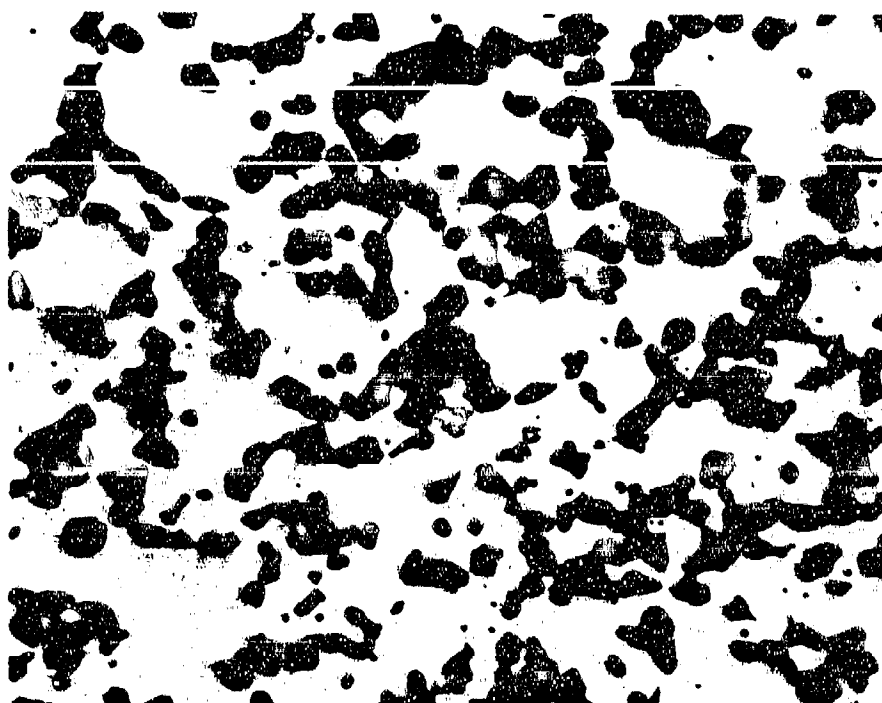
Etched

(b)

500X

Avco Plate No.
4235B

Figure 18. Microstructure of Material III. Billet III05 D0377.

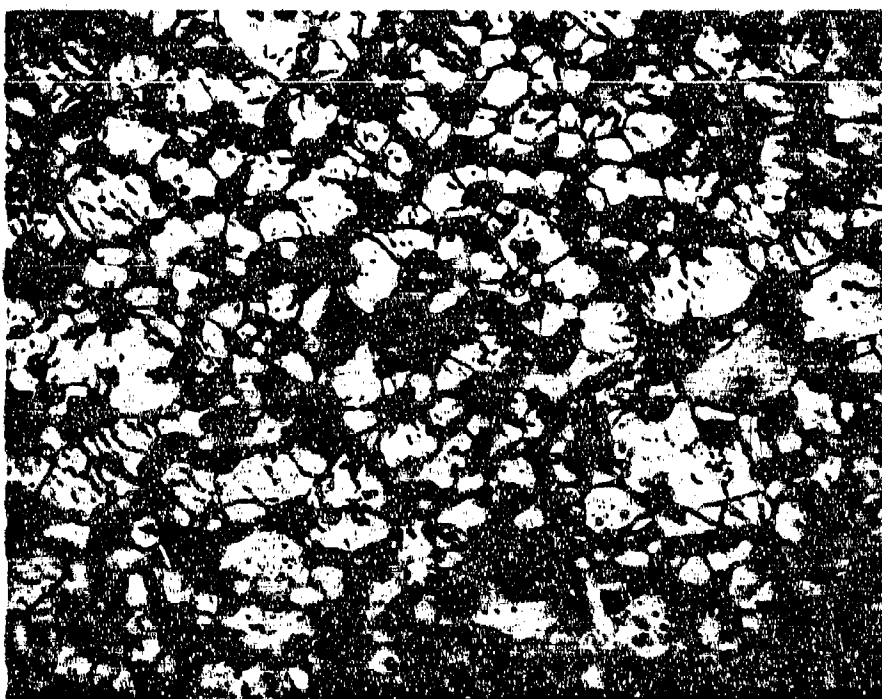


Avco Plate No.
4284J

As-polished

(a)

500X



Avco Plate No.
4284K

Etched

(b)

500X

Figure 19. Microstructure of Material IV. Billet IV05 D0405.

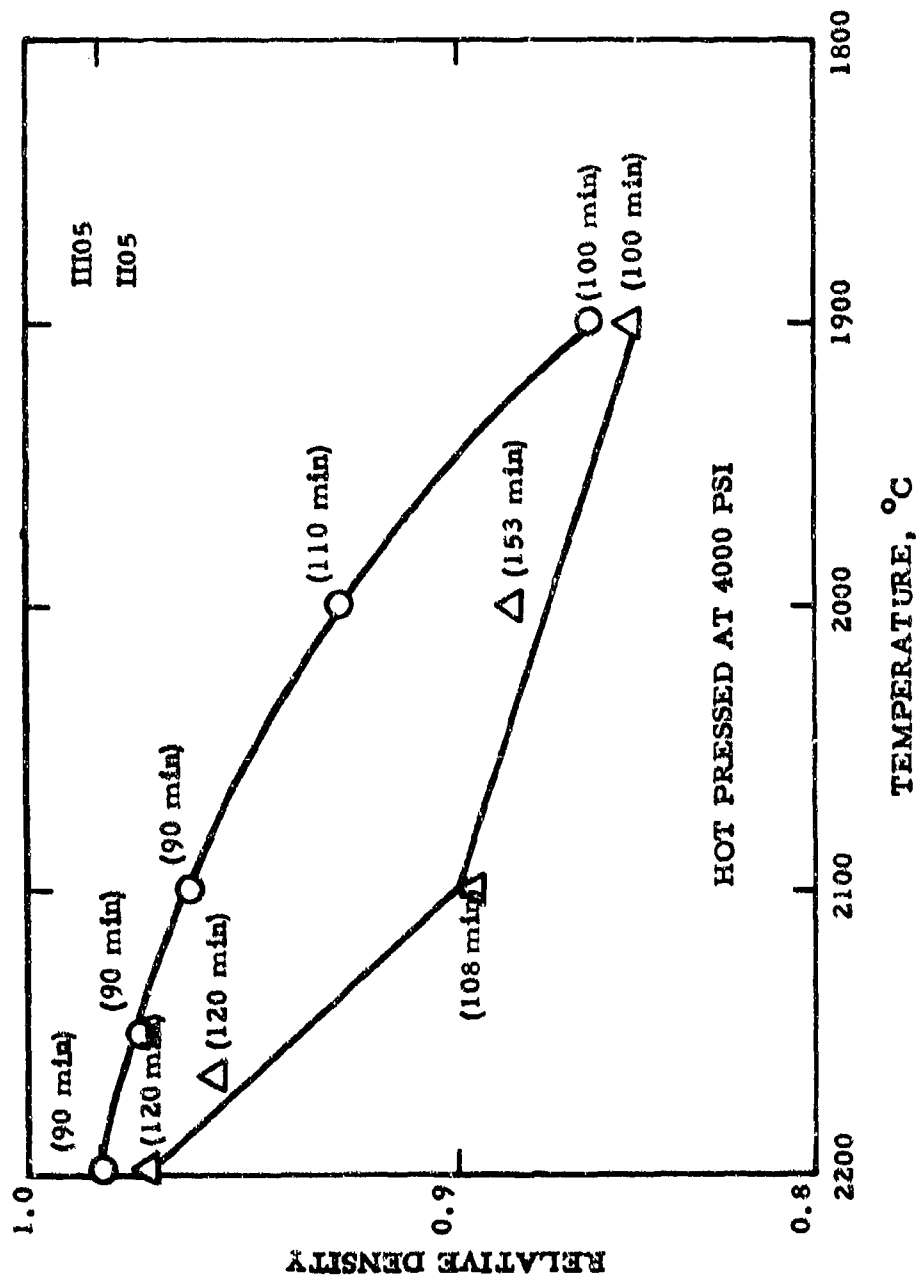
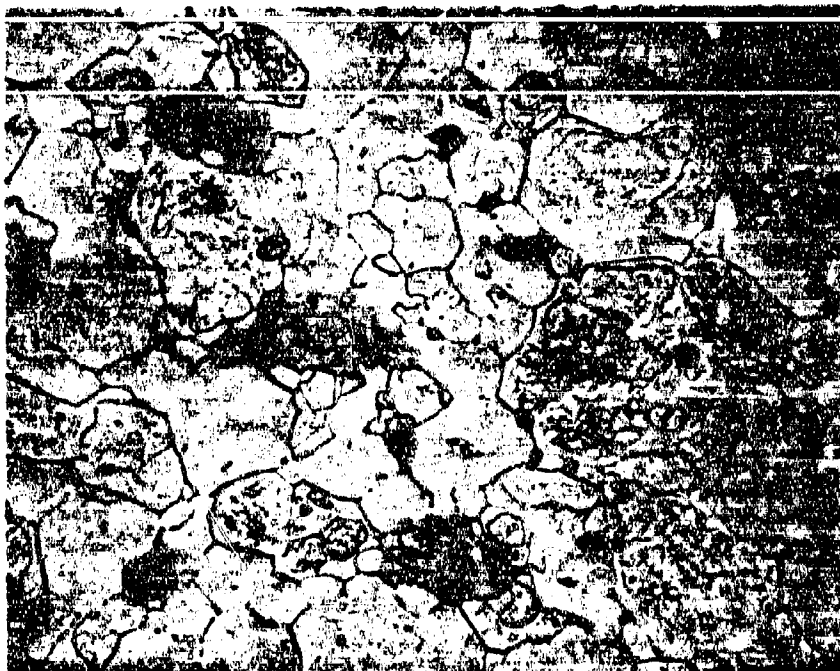


Figure 20. Comparison of Hot Pressing Characteristics of Materials II and III.

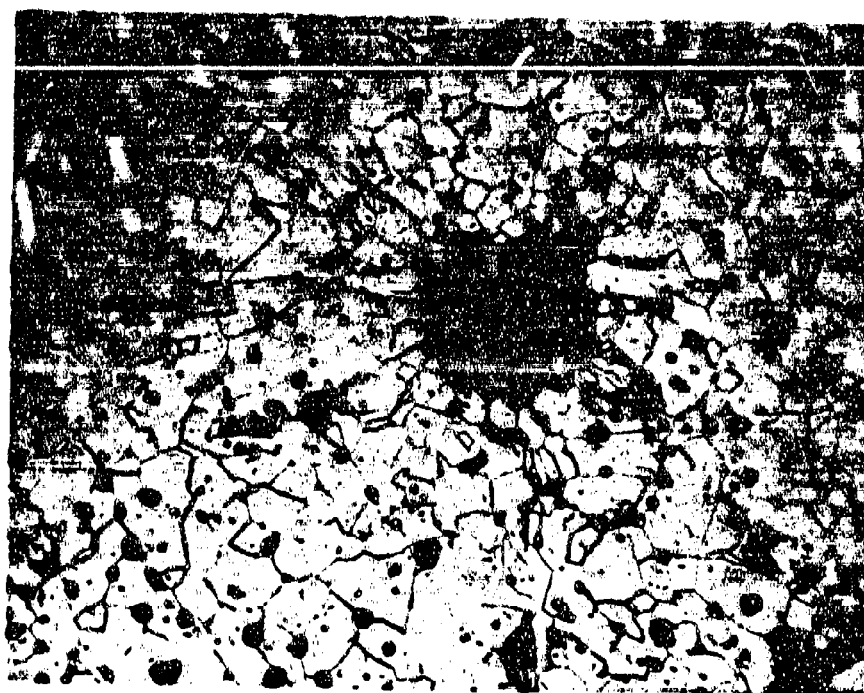


Avco Plate No.
4324K

As-polished

500X

Figure 21. Microstructure of Material VI. Billet VI05 D0462.

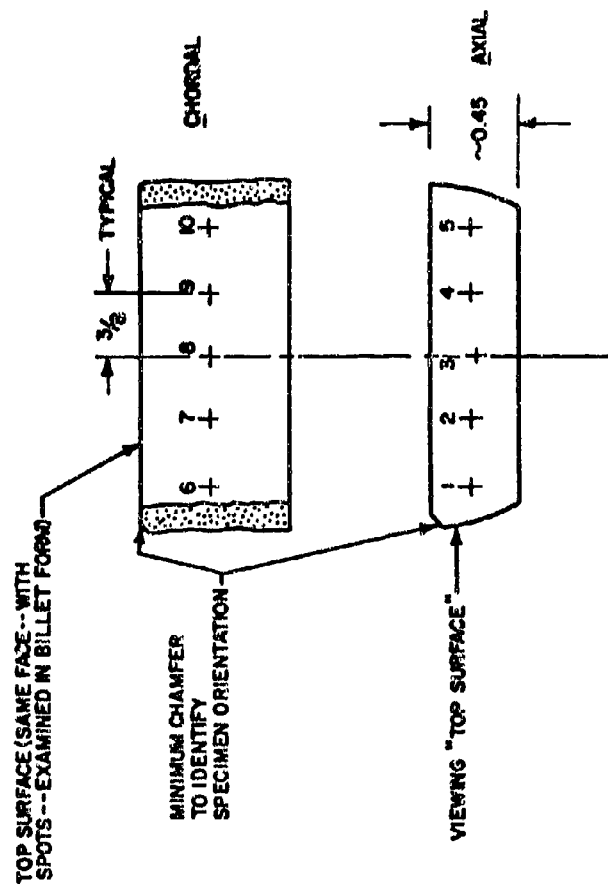


Avco Plate No.
4311C

Etched

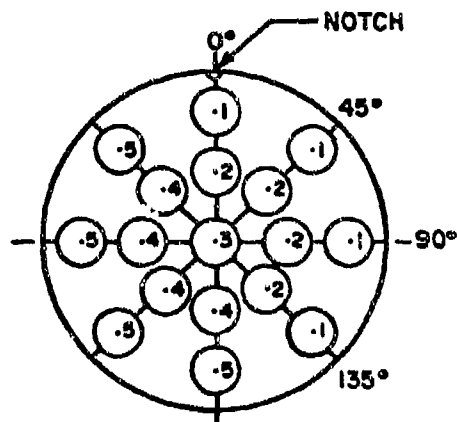
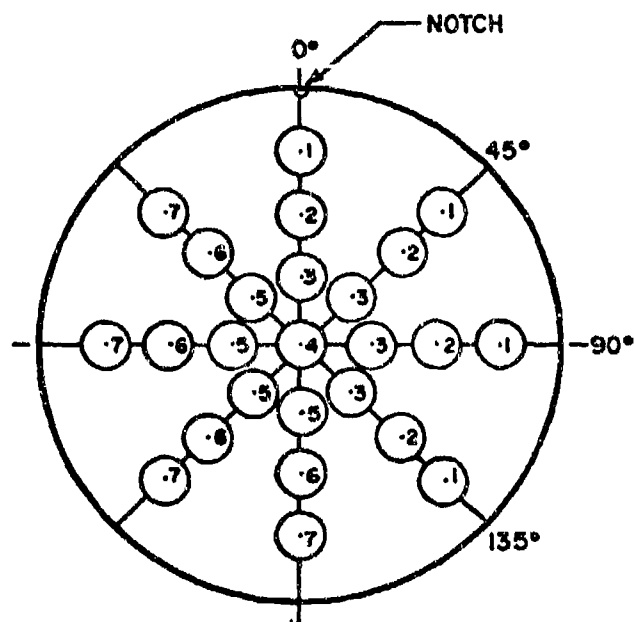
500X

Figure 22. Material Showing Cracks in the Matrix Radially Distributed Around Oxide Inclusion. Billet I03A D0415.



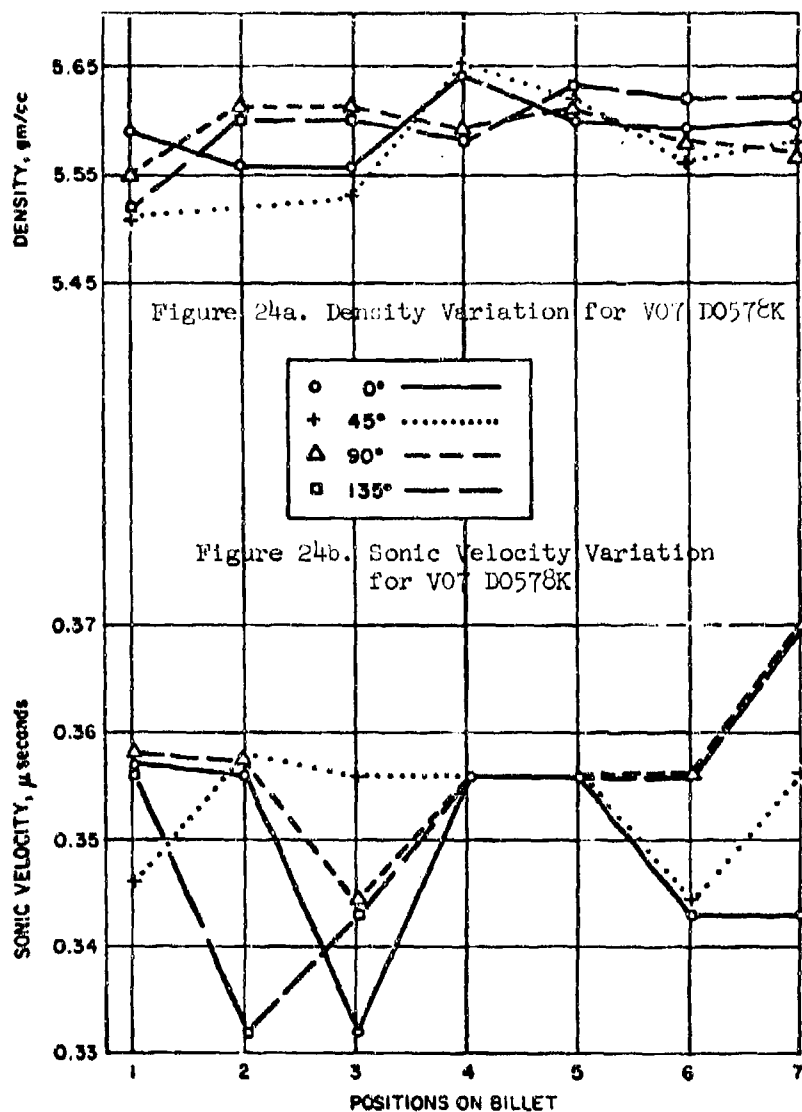
775244D

Figure 23. Location of NDT Measurements on Diametrical Slab.



775243 D

Figure 24. Location of NDT Measurements on 2-Inch and 3-Inch Diameter Billets.



7762470

Figure 25. Density and Sonic Velocity Variations in Billet V07 D0578.

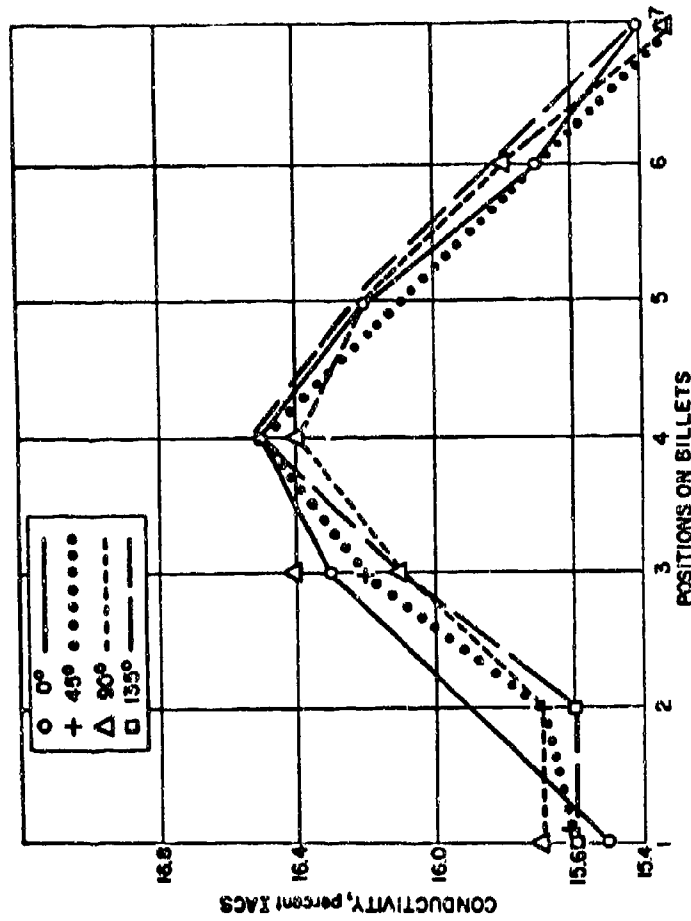
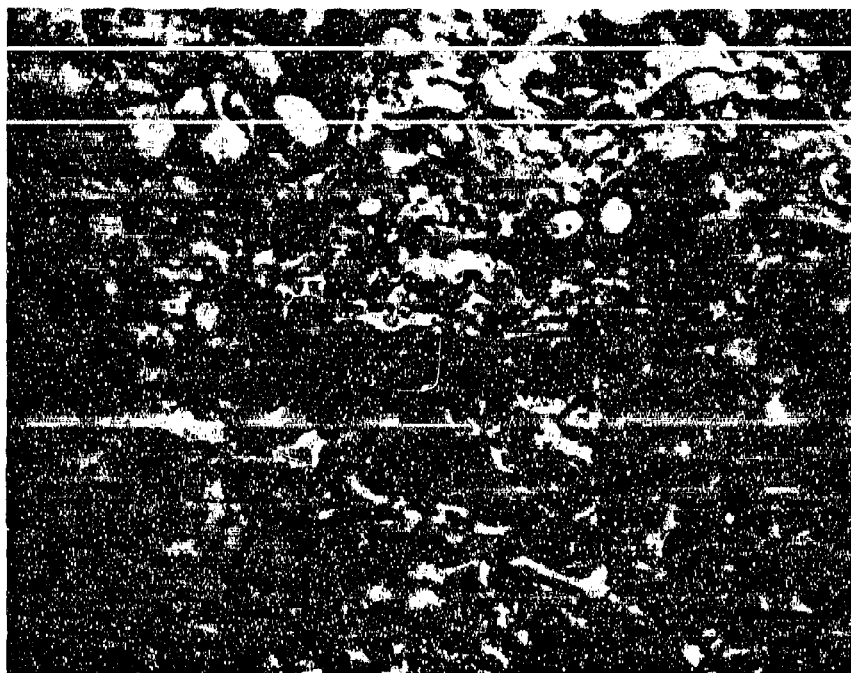


Figure 26. Variation of Electrical Conductivity for V07 D0578K.

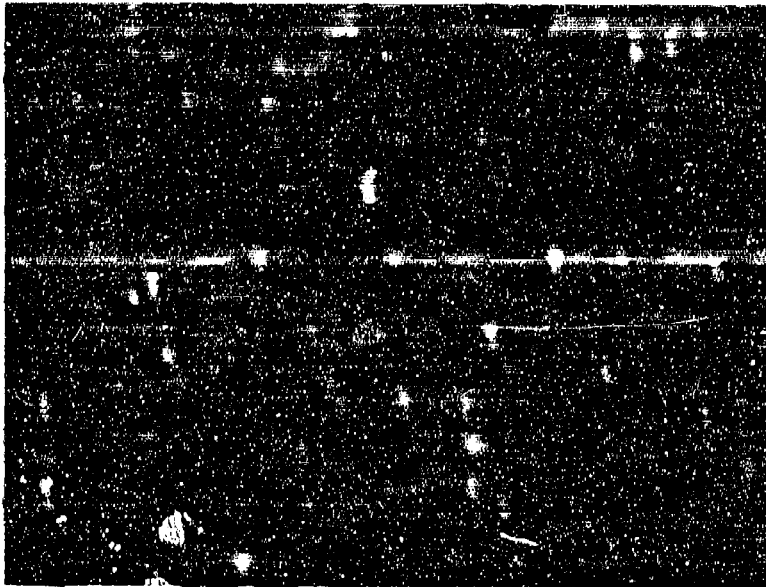


Avco Plate No.
4324M

As-polished

500X

Figure 27. Material I Plasma Sprayed on Stainless Steel.
Billet I02A P0162F.

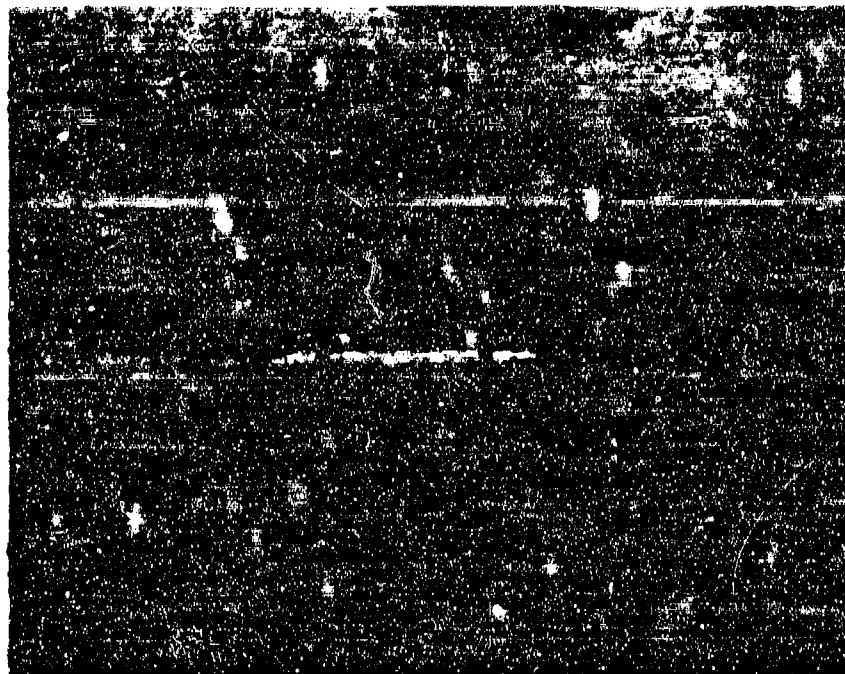


Avco Plate No.
4592

Etched

500X

Figure 28. Microstructure of Dense Area In Sintered Specimen
103A B0005.



Avco Plate No.
4678-A

As Polished

100X

Figure 29. Representative Microstructure of ZrB_2 Reinforced
with Thornel 25 Carbon Fiber, Billet XIII(5) D0644.

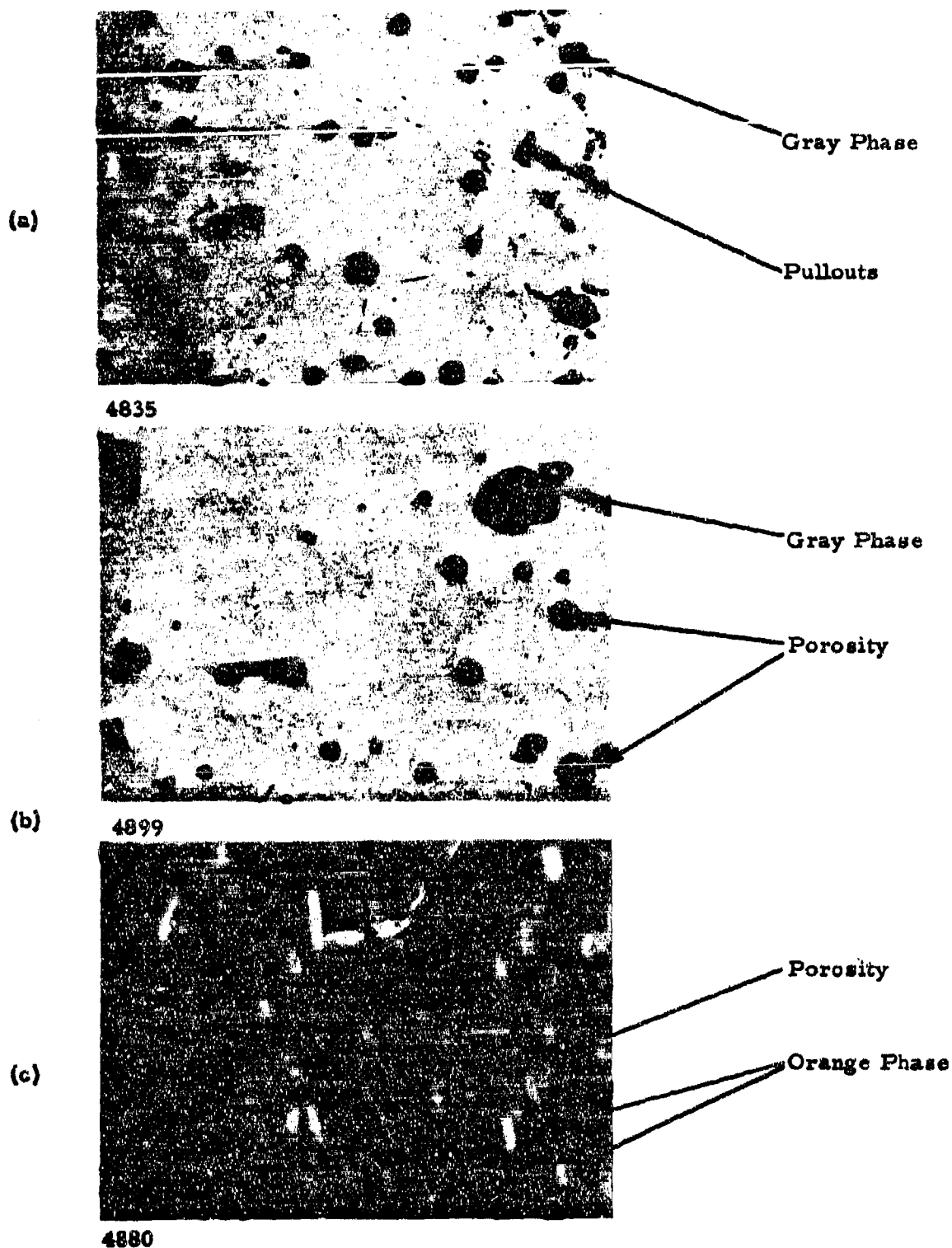
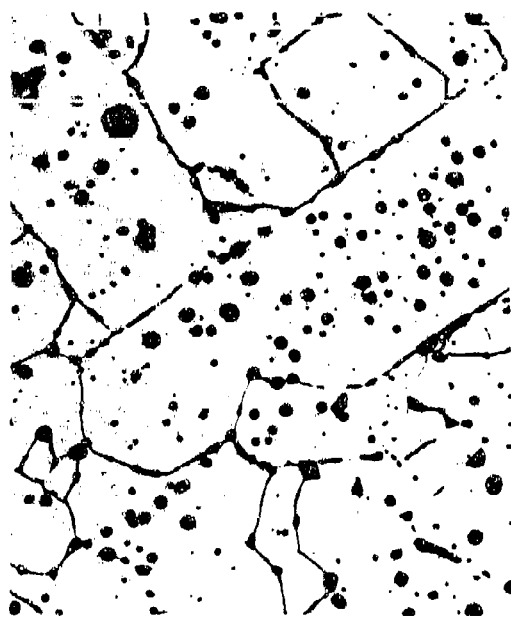
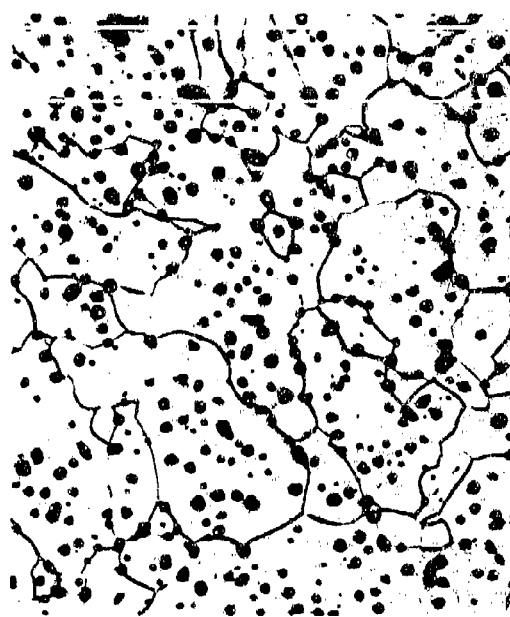


Figure 30. Photomicrographs of Material I07 D0589, As Polished, 500X:
 (a) Original Structure-Area 1, (b) Original Structure-Area 2,
 (c) Annealed at 2200°C (Optical) for 15 Minutes.



4907

(a)



4911

(b)



4910

(c)

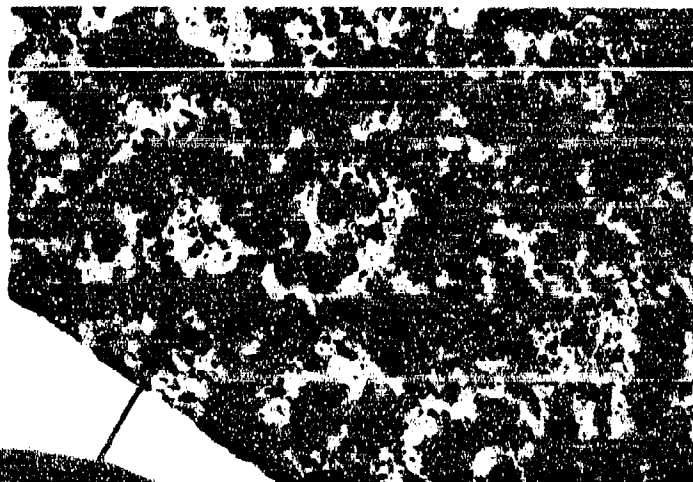


4912

(d)

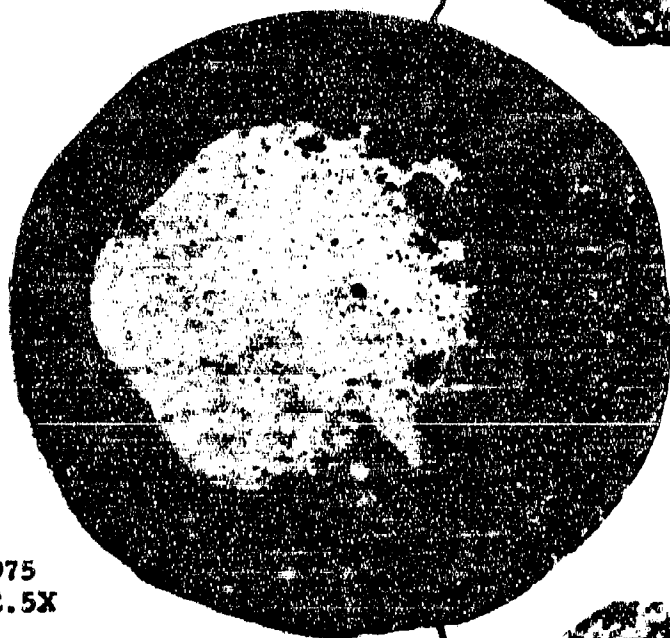
Figure 31. Photomicrographs of Material 107 D0589, Etched, 150X: (a) After Anneal No. 12, (b) After Anneal No. 14, Area 1, (c) After Anneal No. 14, Area 2 and (d) After Anneal No. 14, Area 3.

Depleted
Zone



4976

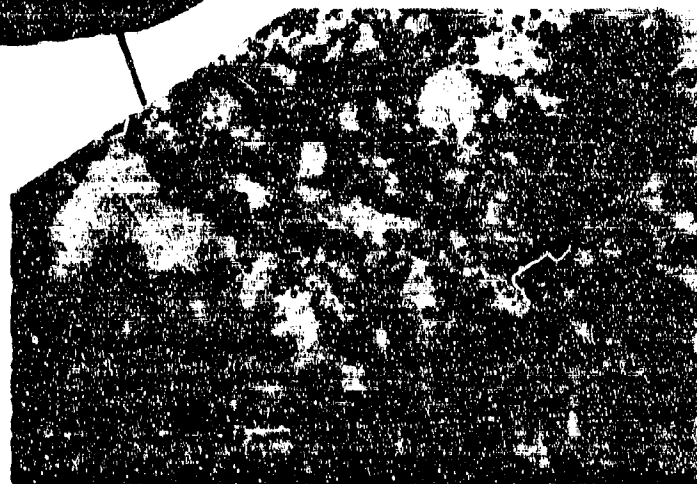
100X



4975
12.5X

4977

500X



Matrix

Figure 32. Photomicrographs of Material VIII, D0498, Annealed at 2200°C (Color Temperature) for 15 Minutes.

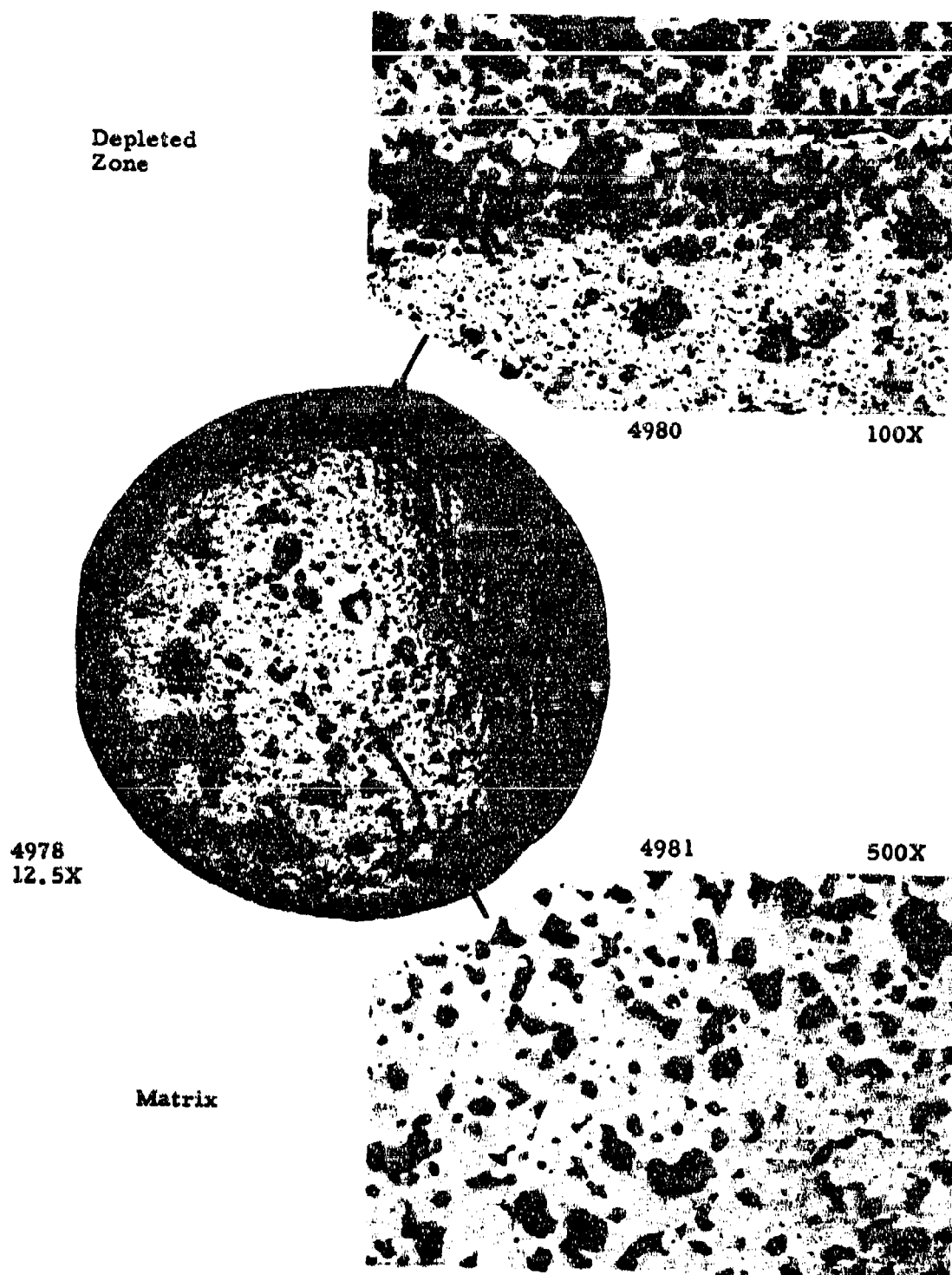


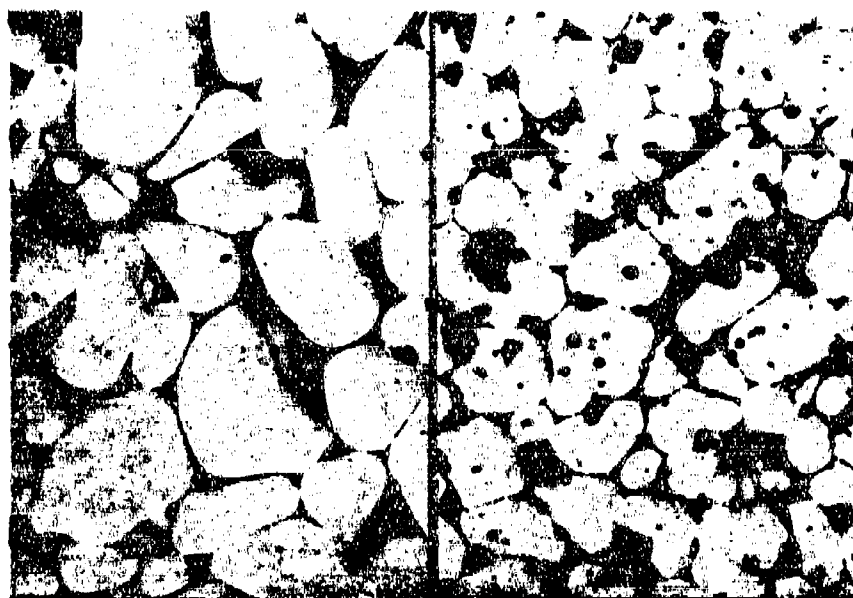
Figure 33. Photomicrographs of Material VIII, D0592, Annealed at 2300°C (Color Temperature) for 15 Minutes.



4844

500X

As Hot Pressed



4985

250X

4986

250X

Near Surface

Center

Figure 34. Photographs of Material X, D0596, Annealed at 2200°C (Color Temperature) for 15 Minutes.

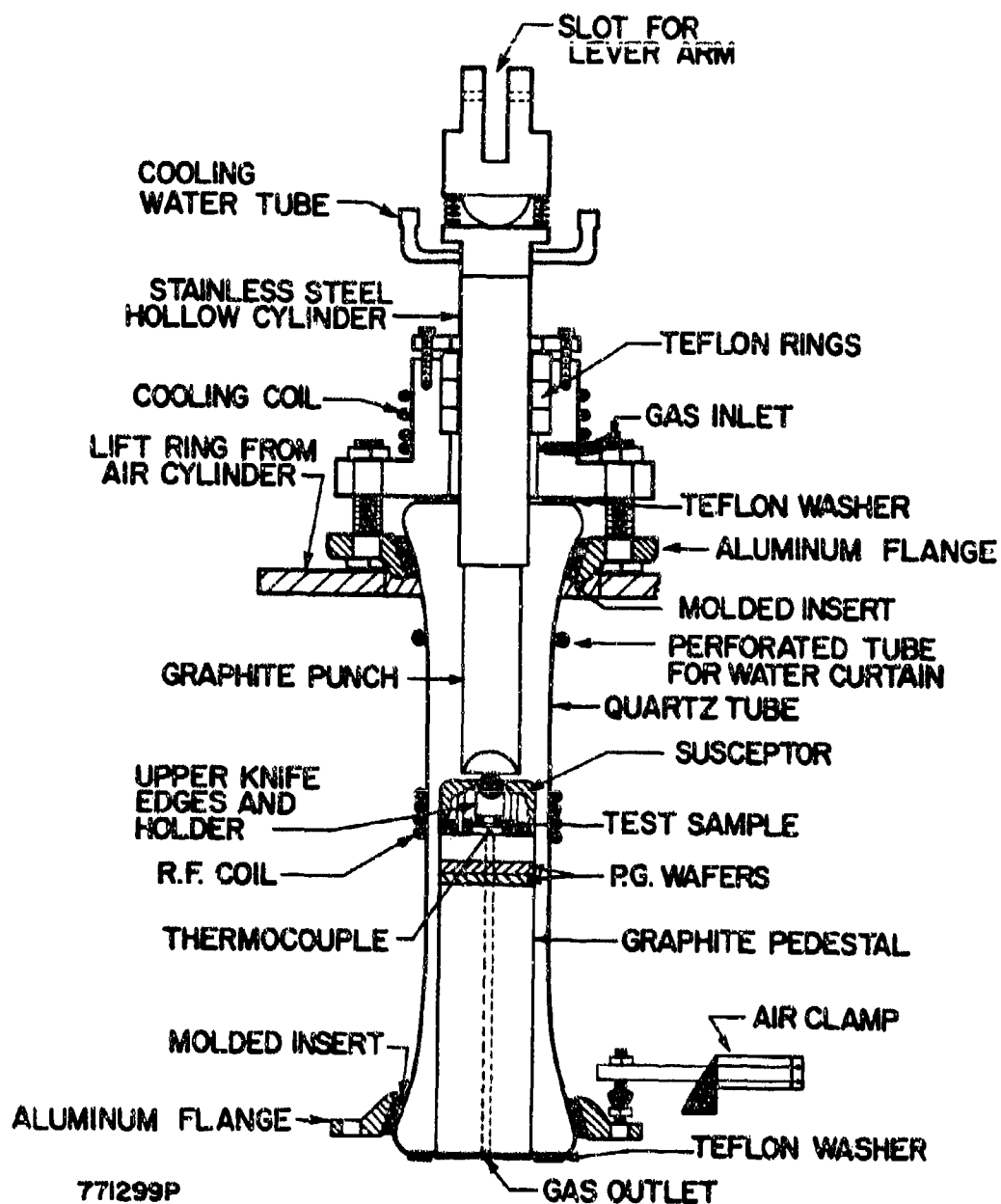


Figure 35. Schematic of High Temperature Lever Arm Bend Test Apparatus.

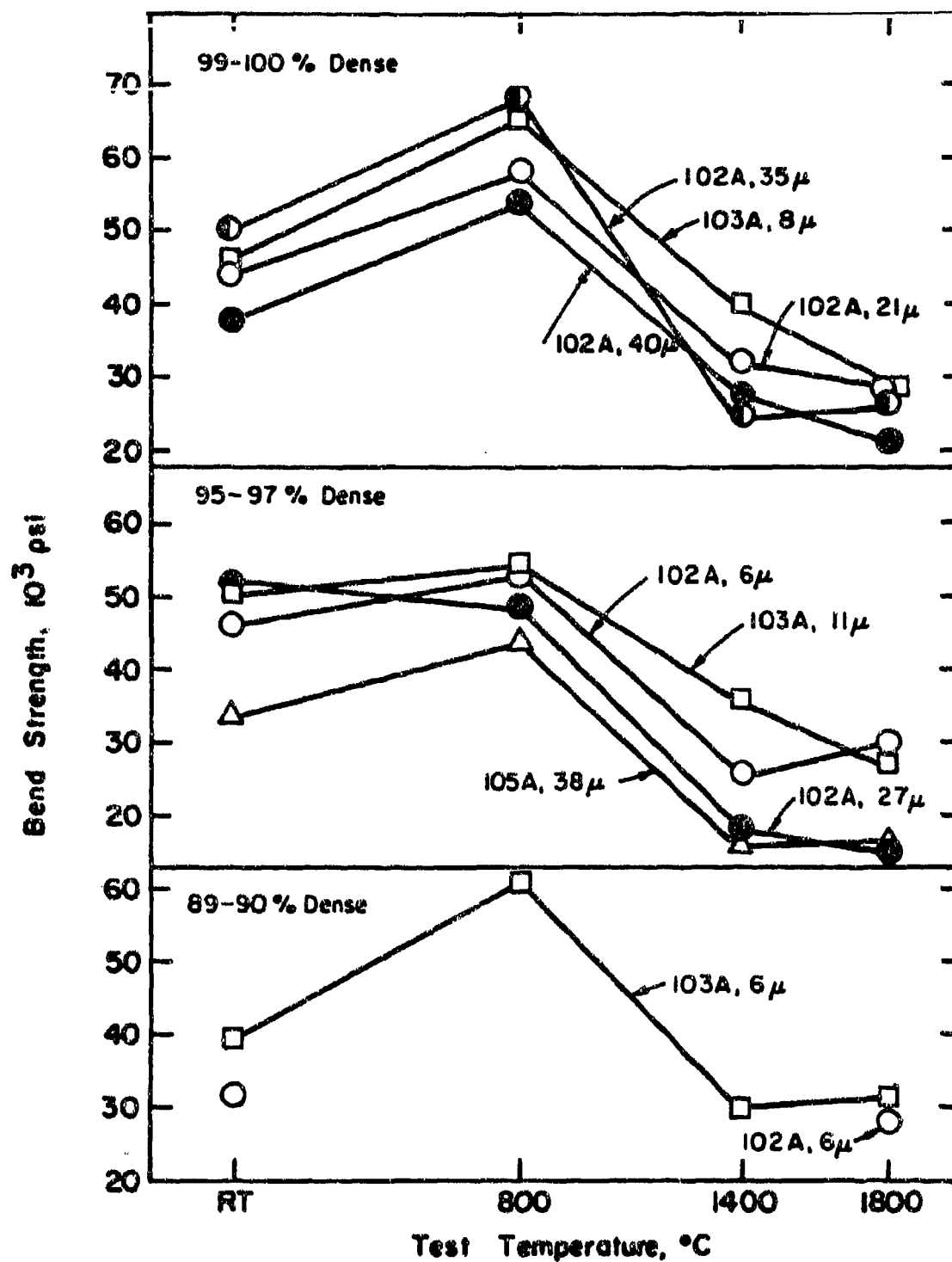


Figure 36. Bend Strength of Material I As A Function of Test Temperature.

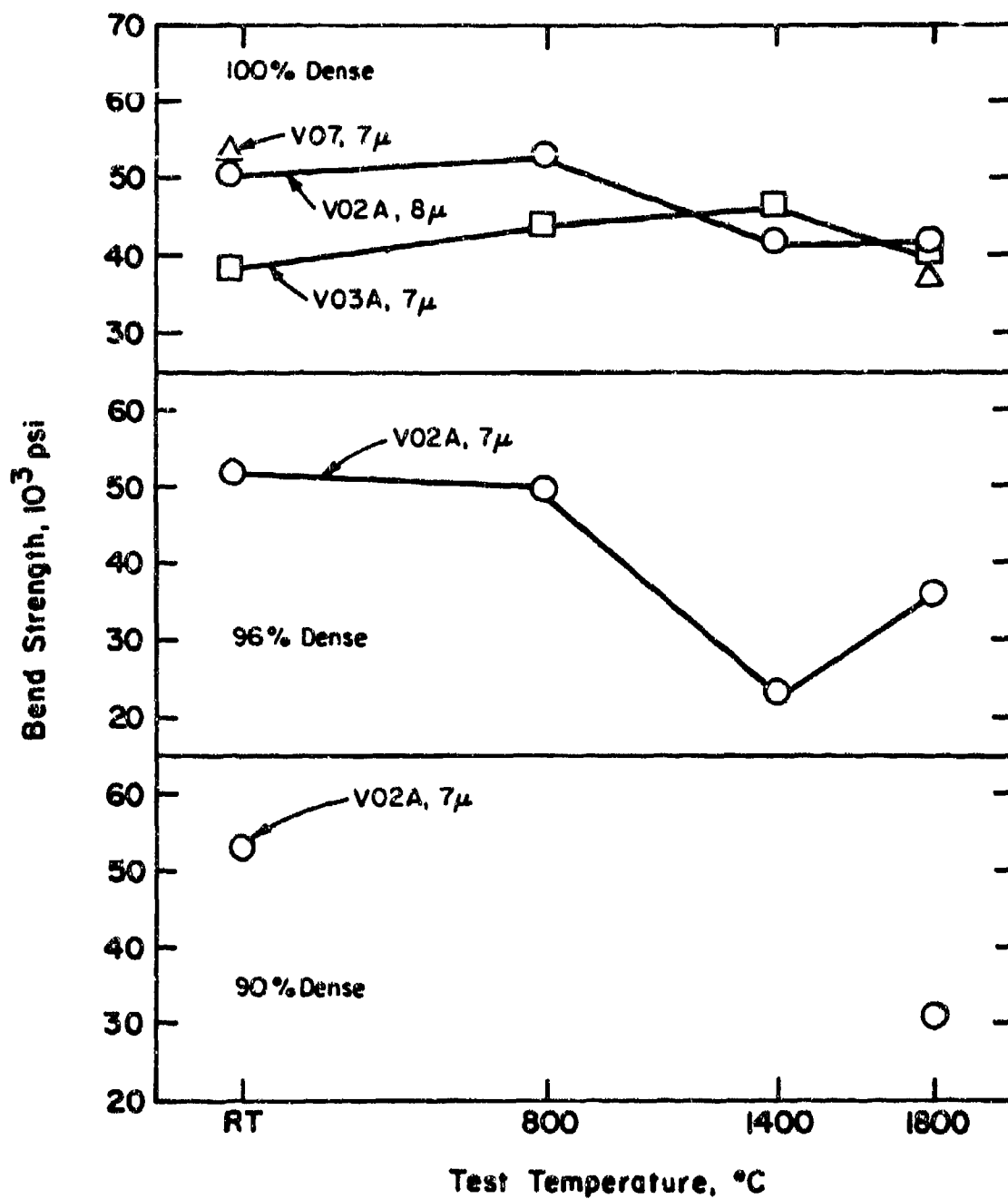


Figure 37. Bend Strength of Material V As A Function of Test Temperature.

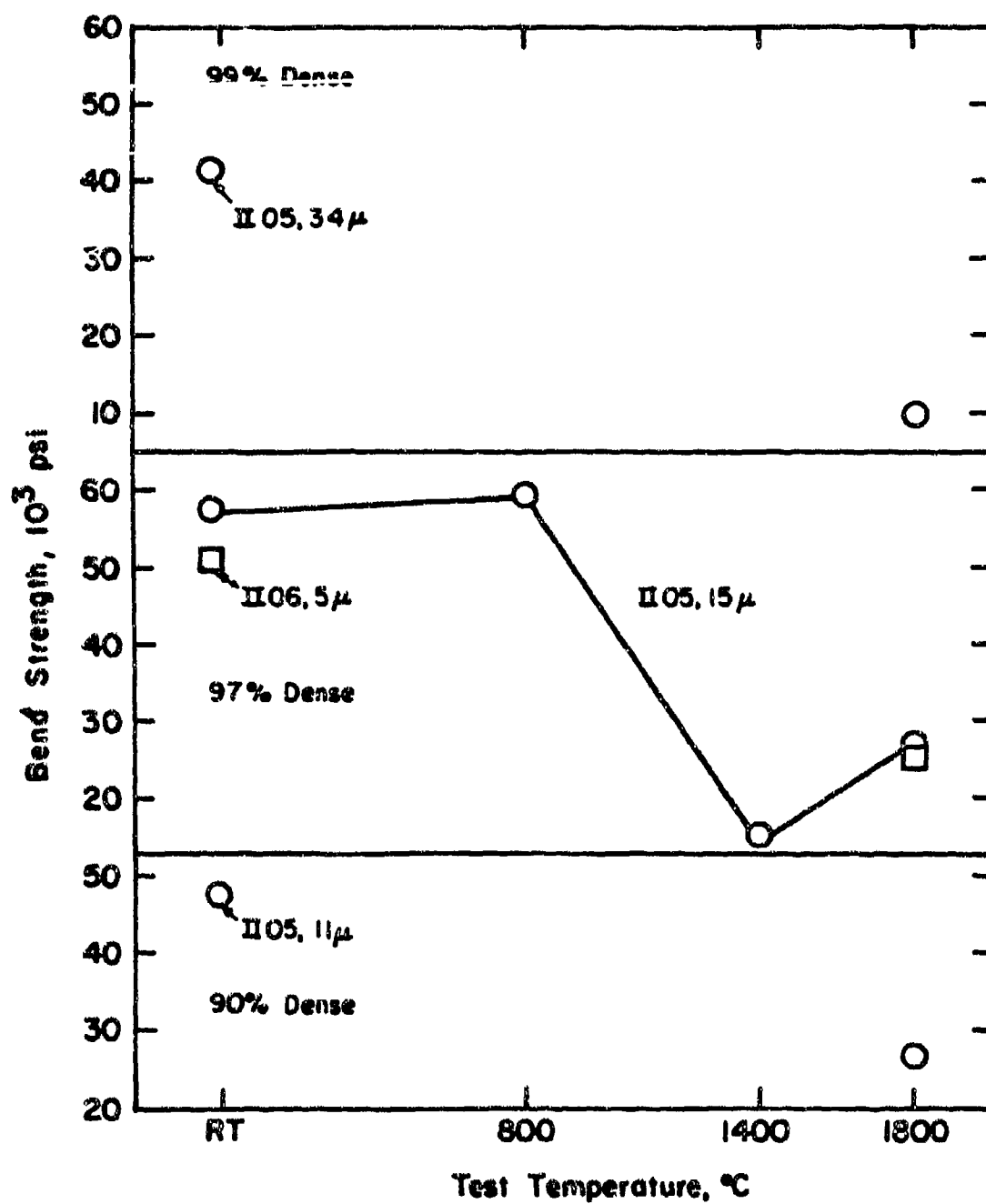


Figure 38. Bend Strength of Material II as a Function of Test Temperature.

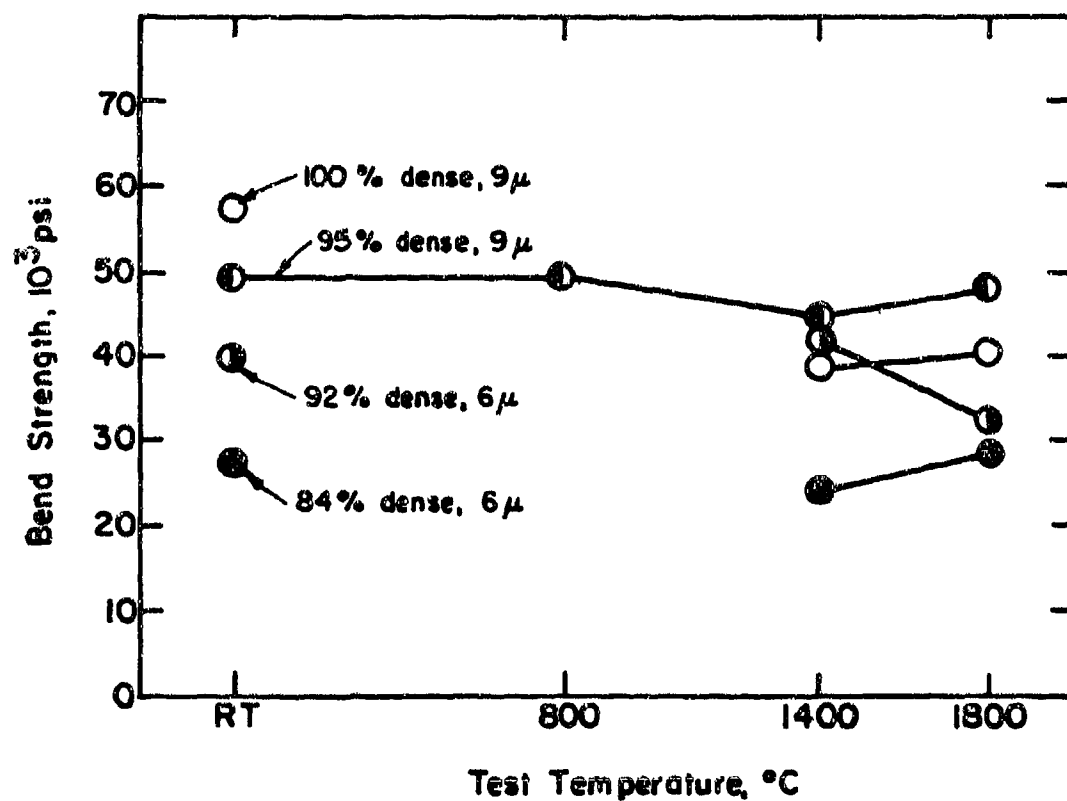


Figure 39. Bend Strength of Material III05 As A Function of Test Temperature.

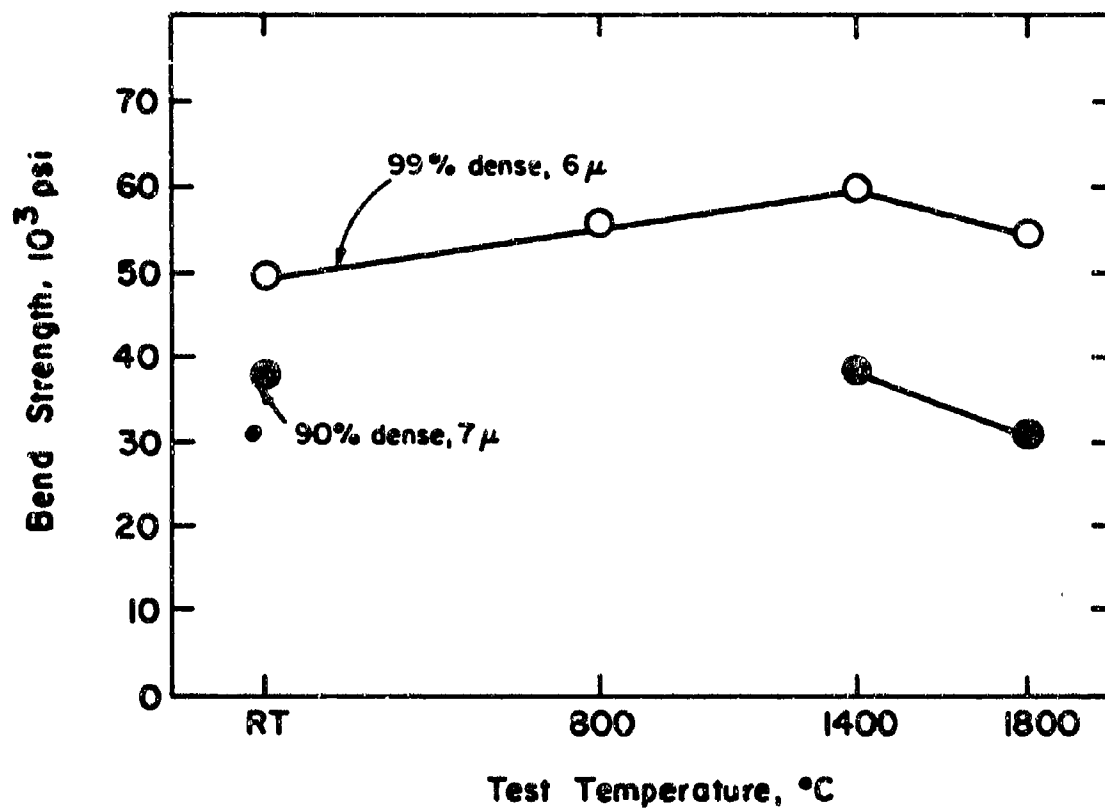


Figure 40. Bend Strength of Material IV05 as a Function of Test Temperature.

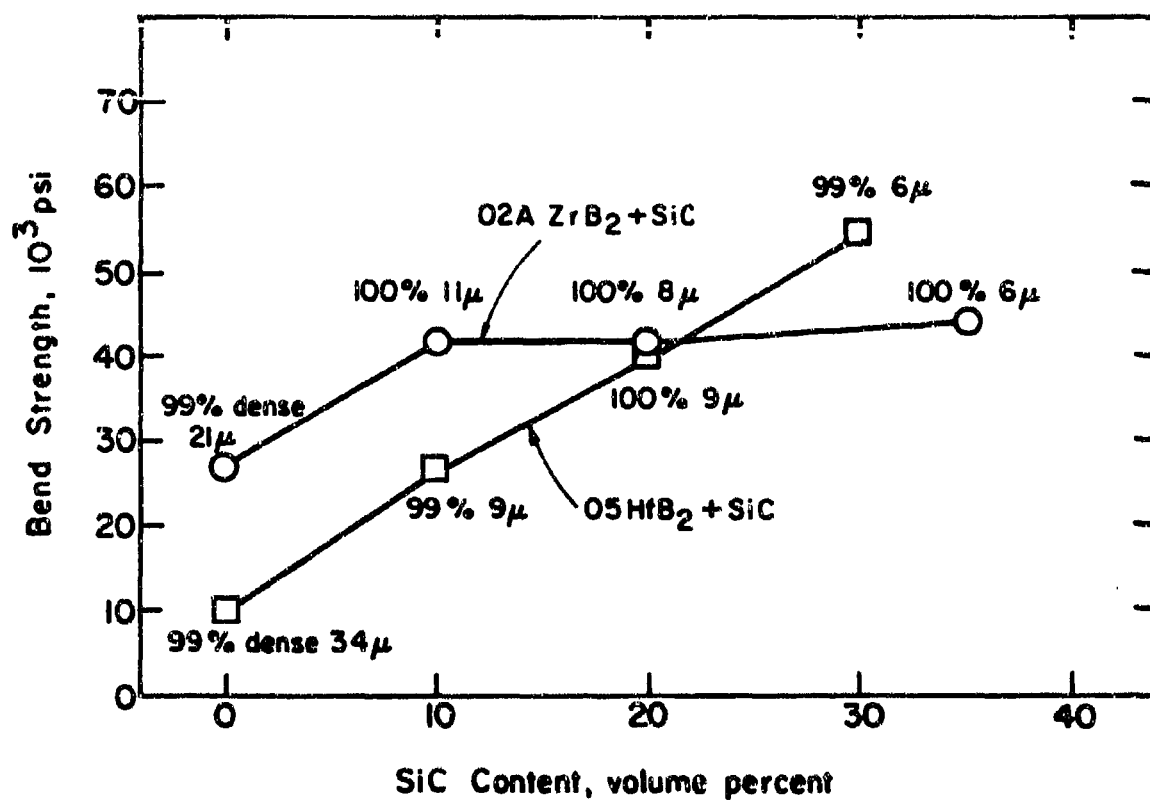


Figure 41. Bend Strength at 1800°C of ZrB_2 -SiC and HfB_2 -SiC Composites As Functions of SiC Content.

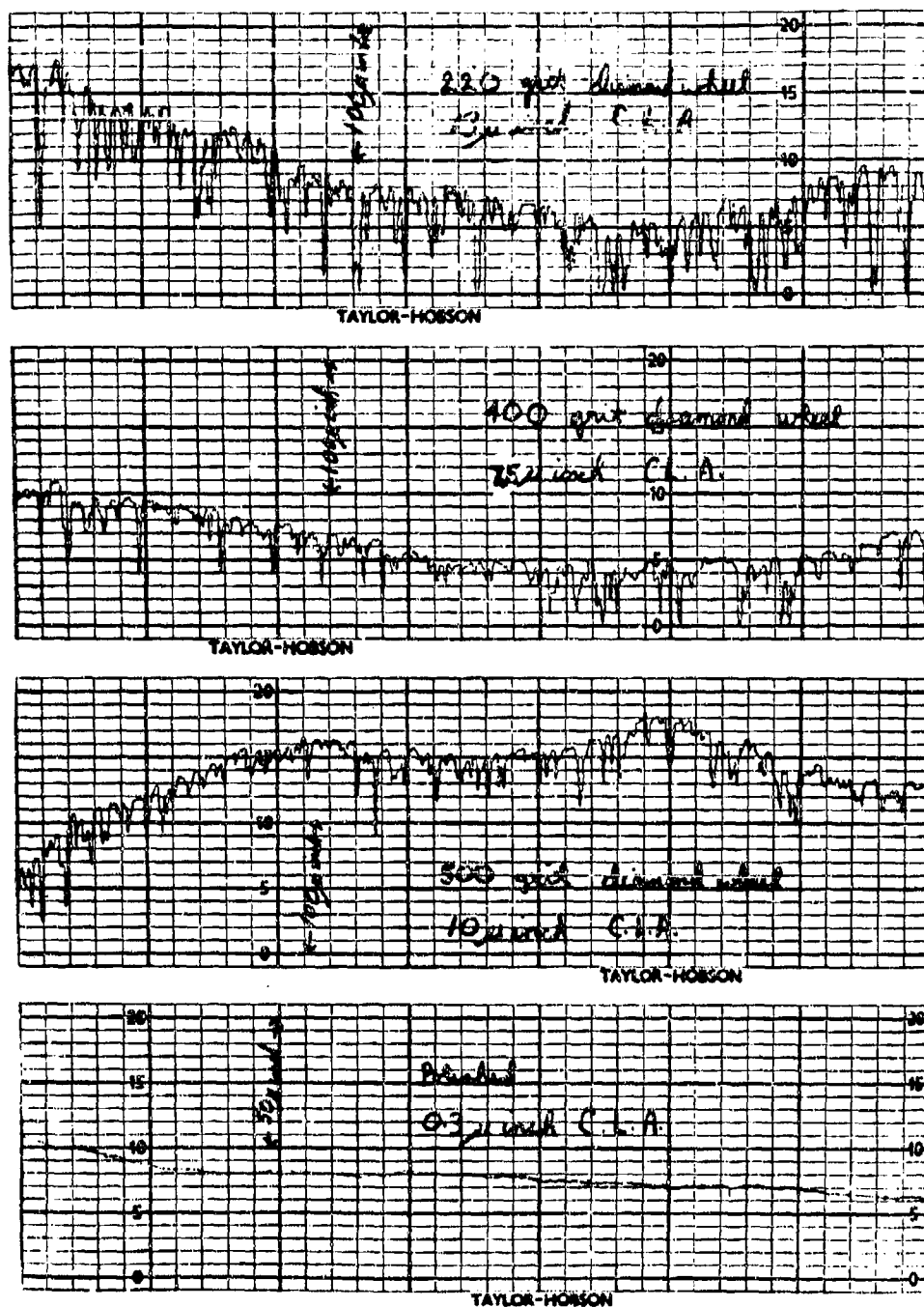
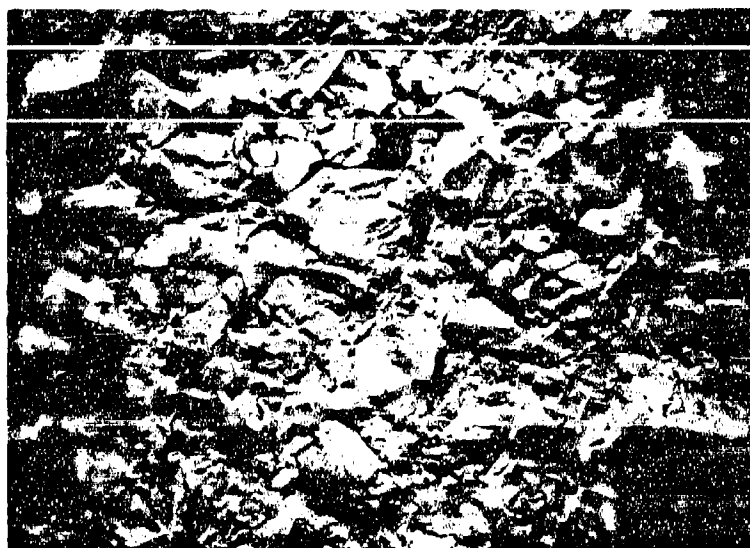


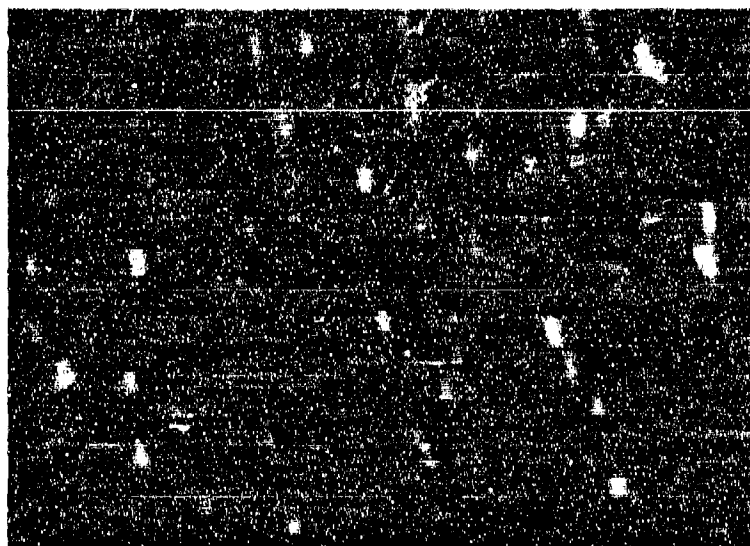
Figure 42. Talysurf Surface Contour Tracers for (a) 220 Grit Finish, (b) 400 Grit Finish, (c) 500 Grit Finish and (d) 0.25 Micron Finish on Billet V07 D0576.



Avco
Plate No.
66715

1500X

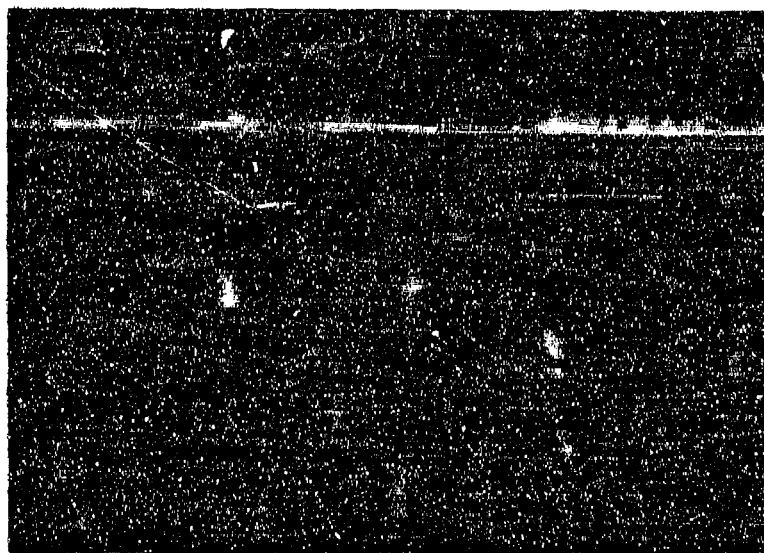
Figure 43. Electron Micrograph of Surface Structure from 200 Grit Finish on V07 D0576. Note Possible Surface Cracks.



Avco
Plate No.
67713

1500X

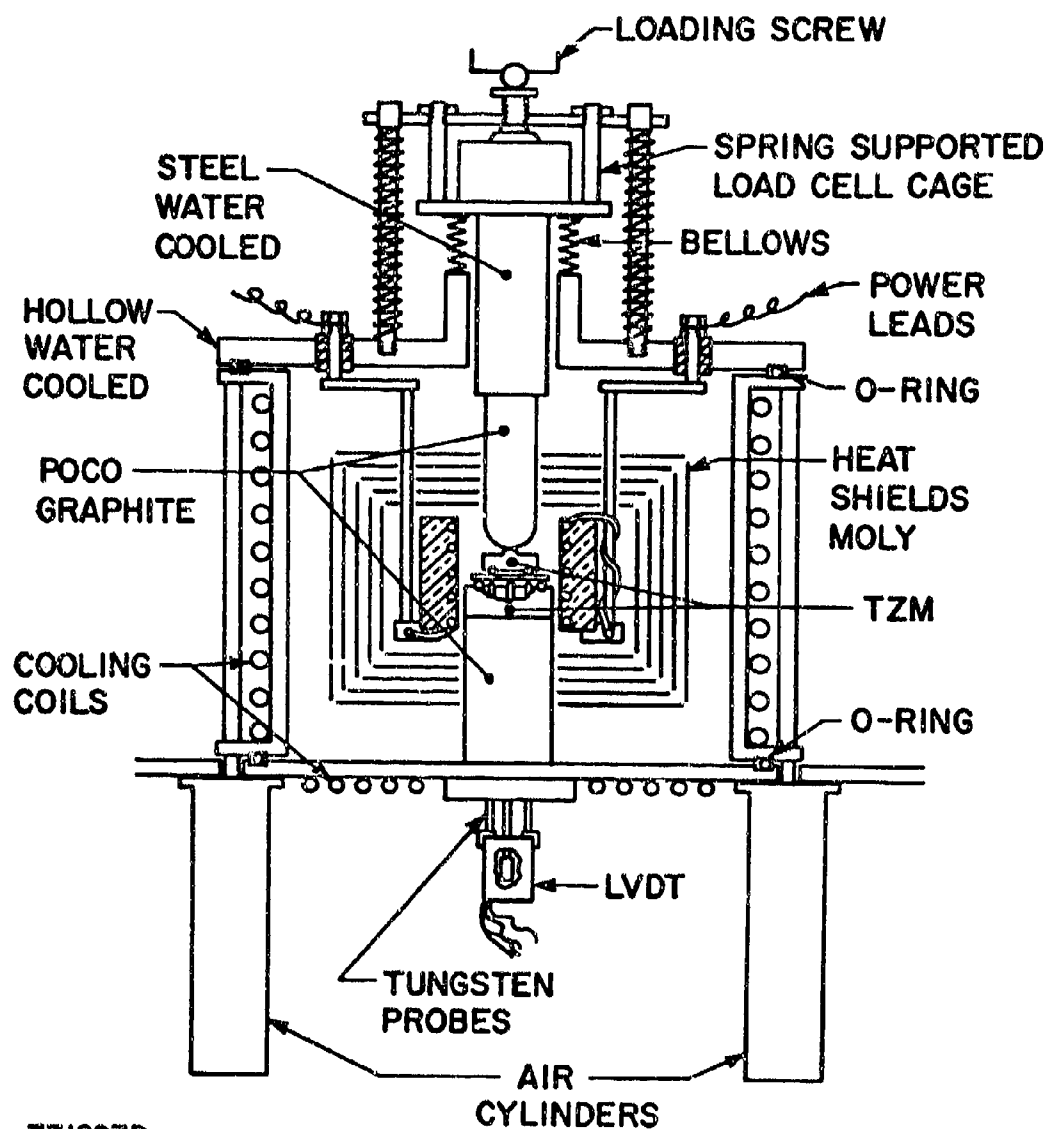
Figure 44. Electron Micrograph of Surface Structure from 400 Grit Finish on V007 D0576.



Avco
Plate No.
67709

1500X

Figure 45. Electron Micrograph of Surface Structure
for 0.25 Micron Diamond on V07 D0576.



771297P

Figure 46. Schematic of High Temperature Apparatus Used for Modulus Measurements.

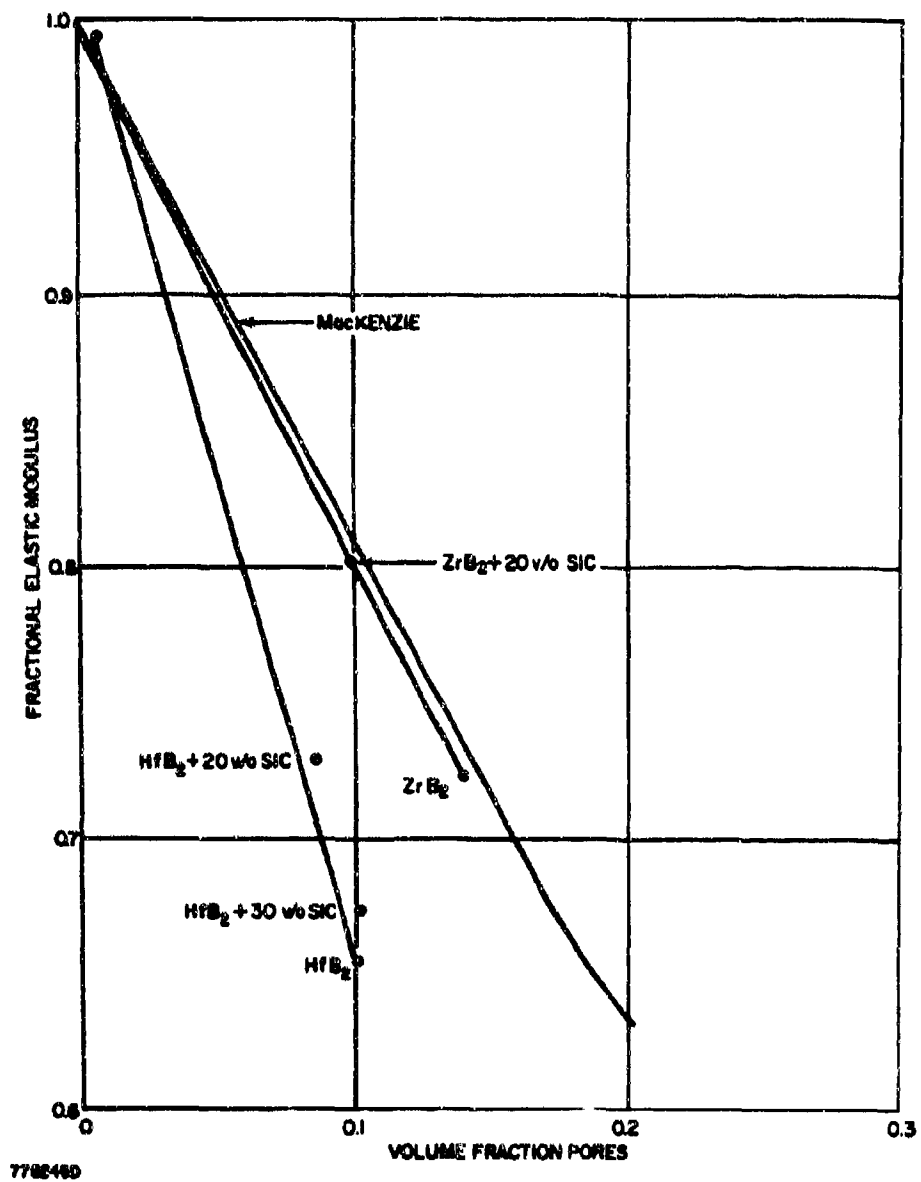
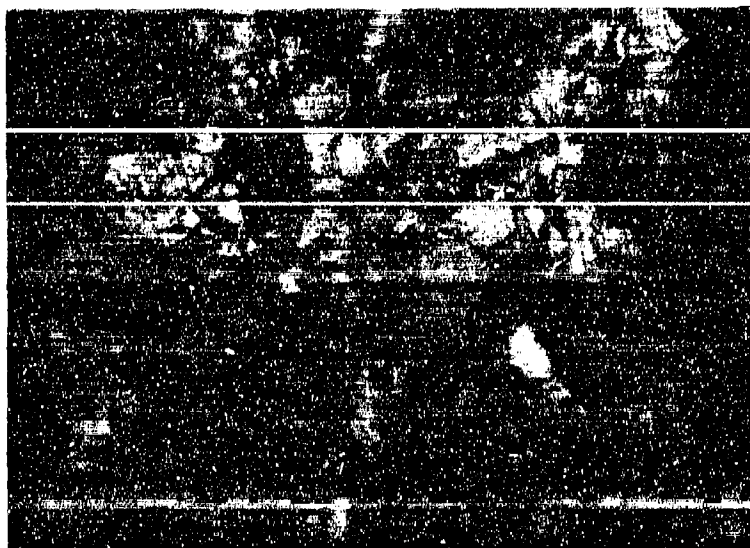


Figure 47. Effect of Porosity on Room Temperature Elastic Modulus for Various Diborides.



Avco
Plate No.
661038

1500X

Figure 48. Electron Fractograph of Material V Tested at 23°C with Bend Strengths of 50,500 psi. Billet V02A D0371.



Avco
Plate No.
661041

1500X

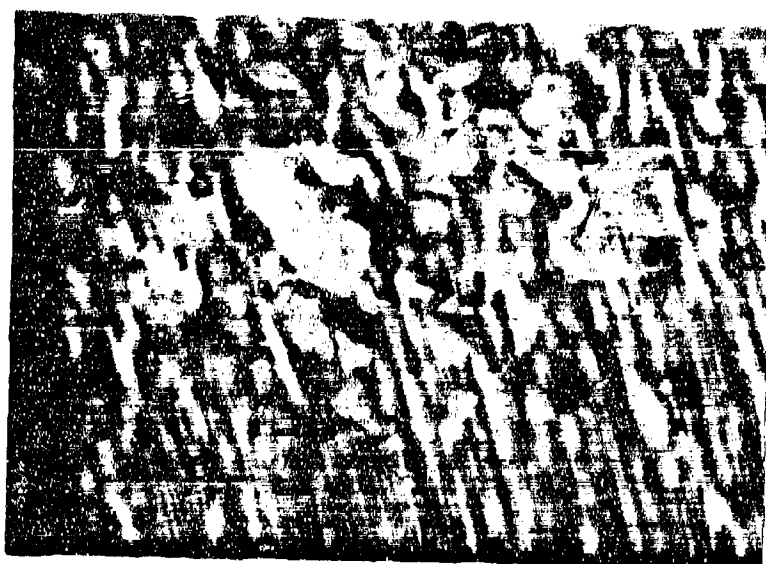
Figure 49. Electron Fractograph of Material V Tested at 800°C with Bend Strength of 52,700 psi. Billet V02A D0371.



Avco
Plate No.
66 1044

1500X

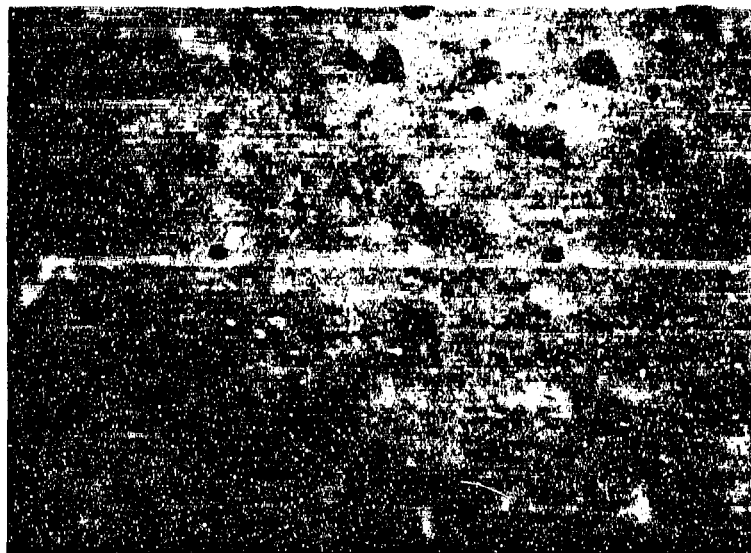
Figure 50. Electron Fractograph of Material V Tested at 1400°C with Bend Strength of 43,000 psi. Billet V02A D0371.



Avco
Plate No.
67235

1500X

Figure 51. Electron Fractograph of Material V Tested at 1800°C with Bend Strength of 44,900 psi. Billet V02A D0371.



Avco
Plate No.
4410A

1000X

Figure 52. Edge of Specimen I02A D0338 After Testing at 1800°C in Argon.

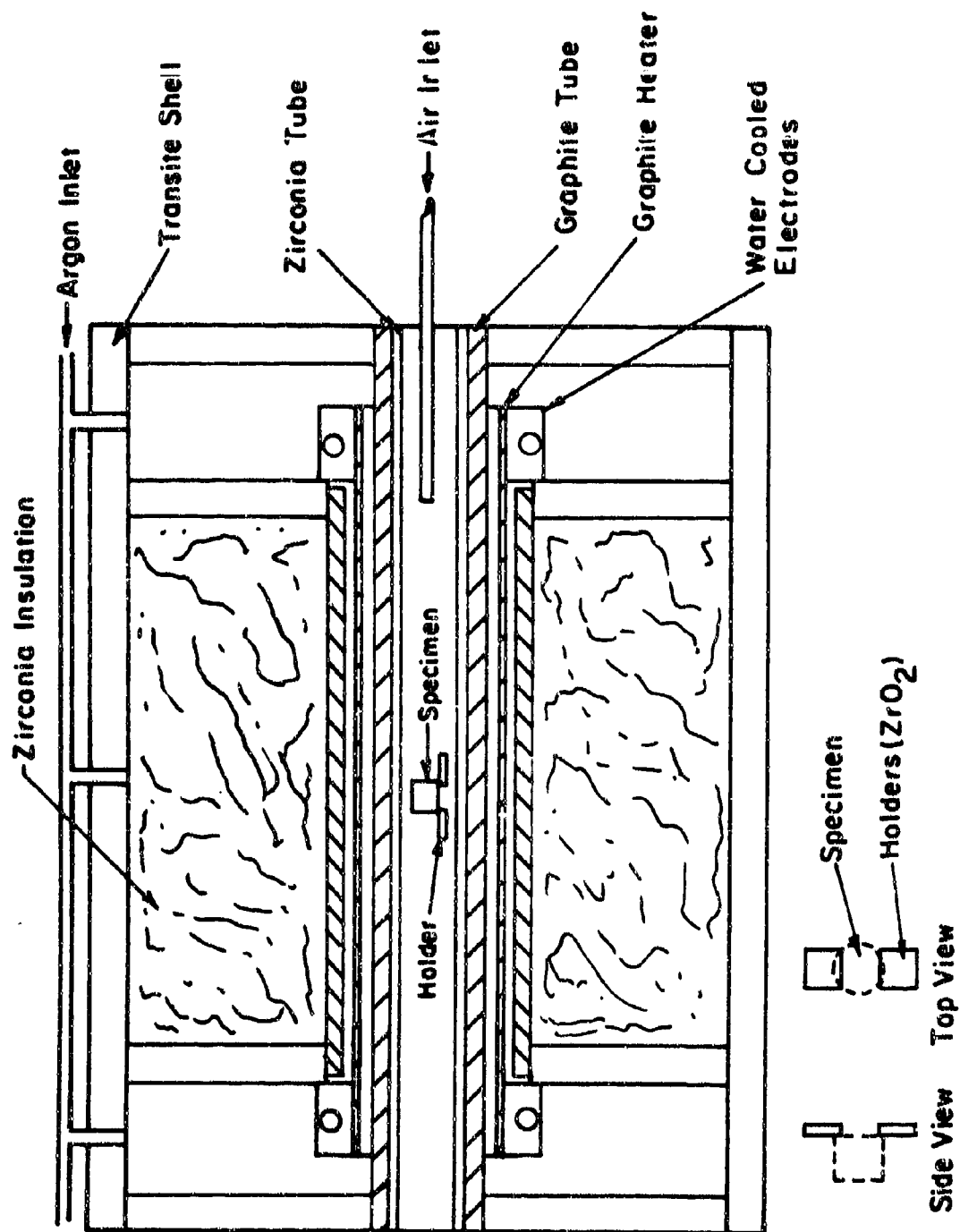


Figure 53. Schematic Diagram of Air Oxidation Furnace.

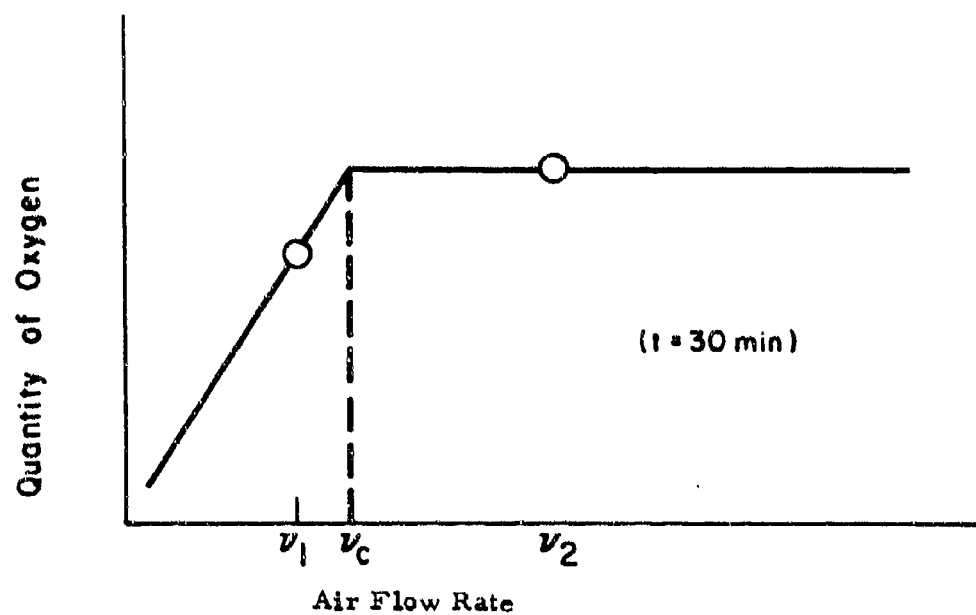
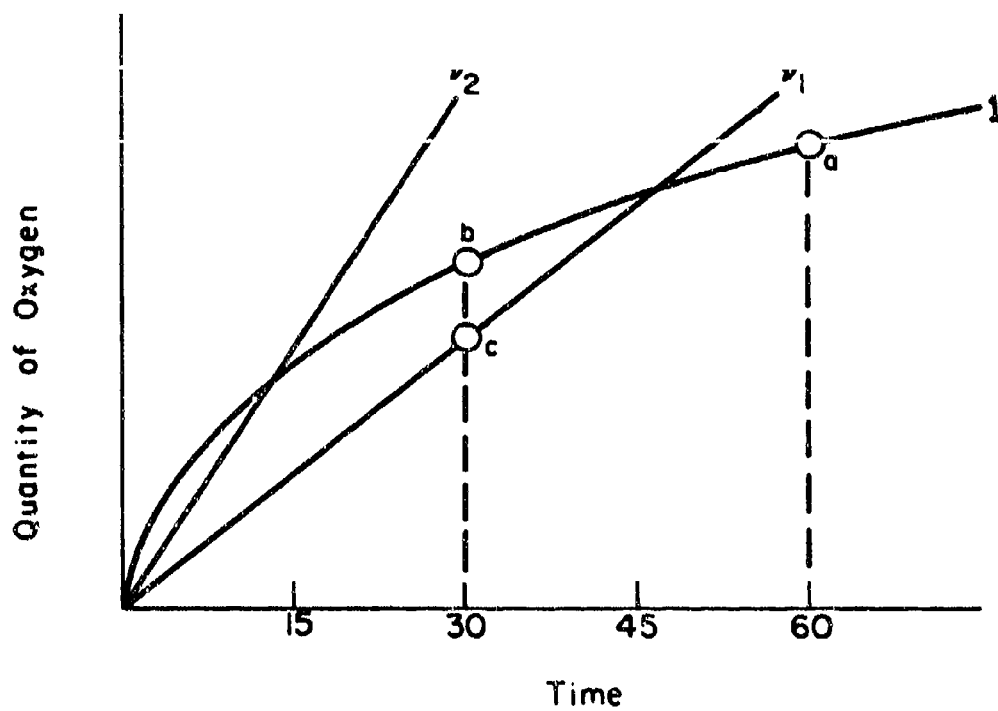


Figure 54. Dependency of Air Flow Rate for Hypothetical Oxidation Experiment at Constant Temperature.

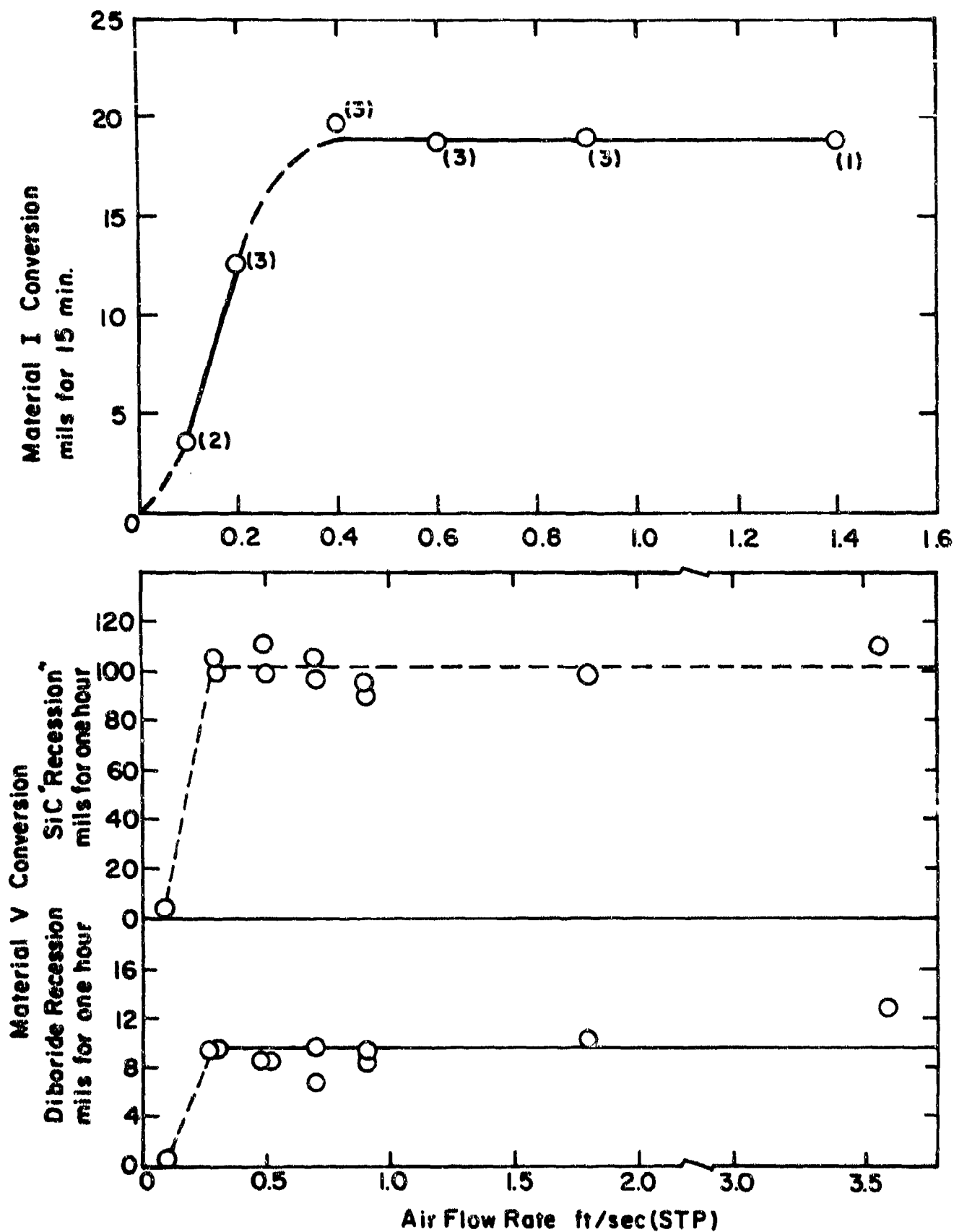


Figure 55. Air Flow Rate Dependence for Material I (1800°C, 15 Minutes and Material III (2120°C, 60 Minutes).

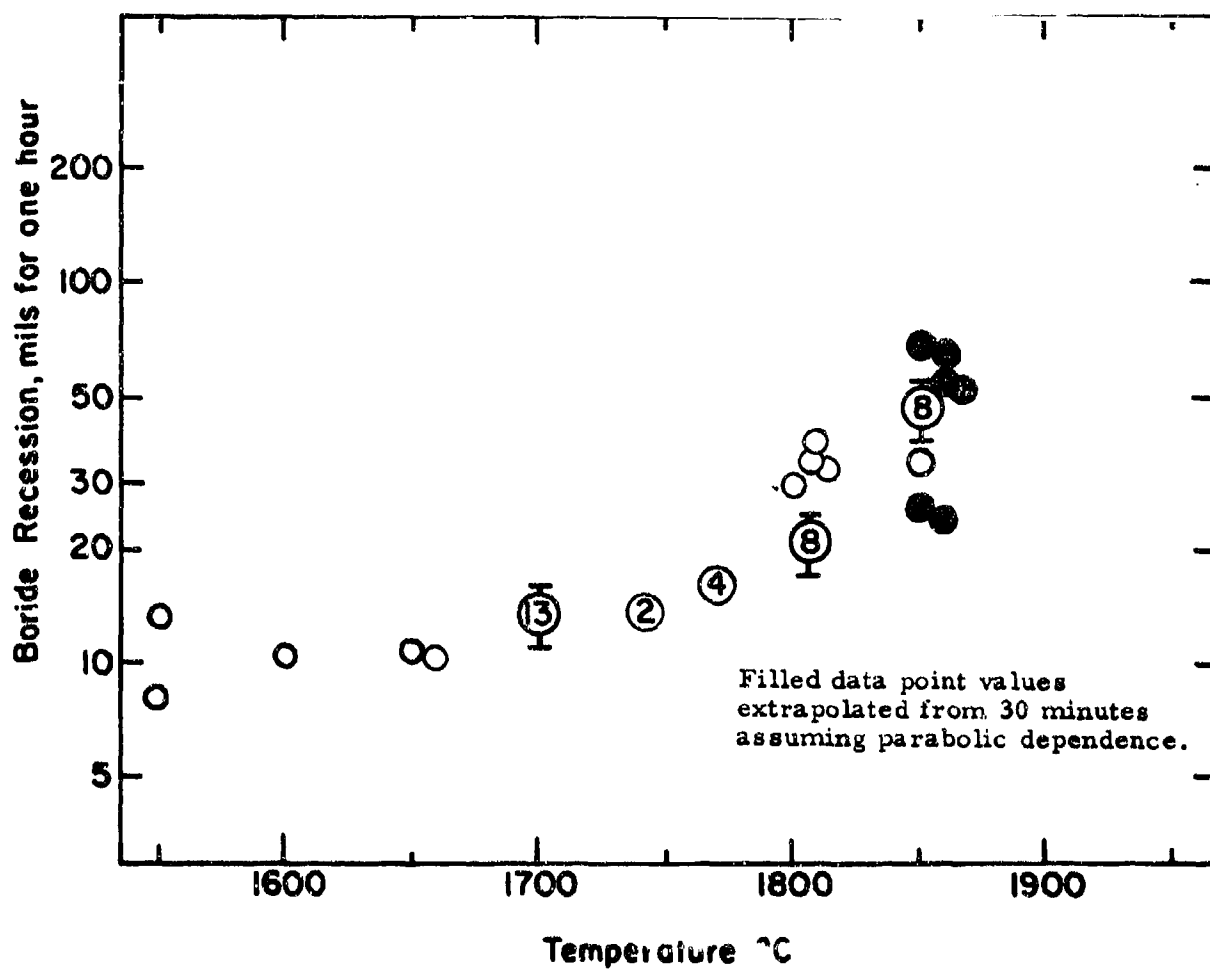


Figure 56. Oxidation Screening: Material I (ZrB_2).

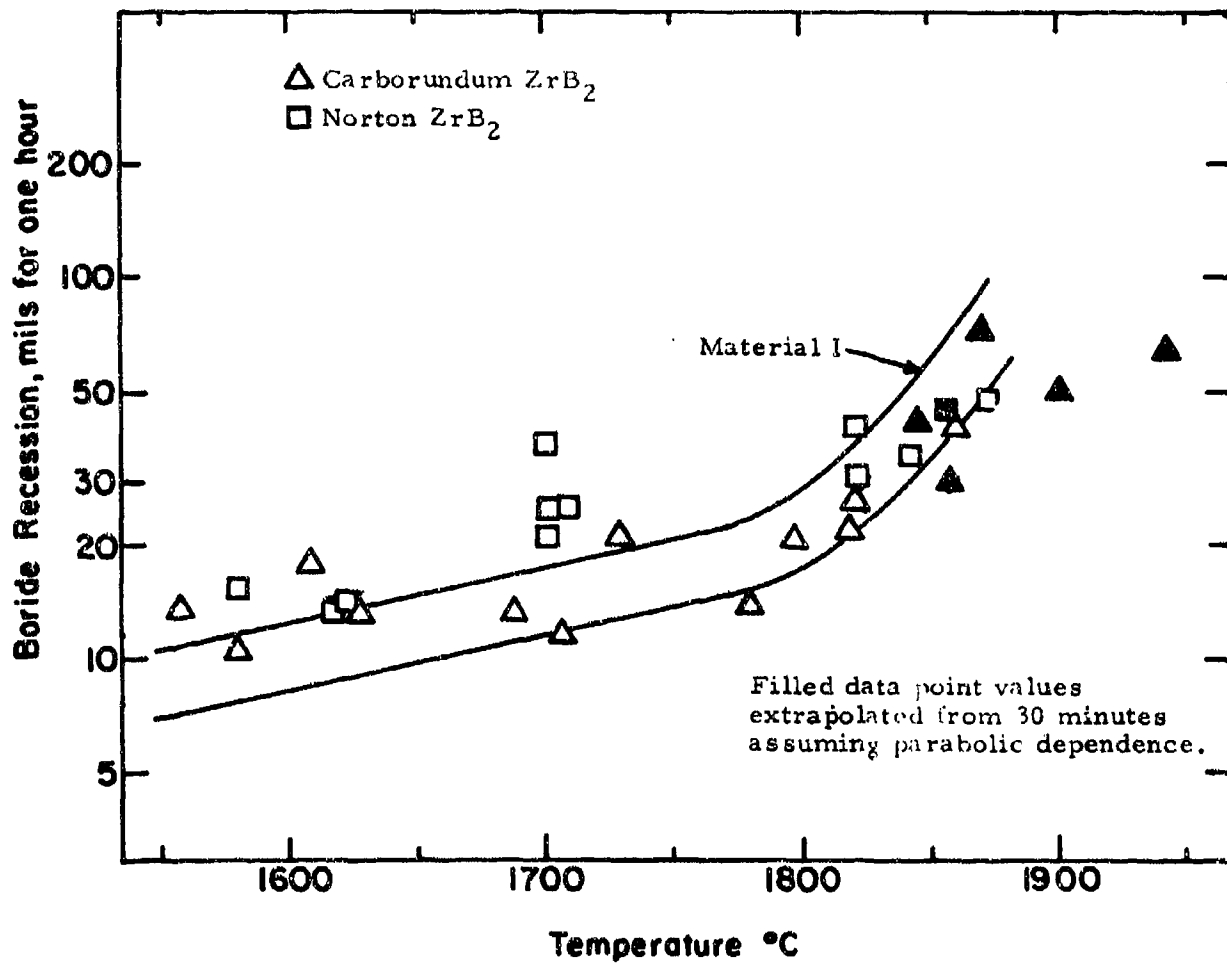


Figure 57. Oxidation Comparison: Commercially Hot Pressed ZrB_2 vs. Material I (ZrB_2).

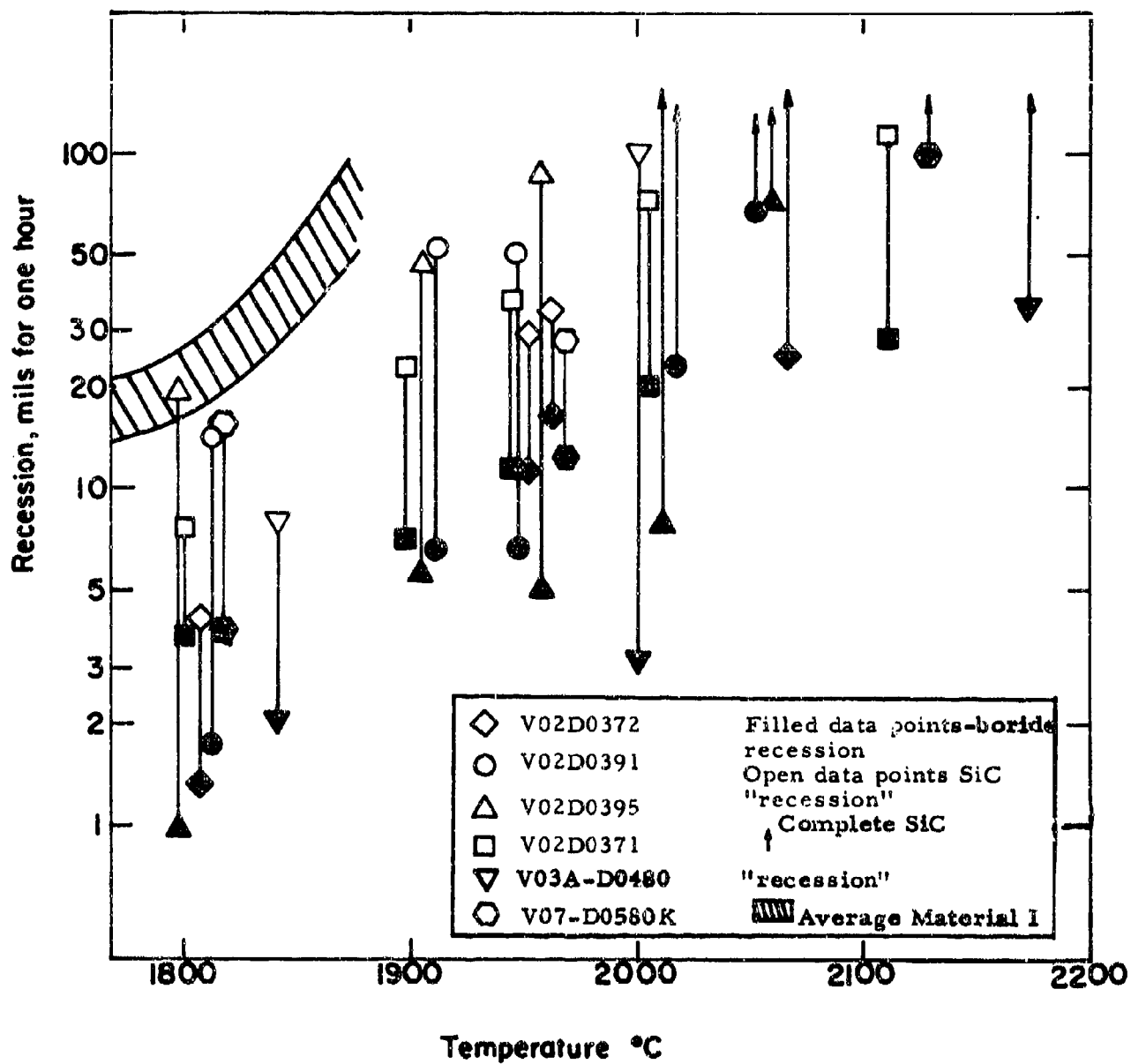


Figure 58. Oxidation Screening: Material V (ZrB_2 -20 v/o SiC).

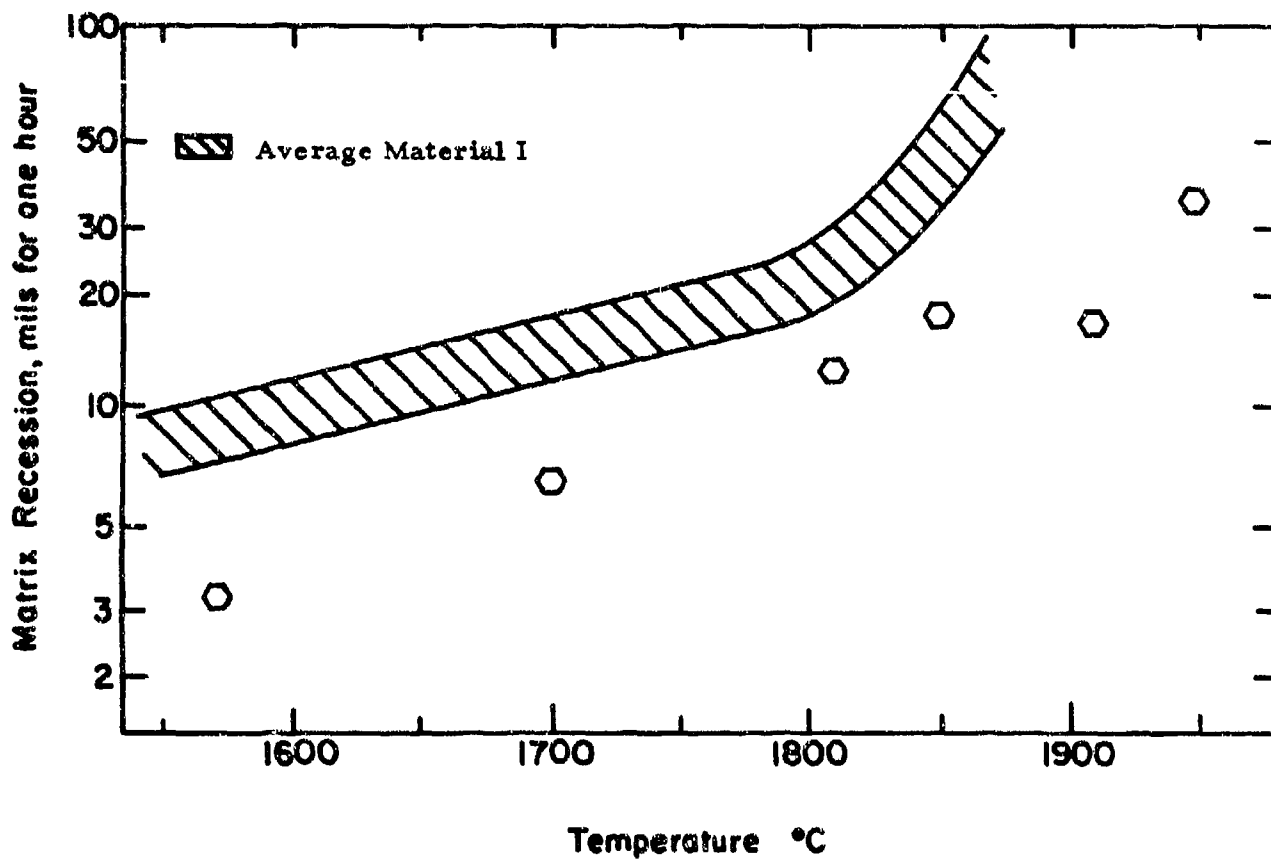


Figure 59. Oxidation Comparison: Boride Z vs. Material I (ZrB_2).

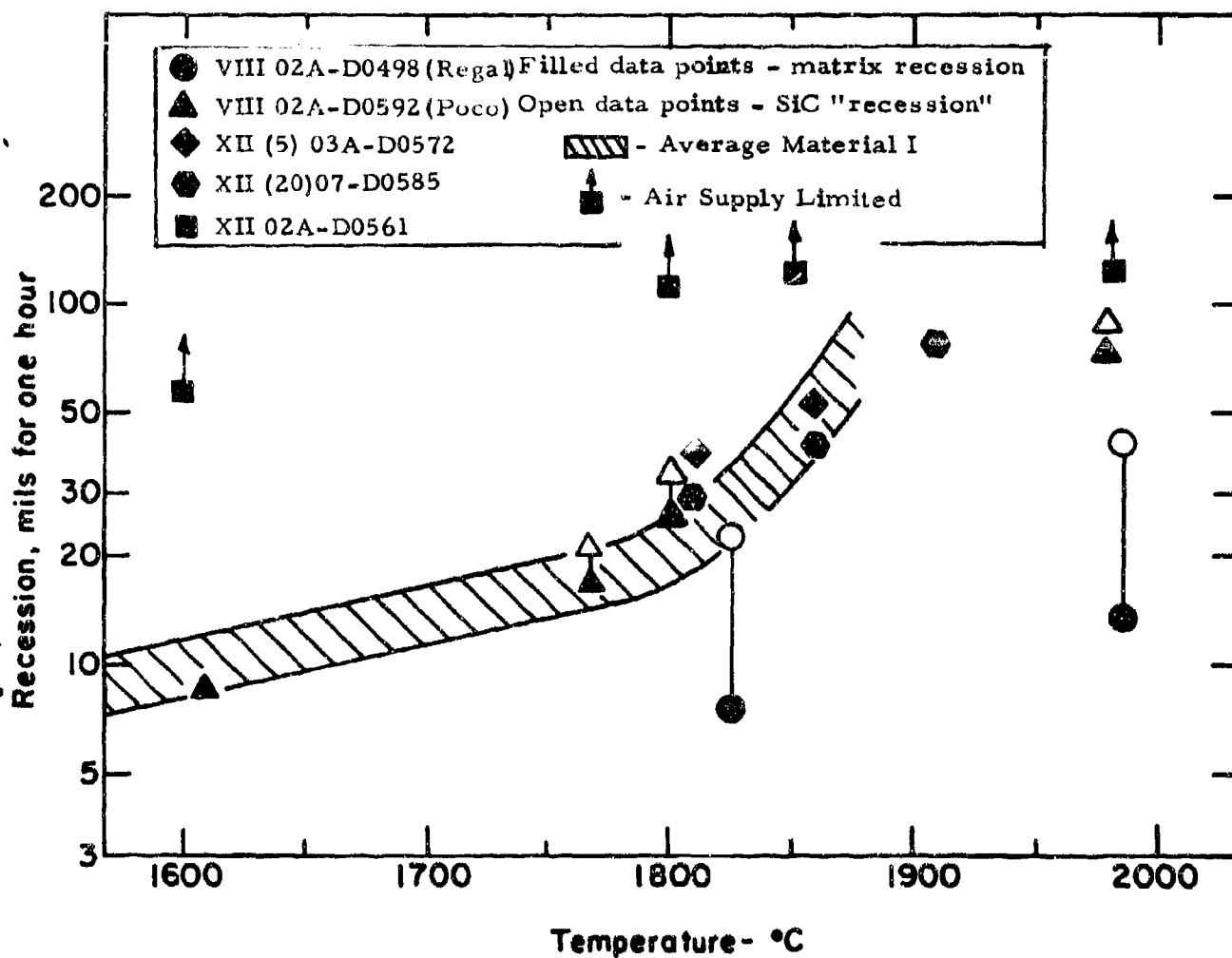


Figure 60 . Oxidation Screening: Material VIII ($\text{ZrB}_2 + 30 \text{ v/o Graphite} + 14 \text{ v/o SiC}$), and Material XII ($\text{ZrB}_2 + 50 \text{ v/o Graphite}$).

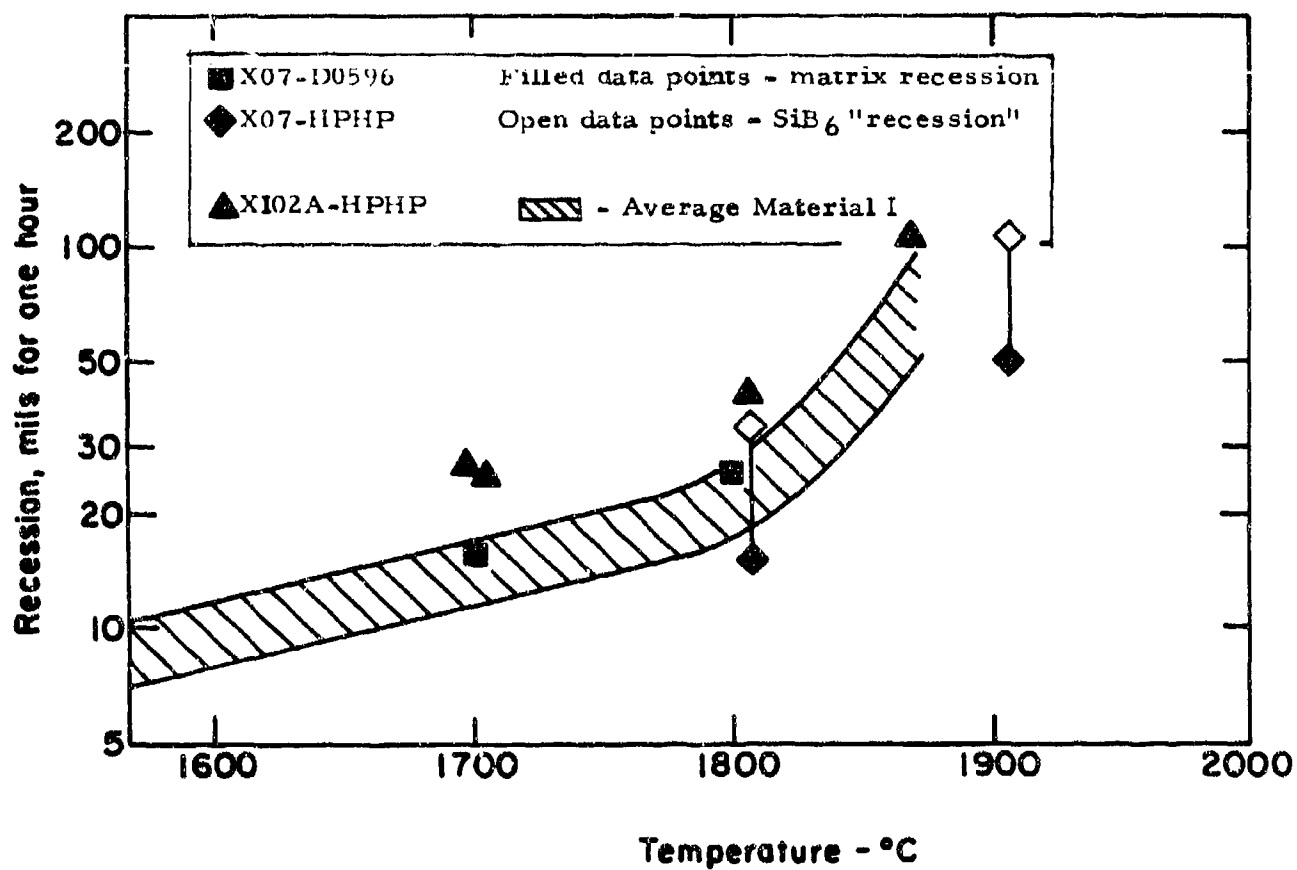


Figure 61. Oxidation Screening: Material X ($\text{ZrF}_2 + 20 \text{ v/o SiB}_6$) and Material XI ($\text{ZrB}_2 + 8 \text{ v/o Cr}$).

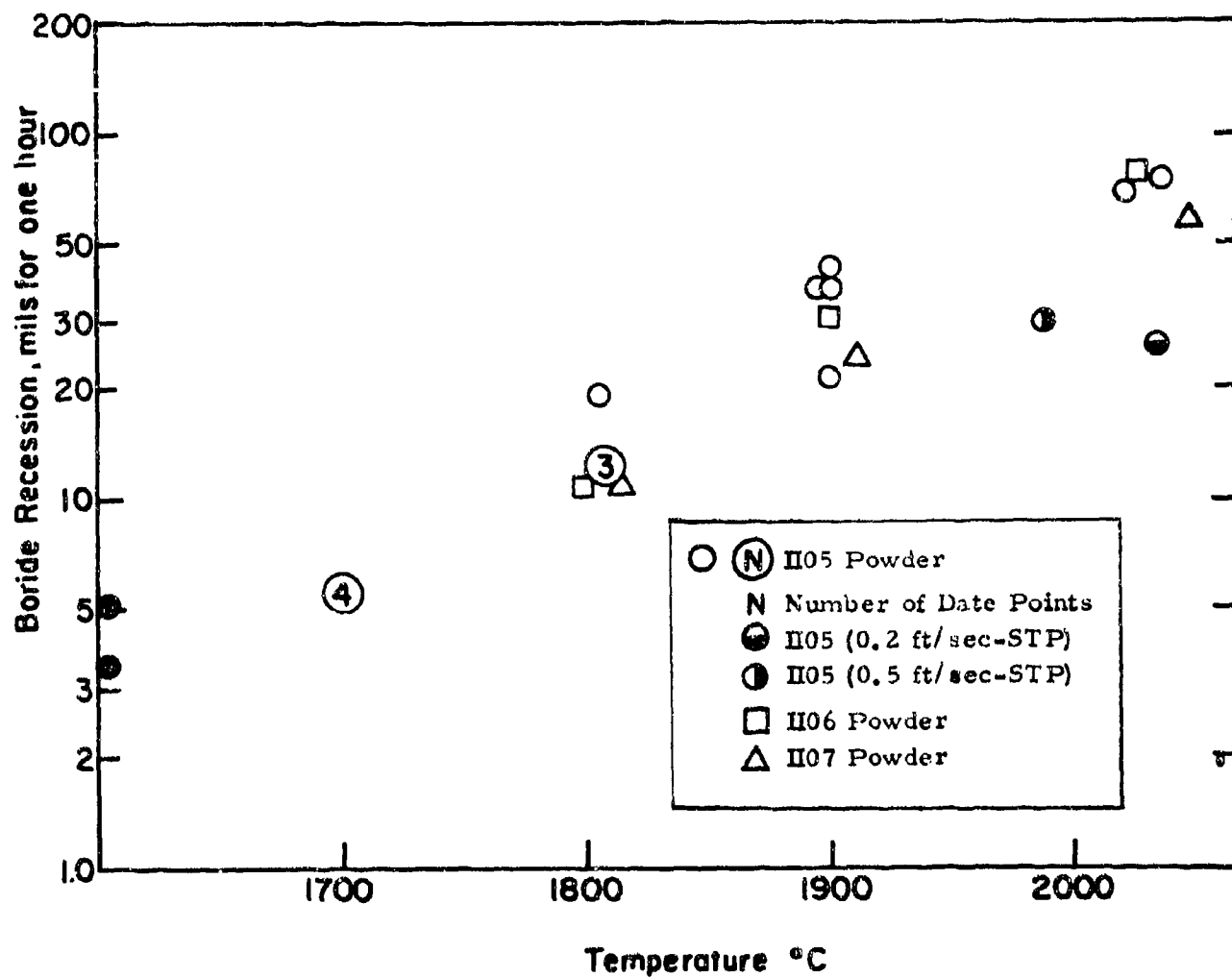


Figure 62. Oxidation Screening: Material II (HfB_2).

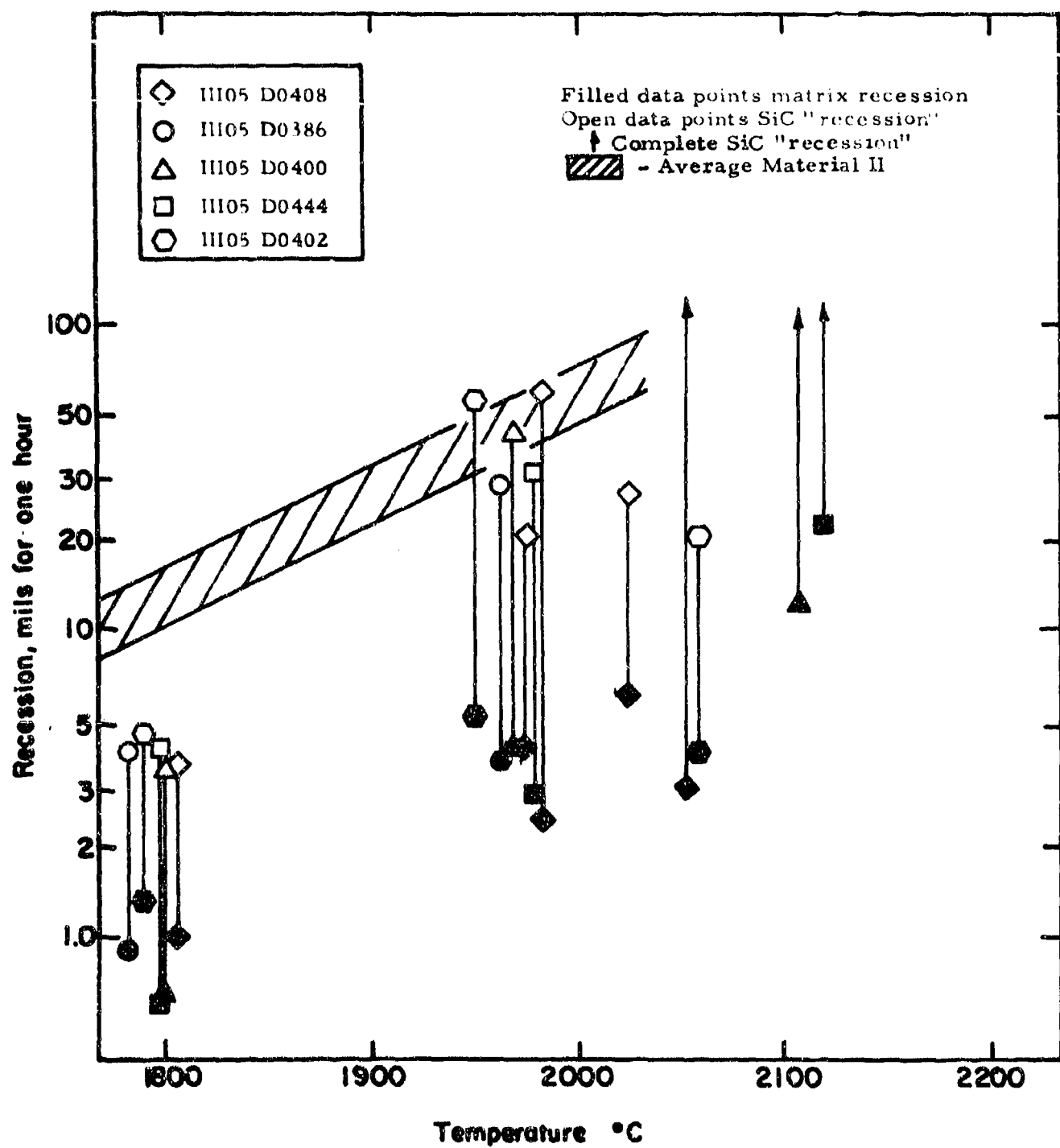


Figure 63. Oxidation Screening: Material III ($\text{HfB}_2 + 20 \text{ v/o SiC}$).

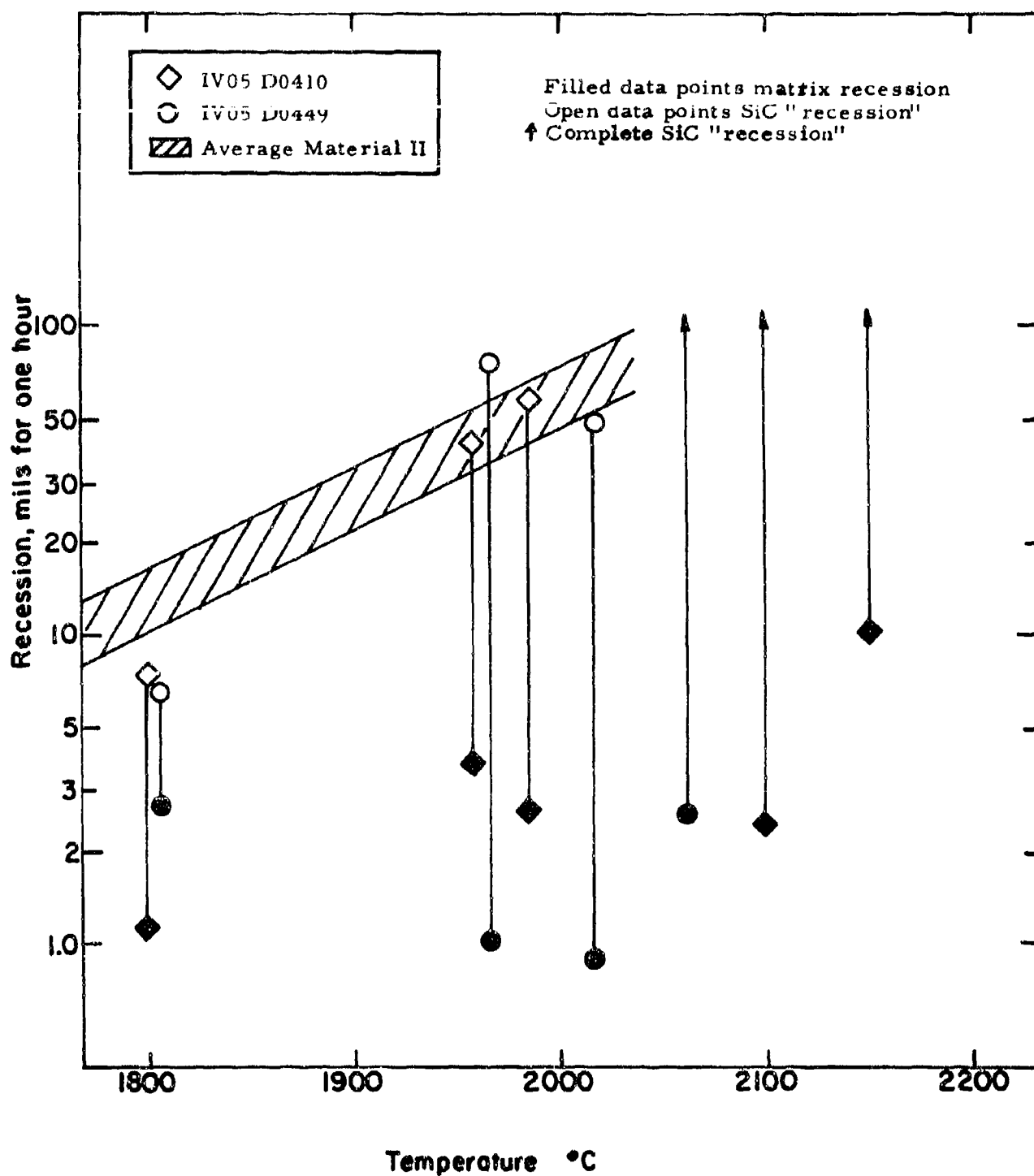


Figure 64. Oxidation Screening: Material IV ($\text{HfB}_2 + 30 \text{ v/o SiC}$).

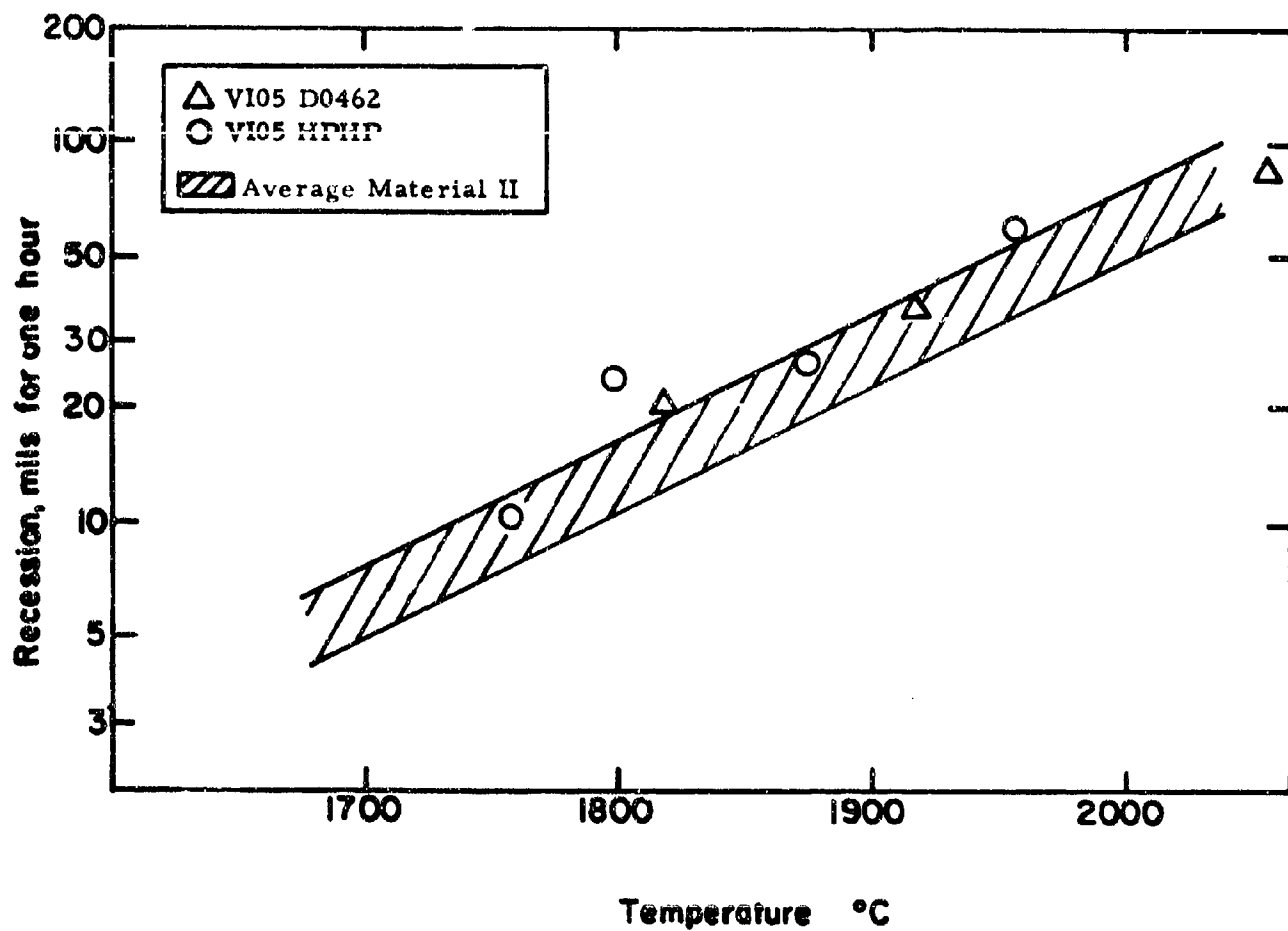
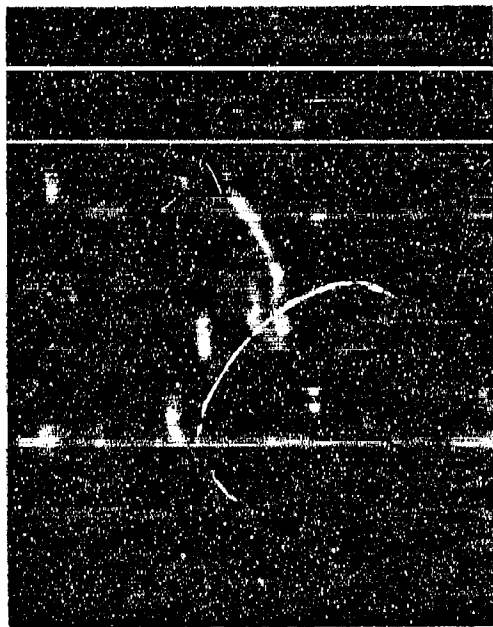


Figure 65. Oxidation Screening: Material VI (HfB_2 + 4 v/o Hf-27 Ta).



1-3321

OX559-1550°C

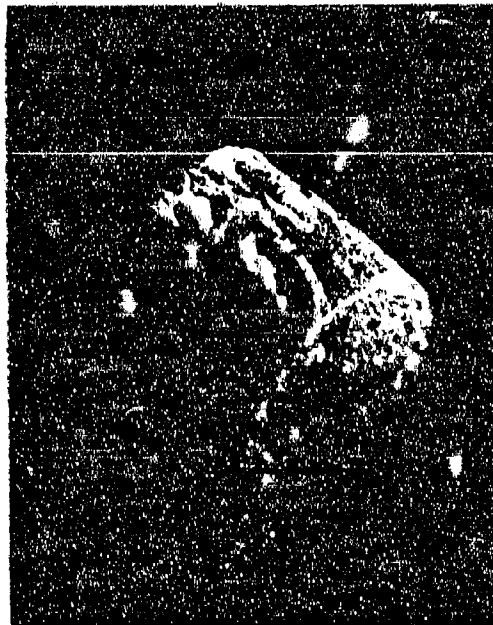
D0326



1-2041

OX295-1700°C

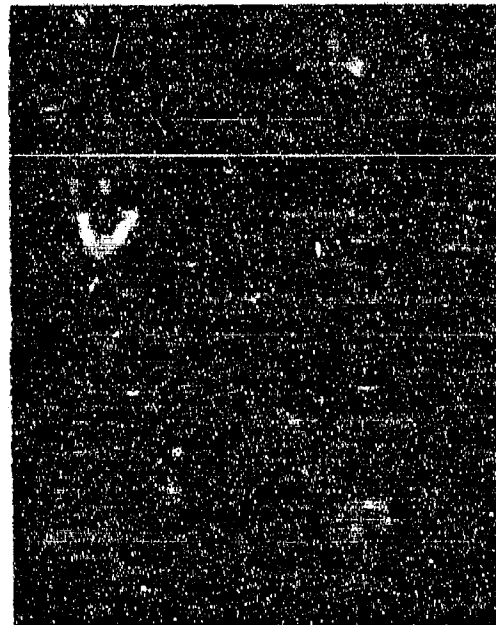
D0345



1-2230

OX335-1810°C

D0345

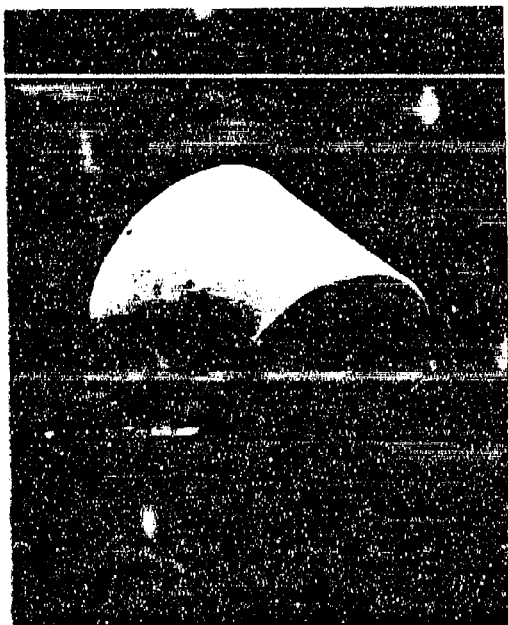


1-3042

OX497-1850°C (30 min.)

D0345

Figure 66. Oxidation Screening, Material I02A: Macrophotographs.



1-3327

OX561-1600°C

D0309



1-1831

OX255-1700°C

D0309



1-2074

OX309-1810°C

D0309

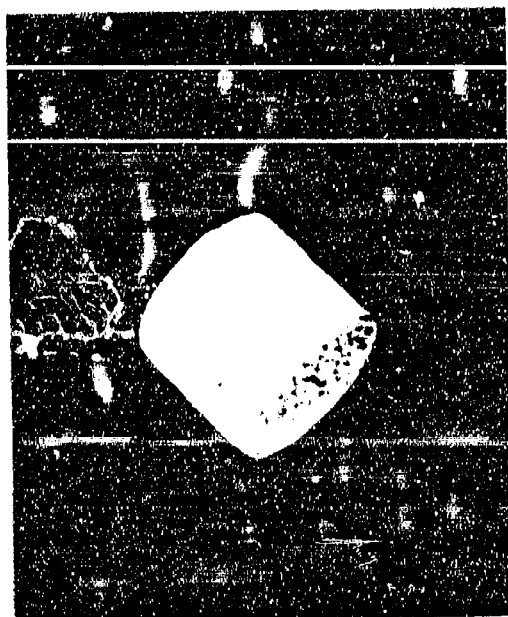


1-2284

OX332-1850°C(30 min.)

D0309

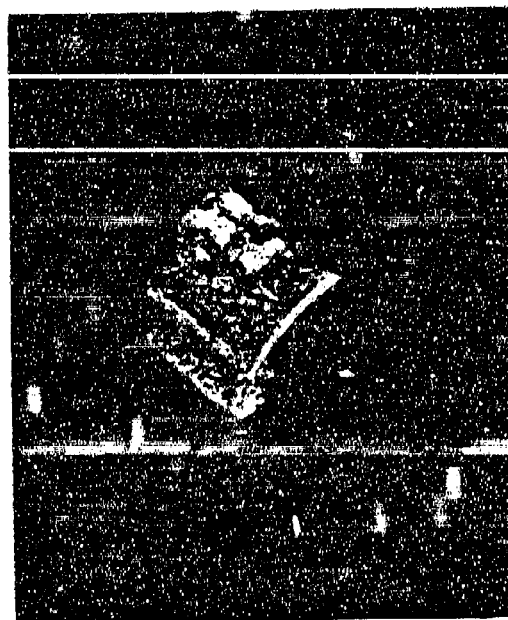
Figure 67. Oxidation Screening, Material I03A: Macrophotographs.



1-5733

D0590

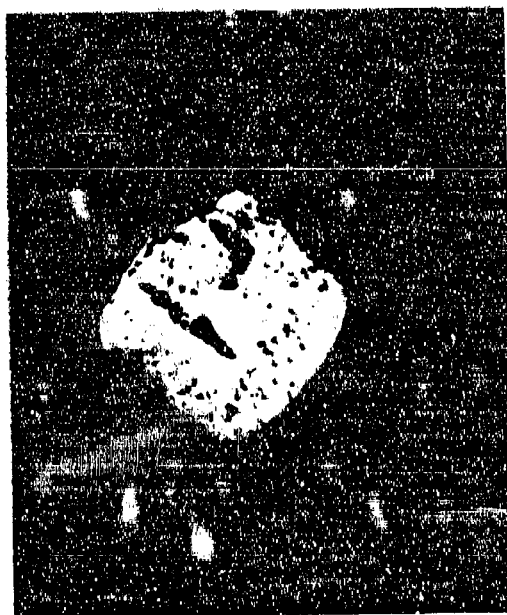
OX899-1700°C



1-6247

D0590

OX1020-1770°C



1-5738

D0590

OX901-1800°C



1-5728

D0590

OX897-1850°C(30 min.)

Figure 68. Oxidation Screening, Material 105A: Macrophotographs.



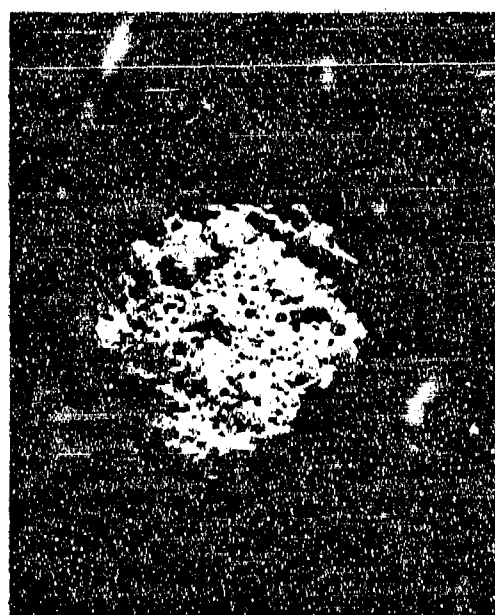
1-5712 D0589
OX894-1700°C



1-6238 D0589
OX1017-1770°C



1-5717 D0589
OX895-1800°C



1-5722 D0589
OX896-1850°C (30 min.)

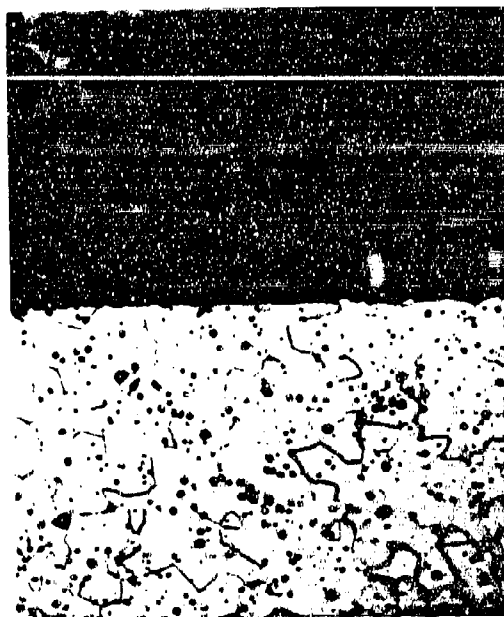
Figure 69. Oxidation Screening, Material 107: Macro photographs.



1-4218

OX559-1550°C

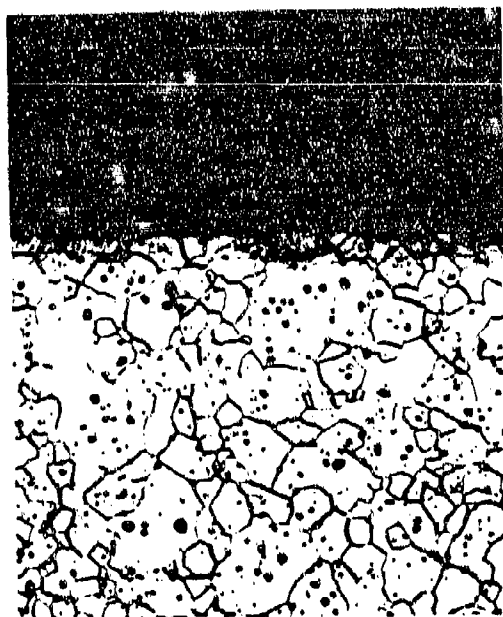
D0326



1-2043

OX295-1700°C

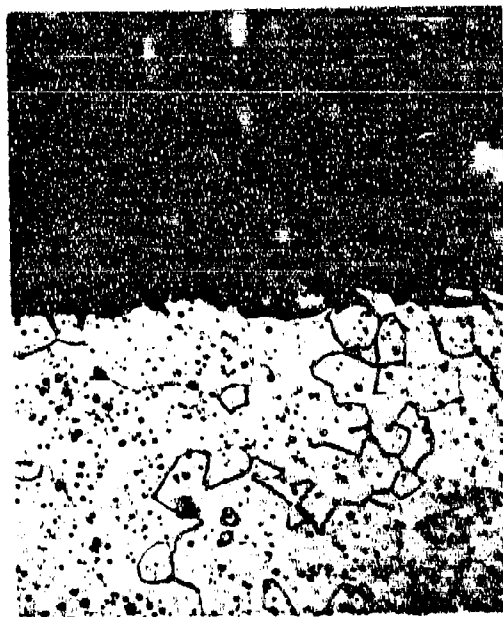
D0345



1-2232

OX335-1810°C

D0345

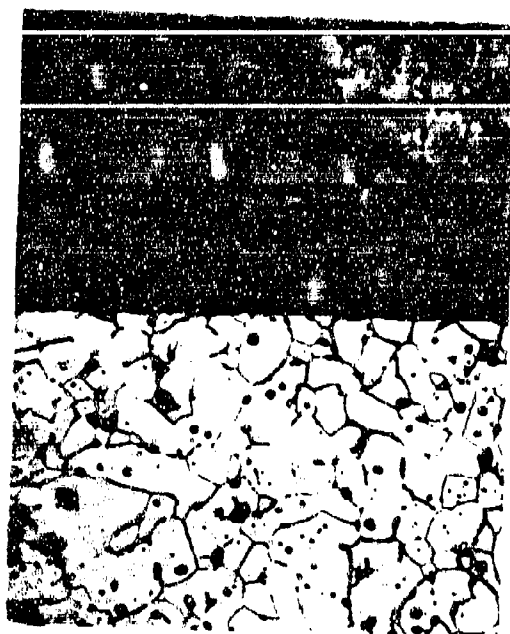


1-4217

OX497-1850°C(30 min.)

D0345

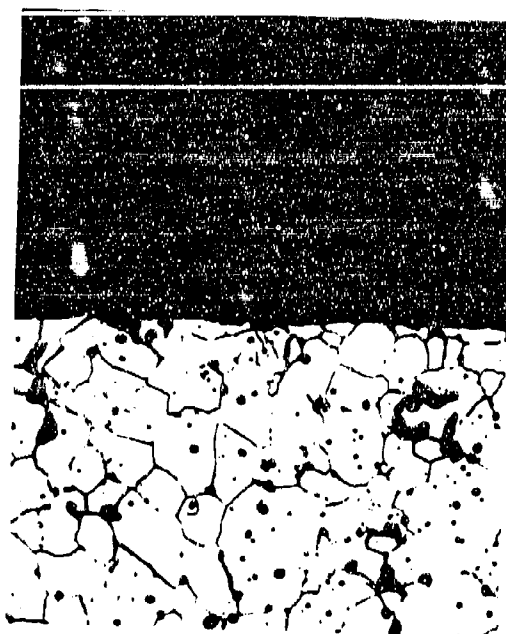
Figure 70. Oxidation Screening, Material 102A: Oxide-Matrix Interfaces, 250X.



1-4216

OX561-1600°C

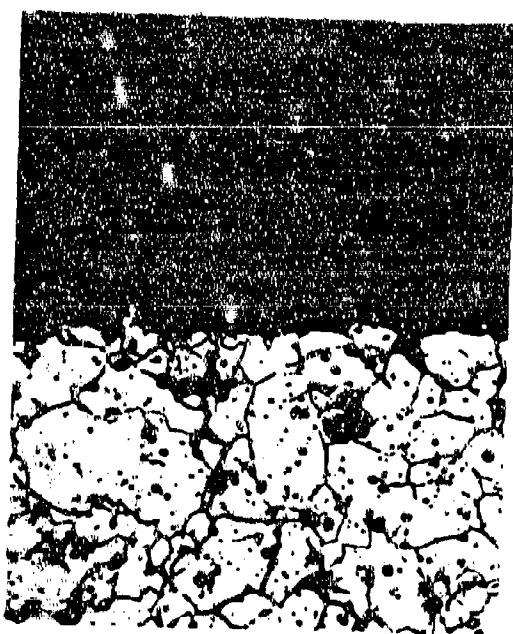
D0309



1-1833

OX255-1700°C

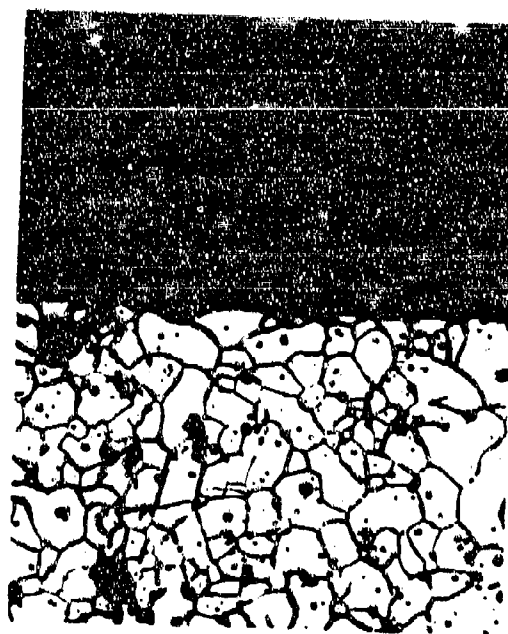
D0309



1-2076

OX309-1810°C

D0309

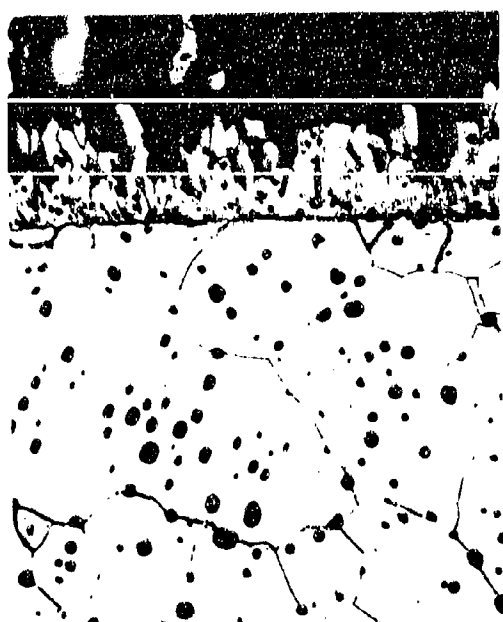


1-2286

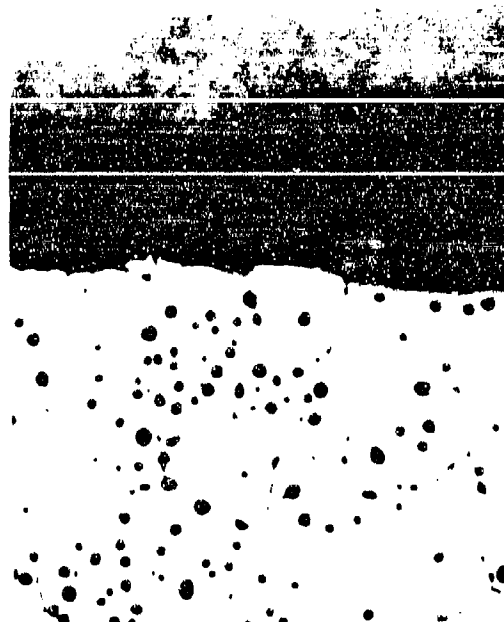
OX332-1850°C(30 min.)

D0309

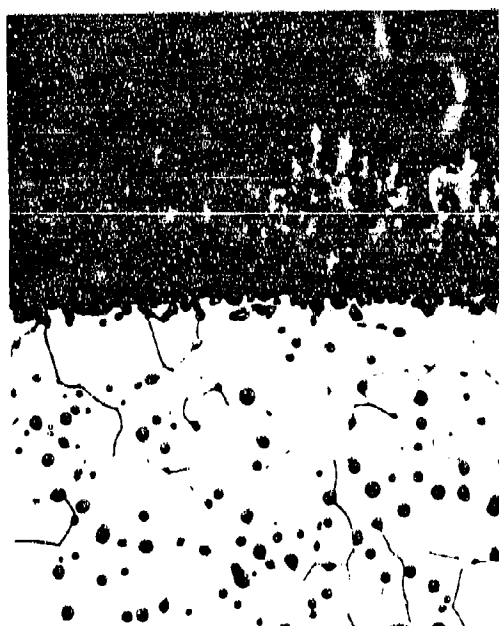
Figure 71. Oxidation Screening, Material 103A: Oxide-Matrix Interfaces, 250X.



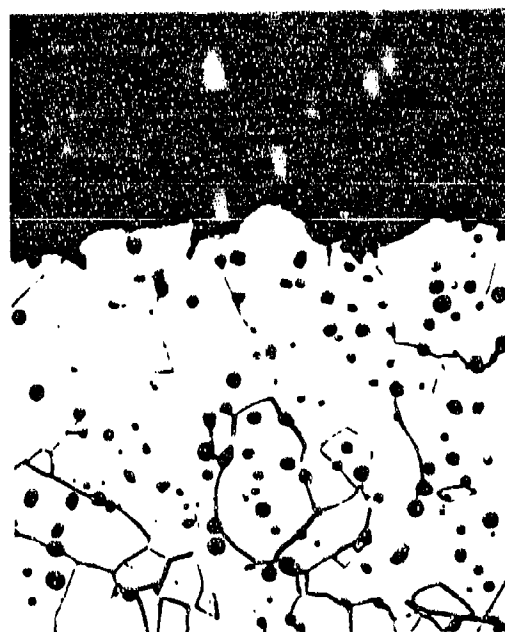
1-5735 I05A-D0590
OX899-1700°C



1-5730 I05A-D0590
OX897-1850°C (30 min.)

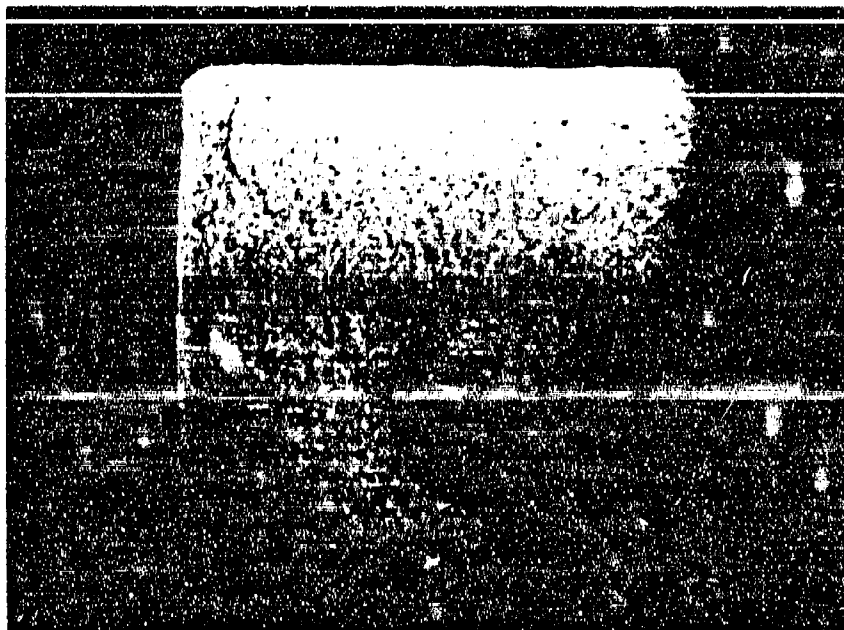


1-5714 I07-D0589
OX894-1700°C



1-5724 I07-D0589
OX896-1850°C (30 min.)

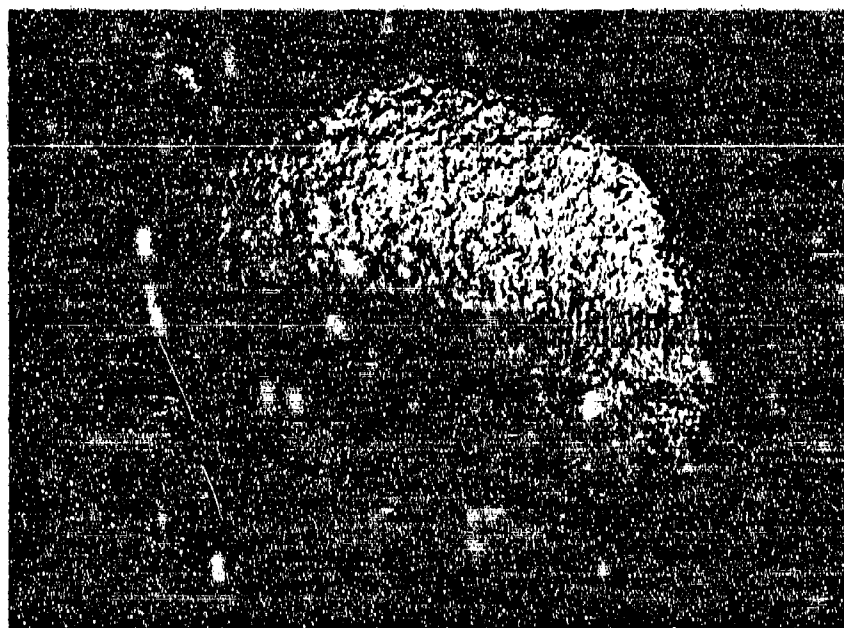
Figure 72. Oxidation Screening, Materials I05A and I07: Oxide-Matrix Interfaces, 250X.



1-2042

Longitudinal

OX295

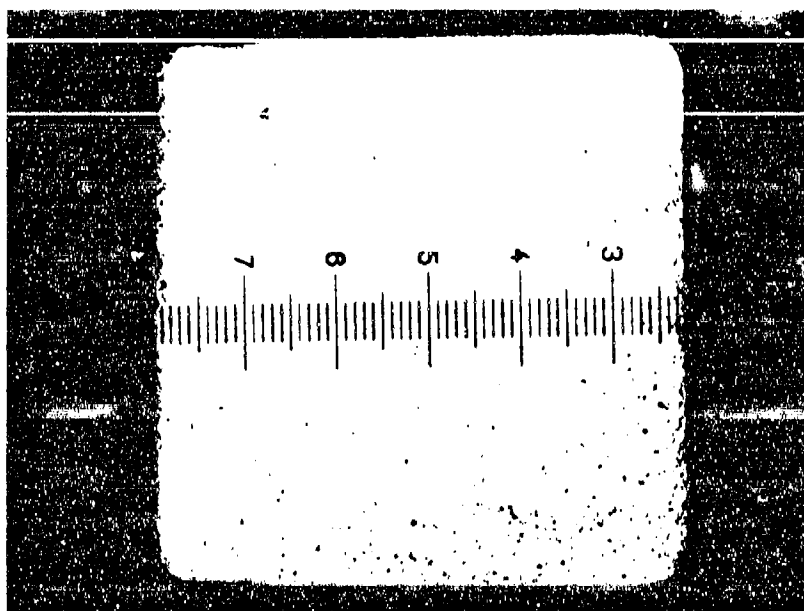


1-2045

Transverse

OX295

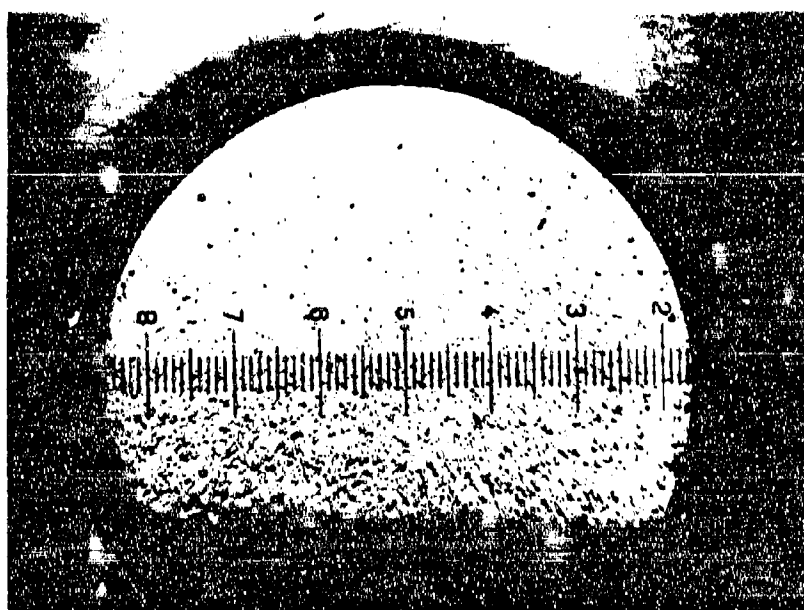
Figure 73. Oxidation Screening, Material I02A: Reticule Photographs (1 div. = 4.86 mils), D0345, 1700°C.



1-1832

Longitudinal

OX255

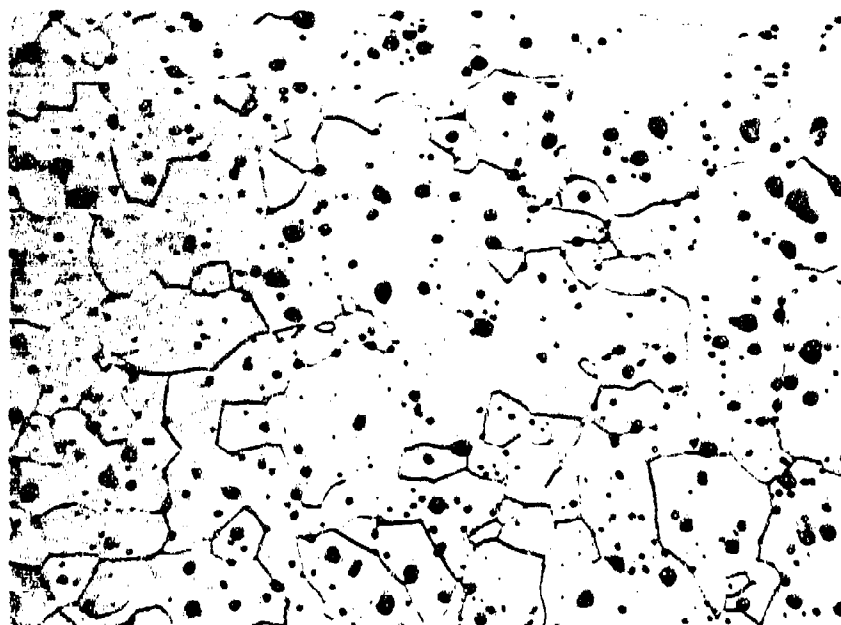


1-1835

Transverse

OX255

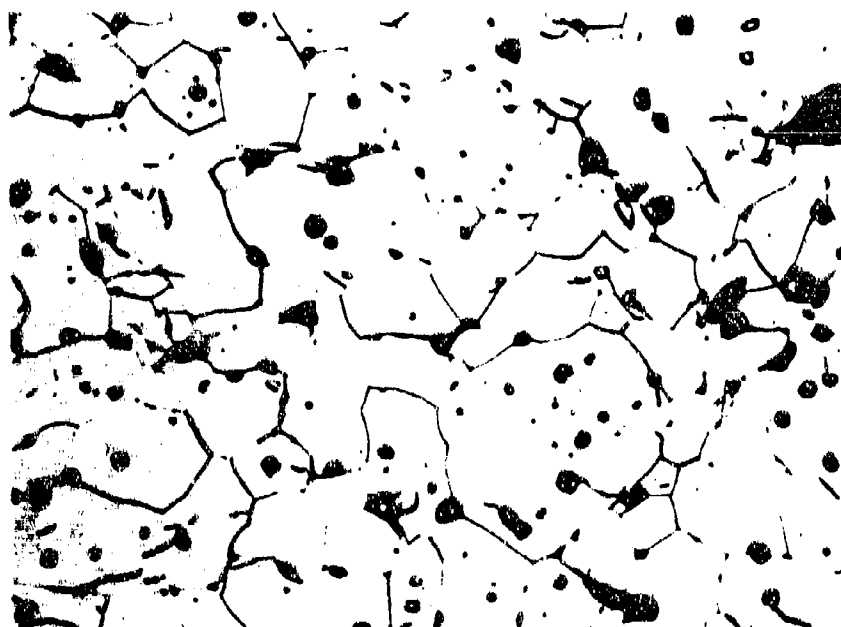
Figure 74. Oxidation Screening, Material I03A: Reticule Photographs (1 div. = 4.86 mils), D0309, 1700°C.



1-2044

102A-D0345

OX295

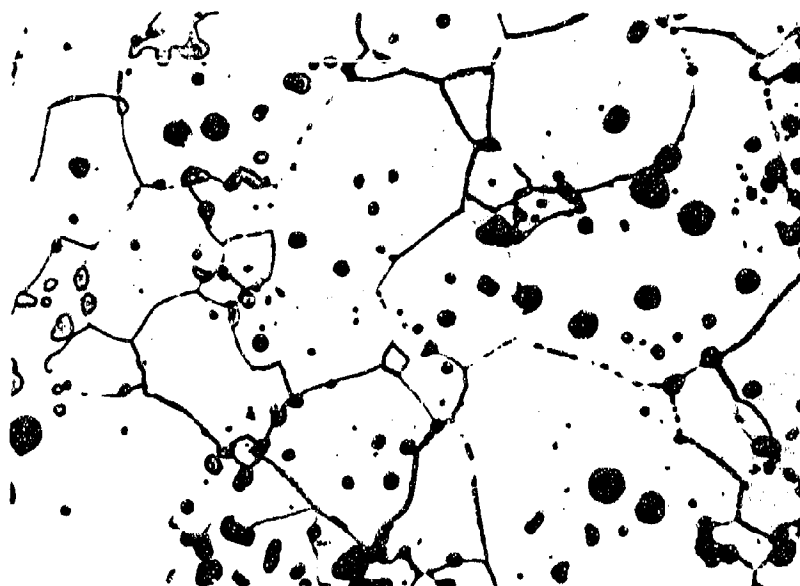


1-1834

103A-D0309

OX255

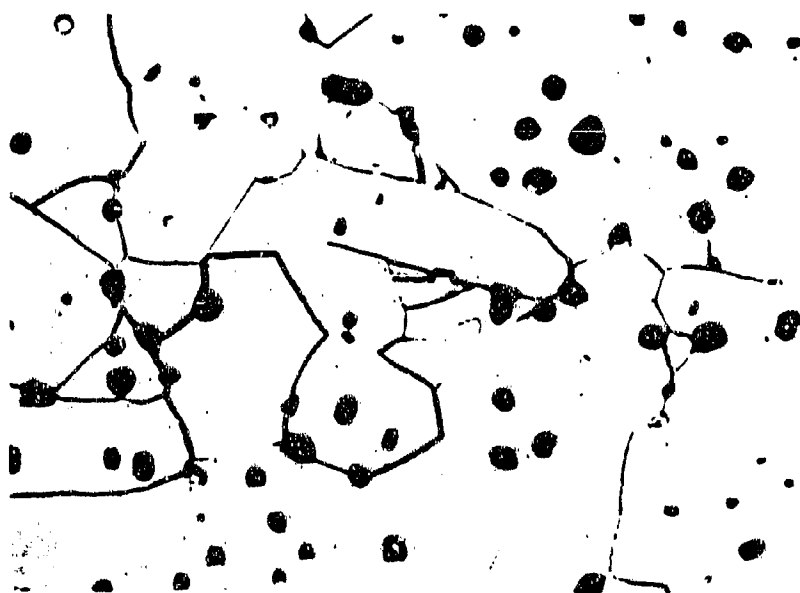
Figure 75. Oxidation Screening, Material I: Representative Matrix Photographs, 1700°C, 500X.



1-5731

I05A-D0590

OX897

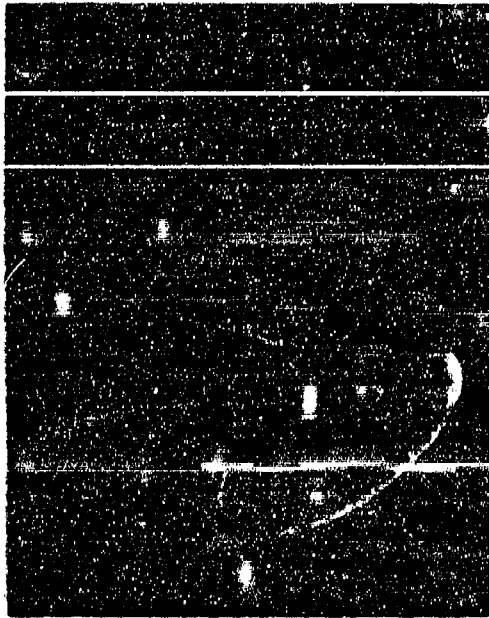


1-5725

I07-D0589

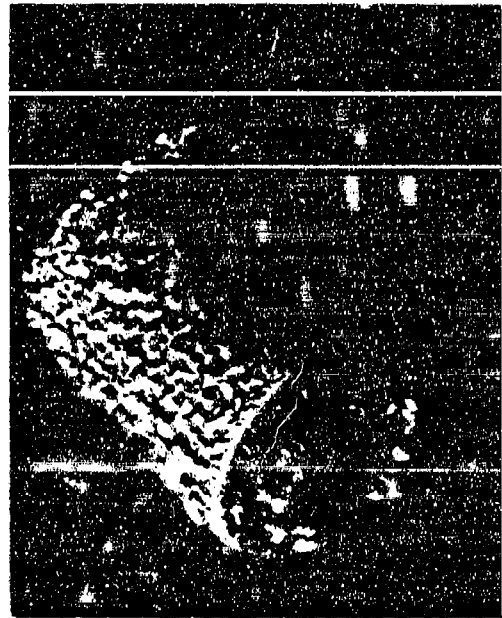
OX896

Figure 76. Oxidation Screening; Material I: Representative Matrix Photographs, 1850°C (30 min.), 500X.



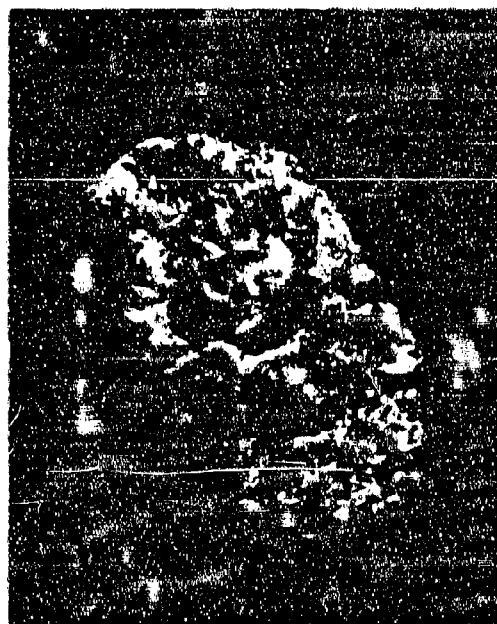
1-1350

OX155 - 1550°C



1-1357

OX156 - 1730°C



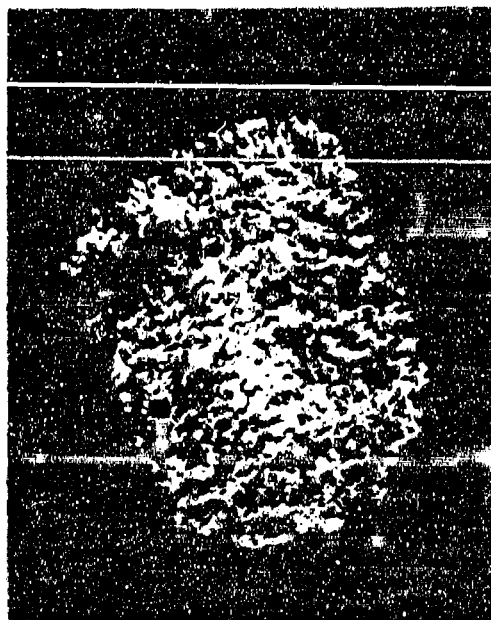
1-1364

OX157 - 1820°C (30 min.)

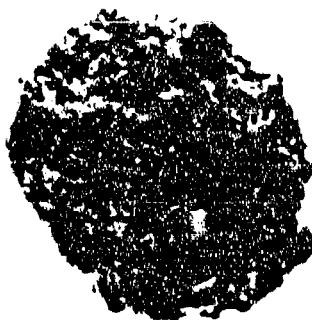
Figure 77. Oxidation Comparison, Carborundum ZrB_2 : Macrophotographs.



1-1111
OX113-1540°C



1-1233
OX132-1740°C



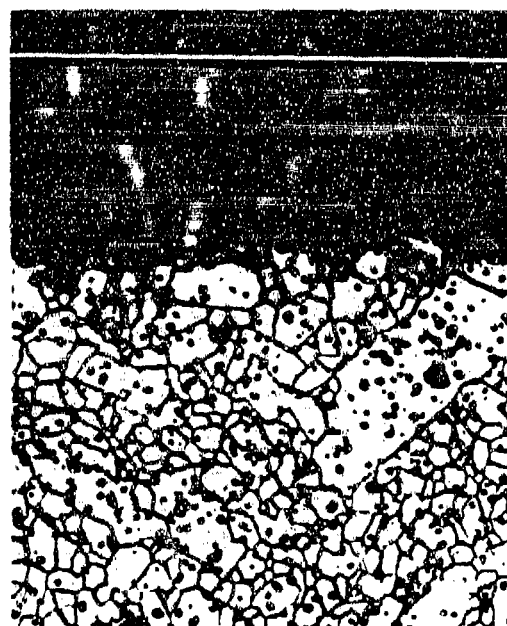
1-1125 OX115-1880°C(30 min.)

Figure 78. Oxidation Comparison, Norton ZrB_2 : Macrophotographs.



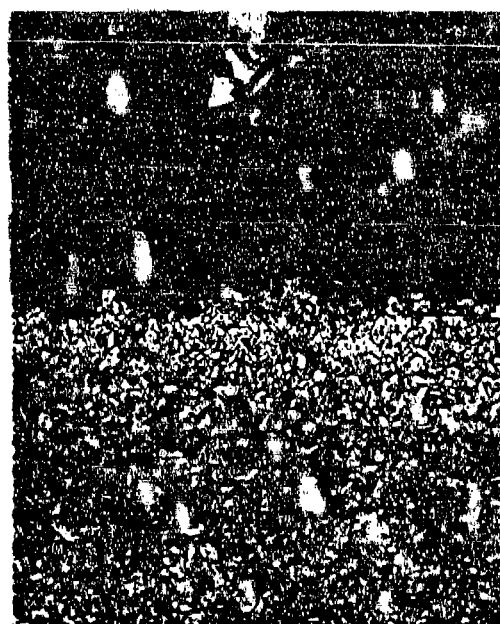
1-1355

OX155-1550°C



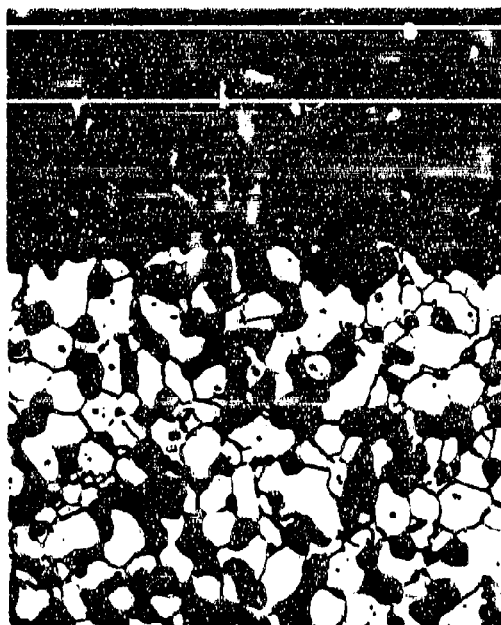
1-1359

OX156-1730°C



1-1366 OX157-1820°C(30 min.) (50X)

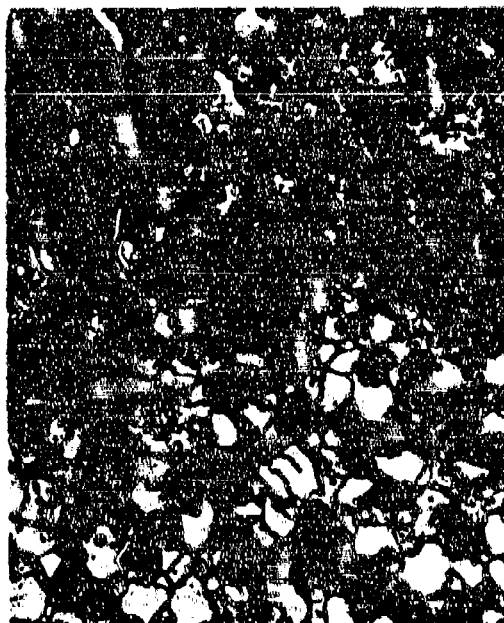
Figure 79. Oxidation Comparison, Carborundum ZrB_2 : Oxide-Matrix Interfaces, 250X.



1-113
OX113-1540°C



1-1235
OX132-1740°C



1-1127
OX115-1880°C(30 min.)

Figure 80. Oxidation Comparison, Norton ZrB_2 : Oxide-Matrix Interfaces, 250X.



1-2245

OX330-1800°C

D0372



1-2273

OX343-1960°C

D0372



1-2399

OX352-2060°C

D0372

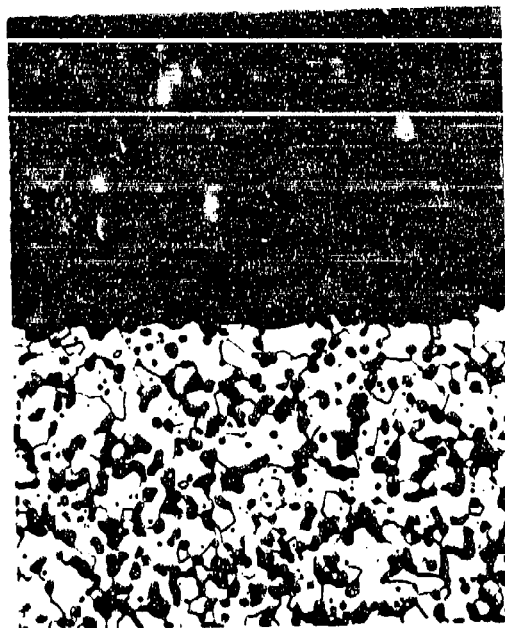
Figure 81. Oxidation Screening, Material V02A: Macrophotographs.



1-2246

OX330-1800°C

D0372



1-2272

OX343-1960°C

D0372



1-2401

OX352-2060°C

D0372

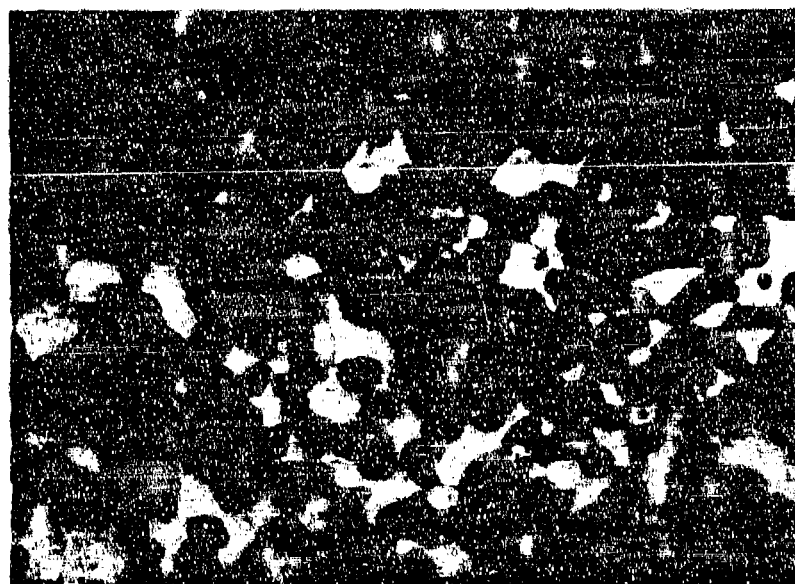
Figure 82. Oxidation Screening, Material V02A: Oxide-Matrix Interface, 250X.



1-3871

Interface

250X



1-3872

Interface

500X

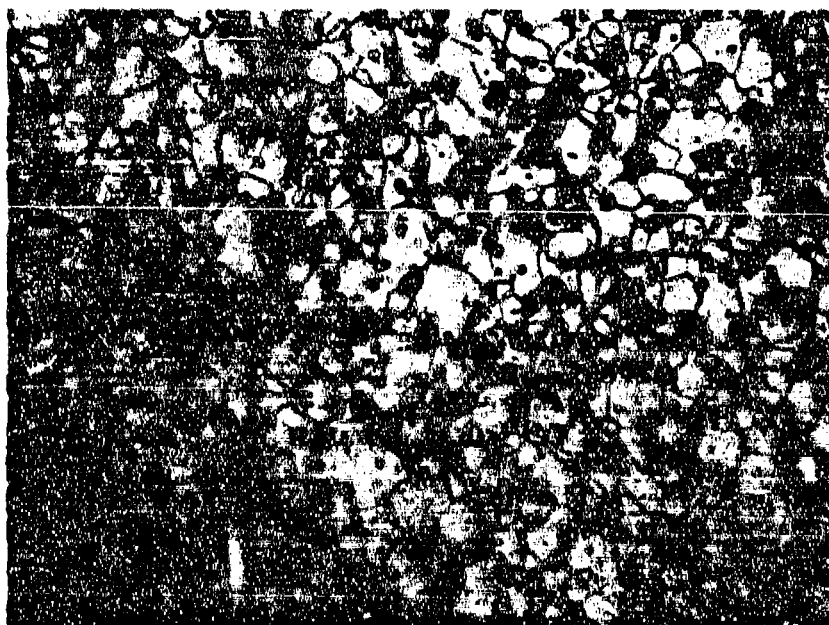
Figure 83. Oxidation Screening, Material V07: D0580K, OX635-2100°C.



1-2276

Interface

160X

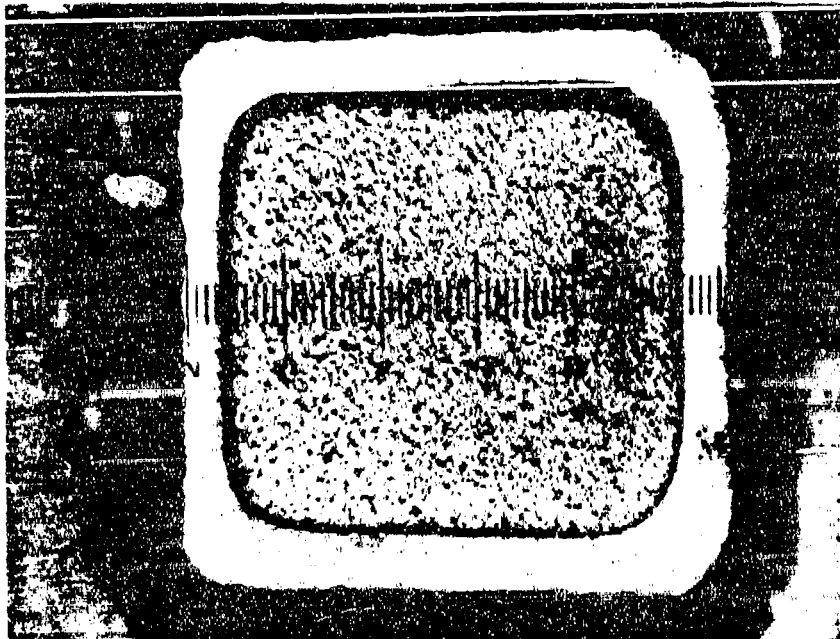


1-2275

Matrix

500X

Figure 84. Oxidation Screening, Material V02A: D0372, OX343, 1960°C.



1-2274

Longitudinal

OX343



1-2277

Transverse

OX343

Figure 85. Oxidation Screening, Material V02A: Reticule Photographs (1 div. = 4.86 mils), D0372, 1960°C.



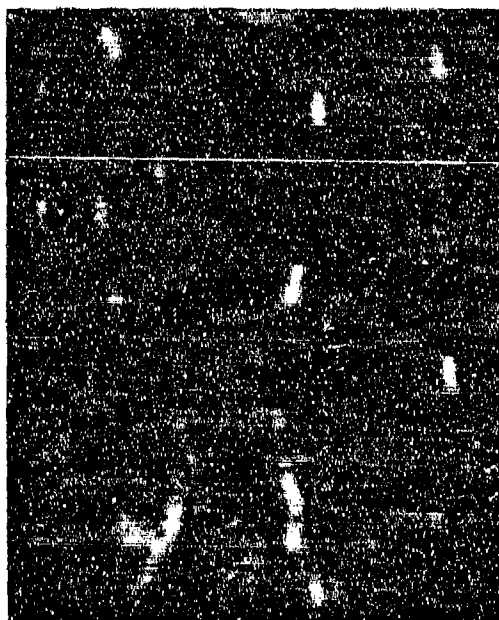
1-3315

OX556-1610°C



1-2893

OX445-1810°C



1-3226

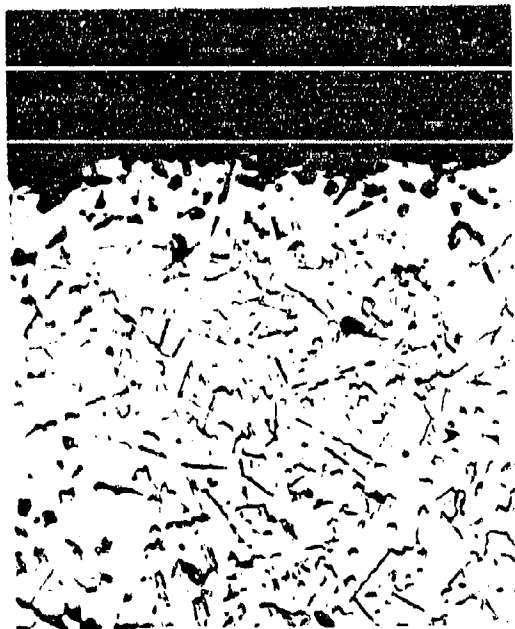
OX530-1910°C



1-3229

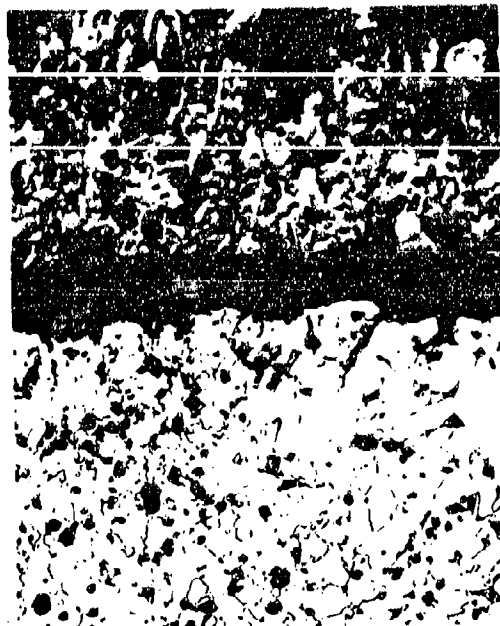
OX531-1950°C

Figure 86. Oxidation Screening, Boride Z: Macrophotographs.



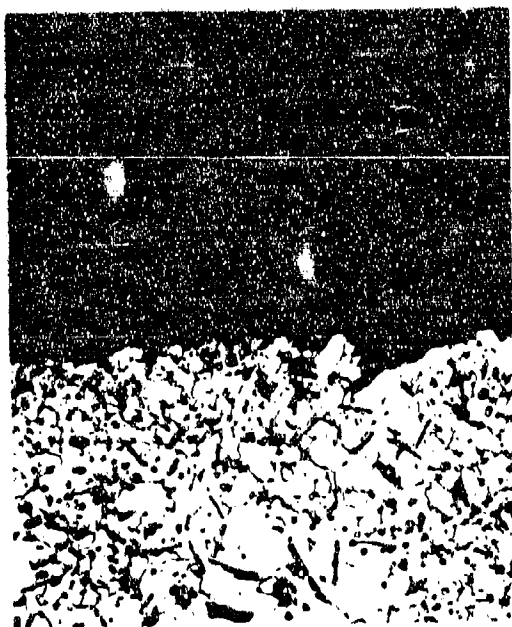
1-4296

OX556-1610°C



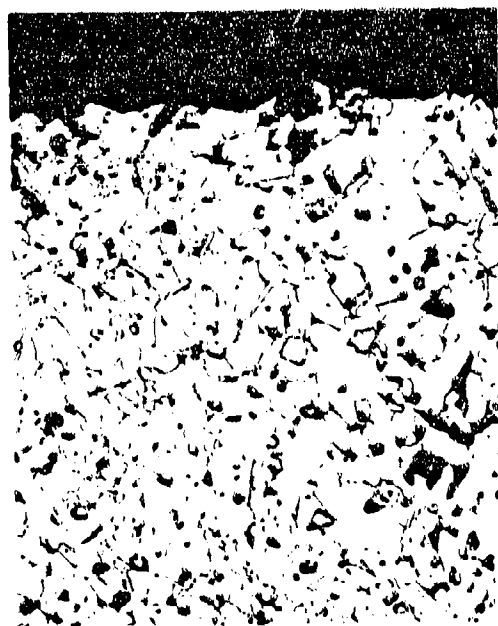
1-2896

OX445-1810°C



1-4299

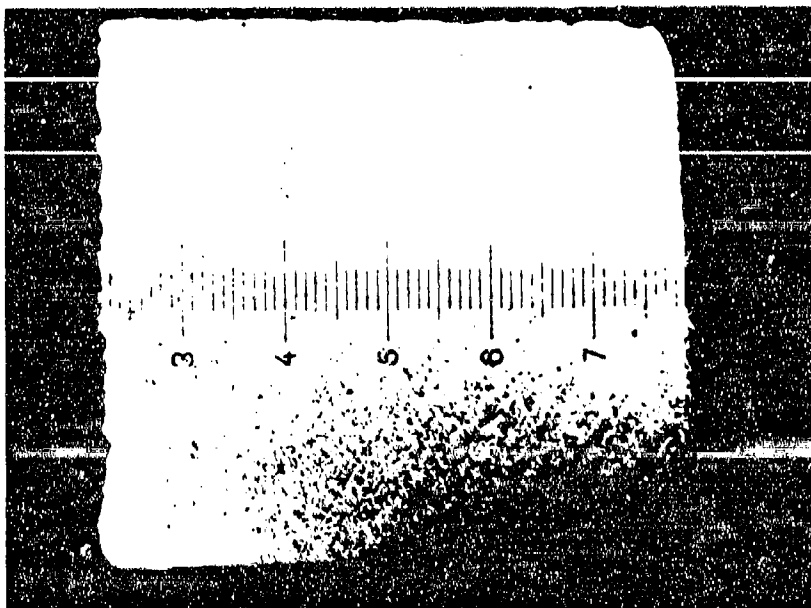
OX530-1910°C



1-4298

OX531-1950°C

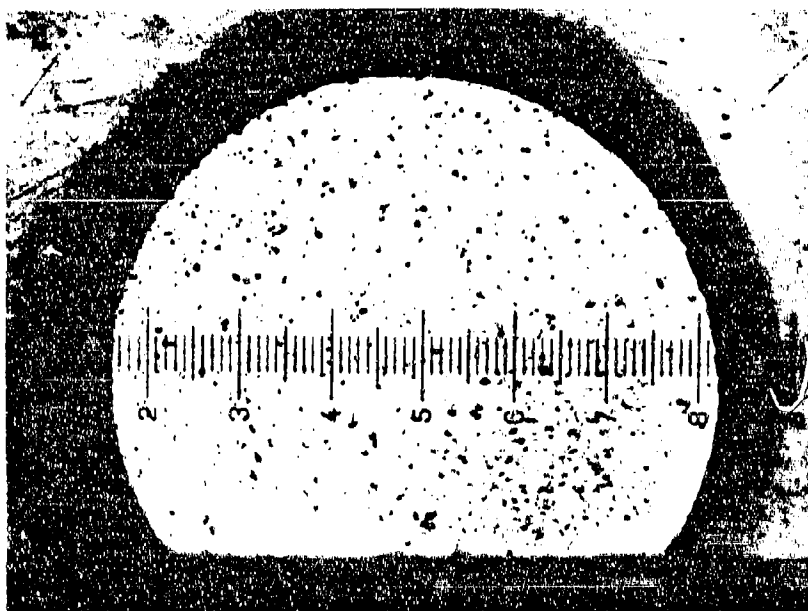
Figure 87. Oxidation Screening, Boride Z: Oxide-Matrix Interfaces, 250X.



1-2894

Longitudinal

OX445

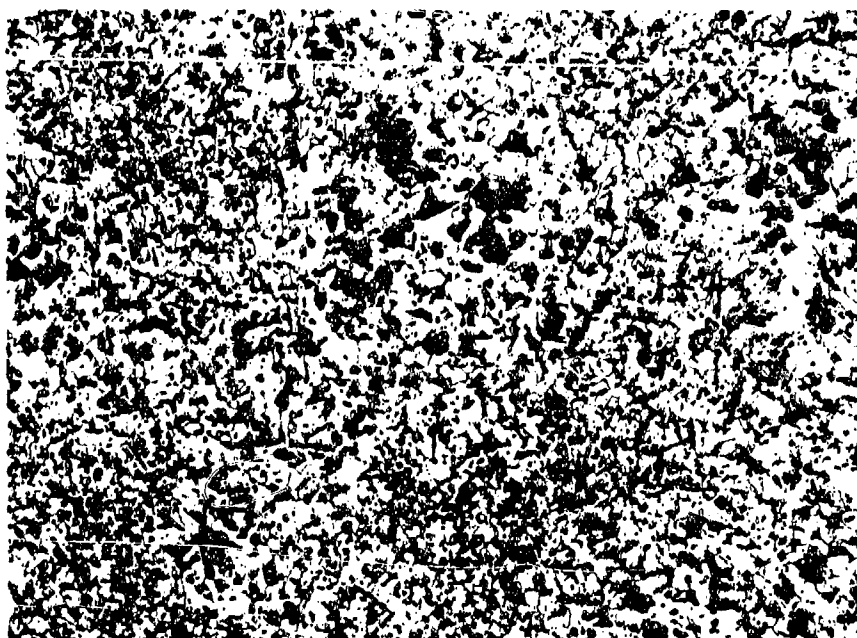


1-2898

Transverse

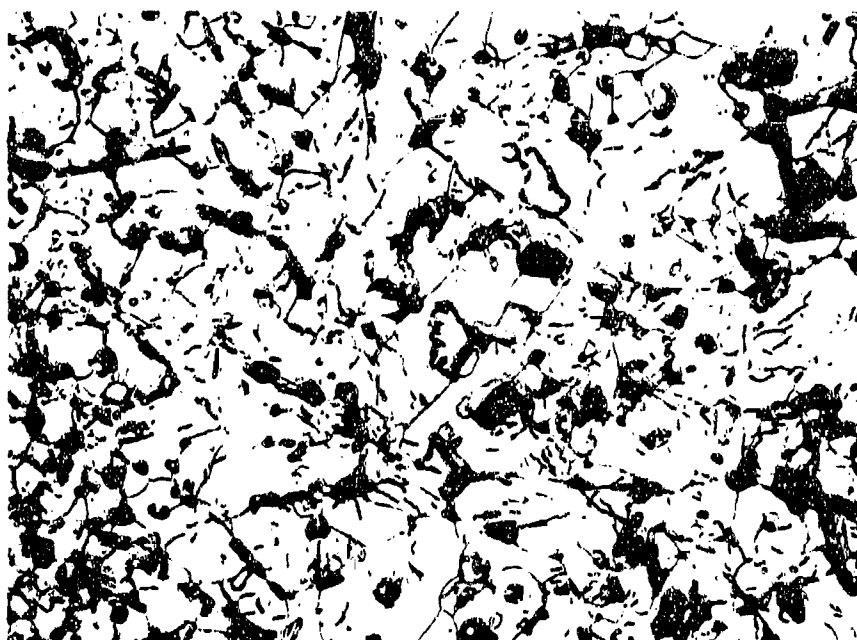
OX445

Figure 88. Oxidation Screening, Boride Z: Reticule Photographs
(1 div. = 4.86 mils), 1810°C.



1-2895

150X



1-2897

500X

Figure 89. Oxidation Screening, Boride Z: Representative Matrix Photographs, 1810°C.



1-3832

OX623-1820°C

D0498



1-3840

OX627-1980°C

D0498



1-5782

OX916-1800°C

D0592

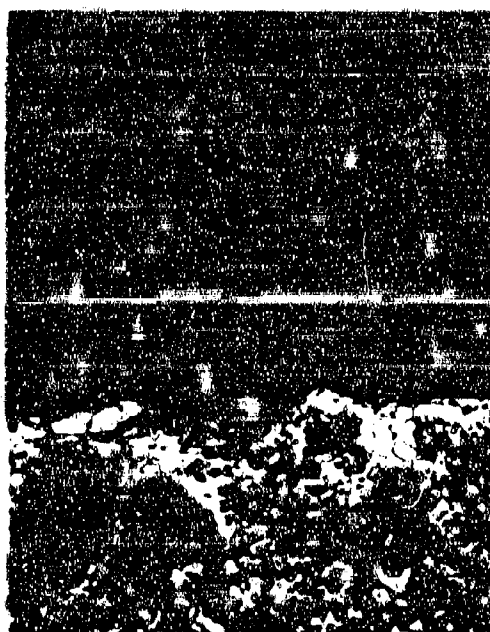


1-5776

OX915-1970°C

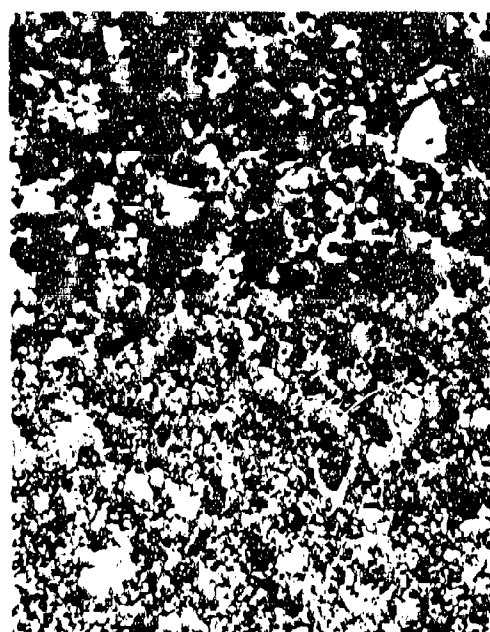
D0592

Figure 90. Oxidation Screening, Material VIII: Macrophotographs.



1-3842

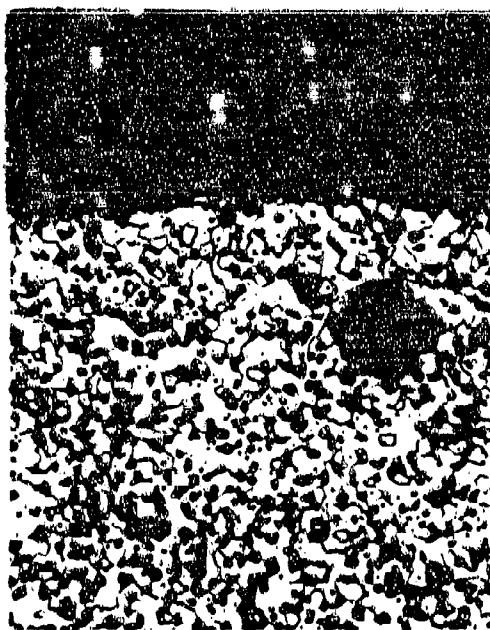
D0498



1-3843

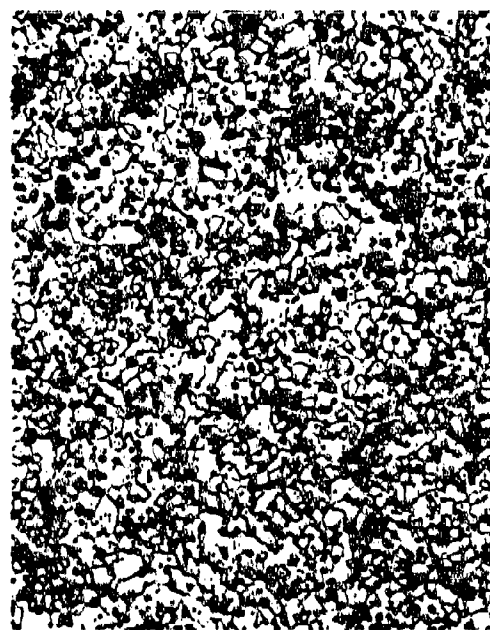
D0498

OX627-1980°C



1-5778

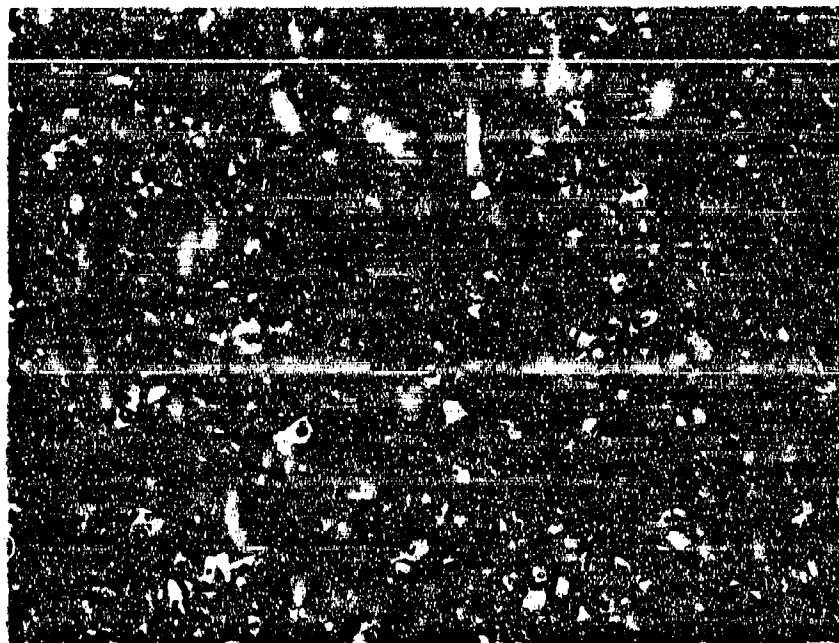
D0592



1-5779

D0592

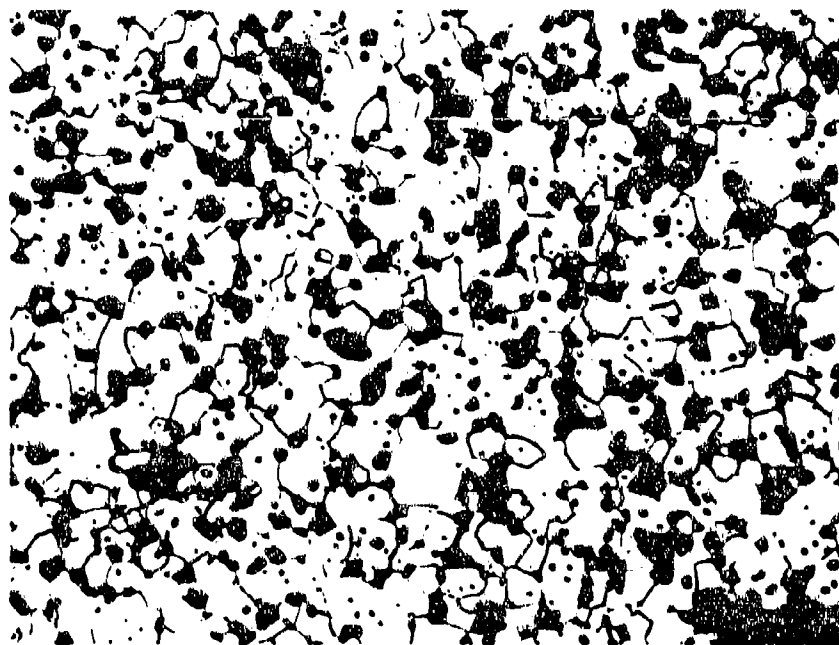
Figure 91. Oxidation Screening, Material VIII: Depleted Matrix-Oxide Interfaces (Left) and Matrix-Depleted Matrix Interfaces (Right), 250X.



1-3844

OX627-1980°C

D0498

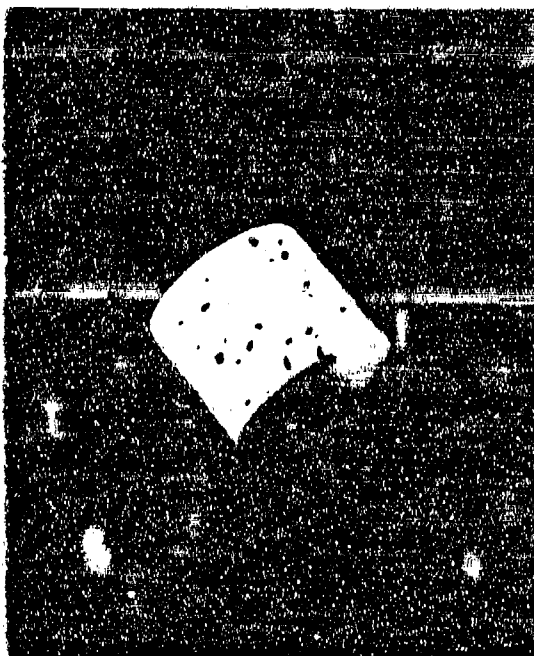


1-5780

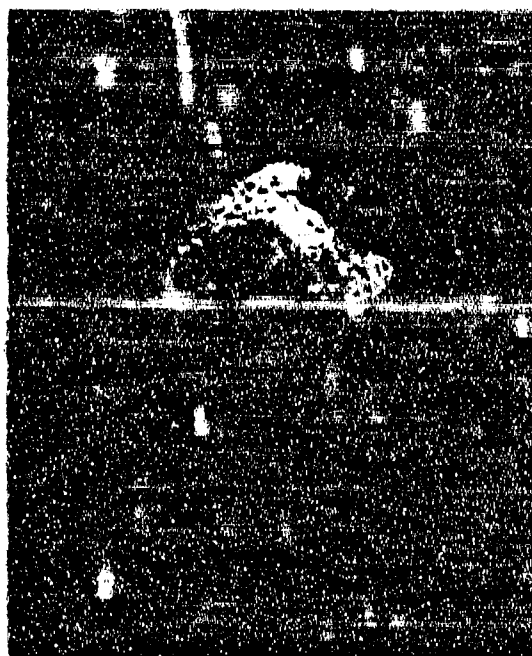
OX915-1970°C

D0592

Figure 92. Oxidation Screening, Material VIII: Representative Matrix Photographs, 500X.



1-5878 XII02A D0561
OX844-1800°C



1-5952 XII(20)07 D0585
OX946-1810°C

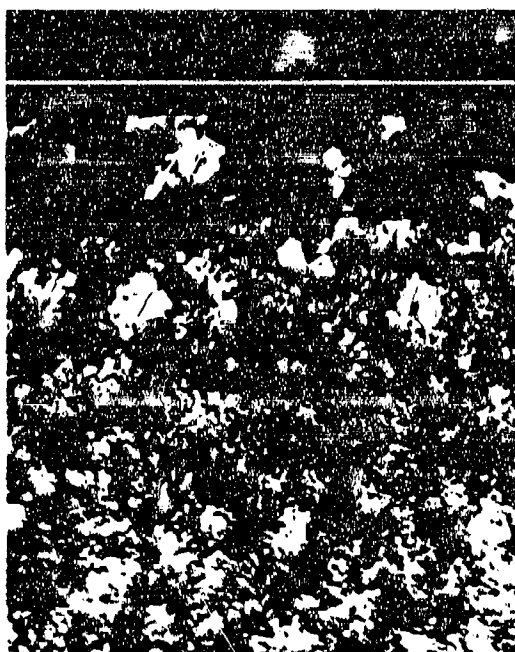


1-5970 XII(20)07 D0585
OX950-1860°C(30 min.)



1-5959 XII(05)03A D0572
OX947-1810°C

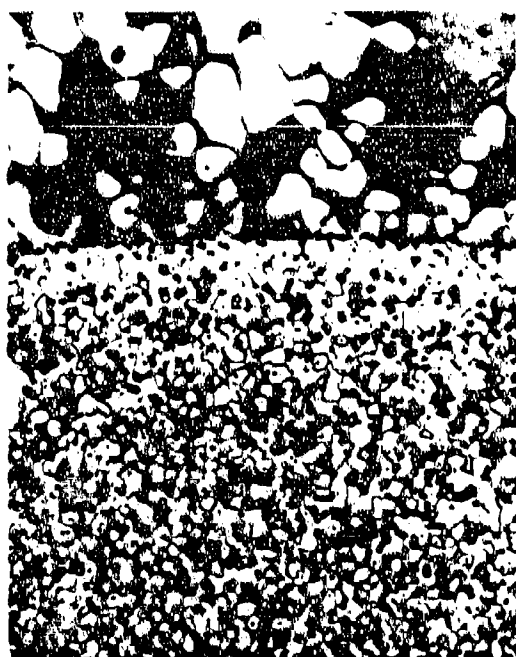
Figure 93. Oxidation Screening, Material XII: Macrophotographs.



1-5880 XII02A D0561
OX844-1800°C



1-5954 XII(20)07 D0585
OX846-1810°C

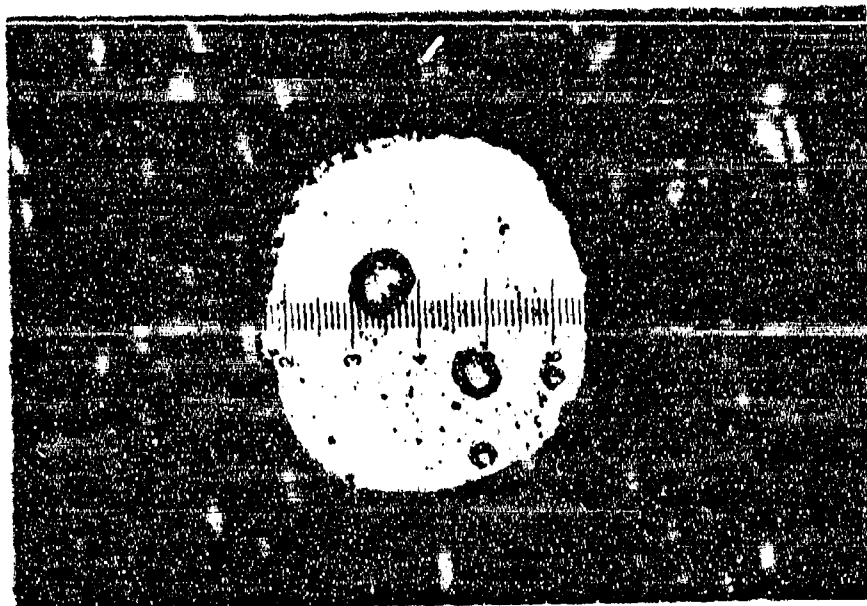


1-5972 XII(20)07 D0585
OX950-1860°C(30 min.)



1-5961 XII(05)03A D0572
OX847-1810°C

Figure 94. Oxidation Screening, Material XII: Matrix-Oxide Interfaces, 250X.

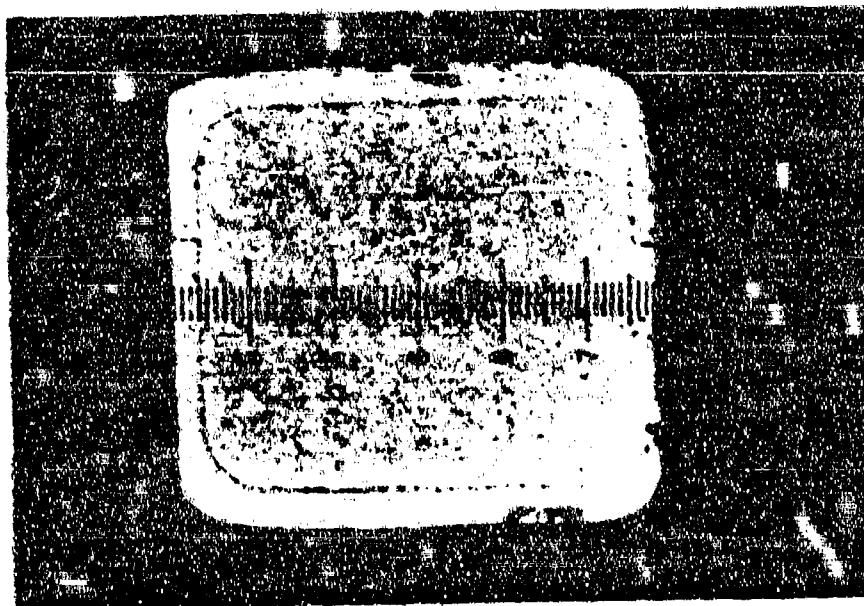


1-5879

(1.97 mils/div.)

XII02A D0561

OX844-1800°C



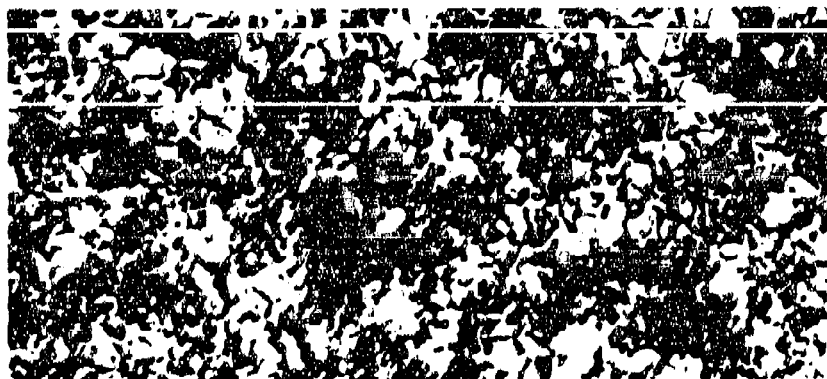
P-5953

(4.86 mils/div.)

XII(20)07 D0585

OX946-1810°C

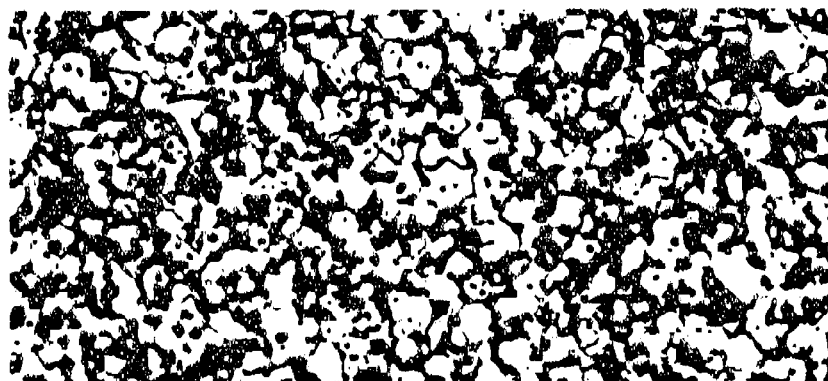
Figure 95. Oxidation Screening, Material XII: Reticule Photographs.



1-5881

OX844-1800°C

XII02A D0561



1-5956

OX946-1810°C

XII(20)07 D0585



1-5962

OX947-1810°C

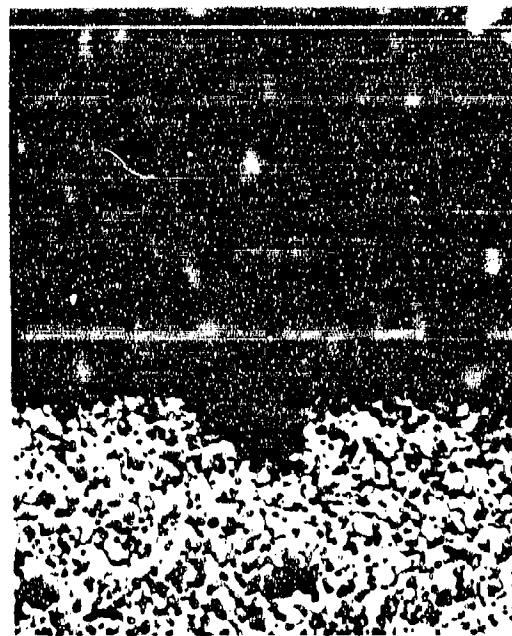
XII(05)03A D0572

Figure 96. Oxidation Screening, Material XII: Representative Matrix Photographs, 500X.



1-5799

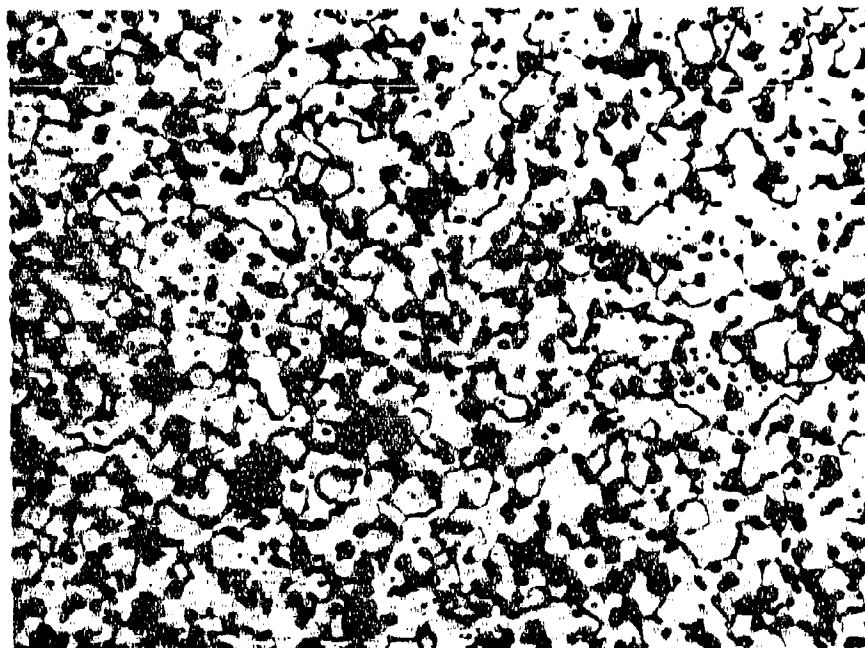
Macrograph



1-5801

Interface

250X



1-5802

Matrix

500X

Figure 97. Oxidation Screening, Material X: Typical Microstructures, Pressing D0596, OX925-1700°C.



1-2623

OX401-1600°C

D0352



1-2378

OX349-1700°C

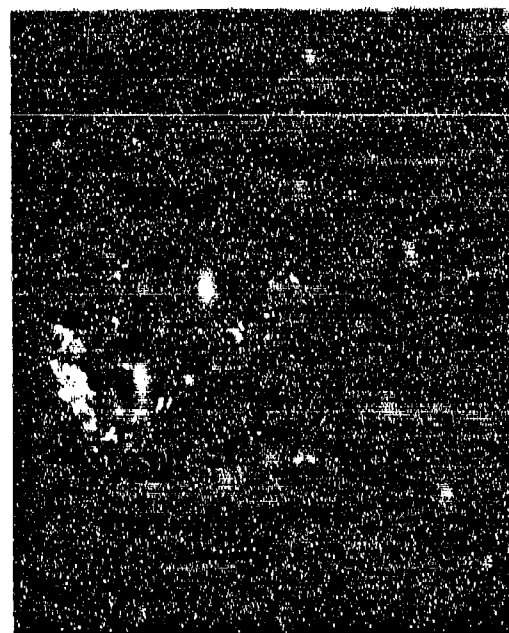
D0352



1-2420

OX366-1810°C

D0352

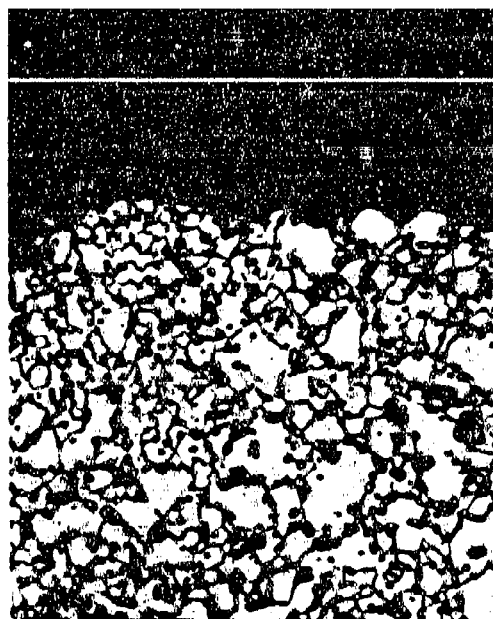


1-2468

OX375-1900°C

D0352

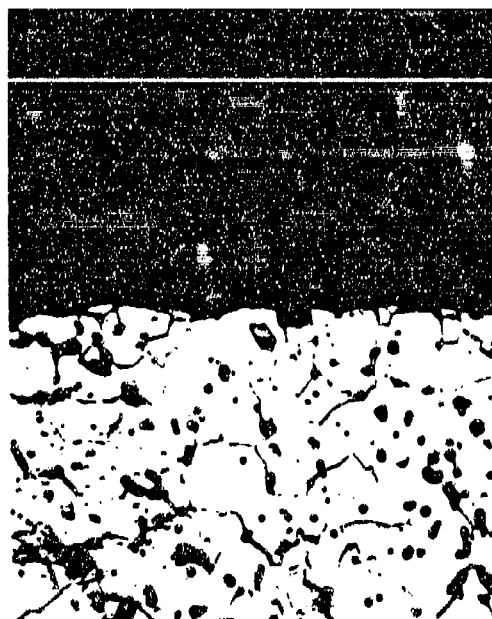
Figure 98. Oxidation Screening, Material II05: Macrophotographs.



1-4209

OX401-1600°C

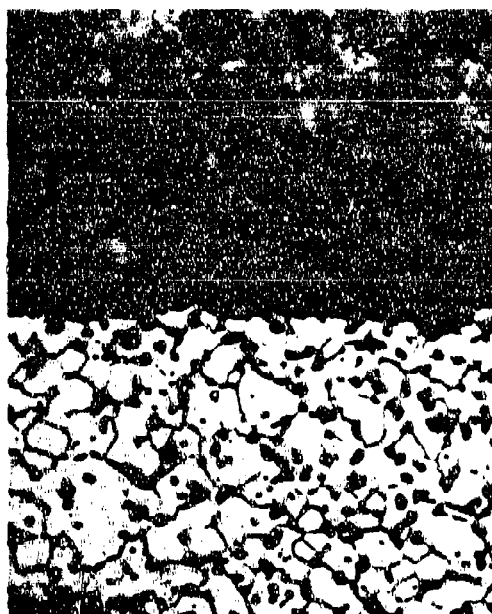
D0352



1-4297

OX349-1700°C

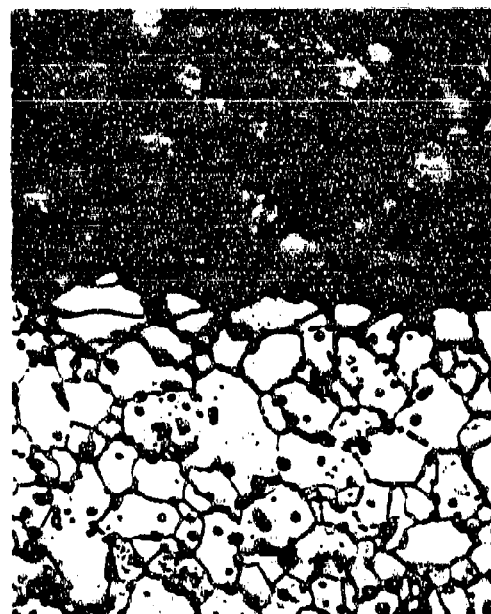
D0352



1-2422

OX366-1810°C

D0352

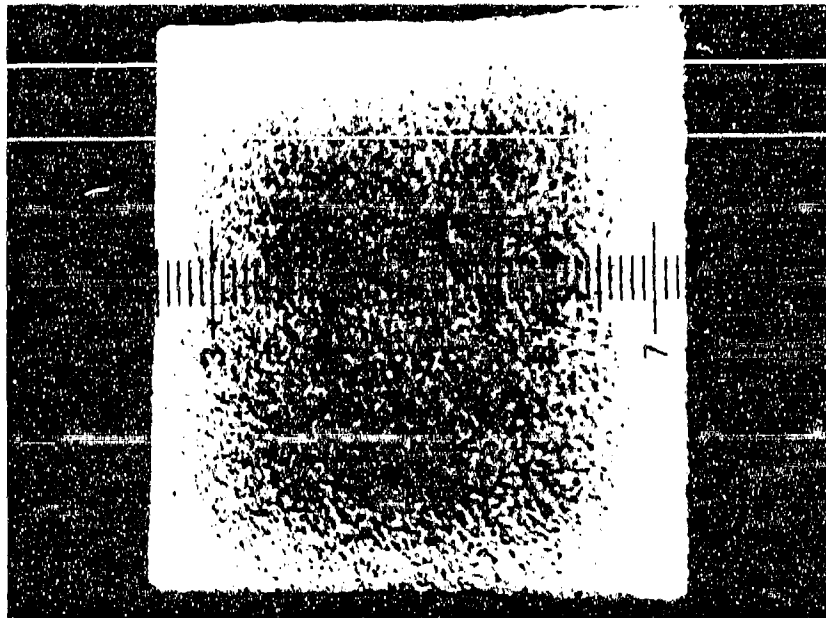


1-2470

OX375-1900°C

D0352

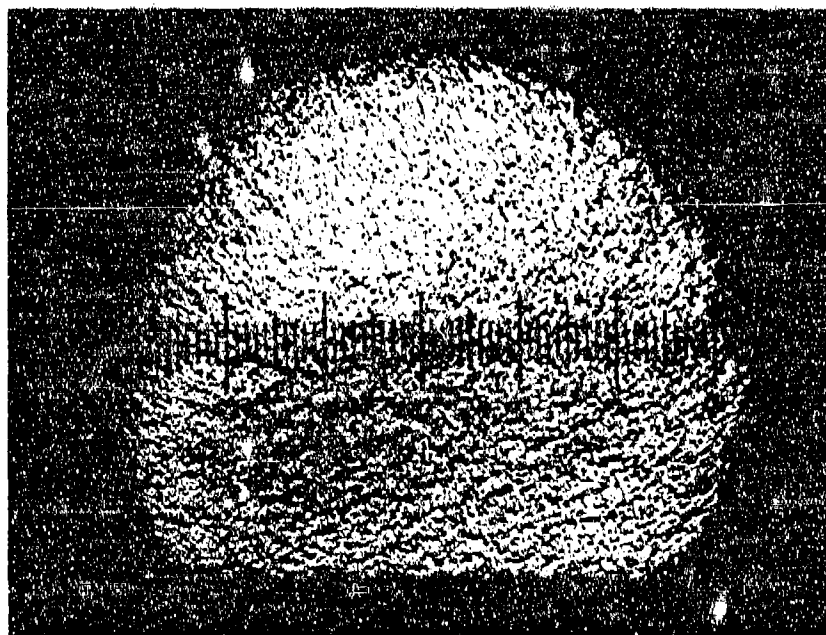
Figure 99. Oxidation Screening, Material H05: Oxide-Matrix Interfaces, 250X.



1-2421

Longitudinal

OX366

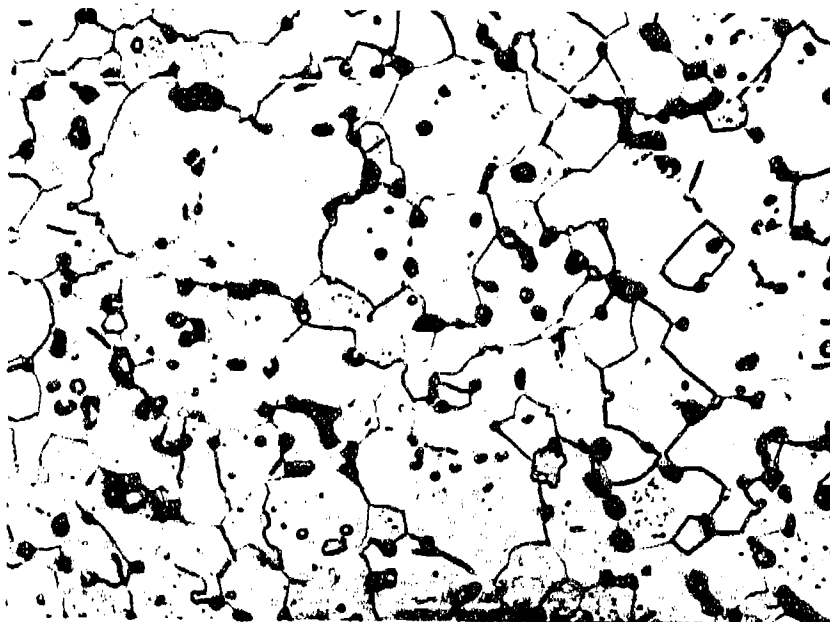


1-2424

Transverse

OX366

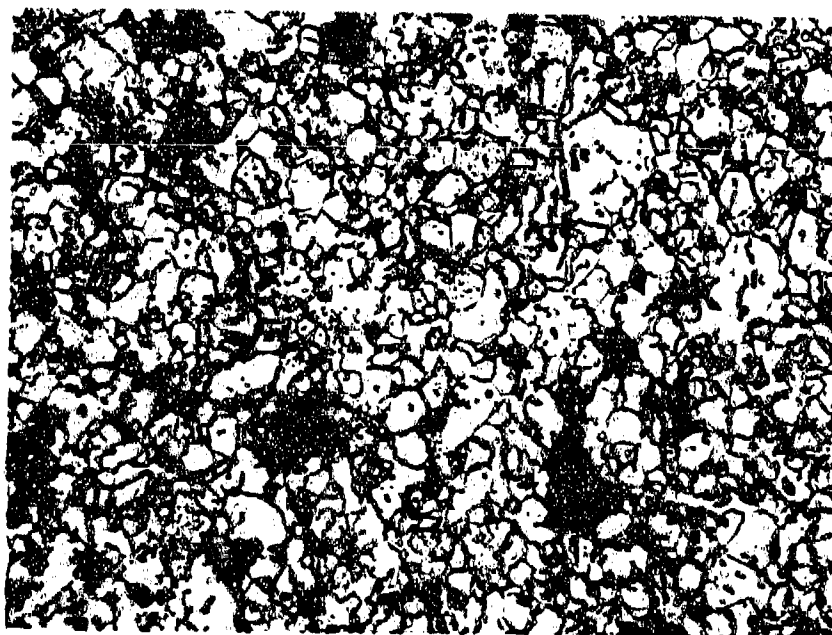
Figure 100. Oxidation Screening, Material II05: Reticule Photographs
(1 div. = 4.86 mils), D0352, 1810°C.



1-2423

II05-D0352

OX366



1-2256

II06-D0383

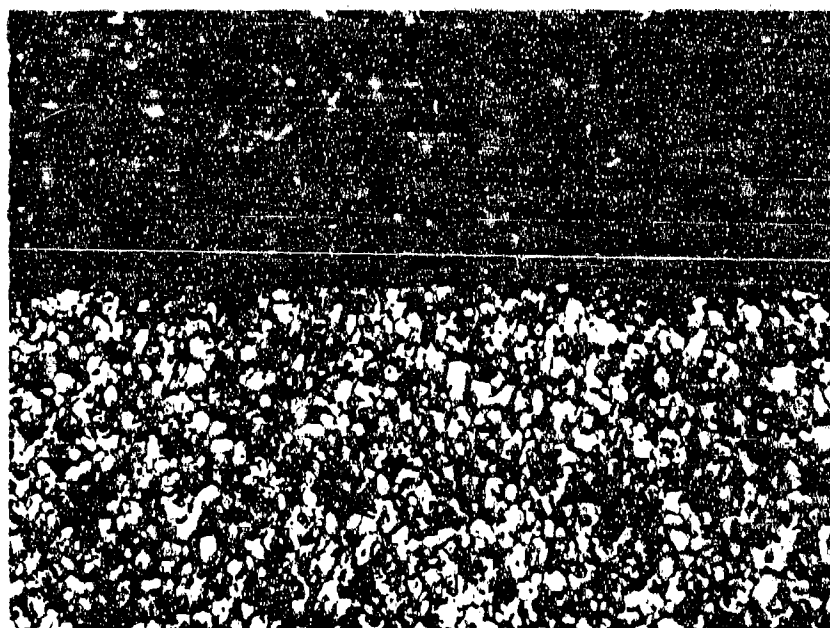
OX327

Figure 101. Oxidation Screening, Material II: Representative Matrix Photographs, 1800°C, 500X.



1-2254

Macrograph

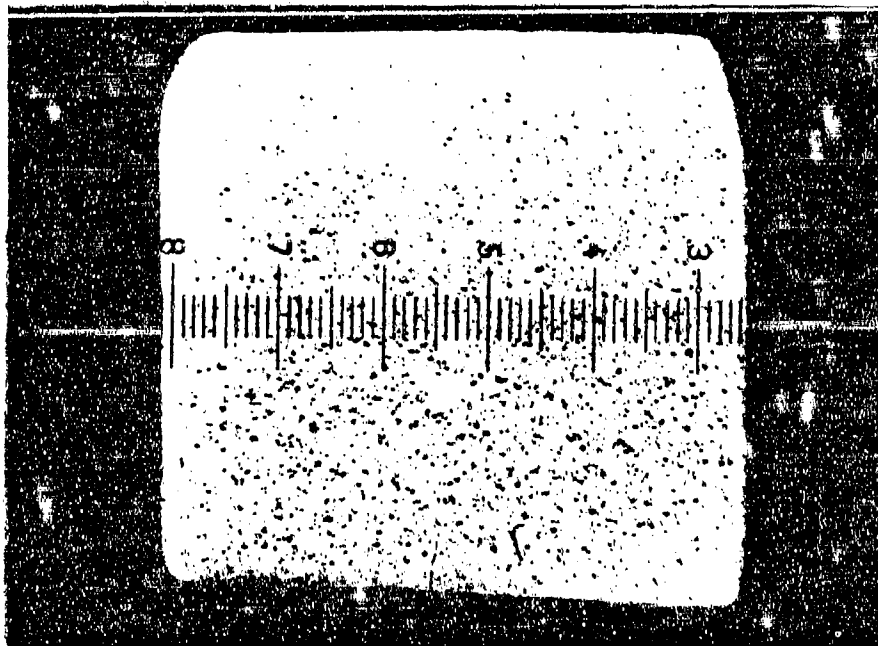


1-2257

Oxide-Matrix Interface

250X

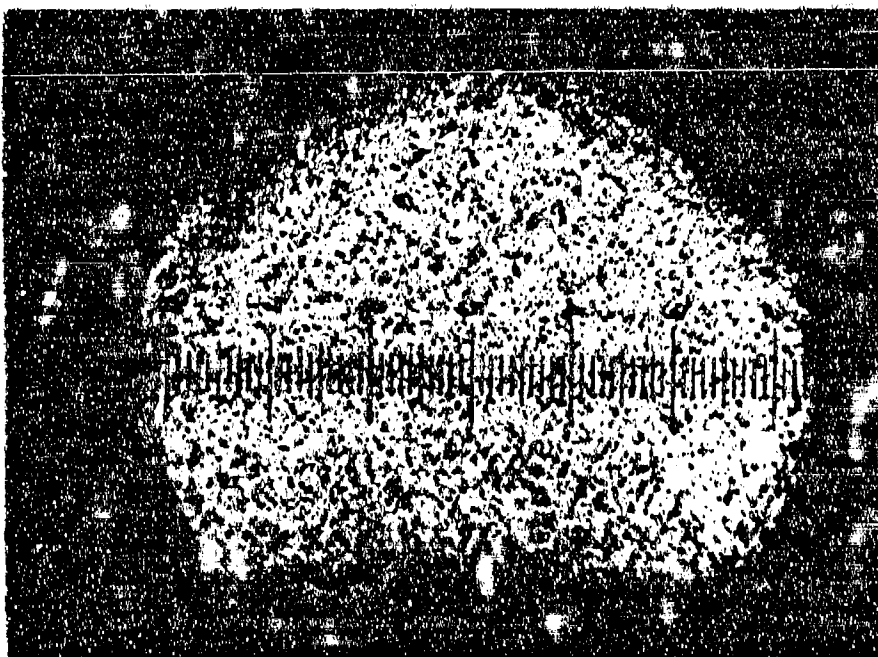
Figure 102. Oxidation Screening, Material II06: OX327, D0383, 1800°C.



1-2255

Longitudinal

OX327

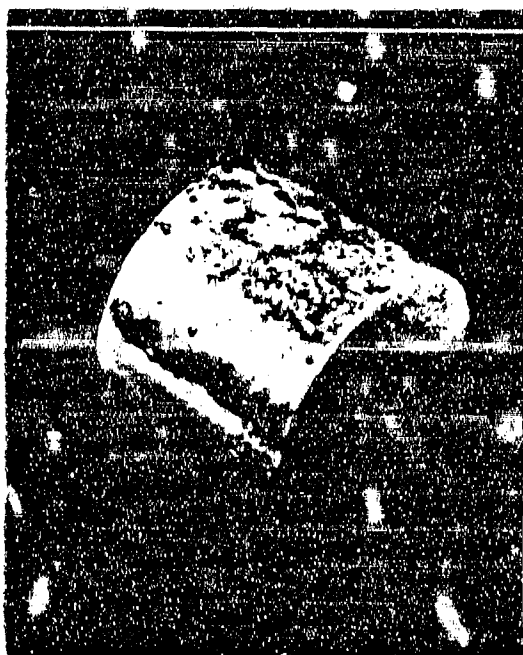


1-2258

Transverse

OX327

Figure 103. Oxidation Screening, Material 1106: Reticule Photographs (1 div. = 4.86 mils), D0383, 1800°C.



1-2267

OX340-1800°C

D0408



1-2278

OX345-1980°C

D0408



1-2511

OX384-2050°C

D0408

Figure 104. Oxidation Screening, Material III: Macrophotographs.



1-4220

OX340-1800°C

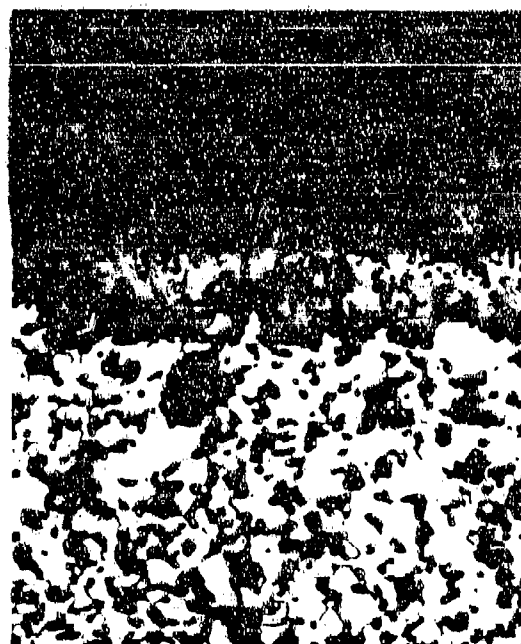
D0408



1-2281

OX345-1980°C

D0408

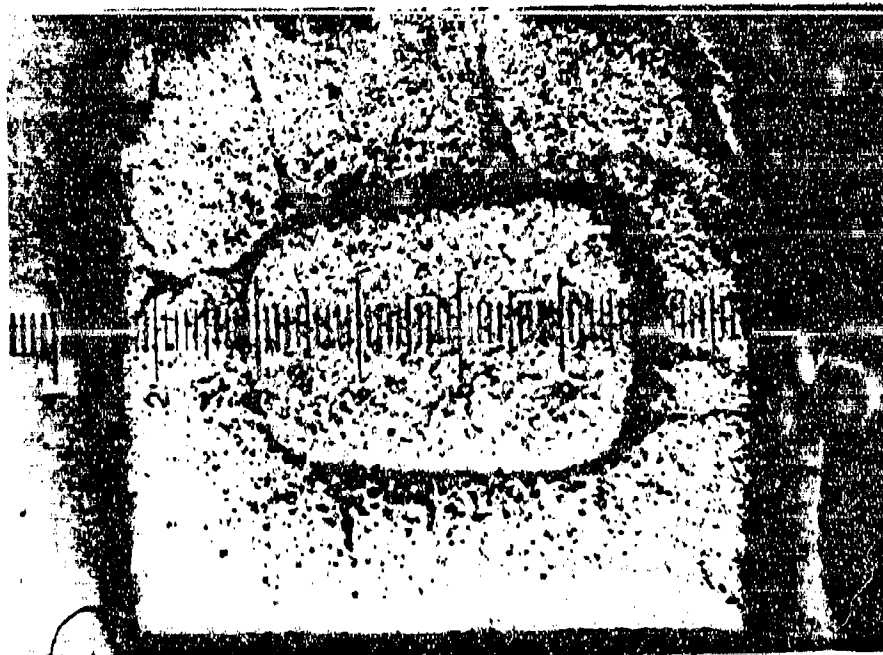


1-2514

OX384-2050°C

D0408

Figure 105. Oxidation Screening, Material III: Oxide-Matrix Interfaces, 250X.



1-2279

Longitudinal

OX345

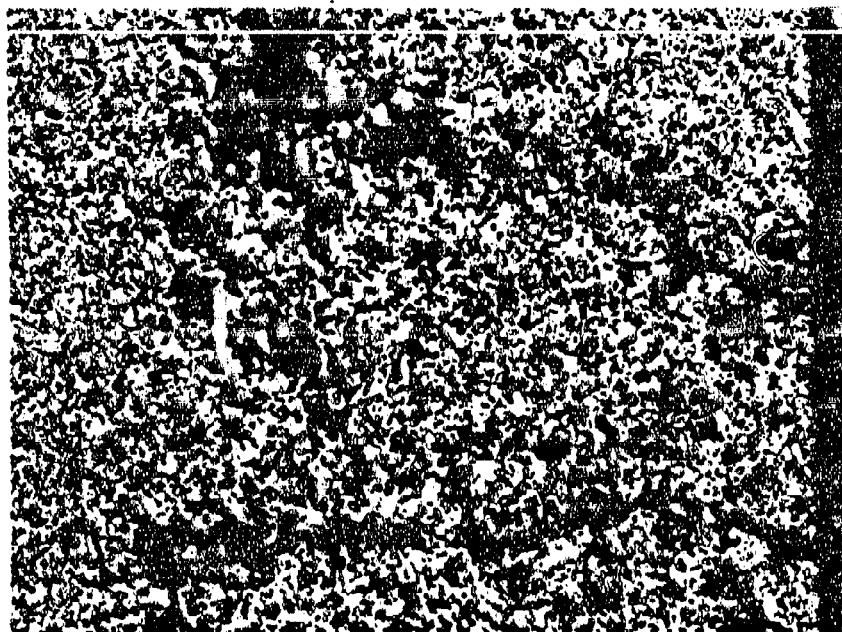


1-2283

Transverse

OX345

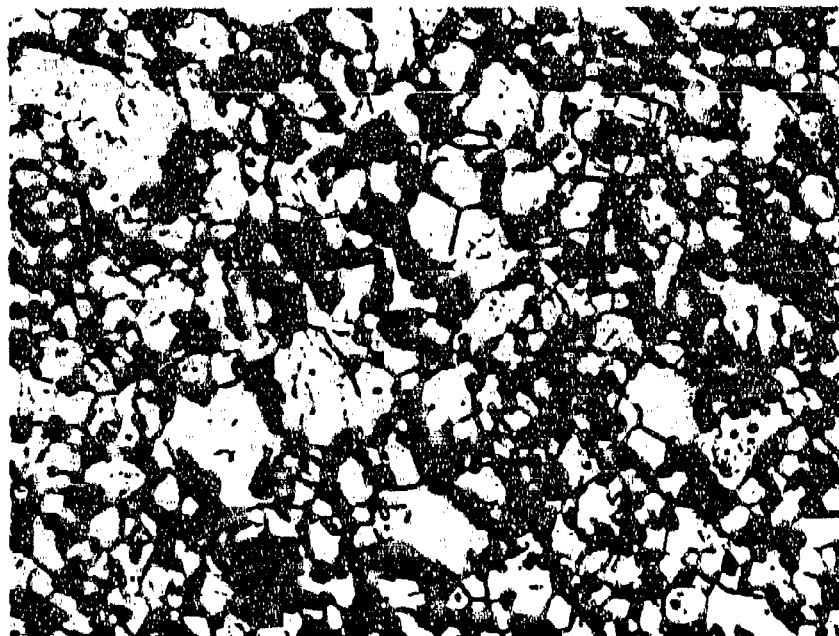
Figure 106. Oxidation Screening, Material III: Reticule Photographs
(1 div. = 4.86 mils), D0408, 1980°C.



1-2280

75X

Interface



1-2282

500X

Matrix

Figure 107. Oxidation Screening, Material III: D0408, OX345, 1980°C.



1-2430

OX368-1800°C

D0410



1-2504

OX383-1960°C

D0410

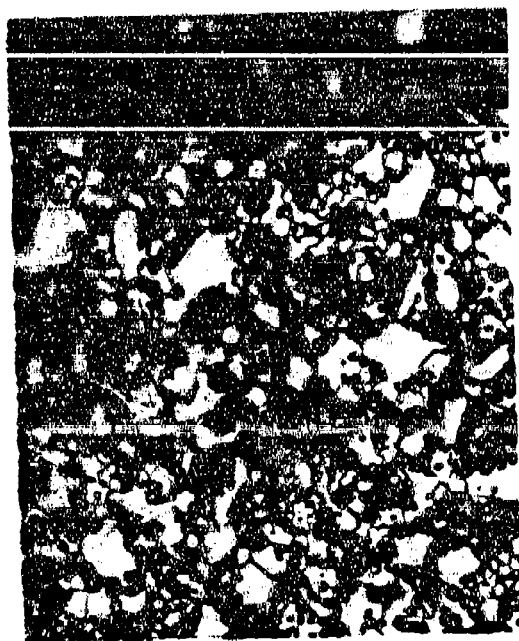


1-2518

OX385-2100°C

D0410

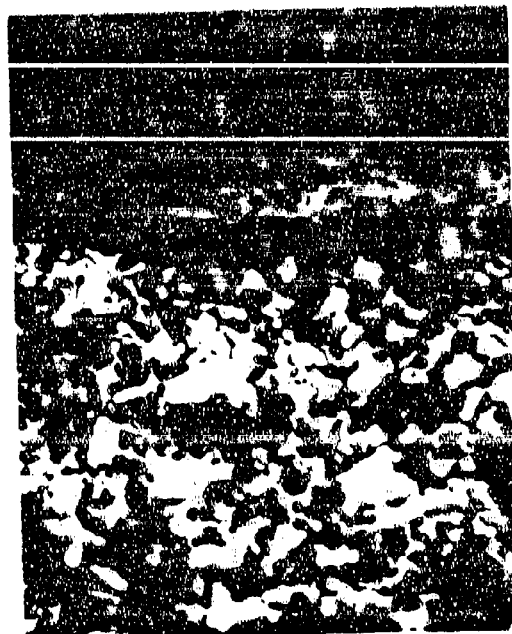
Figure 108. Oxidation Screening, Material IV: Macrophotographs.



1-4221

OX368-1800°C

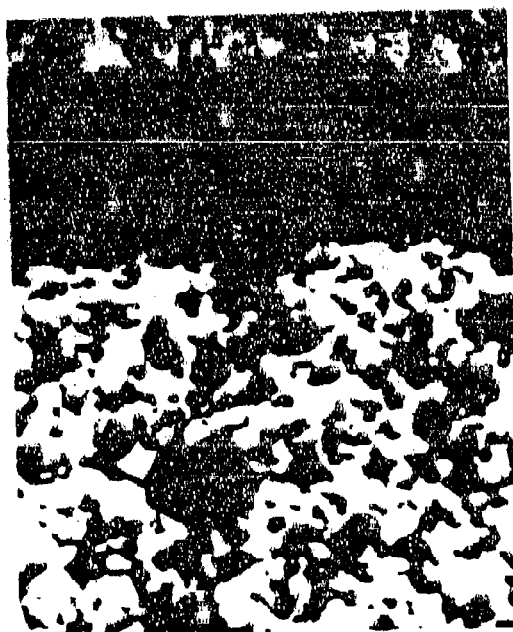
D0410



1-2507

OX383-1960°C

D0410

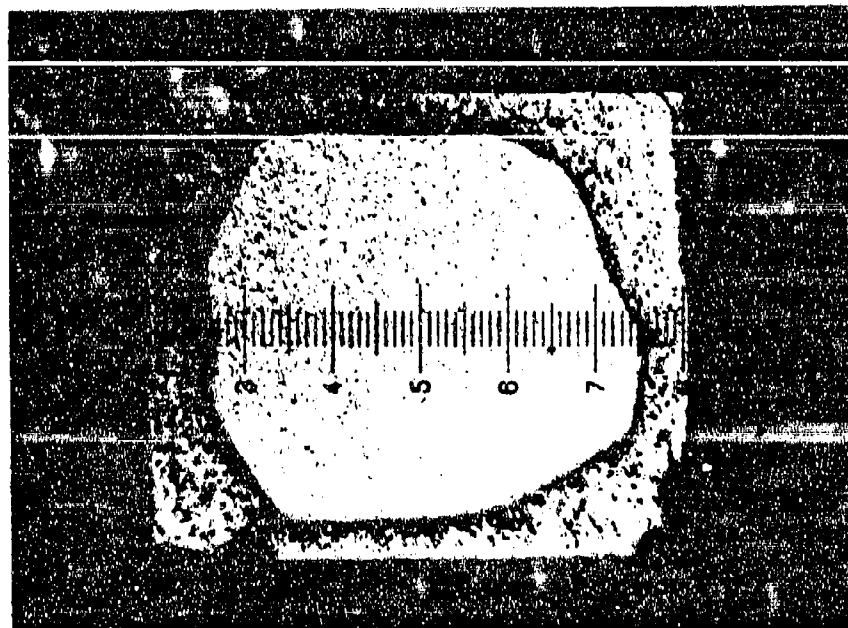


1-2520

OX385-2100°C

D0410

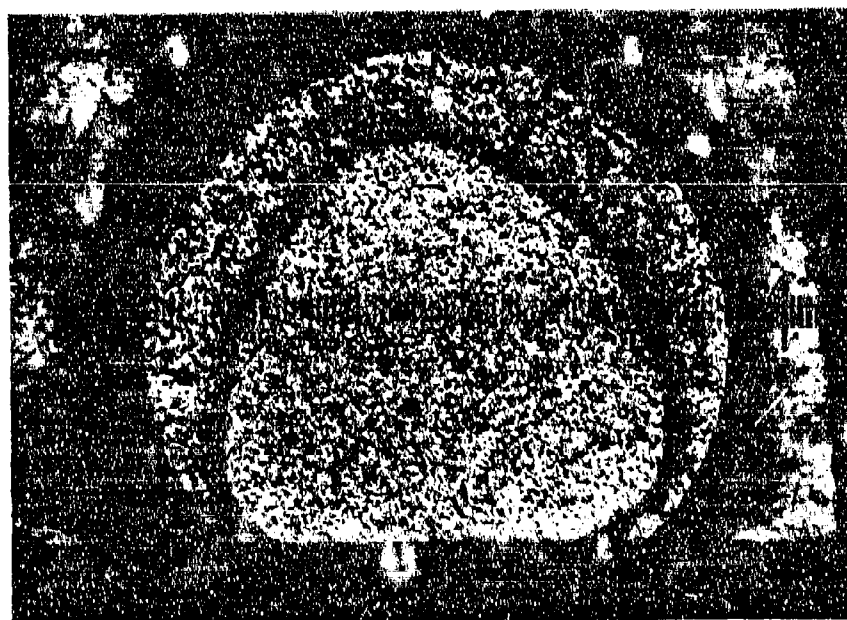
Figure 109. Oxidation Screening, Material IV: Oxide-Matrix Interfaces, 250X.



1-2505

Longitudinal

OX383

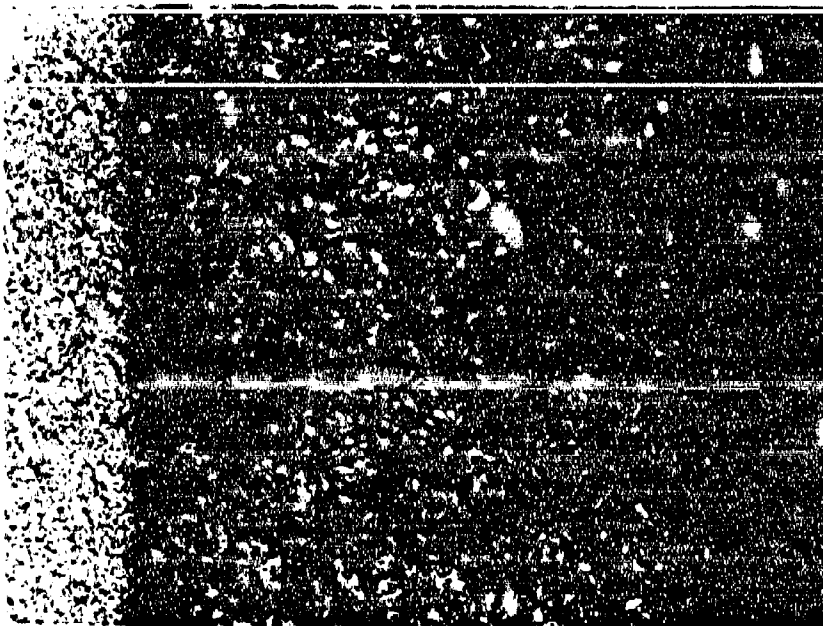


1-2510

Transverse

OX383

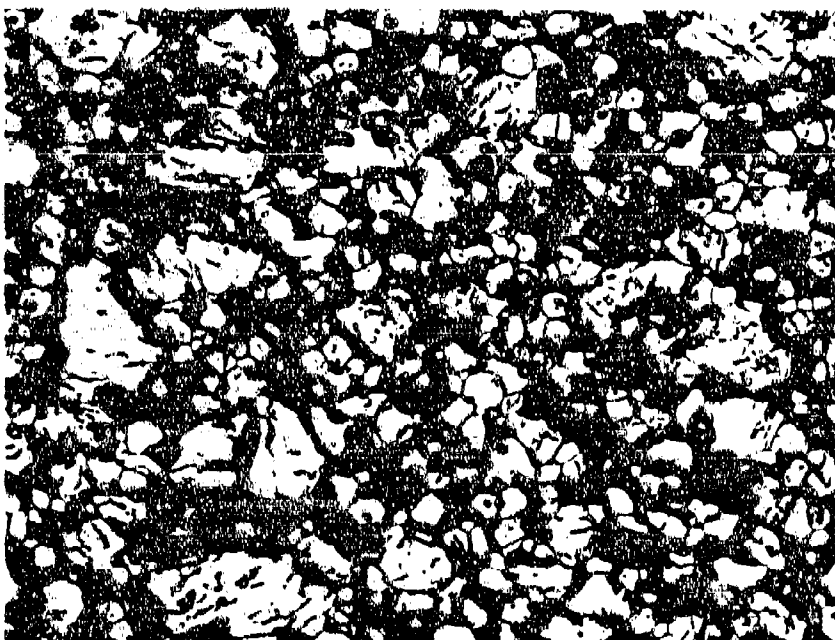
Figure 110. Oxidation Screening, Material IV: Reticule Photographs
(1 div. = 4.86 mils), D0410, 1960°C.



1-4222

Interface

50X



1-2509

Matrix

500X

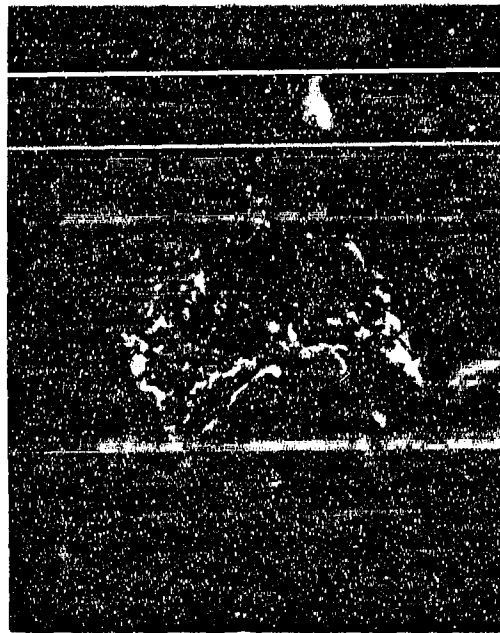
Figure 111. Oxidation Screening, Material IV: D0410, OX383, 1960°C.



1-2826

OX434-1760°C

D0462



1-2707

OX422-1875°C

D0462

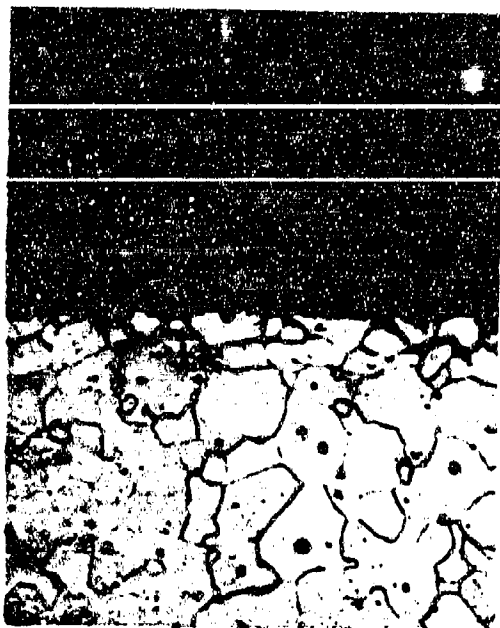


1-2494

OX376-1960°C

D0462

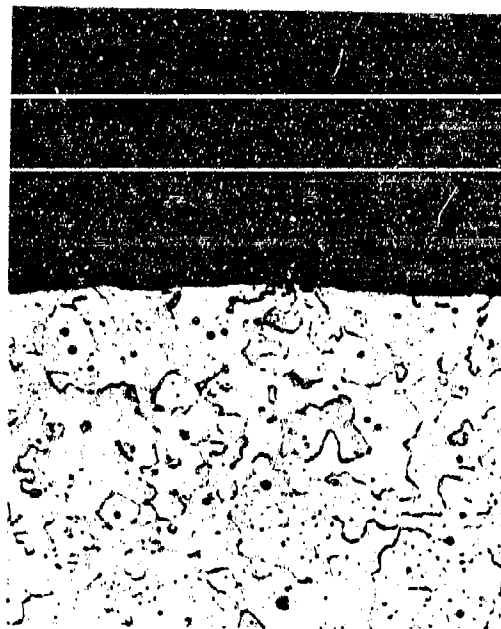
Figure 112. Oxidation Screening, Material VI: Macrophotographs.



1-4294

OX434-1760°C

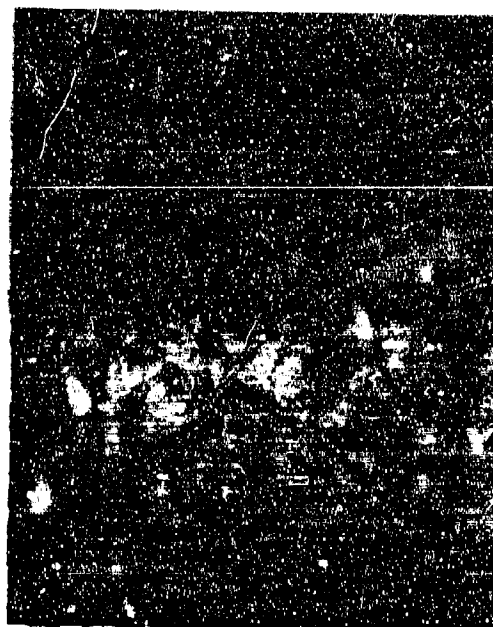
D0462



1-4224

OX422-1875°C (150X)

D0462

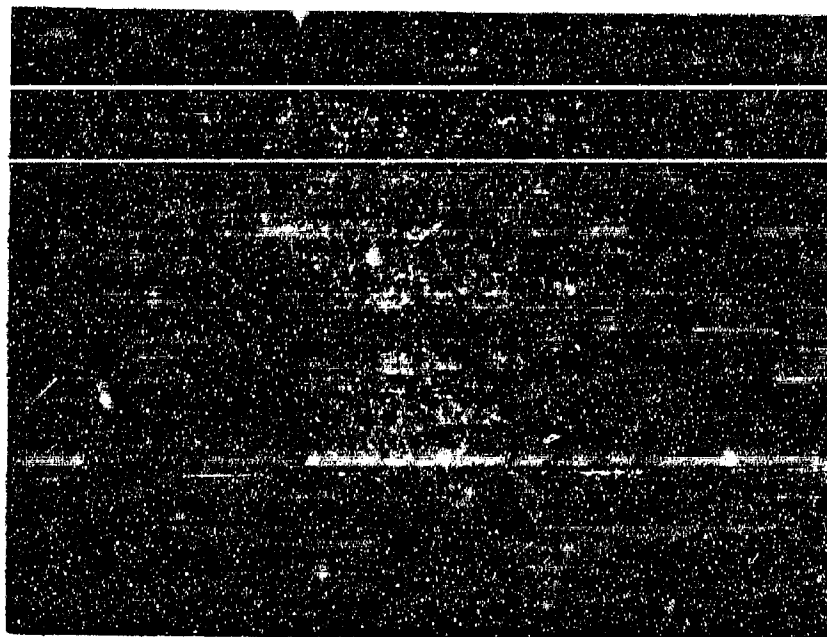


1-2496

OX376-1960°C

D0462

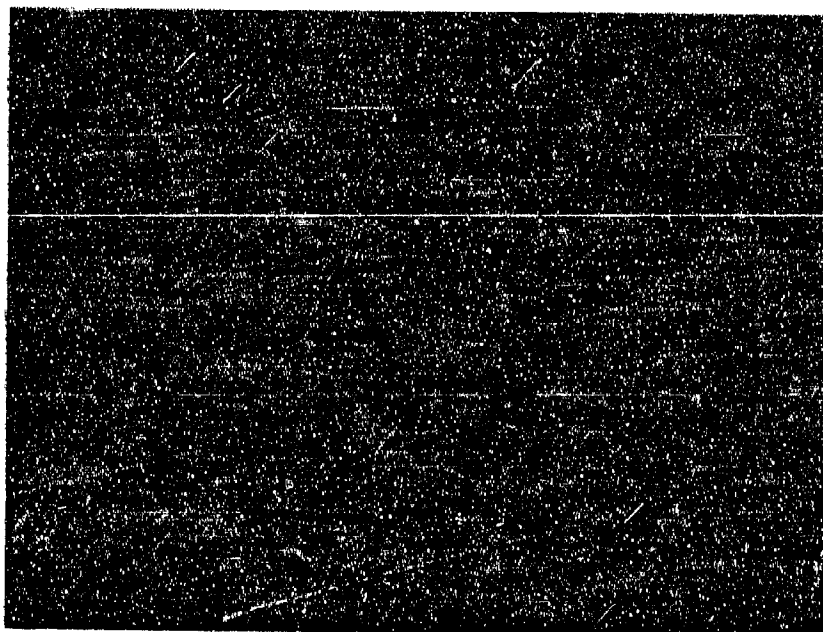
Figure 113. Oxidation Screening, Material VI: Oxide-Matrix Interfaces, 250X.



1-2827

Longitudinal

OX434

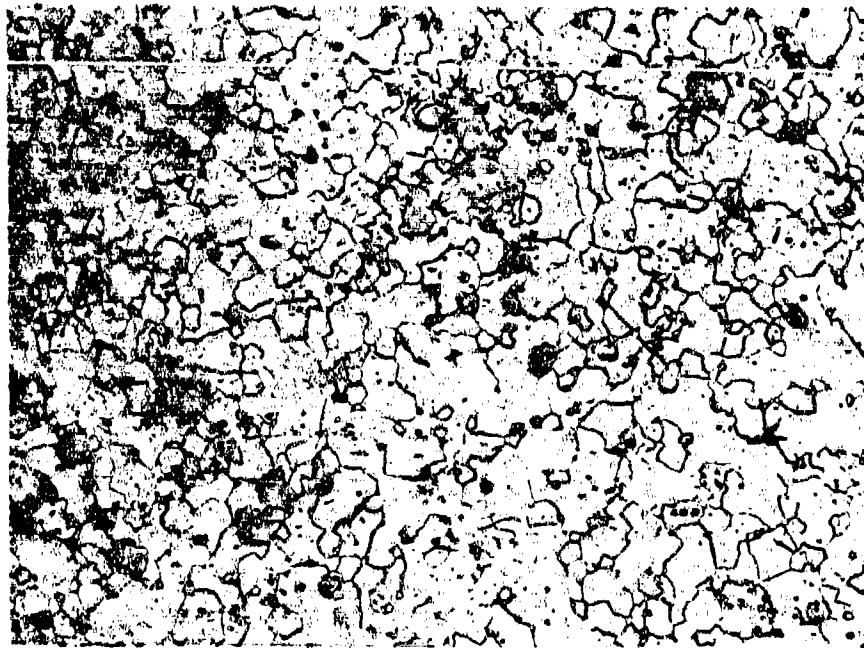


1-4292

Transverse

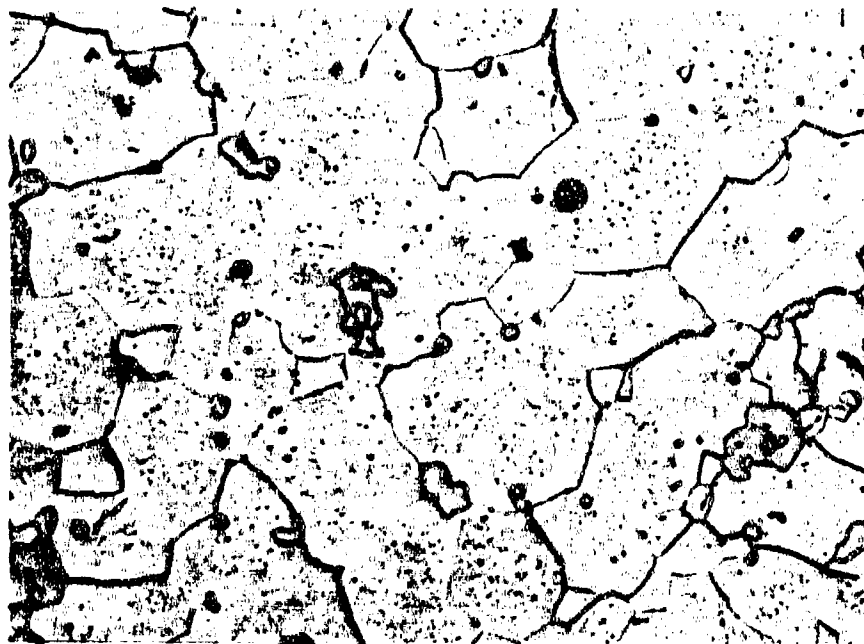
OX434

Figure 114. Oxidation Screening, Material VI: Reticule Photographs (1 div. = 4.86 mils), D0462, 1760°C.



1-4293

150X



1-4295

500X

Figure 115. Oxidation Screening, Material VI: Representative Matrix Photographs, D0462, OX434, 1760°C.

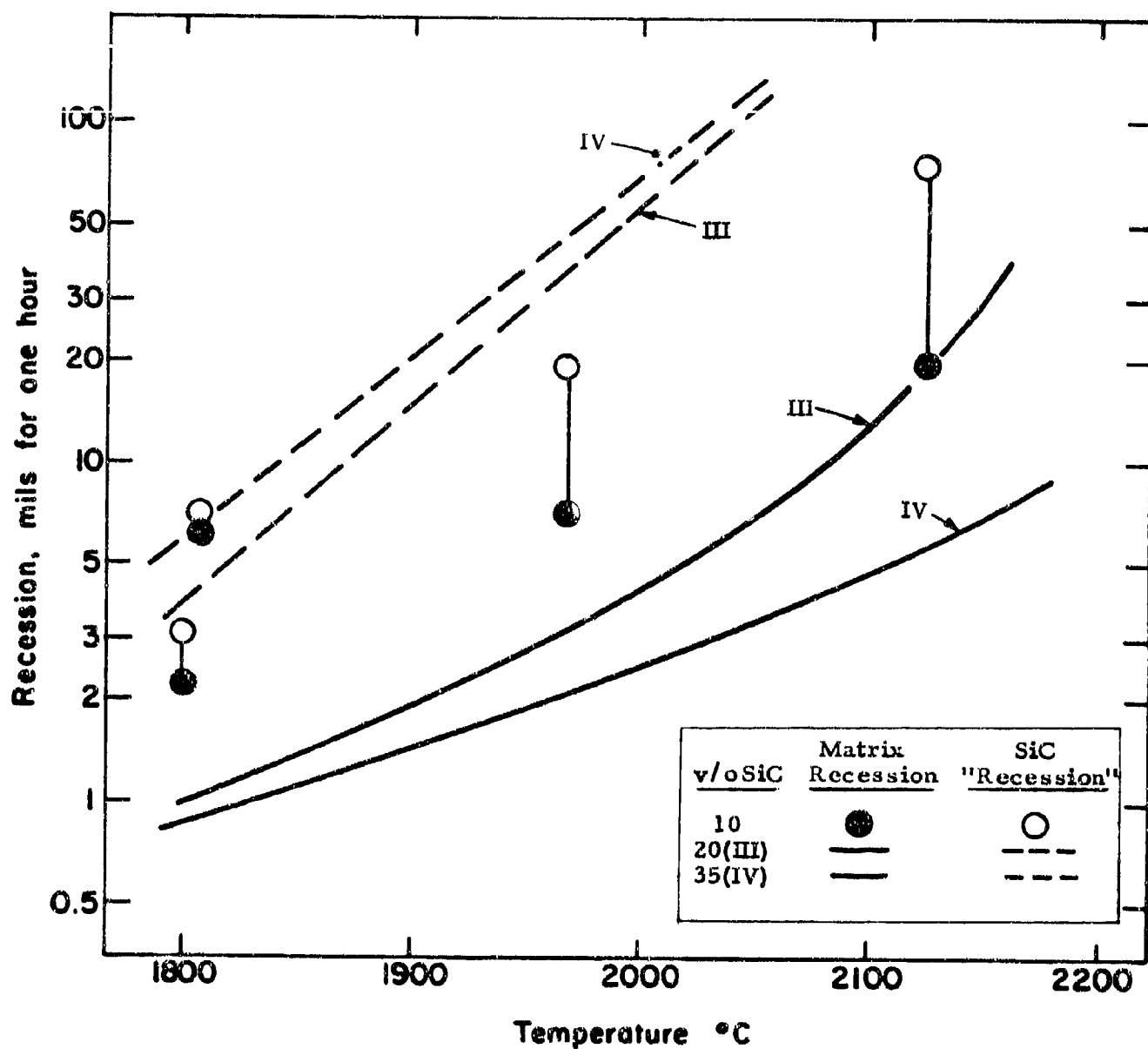


Figure 116. Oxidation Screening: Material III ($\text{HfB}_2 + \text{SiC}$) - Effect of SiC Content.

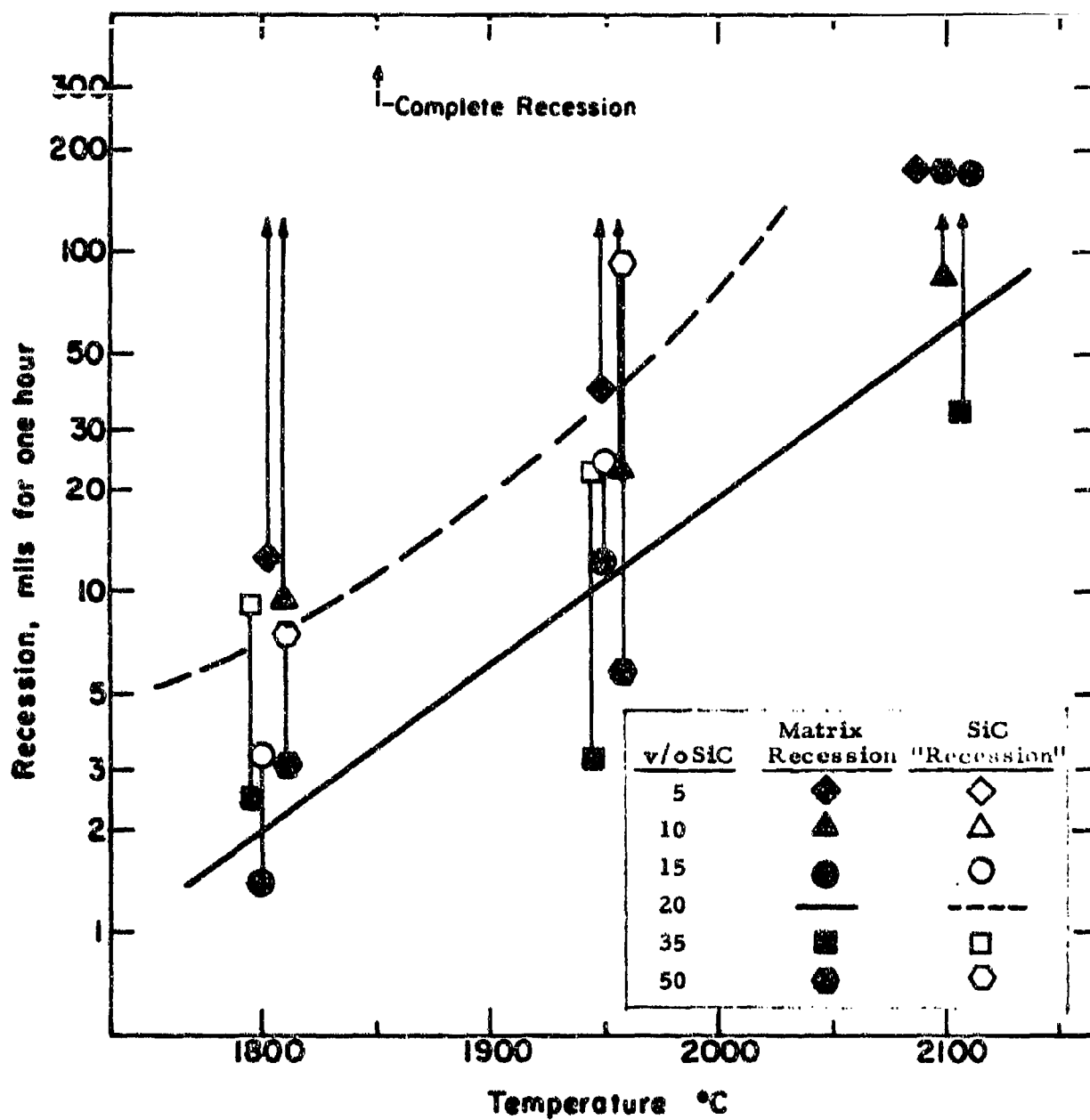


Figure 117. Oxidation Screening: Material V ($ZrB_2 + SiC$) - Effect of SiC Content.

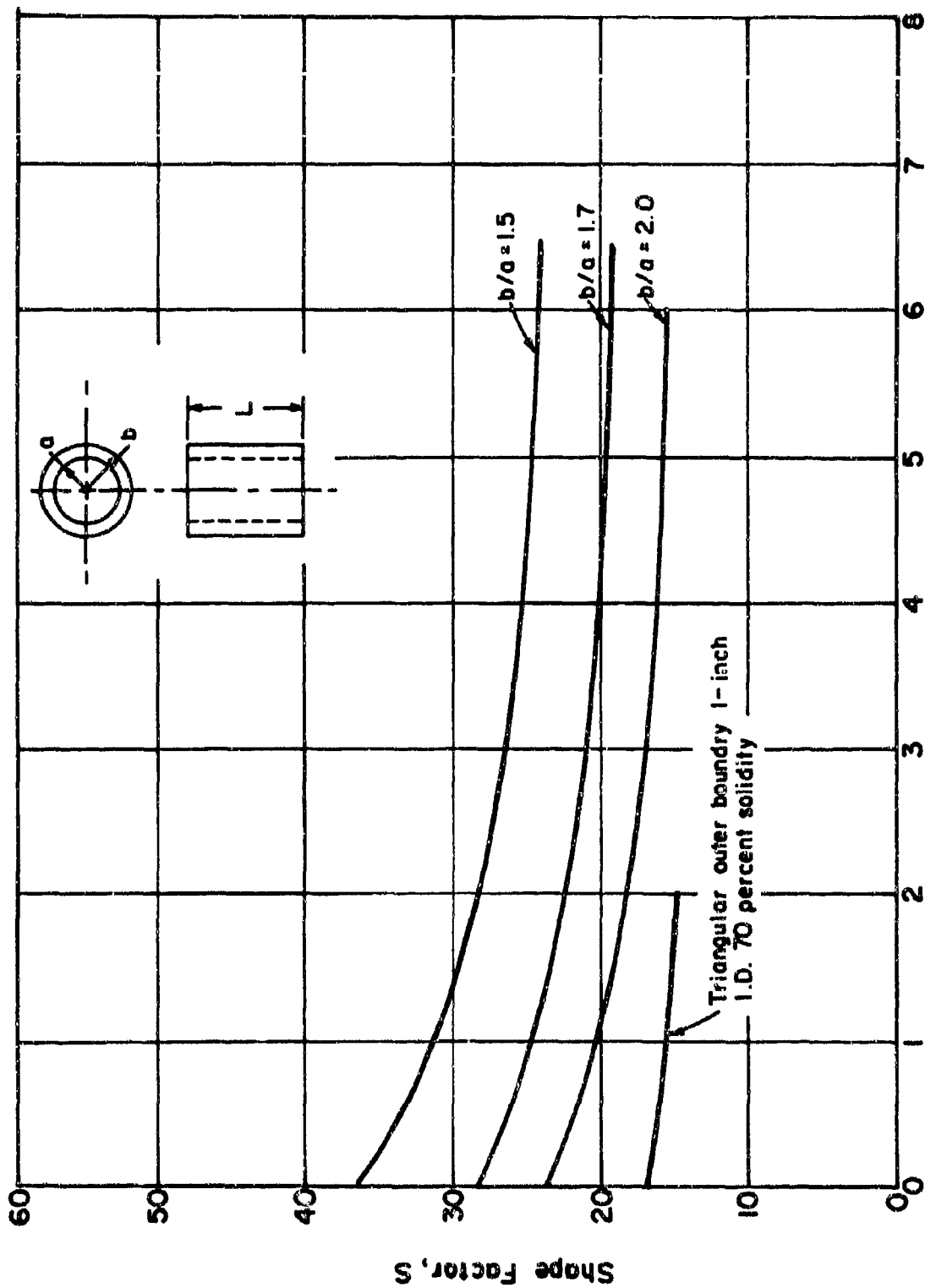


Figure 118. Shape Factors of Circular Cylindrical Thermal Stress Specimens.

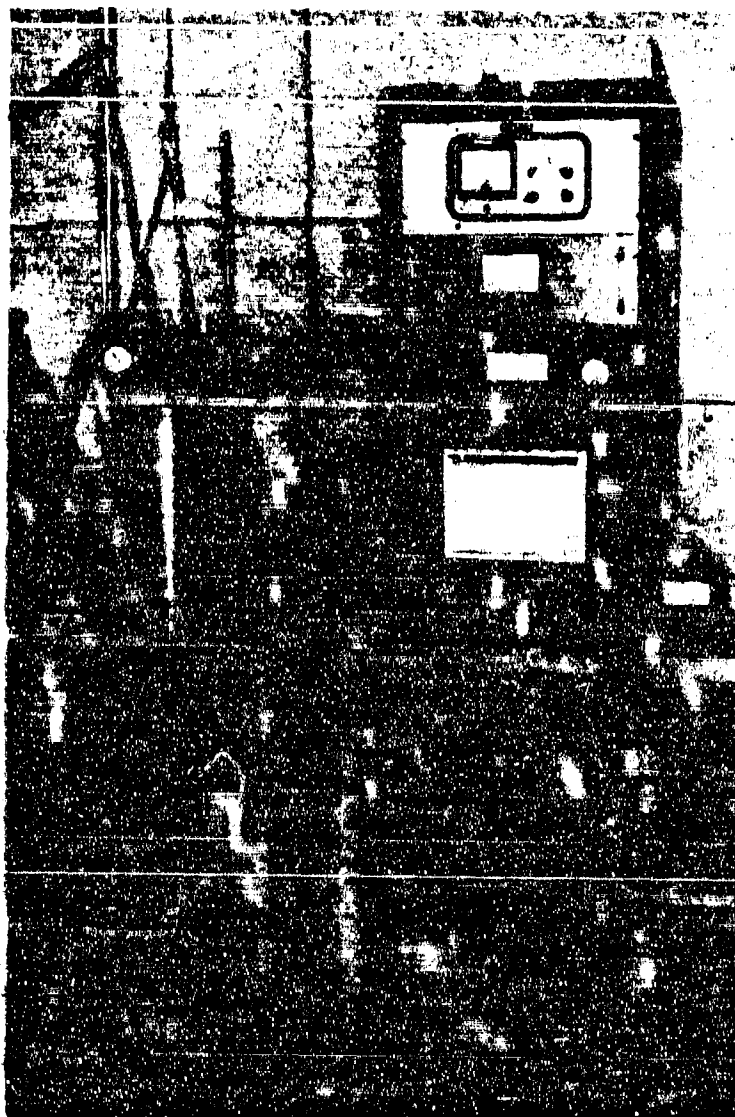


Figure 119. Thermal Stress Apparatus.

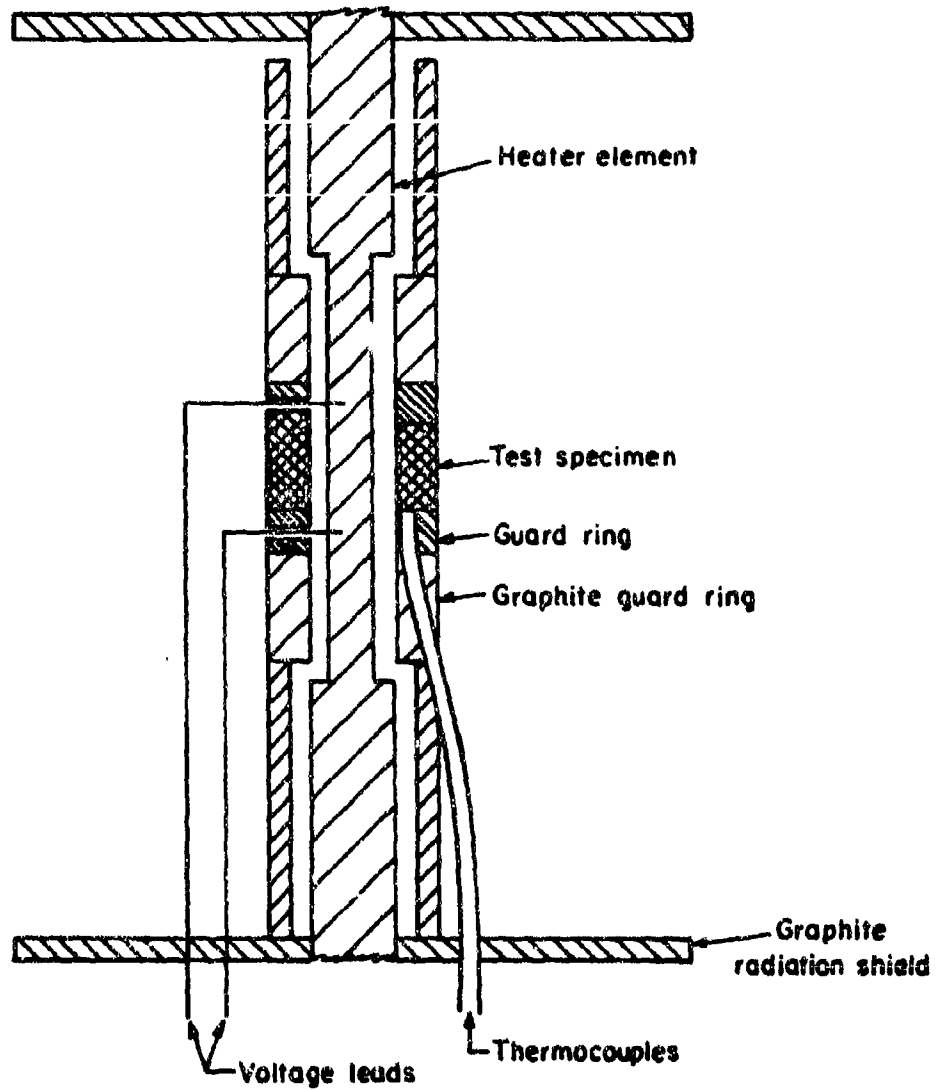


Figure 120. Cross Sectional Schematic of Sample Placement in Thermal Stress Testing Apparatus.

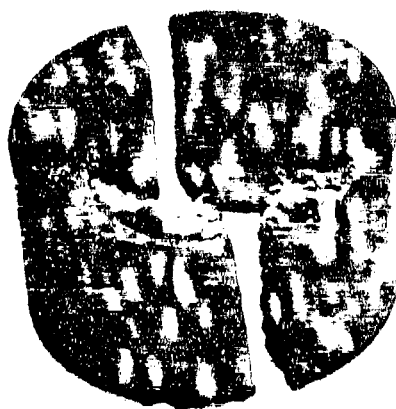


Figure 121. KT SiC Sample Thermal Stress Specimen after Failure.



Figure 122. Material I (I03A D0539) Thermal Stress Specimen Failed in Cooling after Test.

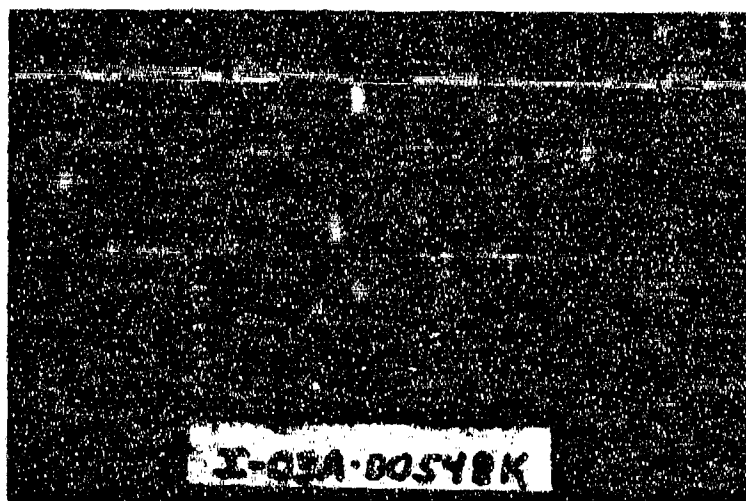


Figure 123. Material I (I03A D0548K) Thermal Stress Specimen Failed Under Transient Heating Conditions.

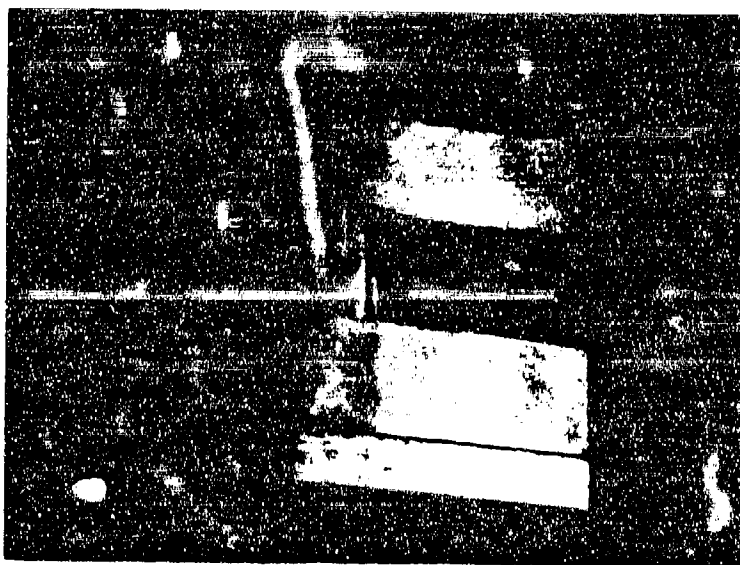


Figure 124. Material II (II05 D0595K) Failed Thermal Stress Specimen Before Removal from Test Apparatus.

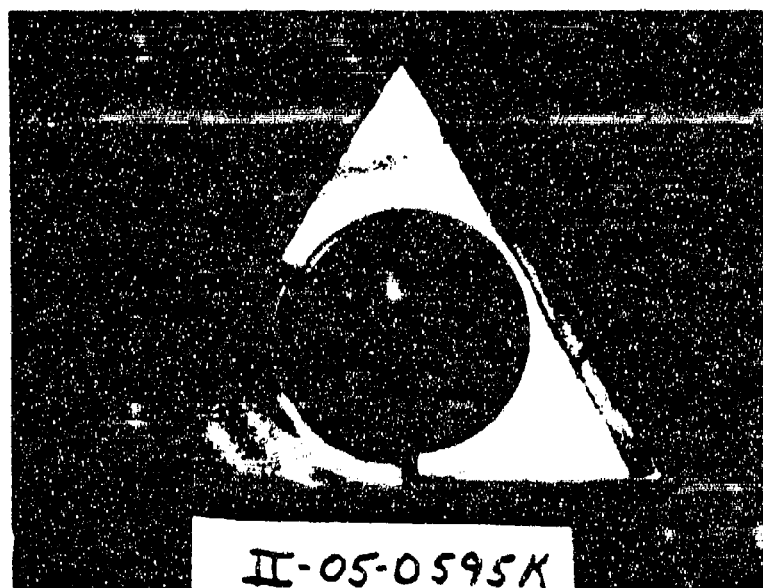


Figure 125. Material II (II05 D0595K) Thermal Stress Specimen after Failure.

TABLE 1
ORGANIZATIONAL RESPONSIBILITIES BREAKDOWN

| | |
|--|--------------------------------------|
| Technical Management | ManLabs |
| Materials Procurement | ManLabs |
| Materials Characterization | ManLabs |
| Fabrication: | |
| Hot Pressing | Avco/SSD |
| Characterization | Avco/SSD |
| Exploratory | Avco/SSD |
| Characterization | Avco/SSD |
| Pyrolytic Depositions | Raytheon Research Division |
| Characterization | ManLabs |
| Thermal and Oxidation Evaluations | ManLabs |
| Mechanical Properties | Avco/SSD |
| Thermal Expansion | ManLabs |
| Thermal Diffusivity | North American/Atomics International |
| Emittance | Avco/SSD |
| Steady State Thermal Stress Resistance | Battelle Memorial Institute |
| Simulated Leading Edge Evaluation | Bell Aerosystems |
| Arc Plasma Evaluations | ManLabs - AF33(615)-3859 |
| Nondestructive Testing | Avco/SSD - AF33(615)-3942 |

TABLE 2
DIBORIDE MATERIAL IDENTIFICATION: PHASE CONSTITUTION
AND BASE COMPOSITION

| <u>Material Diboride</u> | <u>Designation</u> | <u>Remarks and Rationale for Specific Additives</u> |
|------------------------------|--------------------|---|
| I | ZrB_2 | Zirconium diboride, no additive. |
| II | HfB_2 | Hafnium diboride, no additive. |
| III | $HfB_2 + SiC$ | Hafnium diboride with twenty volume per cent silicon carbide to enhance oxidation resistance. |
| IV | $HfB_2 + SiC$ | Hafnium diboride with thirty volume per cent silicon carbide to enhance oxidation resistance. |
| V | $ZrB_2 + SiC$ | Zirconium diboride with twenty volume per cent silicon carbide to enhance oxidation resistance. |
| VI | $HfB_2 + Hf-Ta$ | Hafnium diboride with four volume per cent hafnium tantalum alloy to provide an oxidation resistant metallic binder phase and enhance strength properties. |
| VII | $HfB_2 + SiC$ | Boron rich hafnium diboride with silicon carbide additive to enhance oxidation resistance. |
| VIII | $ZrB_2 + SiC + C$ | Zirconium diboride with fourteen volume per cent silicon carbide, thirty volume per cent carbon to enhance thermal stress resistance and maintain improved oxidation resistance relative to ZrB_2 . |
| IX | $HfB_2 + HfSi$ | Hafnium diboride with twenty volume per cent hafnium silicide to enhance oxidation resistance. |
| X | $ZrB_2 + SiB_6$ | Zirconium diboride with twenty volume per cent silicon hexaboride to enhance oxidation resistance. |
| XI | $ZrB_2 + Cr$ | Zirconium diboride with eight volume per cent chromium to enhance mechanical strength properties. |
| XII | $ZrB_2 + C$ | Zirconium diboride with fifty volume per cent carbon to enhance thermal stress resistance. |
| XIII | $ZrB_2 + W$ | Zirconium diboride with tungsten to enhance mechanical properties. |

TABLE 3
TENTATIVE POWDER SPECIFICATION FOR HOT PRESSING
GRADES OF ZrB_2 AND HfB_2

Limitations of present powder production technology for ZrB_2 and HfB_2 and cost considerations in quantities of the order of 100 pounds for hot pressing purposes will of necessity contain oxygen and carbon impurities. Materials found most suitable for hot pressing without additives or with carbon or SiC additive are characterized by over-all composition such that oxygen and carbon impurities are present as metal oxide, metal carbide or a mixed metal oxy-carbide.

Limitations imposed by present powder production technology of ZrB_2 and HfB_2 for hot pressing purposes in quantities of the order of 100 pounds lead to the presence of 0.5 to 1.5 per cent nonmetallic impurities principally oxygen and carbon. The over-all chemical composition has to be specified to insure that these impurities are present as metal oxide, metal carbide or as metal oxy-carbide. The thermodynamic stability of zirconium and hafnium oxides overrides compositional effects, but over-all metal rich compositions have to be specified to avoid the stabilization of carbon as B_4C . The presence of the latter lowers the temperature required for liquid phase formation relative to that observed for the oxide impurity phases. All metallic impurities have to be kept below 0.1 per cent to maintain basic properties of ZrB_2 and HfB_2 . Of the metallic impurities, iron and titanium are more commonly encountered and both should be kept below the 0.1 per cent level. Powder particle size should be specified as -325 mesh or finer; fluid energy milling can be further specified or performed after delivery of powder to break up particulate aggregates. Chemistry specification are as follows:

| | ZrB_2 Weight Per Cent | HfB_2 Weight Per Cent |
|-----------------------|----------------------------|----------------------------|
| Hf | 1.0 - 3.0 | 88.0 - 89.5 (Hf+Zr) |
| Zr | 79.5 - 80.5 (Hf+Zr) | 1.0 - 3.0 |
| B | 18.0 - 19.0 | 10.0 - 10.5 |
| C | <0.50 | <0.50 |
| O | <0.50 | <0.50 |
| Ti | <0.10 | <0.10 |
| Fe | <0.05 | <0.05 |
| Other Metals | <0.10 | <0.10 |
| N | <0.05 | <0.05 |
| H | <0.05 | <0.05 |
| Atomic Ratio: B/Hf+Zr | <2.0 | <2.0 |

TABLE 4

DIBORIDE POWDER PROCUREMENT SCHEDULE

| <u>Material</u> * | <u>Supplier</u> | <u>Quantity</u> <u>pounds</u> | <u>Purchase Schedule</u> | |
|---------------------|-----------------|----------------------------------|--------------------------|--------------------|
| | | | <u>Ordered</u> | <u>Received</u> |
| I02 | U. S. Borax | 1 | 3/16/66 | 3/28/66 |
| I02A | U. S. Borax | 93 | 4/11/66 | 4/14/66 |
| I03 | U. S. Borax | 1 | 4/11/66 | 4/13/66 |
| I03A | U. S. Borax | 100 | 6/24/66 | 7/14/66 |
| I05 | Shieldalloy | 5 | 6/24/66 | 10/03/66 |
| I05A (Reprocessed) | Shieldalloy | 95 | 3/01/67 | 4/13/67 |
| I07 | U. S. Borax | 400 | 2/27/67 | 4/11/67 |
| II05 | Wah Chang | 20 | 3/18/66 | 7/20/66 |
| II05A | Wah Chang | 80 | 3/18/66 | 9/20/66 |
| II06 | Shieldalloy | 5 | 5/13/66 | 8/29/66 |
| II06A (Reprocessed) | Shieldalloy | 45 | 1/01/67 | 10/01/67 (anticip) |
| II09 | Wah Chang | 300 (100)** | 3/15/67 | 10/01/67 (anticip) |
| II10 | Carborundum | 100 | 9/11/67 | 10/01/67 (anticip) |

*The roman numerals I and II identify the material as zirconium diboride and hafnium diboride, respectively; the designations 02 and 02A refer to different shipments of the same powder lot except where reprocessing is indicated.

**Original order of 300 pounds changed to 100 pounds.

TABLE 5
CHARACTERIZATION OF ZIRCONIUM DIBORIDE POWDER, 102

Supplier: U. S. Borax Research Corporation

Quantity: 102 (1 pound sample) - 102A (94 pound lot)

| | |
|---|---------------------------------------|
| 1. Qualitative Analysis (weight per cent, w/o) | 4. X-ray Phase Identification |
| Ti, Cr, Fe 0.1 - 1.0 | ZrB ₂ |
| V 0.01 - 0.1 | ZrO ₂ (impurity) |
| | ZrC (impurity) |
| 2. Quantitative Analysis (w/o) | 5. Powder Density |
| Zr 79.6 | 6.03 g/cc |
| B 18.3 | |
| C 0.38 | 6. Particle Size Distribution |
| O (AA) 1.05 | |
| Ti 0.02 | Range (μ) w/o |
| Cr 0.10 | 0-5 4.0 |
| Fe 0.08 | 5-10 23.4 |
| Total 99.53 | 10-20 64.5 |
| 3. Atomic Ratio | 20-40 7.6 |
| Over-all B/Zr = 1.94 | >40 0.5 |
| Corrected B/Zr* = 2.07 | |
| 7. Phase Assay (volume per cent) | ZrB ₂ ZrO ₂ ZrC |
| Calculated from Composition | 93.6 4.4 2.0 |

* Atomic ratio corrected for metal assumed to be present as metal dioxide and metal monocarbide.

TABLE 6
CHARACTERIZATION OF ZIRCONIUM DIBORIDE POWDER, 103

Supplier: U. S. Borax Research Corporation

Quantity: 103 (1 pound sample) - 103A (100 pound lot)

| | |
|--|--|
| 1. Qualitative Analysis (weight per cent, w/o) Ca, Fe 0.01 - 0.1 | 4. X-ray Phase Identification ZrB ₂ ZrO ₂ (impurity) |
| 2. Quantitative Analysis (w/o) Zr 79.8 B 17.7 C 0.03 O (AA) <u>1.49</u> Total 99.02 | 5. Powder Density 6.04 g/cc |
| 3. Atomic Ratio Over-all B/Zr = 1.87 Corrected B/Zr* = 1.98 | 6. Particle Size Distribution Range (μ) w/o 0-5 7.5 5-10 37.9 10-20 48.9 20-40 5.5 >40 0.2 |
| 7. Phase Assay (volume per cent) Calculated from Composition | ZrB ₂ ZrO ₂ ZrC 93.5 6.3 0.2 |

* Atomic ratio corrected for metal assumed to be present as metal dioxide and metal monocarbide.

TABLE 7
CHARACTERIZATION OF ZIRCONIUM DIBORIDE POWDER, 107

Supplier: U. S. Borax Research Corporation

Quantity: 400 pounds¹

| | | | | | | | | |
|-----------|---|---------|-------|-------|----|---|------------------|-----|
| 1. | Qualitative Analysis (weight per cent, w/o) Fe, Ca, Ti 0.01 - 0.1 | | | | 4. | X-ray Phase Identification ZrB ₂ ZrO ₂ (impurity) | | |
| 2. | Quantitative Analysis (w/o) | | | | 5. | Powder Density 5.96 g/cc | | |
| | A | B | C | Ave. | | | | |
| Zr | 78.5 | 78.6 | 78.4 | 78.5 | | | | |
| B | 19.1 | 18.4 | 18.2 | 18.6 | | | | |
| C | 0.22 | 0.31 | 0.25 | 0.26 | | | | |
| O(AA) | 1.30 | 1.31 | 1.31 | 1.31 | | | | |
| O(VF) | - | (1.15) | - | - | | | | |
| Total | 99.12 | 98.62 | 98.16 | 98.67 | | | | |
| 3. | Atomic Ratio | | | | 6. | Particle Size Distribution | | |
| Over-all | B/Zr _* = 1.99 | | | | | Range (μ) w/o | | |
| Corrected | B/Zr = 2.14 | | | | | 0-5 7.9 | | |
| | | | | | | 5-10 33.8 | | |
| | | | | | | 10-20 52.1 | | |
| | | | | | | 20-40 5.0 | | |
| | | | | | | >40 1.2 | | |
| 7. | Phase Assay (volume per cent) | | | | | ZrB ₂ | ZrO ₂ | ZrC |
| | Calculated from Composition | | | | | 93.2 | 5.4 | 1.4 |

¹ The four hundred pound lot was blended then shipped in three separated containers designated A, B and C.

*Atomic ratio corrected for metal assumed to be present as metal dioxide and metal monocarbide.

TABLE 8
CHARACTERIZATION OF ZIRCONIUM DIBORIDE POWDER, I05A

Supplier: Shieldalloy Corporation (H. C. Starck Berlin)

Quantity: 100 pounds¹

| | |
|--|---|
| 1. Qualitative Analysis (weight per cent, w/o) Ti, Fe, Co 0.01 - 0.1 | 4. X-ray Phase Identification ZrB ₂ |
| 2. Quantitative Analysis (w/o) Zr 79.3 B 18.65 C 0.02 O(AA) <u>0.42</u> Total 98.39 | 5. Powder Density 5.97 g/cc |
| 3. Atomic Ratio Over-all B/Zr = 1.97 Corrected B/Zr* = 2.02 | 6. Particle Size Distribution Range (μ) w/o 0-5 7.7 5-10 26.6 10-20 44.7 20-40 17.8 >40 1.1 |
| 7. Phase Assay (volume per cent) Calculated from Composition | ZrB ₂ ZrO ₂ ZrC 98.1 1.8 0.1 |

¹ The original five pound sample designated I05 was found unsatisfactory for this program as it contained significant amounts of ZrO₂ and ZrC. The I05A was obtained by reprocessing the I05.

* Atomic ratio corrected for metal assumed to be present as metal dioxide and metal monocarbide.

TABLE 9

CHARACTERIZATION OF HAFNIUM DIBORIDE POWDER, H05 AND H05A

Supplier: Wah Chang Corporation

Quantity: H05 (20 pound sample) - H05A (80 pound lot)

| | | | | | |
|---|-------------------|------------------|-------------------------------|------|--|
| 1. Qualitative Analysis (weight per cent, w/o) | | | 4. X-ray Phase Identification | | |
| Zr | | 1 - 10 | HfB ₂ | | |
| Si | | 0.1 - 1.0 | HfC (impurity) | | |
| Al | | 0.01 - 0.1 | | | |
| 2. Quantitative Analysis (w/o) | | | 5. Powder Density | | |
| | H05 | H05A | 10.69 g/cc | | |
| Hf+Zr | 89.7 | 89.4 | | | |
| Zr | 1.15 | - | | | |
| B | 10.4 | 10.5 | | | |
| C | 0.21 | 0.12 | | | |
| O | 0.07 | 0.11 | | | |
| Total | 100.38 | 100.13 | | | |
| 3. Atomic Ratio | | | 6. Particle Size Distribution | | |
| Over-all | B/Hf _* | = 1.96 | Range (μ) | w/o | |
| Corrected | B/Hf _* | = 2.03 | 0-5 | 7.7 | |
| | | | 5-10 | 29.7 | |
| | | | 10-20 | 32.2 | |
| | | | 20-40 | 30.1 | |
| | | | >40 | 0.3 | |
| 7. Phase Assay (volume per cent) | | | | | |
| Calculated from Composition | HfB ₂ | HfO ₂ | HfC | | |
| | 97.6 | 1.8 | 1.9 | | |

*Atomic ratio corrected for metal assumed to be present as metal dioxide and metal monocarbide.

TABLE 10
ADDITIVE MATERIAL PROCUREMENT SCHEDULE

| <u>Purchase Schedule</u> | | | | |
|--------------------------|------------------|---------------------------|----------------|-----------------|
| <u>Material</u> | <u>Supplier</u> | <u>Quantity</u> pounds | <u>Ordered</u> | <u>Received</u> |
| Silicon Carbide: | | | | |
| Powder | Carborundum | 30 | 3/18/66 | 5/10/66 |
| Fiber | Carborundum | 1 | 3/27/67 | 3/31/67 |
| Silicides: | | | | |
| B ₆ Si | Cerac | 1 | 3/9/67 | 3/14/67 |
| HfSi | Wah Chang | 1 | 3/18/66 | 6/10/66 |
| Metals: | | | | |
| Hf | Wah Chang | 5 | 3/18/66 | 4/ 5/66 |
| Hf-27Ta (01)* | Wah Chang | 0.9 | 5/16/66 | 5/20/66 |
| Hf-27Ta (02)* | Wah Chang | 6 | 3/15/67 | 7/15/67 |
| W (Filament) | General Electric | 1 | 4/13/67 | 5/ 5/67 |
| Cr | J. Hardy | 5 | MANLABS STOCK | |
| Graphites: | | | | |
| Poco (Powder) | AFML | 5.0 | | 2/17/67 |
| Thornel 25 (Fiber) | AFML | 0.5 | | 4/ /67 |

*The designations of (01), (02) refer to different orders of a given material.

TABLE 11

CHARACTERIZATION OF SILICON CARBIDE ADDITIVES

Silicon Carbide Powder, SiC (04)

Qualitative Spectroscopic Analysis:

Si, > 10%; Ti, 0.1-1%; V, 0.01-0.1%; all other
metallic impurities less than 0.01%

Quantitative Chemical Analysis:

Si, 69.8%; C, 29.5%

X-ray Phase Identification:

SiC

Silicon Carbide Fibers

Qualitative Spectroscopic Analysis:

Si > 10%; B, 0.1-1.0%; Mg, Ca, Fe, 0.01-0.1%;
all other metallic impurities less than 0.01%

Suppliers Specifications:

0.5 - 3.0 μ - Diameter

100 - 750 μ - Long

Composition Si + C \geq 95%

TABLE 12
CHARACTERIZATION OF METALS AND ALLOYS

Hafnium Metal Powder, Hf(04)

Qualitative Spectroscopic Analysis:

Hf, > 10%; Zr, 0.1-1%; all other metallic impurities less than 100 ppm.

Qualitative Spectroscopic Analysis (by Supplier):

Zr, 2.50%; all other metallic impurities less than 200 ppm.

Quantitative Chemical Analysis (by Supplier):

O, 790 ppm; C, < 30 ppm.

X-ray Phase Identification:

Hf

Hafnium-Tantalum Alloy Powder, Hf-27Ta(01)

Qualitative Spectroscopic Analysis:

Hf, Ta, > 10%; Zr, 1-10%; all other metallic impurities less than 0.01%.

Quantitative Spectroscopic Analysis (by Supplier):

Zr, 1.9%; W, 0.11%; Mo, 0.06%; all other metallic impurities less than 125 ppm.

Quantitative Chemical Analysis (by Supplier):

Ta, 23.7%; O, 0.15%; C, 50 ppm.

X-ray Phase Identification:

α Hf, β Ta Consistent with phase diagram for this composition.

Tungsten Filament

Qualitative Spectroscopic Analysis:

Th, B, 0.1-1.0%; all other metallic impurities less than 0.01%.

Dimensions:

0.001 inch diameter, 1/8 inch \pm 1/64 inch long.

TABLE 13

CHARACTERIZATION OF SILICIDE ADDITIVES

Hafnium Silicide Powder, HfSi(01)

Qualitative Spectroscopic Analysis:

Hf, Si, > 10%; Zr, 1-10%; all other metallic impurities less than 0.01%.

Quantitative Chemical Analysis (by Supplier):

Atomic Ratio Si/Hf = 1.35.

X-ray Phase Identification:

HfSi, HfSi₂

Boron Silicide Powder, B₆Si(01)

Qualitative Spectroscopic Analysis:

B, Si, > 10%; Mg, 0.1-1.0%; Ca, Mn, Fe, Sn, 0.01-0.1%; all other metallic impurities less than 0.01%.

Quantitative Chemical Analysis:

Si, 31.0

Atomic Ratio:

B/Si = 5.7 (calculated for 68.0% B determined by difference).

X-ray Phase Identification:

SiB₆

TABLE 14

CHARACTERIZATION OF GRAPHITE AND CARBON ADDITIVES

Poco Graphite Powder

Qualitative Spectroscopic Analysis:

B, > 1%; Cr, Mn, Fe, Co, Pb, 0.01-0.1%; all other metallic impurities less than 0.01%.

Particle Size:

-400 mesh.

Thornel 25 Graphite Fibers

Qualitative Spectroscopic Analysis:

All metallic impurities less than 0.01%.

Dimensions:

Regal 330 Carbon Powder

Suppliers (Cabot Corp.) Specification:

Per cent C, 99; per cent volatiles, 1; physical state, amorphorous; particle size, 200A.

TABLE 15

FABRICATION CONDITIONS AND BILLET CHARACTERISTICS FOR
RESULTING DENSITIES FOR CUSTOM PRESSINGS
PERFORMED BY CARBORUNDUM

| <u>Ident. No.</u> | <u>Temp. °C</u> (optical) | <u>Press.</u> (psi) | <u>Hold Time</u> (min) | <u>Density</u> (g/cc) | <u>Billet Characteristics</u> |
|--|------------------------------|------------------------|---------------------------|--------------------------|-------------------------------|
| <u>Carborundum Powder Lot: Carbo 166</u> | | | | | |
| <u>Triplicate Pressing No. 1</u> | | | | | |
| 1A | 2150 | 3000 | 45 | 5.81 | Crack free |
| 1B | | | | 5.79 | Crack free |
| 1C | | | | 5.75 | Crack free |
| <u>Triplicate Pressing No. 2</u> | | | | | |
| 2A | 2000 | 2000 | 45 | 5.70 | Crack free |
| 2B | | | | 5.60 | Circumferential cracks |
| 2C | | | | 5.60 | Circumferential cracks |
| <u>ManLabs Powder Lot I02A</u> | | | | | |
| <u>Single Pressings</u> | | | | | |
| 3 | 1900 | 4000 | 50 | 4.78 | Crack free |
| 4 | 2160 | 4000 | 90 | 6.01 | Crack free |
| 7 | 2160 | 4000 | 50 | 6.04 | Crack free |
| <u>Triplicate Pressing No. 9</u> | | | | | |
| 9A | 2160 | 4000 | 50 | 5.97 | 1/2 inch Radial edge crack |
| 9B | | | | 6.00 | Extensive crack- ing |
| 9C | | | | 6.02 | 1/2 inch Radial edge crack |
| <u>ManLabs Powder Lot I03A</u> | | | | | |
| 5 | 2000 | 4000 | 60 | 5.52 | Crack free |
| 6 | 1900 | 4000 | 100 | 4.88 | Crack free |
| 8 | 2200 | 4000 | 50 | 5.96 | Crack free |
| <u>Triplicate Pressing No. 10</u> | | | | | |
| 10A | 2200 | 4000 | 50 | 6.00 | Extensive crack- ing |
| 10B | | | | 6.03 | Extensive crack- ing |
| 10C | | | | 6.00 | 1/2 inch Radial edge crack |

TABLE 16
POWDER DENSITIES AND MAXIMUM BILLET DENSITIES
FOR MATERIALS I TO XII

| <u>Material Designation</u> | <u>Air Pycnometric Powder Density or Calculated Density (c) gm/cc</u> | <u>Maximum Density Based On A Fabrication gm/cc</u> |
|---------------------------------|---|---|
| I02A | 6.03 \pm .02 | * |
| I03A | 6.04 \pm .01 | * |
| I04 | 6.00 \pm .02 | * |
| I05 | 6.33 \pm .02 | * |
| I06 | 5.96 \pm .02 | 6.03 |
| I07 | 5.96 \pm .02 | * |
| II05 | 10.69 \pm .04 | * |
| II06 | 11.15 \pm .04 | 11.17 |
| II07 | 10.25 \pm . | ** |
| II08 | 9.57 \pm .03 | 10.21 |
| III05 | 9.20 (c) | 9.50 |
| IV05 | 8.45 (c) | 8.62 |
| V02A | 5.47 (c) | 5.54 |
| V03A | 5.47 (c) | * |
| V07 | 5.42 (c) | 5.56 |
| VI05 | 10.89 \pm .02 | 10.97 |
| VIII02A Regal | 4.37 (c) | 4.50 |
| VIII07 Regal | 4.33 (c) | 4.66 |
| VIII07 Poco | 4.44 (c) | * |
| X07 | 5.24 (c) | 5.53 |
| XII02 | 4.11 (c) | * |
| XII07 Poco | 4.32 (c) | * |
| XII07 Regal | 3.88 (c) | * |

* All hot pressed billets were equal to or less than powder density.
** Powder reacted with die.

TABLE 17

MATERIAL LOT PRESSING CONDITIONS AND RESULTS

| <u>Material Designation</u> | <u>Temp.</u> °C | <u>Pressure</u> psi | <u>Time</u> min | <u>Density</u> gm/cc | <u>Grain Intercept</u> μ | <u>Furnace No.</u> |
|---------------------------------|--------------------|------------------------|--------------------|-------------------------|---------------------------------|------------------------|
| I02A D0282 | 2100 | 6000 | 120 | 5.91 | 32 | |
| I02A D0283 | 2050 | 6000 | 60 | 5.87 | 24 | |
| I02A D0289 | 2050 | 6000 | 30 | 5.80 | 22 | |
| I02A D0290 | 2050 | 8000 | 30 | 5.85 | 26 | |
| I02A D0291 | 2200 | 6000 | 30 | 5.78 | 27 | |
| I02A D0304* | 2070 | 6000 | 60 | 5.83 | 35 | |
| I02A D0305F ¹ | 2075 | 6000 | 60 | 5.99 | 35 | |
| I Stark D0306 | 2070 | 6000 | 60 | 6.08 | 10 | |
| I02A D0307F | 2000 | 6000 | 60 | 5.95 | 30 | |
| I03A D0308 | 2070 | 6000 | 60 | 6.05 | 25 | |
| I03A D0309 | 1980 | 6000 | 60 | 6.04 | 20 | |
| I03A D0310 | 1900 | 6000 | 90 | 5.97 | 13 | |
| I03A D0311 | 1800 | 6000 | 120 | 5.54 | 9 | |
| I03A D0312 | 1800 | 6-8000 | 60 | 5.66 | 7 | |
| I03A D0313 | 1900 | 4000 | 60 | 5.99 | 10 | |
| I03A D0314F | 1800 | 6000 | 120 | 6.00 | 8 | |
| I02A D0318** | 2080 | 6000 | 60 | ++ | -- | |
| I03A D0320** | 1900 | 6000 | 60 | 5.81 | 10 | |
| I02A D0322 | 2200 | 4000 | 90 | ++ | -- | |
| I03A D0323 | 1800 | 6000 | 60 | 5.19 | -- | |
| I03A D0324 | 1800 | 6000 | 30 | 5.56 | 7 | |
| I03A D0325 | 1800 | 6000 | 15 | 5.18 | -- | |
| I02A D0326 | 2100 | 6000 | 240 | 6.02 | 40 | |
| I02A D0327 | 1900 | 6000 | 60 | 5.68 | 7 | |
| I03A D0328 | 1800 | 6000 | 25 | 5.37 | 6 | |
| I03A D0329 | 1900 | 4000 | 60 | 6.00 | -- | |
| I03A D0330 | 1900 | 4000 | 90 | 5.98 | -- | |
| I03A D0331 | ---- | ---- | reacted | | -- | |
| I03A D0332 | 1900 | 4000 | 120 | 5.39 | -- | |
| I03A D0333 | 1900 | 4000 | 30 | 4.89 | -- | |
| I03A D0334 | 1900 | 4000 | 180 | 5.94 | -- | |
| I03A D0335 | 2000 | 4000 | 60 | 5.93 | -- | |
| I02A D0336 | 2000 | 4000 | 35 | 5.65 | -- | |
| I02A D0337 | 1900 | 4000 | 90 | 5.62 | 9 | |
| I02A D0338 | 1900 | 4000 | 50 | 5.32 | 30 | |
| I03A D0339 | 1900 | 4000 | 100 | 5.52 | 9 | |
| I03A D0340 | 1900 | 4000 | 145 | 5.82 | 11 | |

* Ball milled with WC balls.

** Sample size 1 inch diameter by 1 inch high.

¹ The letter "F" identifies fluid energy milled powder.

TABLE 17(CONT)

MATERIAL I HOT PRESSING CONDITIONS AND RESULTS

| <u>Material Designation</u> | <u>Temp.</u> °C | <u>Pressure</u> psi | <u>Time</u> min | <u>Density</u> gm/cc | <u>Grain Intercept</u> μ | <u>Furnace No.</u> |
|---------------------------------|--------------------|------------------------|--------------------|-------------------------|---------------------------------|------------------------|
| I02A D0341 | 2100 | 6000 | 90 | 5.89 | 31 | |
| I02A D0342 | 2200 | 4000 | 40 | 4.88 | -- | |
| I02A D0343 | 2000 | 4000 | 60 | 5.43 | 6 | |
| I02A D0344 | 2100 | 4000 | 25 | 5.40 | -- | |
| I02A D0345F | 1950 | 6000 | 225 | 5.97 | 21 | |
| I02A D0347 | 2100 | 4000 | 40 | 5.66 | -- | |
| I03A D0359 | 2000 | 4000 | 75 | 5.94 | -- | |
| I03A D0360 | 2000 | 4000 | 75 | 5.77 | -- | |
| I02A D0361 | 2160 | 4000 | 50 | 5.70 | | |
| I02A D0362 | 2160 | 4000 | 35 | 5.76 | | |
| I02A D0363F | 2100 | 4000 | 80 | 3.87 | 24 | |
| I02A D0364 | 2160 | 4000 | 90 | 5.91 | | |
| I02A D0365 | Reacted | | | | | |
| I03A D0366 | 2000 | 4000 | 75 | 5.92 | | |
| I03A D0367 | 2000 | 4000 | 75 | 5.85 | | |
| I03A D0368 | 2000 | 4000 | 75 | 5.68 | | |
| I03A D0369 | 2000 | 4000 | 75 | 6.00 | | |
| I03A D0414 | 2000 | 4000 | 120 | 5.88 | 15 | |
| I03A D0415 | 2000 | 4000 | 73 | 5.78 | 12 | |
| I03A D0416 | 2000 | 4000 | 110 | 3.95 | | |
| I03A D0417 | 1900 | 6000 | 105 | Reacted | | |
| I02A D0418 | 2100 | 6000 | 163 | 5.88 | | |
| I02A D0419F | 1900 | 6000 | 102 | 5.80 | 13 | |
| I03A D0420F | 1800 | 6000 | 220 | 5.81 | | |
| I02A D0421F | 2000 | 6000 | 115 | 5.93 | 30 | |
| I03A D0422 | 1900 | 6000 | 120 | 6.00 | | |
| I05 D0455 | 1900 | 4000 | 110 | 4.95 | | 1B |
| I05 D0446 | 2000 | 2500 | 31 | 3.94 | | 2B |
| I04 D0447 | 2000 | 6000 | 80 | 5.64 | 10 | 3B |
| I05 D0450 | 2100 | 6000 | 130 | 6.11 | 8 | 1B |
| I05 D0451 | 2000 | 6000 | 80 | 4.76 | | 2B |
| I04 D0452 | 2100 | 6000 | 150 | 5.81 | 19 | 3B |
| I04 D0453 | 2000 | 6000 | 70 | 4.35 | | 2B |
| I05 D0454 | 2100 | 4000 | 80 | 5.08 | | 1B |
| I05 D0455 | 2200 | 4000 | 75 | 6.22 | | 3B |
| I02A D0481 | 2150 | 5000 | 33 | | | 3C |
| I03A D0483 | 2080 | 4000 | 1000 | 5.87 | | 2C |
| I03A D0484 | 2080 | 4000 | 90 | 5.91 | 13 | 2C |
| I02A D0485 | 2100 | 6000 | 270 | 5.02 | | 1C |
| I06 D0486 | 2100 | 6000 | 180 | Reacted | | 3C |
| I06 D0489 | 2000 | 6000 | 160 | 6.03 | | 3C |

TABLE 17 (CONT)

MATERIAL I HOT PRESSING CONDITIONS AND RESULTS

| <u>Material Designation</u> | <u>Temp.</u> °C | <u>Pressure</u> psi | <u>Time</u> min | <u>Density</u> gm/cc | <u>Grain Intercept</u> μ | <u>Furnace No.</u> |
|---------------------------------|--------------------|------------------------|--------------------|-------------------------|---------------------------------|------------------------|
| I03A D0475K* | 2100 | 2500 | 120 | 5.99 | 23 | 2B |
| I03A D0459K | 2000 | 2500 | 55 | 5.5 | | 3C |
| I05 D0463 | 2220 | 6000 | 180 | 5.63 | 7 | 3C |
| I03A D0466 | 2220 | 8000 | 90 | 6.03 | 29 | 1C |
| I02A D0481 | 2150 | 5000 | 33 | | | 3C |
| I03A D0483 | 2080 | 4000 | 100 | 5.87 | 33 | 2C |
| I03A D0484 | 2080 | 4000 | 90 | 5.91 | 13 | 2C |
| I02A D0485 | 2100 | 6000 | 270 | 5.02 | | 1C |
| I06 D0486 | 2100 | 6000 | 240 | | | 3C |
| I06 D0489 | 2000 | 6000 | 160 | 6.03 | 7 | 3C |
| I03A VB01 | 1500- | 4000 | 400 | 4.01 | 31 | |
| | 1600 | | (vacuum) | | | |
| I03A D0539K | 2100 | 2500 | 120 | 6.06 | | 1E |
| I03A D0542K | 2000 | 2500 | 75 | | | |
| I03A D0545K | 2000 | 2500 | 110 | | | 2E |
| I03A D0548K | 2000 | 4000 | 60 | 5.17 | 97 | 2E |
| I07 D0555 | 2000 | 4000 | 60 | 5.75 | 22 | 1E |
| I07 D0558 | 2000 | 4000 | 150 | 5.81 | | 1E |
| I07 D0560 | 1950 | 3000 | 60 | 5.69 | | 1E |
| I03A D0563K | 2050 | 2500 | 105 | 5.94 | 56 | 3E |
| I07 D0574 | 2050 | 4000 | 80 | 5.83 | 35 | 3E |
| I07 D0575 | 2100 | 4000 | 75 | 5.75 | 34 | 1E |
| I05A D0587 | 2100 | 4000 | 65 | 5.90 | 69 | 3E |
| I07 D0589 | 2150 | 4000 | 120 | 5.90 | 38 | 1E |
| I05A D0590 | 2050 | 4000 | 80 | 5.93 | 15 | 1E |
| I02A D0610 | 2100 | 4000 | 60 | 5.81 | | 2 |
| I02A D0613 | 2060 | 4000 | 60 | 5.45 | 18 | 2 |
| I03 D0619 | 2000 | 2500 | 140 | 6.02 | | 2 |
| I07 D0628F | 2060 | 4000 | 55 | 5.98 | | 2 |
| I05A D0650K | 2080 | 2500 | 120 | 5.92 | | |
| I03A D0656 | 1900 | 4000 | 58 | | | 3 |
| I03A D0657 | 2100 | 4000 | 60 | | | 2 |

* Letter "K" designated billets 3 inch diameter by 1 inch high, all other billets 2 inch diameter by 0.7 inch high.

TABLE 18
QUANTITATIVE METALLOGRAPHIC PHASE ANALYSIS
FOR HOT PRESSED ZrB_2

| <u>Phase</u> | <u>Volume Percentage*</u> | |
|----------------------|---------------------------|-------------------|
| | <u>I03A D0308</u> | <u>I02A D0283</u> |
| ZrB_2 | 87.85 | 87.7 |
| Orange Phase | 2.33 | 1.1 |
| ZrO_2 (Gray Phase) | 9.82 | 8.5 |
| Pores by Density | | 2.7 |

* Data obtained from twelve lineal analysis traces of approximately 500 microns each.

TABLE 19

MATERIAL I WITH INTENTIONAL IMPURITY PHASE ADDITIONS,
FABRICATION CONDITIONS AND RESULTS

| <u>Material Designation</u> | <u>Temp.</u> °C | <u>Pressure</u> psi | <u>Time</u> min | <u>Density</u> gm/cc |
|--|--------------------|------------------------|--------------------|-------------------------|
| I02A D0302 (+5 w/o ZrO ₂) | 2070 | 6000 | 30 | 6.03 |
| I02A D0303 (+5 w/o ZrC) | 2070 | 6000 | 30 | 6.04 |
| I02A D0504 (+10 w/o Y ₂ O ₃ - ZrO ₂) | 1950 | 4000 | 60 | 4.99 |
| I02A D0505 (+10 w/o ZrO ₂) | 1950 | 4000 | 70 | |

TABLE 20

MATERIAL V FABRICATION CONDITIONS AND RESULTS

| <u>Material Designation</u> | <u>Temp.</u> °C | <u>Pressure</u> psi | <u>Time</u> min | <u>Density</u> gm/cc | <u>Grain Intercept</u> μ | <u>Furnace No.</u> |
|-----------------------------|--------------------|------------------------|--------------------|-------------------------|-----------------------------|--------------------|
| V02A D0370 | 2160 | 4000 | 50 | 5.49 | 9 | 3 |
| V02A D0371 | 2160 | 6000 | 58 | 5.49 | 8 | 2 |
| V02A D0372 | 2100 | 4000 | 67 | 5.47 | 8 | 1 |
| V02A D0378 | 2160 | 6000 | 120 | 5.55 | 11 | 2 |
| V03A D0381 | 2000 | 4000 | 60 | 5.83 | | 1 |
| V02A D0382 | 2100 | 4000 | 60 | 5.51 | | 2A |
| V03A D0384 | 2000 | 4000 | 70 | 5.54 | | 1A |
| V02A D0387 | 2100 | 4000 | 20 | 5.45 | 7 | 1A |
| V02A D0388 | 1900 | 4000 | 30 | 4.79 | 5 | 2A |
| V03A D0389 | 1900 | 4000 | 40 | 5.30 | | 3A |
| V02A D0390F* | 2000 | 4000 | 25 | 5.11 | 7 | 3A |
| V02A D0391F | 2000 | 4000 | 15 | 5.02 | 7 | 1B |
| V02A D0392F | 2000 | 4000 | 45 | 5.21 | 7 | 1B |
| V02A D0393F | 2000 | 4000 | 35 | 5.40 | 6 | 2B |
| V02A D0394F | 2000 | 4000 | 50 | 5.47 | 6 | 3B |
| V02A D0395 | 1900 | 4000 | 115 | 5.22 | 7 | 3B |
| V02A D0396 | 1900 | 4000 | 125 | 5.49 | 7 | 2B |
| V02A D0397 | 1900 | 4000 | 110 | 5.28 | 8 | 1B |
| V02A D0398 | 1800 | 6000 | 120 | 5.23 | 6 | 2B |
| V03A D0473 | 2000 | 4000 | 40 | 5.24 | 7 | 1C |
| V03A D0474 | 2000 | 4000 | 40 | 5.29 | | 2C |
| V03A D0477 | 2100 | 4000 | 45 | 5.33 | | 3C |
| V03A D0478 | 2000 | 2500 | 50 | 5.02 | 7 | 1C |
| V03A D0479 | 2000 | 2500 | 20 | 4.50 | | 2C |
| V03A D0480 | 2000 | 6000 | 90 | 5.54 ⁺ | 7 | 1C |
| V02A Q2206L | 2000 | 2500 | 90 | 5.40 ⁺ | | 4A |
| V02A Q2221L | 2000 | 1000 | 75 | 5.12 | | 4A |
| V02A Q2235L | 2050 | 1000 | 60 | | | |
| | | 2000 | 60 | 5.31 | | 4A |
| V(5)02 D0531 | 2050 | 4000 | 60 | 5.84 | 11 | 1D |
| V(10)02 D0532 | 2050 | 4000 | 60 | 5.80 | 10 | 1D |
| V(15)02 D0533 | 2050 | 4000 | 60 | 5.66 | 6 | 1D |
| V(35)02 D0541 | 2050 | 4000 | 50 | 5.04 | 6 | |
| V(50)02 D0557 | 2000 | 4000 | 105 | 3.57 | 5 | 3E |
| V02A D0570 | 2100 | 4000 | 85 | 5.44 | | 2E |
| V07 D0571K ⁺⁺ | 2000 | 2500 | 50 | 5.20 | | 1E |

* F Fluid Energy milled.

** L designates billet size 5-3/4 inch x 5-3/4 inch x 1 inch.

⁺ Cracked during extraction from the die.

⁺⁺ K designates billet size 3 inch diameter x 1 inch high.

TABLE 20 (CONT)

MATERIAL V FABRICATION CONDITIONS AND RESULTS

| <u>Material Designation</u> | <u>Temp.</u> °C | <u>Pressure</u> psi | <u>Time</u> min | <u>Density</u> gm/cc | <u>Grain Intercept</u> μ | <u>Furnace No.</u> |
|---------------------------------|--------------------|------------------------|--------------------|-------------------------|---------------------------------|------------------------|
| V07 D0576K | 2100 | 2500 | 90 | 5.39 | | 2E |
| V07 D0578K | 2100 | 2500 | 40 | 5.59 | | 2E |
| V07 D0580K | 2100 | 2500 | 55 | 5.56 | 7 | 2E |
| V07 D0582K | 2100 | 2500 | 50 | 5.53 | | 3E |
| V07 D0586K | 2100 | 4000 | 37 | 5.55 | | 1E |
| V07 D0594 | 2100 | 4000 | 160 | 5.54 | | 1E |
| V02A D0612 | 2060 | 4000 | 60 | 5.44 | | 1 |
| V02A D0614 | 1900 | 4000 | 60 | 4.93 | | 1 |
| V07 D0616 | 2060 | 4000 | 40 | 5.39 | | 2 |
| V05 D0617 | 2060 | 4000 | 45 | 5.71 | | 1 |
| V05A D0618 | 2060 | 4000 | 80 | 5.54 | 9 | 1 |
| V07Q 2295L | 2000 | 2500 | 132 | 5.53 | | |
| V05A D0622 | 2100 | 4000 | 125 | 3.76 | | 1 |
| V07Q 2297L | 2000 | 2500 | 80 | 5.50 | | 2 |
| V03A D0658 | 1900 | 4000 | 60 | 4.95 | | 3 |
| V03A D0659 | 2100 | 4000 | 60 | 5.49 | | 3 |

TABLE 21
FABRICATION CONDITIONS FOR SPECIAL MATERIALS USED
FOR MATERIAL V PHASE ANALYSIS

| <u>Composition</u> | <u>Billet</u> | <u>Temp.</u> °C | <u>Pressure</u> psi | <u>Time</u> min | <u>Furnace</u> <u>No.</u> |
|--|---------------|--------------------|------------------------|--------------------|------------------------------|
| 20 v/o ZrC 80 v/o SiC | D0623 | 2100 | 4000 | 160 | 1 |
| 20 v/o ZrO ₂ 80 v/o SiC | D0624 | 2050 | 4000 | 120 | 1 |
| 20 v/o I05A 20 v/o ZrC 60 v/o SiC | D0625 | 2050 | 4000 | 110 | 2 |
| 20 v/o I05A 20 v/o ZrO ₂ 60 v/o SiC | D0626 | 2050 | 4000 | 100 | 1 |
| 20 v/o ZrC 20 v/o ZrO ₂ 60 v/o SiC | D0627 | 2050 | 4000 | 155 | 1 |

TABLE 22

MICROSTRUCTURE STUDY OF SPECIAL MATERIALS USED FOR MATERIAL V ANALYSIS

| Billet No. | Power Mixture Composition | X-ray Phase Identification | | Microhardness, KHN [*] | | Color | Result of Etching with | | |
|------------|--|----------------------------|------------------|--|---------------------------------------|-------|------------------------|------------------|--------------------------------|
| | | | | | | | HNO ₃ +HF | HNO ₃ | H ₂ SO ₄ |
| | | Before | After | Accepted Kg/mm ² | Measured Kg/mm ² | | | | |
| D0622 | 20v/o ZrB ₂ 80v/o SiC | ZrB ₂ | ZrB ₂ | 950 (50g) 1030 (100g) 3000 (100g) 1875 (100g) | 967 (25g) 1231 (25g) 2241 (25g) | white | etched | no attack | no attack |
| | | SiC | SiC | | | gray | etched | etched | etched |
| D0623 | 20v/o ZrC 80v/o SiC | ZrC | ZrC | 950 (50g) 1030 (100g) 3000 (100g) 1875 (100g) | 967 (25g) 1231 (25g) 2241 (25g) | white | etched | no attack | no attack |
| | | SiC | SiC | | | gray | etched | etched | etched |
| D0624 | 20v/o ZrO ₂ 80v/o SiC | ZrO ₂ | ZrO ₂ | 950 (50g) 1030 (100g) 3000 (100g) 1875 (100g) | 967 (25g) 1231 (25g) 2241 (25g) | white | etched | no attack | no attack |
| | | SiC | SiC | | | gray | etched | etched | etched |
| D0625 | 20v/o ZrB ₂ 20v/o ZrC 60v/o SiC | ZrB ₂ | ZrB ₂ | 950 (50g) 1030 (100g) 3000 (100g) 1875 (100g) | 967 (25g) 1231 (25g) 2241 (25g) | white | etched | no attack | no attack |
| | | ZrC | ZrC | | | gray | etched | etched | etched |
| D0626 | 20v/o ZrB ₂ 20v/o ZrO ₂ | ZrB ₂ | ZrB ₂ | 950 (50g) 1030 (100g) 3000 (100g) 1875 (100g) | 967 (25g) 1231 (25g) 2241 (25g) | white | etched | no attack | no attack |
| | | ZrO ₂ | ZrO ₂ | | | gray | etched | etched | etched |
| D0627 | 20v/o ZrC 20v/o ZrO ₂ 60v/o SiC | ZrC | ZrC | 950 (50g) 1030 (100g) 3000 (100g) 1875 (100g) | 967 (25g) 1231 (25g) 2241 (25g) | white | etched | no attack | no attack |
| | | ZrO ₂ | ZrO ₂ | | | gray | etched | etched | etched |

* Load values shown in parentheses.

TABLE 23
MATERIAL VIII FABRICATION CONDITIONS AND RESULTS

| <u>Material Designation</u> | <u>Graphite Source</u> | <u>Temp.</u> °C | <u>Pressure</u> psi | <u>Time</u> min | <u>Density</u> gm/cc | <u>Grain Inter- cept</u> μ | <u>Furnace No.</u> |
|---------------------------------|----------------------------|--------------------|------------------------|--------------------|-------------------------|---------------------------------------|------------------------|
| VIII02 D0497 | Regal | 2200 | 4000 | 90 | Reacted | | |
| VIII02 D0498 | Regal | 2100 | 4000 | 90 | 4.53 | 5 | 3C |
| VIII02A D0592 | Poco | 2050 | 4000 | 100 | 4.50 | 5 | 3E |
| VIII07 D0605K | Regal | 2100 | 2500 | 48 | Reacted | | 2 |
| VIII07 D0606K | Regal | 2050 | 2500 | 190 | 4.55 | | 3 |
| VIII07 D0607 | Poco | 2050 | 4000 | 82 | 4.42 | 4 | 3 |
| VIII07 D0609 | Aquadag | 2050 | 4000 | 70 | 4.57 | 4 | 2 |
| VIII(17)(15)07 D0620 | Regal | 2050 | 4000 | 120 | 5.04 | 4 | 2 |
| VIII07 D0621K | Regal | 2060 | 2500 | 155 | 4.47 | | 1 |
| VIII07 Q2301L | Regal | 2000 | 2500 | 140 | 4.27 | | |

TABLE 24
MATERIAL X FABRICATION CONDITIONS AND RESULTS

| <u>Material Designation</u> | <u>Temp.</u> °C | <u>Pressure</u> psi | <u>Time</u> min | <u>Density</u> gm/cc | <u>Grain Intercept</u> μ | <u>Furnace No.</u> |
|---------------------------------|--------------------|------------------------|--------------------|-------------------------|---------------------------------|------------------------|
| X07 D0596 | 1900 | 4000 | 40 | 5.53 | 12 | 1 |
| X07 D0597 | 1800 | 4000 | 50 | 5.28 | 4 | 1 |
| X07 D0634 | 1700 | 4000 | 195 | 5.28 | 5 | 1 |
| X07 D0635 | 2000 | 4000 | 140 | 5.81 | 15 | 3 |

TABLE 25

MATERIAL XII FABRICATION CONDITIONS AND RESULTS

| <u>Material Designation</u> | <u>Graphite Source</u> | <u>Temp.</u> °C | <u>Pressure</u> psi | <u>Time</u> min | <u>Density</u> gm/cc | <u>Grain Intercept</u> μ | <u>Furnace No.</u> |
|---------------------------------|----------------------------|--------------------|------------------------|--------------------|-------------------------|---------------------------------|------------------------|
| XII02 D0544 | Poco | 2200 | 4000 | 60 | Reacted | | 2E |
| XII02 D0546 | Poco | 2100 | 4000 | 120 | 3.64 | | 2E |
| XII07 D0579 | Poco | 2100 | 4000 | 80 | 4.06 | 4 | 3E |
| XII(20)07 D0585 | Poco | 2100 | 4000 | 50 | 5.30 | 5 | 1E |
| XII(5)07 D0500 | Poco | 2100 | 4000 | 80 | Reacted | | 1E |
| XII(10)07 D0601 | Poco | 2100 | 4000 | Reacted | | | 2E |
| XII(5)07 D0602 | Poco | 2050 | 4000 | 145 | 5.89 | | 2 |
| XII(15)07 D0603 | Poco | 2050 | 4000 | 105 | 5.42 | 6 | 3 |
| XII(35)07 D0604 | Poco | 2050 | 4000 | 190 | 4.61 | 4 | 2 |
| XII(20)07 D0608 | Regal | 2050 | 4000 | 80 | 5.23 | 5 | 2 |
| XII(5)07 D0615 | Thornel | 2060 | 4000 | 103 | 5.89 | | 1 |
| XII07 D0629K | Regal | 2060 | 2500 | 113 | 3.88 | | 2 |
| XII07 D0630K | Regal | 2060 | 2500 | 69 | Porous | | 1 |
| XII(5)07 D0638 | Regal | 2080 | 4000 | 73 | 5.89 | | 3 |
| XII(10)07 D0634 | Regal | 2080 | 4000 | 80 | 5.61 | | 1 |
| XII(15)07 D0641 | Regal | 2080 | 4000 | 85 | 5.51 | | 1 |
| XII(20)07 D0642 | Regal | 2080 | 4000 | 80 | 5.19 | | 3 |
| XII(5)07 D0665 | Poco | 1900 | 4000 | 120 | | | 3 |
| XII(10)07 D0667 | Poco | 2050 | 4000 | 202 | | | 3 |
| XII(5)07 D0668 | Poco | 2050 | 4000 | 200 | | | 1 |

TABLE 26

MATERIAL II HOT PRESSING CONDITIONS AND RESULTS

| <u>Material Designation</u> | <u>Temp.</u> °C | <u>Pressure</u> psi | <u>Time</u> min | <u>Density</u> gm/cc | <u>Grain Intercept</u> μ | <u>Furnace No.</u> |
|---------------------------------|--------------------|------------------------|--------------------|-------------------------|---------------------------------|------------------------|
| II05 D0315 | 2000 | 6000 | 150 | 9.23 | 9 | |
| II05 D0316 | 2200 | 6000 | 120 | 10.62 | 40 | |
| II05 D0346 | 2100 | 6000 | 60 | 9.52 | 12 | |
| II05 D0348 | 2200 | 6000 | 200 | 10.58 | 34 | |
| II05 D0349 | 2150 | 6000 | 30 | 9.53 | 11 | |
| II05 D0351 | 2200 | 4000 | 200 | 10.53 | 31 | |
| II05 D0352 | 2100 | 4000 | 150 | 10.25 | 15 | |
| II05 D0353 | 2200 | 4000 | 140 | 10.52 | 37 | |
| II05 D0354A | 2165 | 4000 | 120 | 10.32 | | |
| II05 D0354B | 2165 | 4000 | 120 | 10.53 | | |
| II05 D0355A | 2200 | 4000 | 120 | 10.50 | 42 | |
| II05 D0355B | 2200 | 4000 | 120 | 10.46 | 41 | |
| II05 D0356A | 2170 | 4000 | 120 | 10.07 | | |
| II05 D0356B | 2170 | 4000 | 120 | 10.19 | 19 | |
| II05 D0357 | 2150-2200 | 4000 | 120 | 9.93 | 14 | |
| II06 D0373 | 2200 | 4000 | 55 | 11.10 | | 2A |
| II06 D0374 | 2100 | 4000 | 42 | 11.17 | | 3A |
| II06 D0375 | 2000 | 4000 | 68 | 11.15 | | 1A |
| II06 D0376 | 1900 | 4000 | 145 | 11.14 | 7 | 3A |
| II06 D0379 | 1800 | 4000 | 130 | 10.84 | 5 | 3A |
| II06 D0383 | 2000 | 4000 | 40 | 11.17 | | 3A |
| II05 D0399 | 1900 | 4000 | 100 | 9.10 | | 3B |
| II05 D0409 | 2000 | 6000 | 180 | 9.80 | 8 | 3B |
| II05 D0413 | 2100 | 2500 | 124 | 9.54 | | 3B |
| II05 D0423 | 1900 | 6000 | 180 | 9.26 | 9 | 2B |
| II05 D0425 | 2000 | 4000 | 153 | 9.45 | 9 | 1B |
| II05 D0427 | 2100 | 4000 | 108 | 9.57 | 15 | 2B |
| II05 D0429 | 2100 | 6000 | 137 | 10.13 | | 1B |
| II05 D0430 | 2200 | 2500 | 60 | Reacted | | 3B |
| II05 D0435 | 2100 | 6000 | 95 | 9.84 | | 3B |
| II05 D0437 | 2200 | 2500 | 110 | 9.93 | | 2B |
| II07 D0458 | 2200 | 4000 | 53 | Reacted | 22 | 1B |
| II05 D0471 | 2000 | 8000 | 30 | 9.36 | | 3C |
| II05 D0482F | 2100 | 6000 | 40 | 10.24 | | 3C |
| II05 D0482A | 1980 | 6000 | 60 | 10.21 | | 2C |
| II08 D0487 | 2200 | 4000 | 120 | 9.95 | 46 | 2C |
| II08 D0490 | 2100 | 4000 | 160 | 10.21 | 23 | 2C |
| II05 D0595K | 2100 | 2500 | 20 | 9.51 | | 3E |
| II06 D0672 | 1900 | 4000 | 165 | 10.67 | | |

TABLE 27
 PHASE DISTRIBUTIONS FOR HOT PRESSED BILLETS
 OF MATERIALS II, III AND IV

| <u>Material Designation</u> | <u>HfB₂</u> | <u>SiC</u> | <u>Volume Per Cent</u> | | |
|---------------------------------|------------------------|------------|-------------------------------------|-------------------------------------|--------------|
| | | | <u>Major Impurity Phase</u> | <u>Grain Boundary Phase</u> | <u>Pores</u> |
| II05 D0316 | 91.4 | 0 | 7.8 | 0.1 | 0.7 |
| III05 D0377 | 71.8 | 24.8 | 3.4 | 0 | 0 |
| IV05 D0405 | 69.2 | 29.5 | 1.3 | 0 | 0 |

TABLE 28

MATERIAL III HOT PRESSING CONDITIONS AND RESULTS

| <u>Material Designation</u> * | <u>Temp.</u> °C | <u>Pressure</u> psi | <u>Time</u> min | <u>Density</u> gm/cc | <u>Grain Intercept</u> μ | <u>Furnace No.</u> |
|-----------------------------------|--------------------|------------------------|--------------------|-------------------------|---------------------------------|------------------------|
| III05 D0377 | 2200 | 4000 | 90 | 9.50 | 16 | 2A |
| III05 D0380 | 2150 | 4000 | 90 | 9.41 | 12 | 1A |
| III05 D0385 | 2050 | 4000 | 75 | 9.25 | 9 | 2A |
| III05 D0386 | 2050 | 4000 | 60 | 9.26 | 9 | 3A |
| III05 D0400 | 2000 | 4000 | 110 | 8.86 | 9 | 1B |
| III05 D0401 | 1900 | 4000 | 100 | 8.19 | 5 | 2B |
| III05 D0402 | 1900 | 6000 | 160 | 7.84 | 6 | 1B |
| III05 D0403 | 2100 | 4000 | 90 | 9.28 | 8 | 2B |
| III05 D0404 | 1800 | 5000 | 120 | 7.34 | | 3B |
| III05 D0408 | 2000 | 6000 | 160 | 9.03 | 5 | 1B |
| III05 D0412 | 2100 | 2500 | 132 | 9.12 | 10 | 1B |
| III05 D0426 | 2000 | 4000 | 128 | 9.06 | 7 | 3B |
| III05 D0431 | 2200 | 2500 | 80 | 8.61 | | 3B |
| III05 D0433 | 2200 | 4000 | 39 | 9.33 | 11 | 1B |
| III05 D0438 | 2100 | 2500 | 100 | 9.04 | | 1B |
| III05 D0440 | 2000 | 2500 | 128 | 7.82 | | 1B |
| III05 D0444 | 2000 | 4000 | 100 | 8.52 | 6 | 1B |
| III(5) 05 D0496 | 2200 | 4000 | 90 | 10.16 | 63 | 2C |
| III(10)05 D0503 | 2150 | 4000 | 90 | 10.00 | | 3C |
| III(10)05 D0538 | 2030 | 4000 | 70 | 9.81 | 9 | 1D |
| III(10)05 D0559 | 1950 | 3000 | 60 | 7.35 | | 3E |
| III05 D0573 | 2100 | 4000 | 80 | 9.18 | | 2E |
| III05 D0583K | 2100 | 4000 | 80 | 9.30 | | 2E |
| III(50)05 D0593 | 2050 | 4000 | 120 | 6.79 | | 3E |
| III05 D0599K | 2100 | 2500 | 40 | 9.23 | | 1E |

*The basic composition of Material III contains 20 vol. % SiC. Composition variations from this base are denoted by placing the vol. % of SiC in parenthesis following the roman numeral III.

TABLE 29

MATERIAL IV FABRICATION CONDITIONS AND RESULTS

| <u>Material *</u> <u>Designation</u> | <u>Temp.</u> °C | <u>Pressure</u> psi | <u>Time</u> min | <u>Density</u> gm/cc | <u>Grain</u> <u>Intercept</u> μ | <u>Furnace</u> <u>No.</u> |
|---|--------------------|------------------------|--------------------|-------------------------|---------------------------------------|------------------------------|
| IV05 D0405 | 2200 | 4000 | 103 | 8.62 | 13 | 1B |
| IV05 D0406 | 2100 | 4000 | 70 | 8.60 | 8 | 2B |
| IV05 D0407 | 2000 | 4000 | 110 | 7.92 | 8 | 2B |
| IV05 D0410 | 2000 | 6000 | 191 | 8.57 | 6 | 2B |
| IV05 D0411 | 2100 | 2500 | 160 | 7.91 | 7 | 1B |
| IV05 D0424 | 1900 | 6000 | 122 | 7.78 | 7 | 1B |
| IV05 D0428 | 1900 | 4000 | 127 | 6.98 | | 2B |
| IV05 D0432 | 2200 | 2500 | 60 | Reacted | | 1B |
| IV05 D0434 | 2000 | 4000 | 80 | 8.45 | 8 | 2B |
| IV05 D0436 | 2100 | 2500 | 120 | 7.97 | | 3B |
| IV05 D0439 | 2100 | 4000 | 68 | 8.57 | 8 | 2B |
| IV05 D0441 | 2000 | 2500 | 80 | 6.88 | | 3B |
| IV05 D0442 | 1900 | 4000 | 141 | 6.97 | | 2B |
| IV05 D0443 | 2000 | 4000 | 90 | 7.99 | | 3B |
| IV05 D0448 | 2150 | 2500 | 50 | 8.59 | 10 | 3B |
| IV05 D0449 | 2050 | 4000 | 140 | 7.78 | 7 | 2B |
| IV05 D0476 | 2000 | 5000 | 95 | 7.94 | 6 | 2C |
| IV05 D0547 | 2000 | 4000 | 80 | Cracked | | 2E |
| IV05 D0549 | 2000 | 4000 | 140 | 8.53 | | 3E |

* The basic composition of Material IV contains 30 vol. % SiC.

TABLE 30

MATERIAL VI FABRICATION CONDITIONS AND RESULTS

| <u>Material Designation</u> | <u>Temp.</u> °C | <u>Pressure</u> psi | <u>Time</u> min | <u>Density</u> gm/cc | <u>Grain Intercept</u> μ | <u>Furnace No.</u> |
|---------------------------------|--------------------|------------------------|--------------------|-------------------------|---------------------------------|------------------------|
| VI05 D0460 | 2000 | 6000 | 120 | 9.01 | | 2C |
| VI05 D0461 | 2100 | 6000 | 160 | 10.03 | 8 | 1C |
| VI05 D0462 | 2200 | 4000 | 190 | 10.97 | 14 | 1C |

TABLE 31
 PHASE DISTRIBUTION FOR MATERIAL VI
 BILLET VI05 D0462

| <u>Phase</u> | <u>Volume Per Cent</u> |
|------------------|------------------------|
| HfB ₂ | 92 |
| Hf-Ta Phase | 6.3 |
| Gray Phase | 1.7 |
| Porosity | 0.0 |

TABLE 32
INCIDENCE OF BILLET CRACKING FOR
MATERIALS I AND II

| <u>Designation</u> | <u>Powder</u> | | <u>Number/ Total</u> | <u>Per Cent</u> |
|--------------------|---------------|-------------------------------|--------------------------|-----------------|
| I | 02A | severe cracks*/total examined | 0/13 | 0 |
| | 02A | edge cracks/total examined | 4/13 | 31 |
| | 02A | total cracked/total examined | 4/13 | 31 |
| | 03A | severe cracks/total examined | 4/19 | 21 |
| | 03A | edge cracks/total examined | 6/19 | 31 |
| | 03A | total cracked/total examined | 10/19 | 53 |
| | all** | severe cracks/total examined | 6/38 | 16 |
| | all | edge cracks/total examined | 12/38 | 31 |
| | all | total cracked/total examined | 18/38 | 47 |
| II | 05 | severe cracks/total examined | 3/24 | 13 |
| | 05 | edge cracks/total examined | 4/24 | 17 |
| | 05 | total cracked/total examined | 7/24 | 29 |
| | 06 | severe cracks/total examined | 4/5 | 80 |
| | 06 | edge cracks/total examined | 0/5 | 0 |
| | 06 | total cracks/total examined | 4/5 | 80 |

*Severe cracks, indicates billet scraped.

**Includes I02A, I03A, I04, I05 and I06 powders.

TABLE 33
PRESS FORGING OF MATERIAL I

| <u>Material Designation</u> | <u>Original Billet</u> | <u>Original Density %</u> | <u>Forging Temp. °C</u> | <u>Forging Pressure psi</u> | <u>Forging Time min</u> | <u>Final Density %</u> | <u>Reduction in Height %</u> |
|-----------------------------|------------------------|---------------------------|-------------------------|-----------------------------|-------------------------|------------------------|------------------------------|
| I05 D0463 | D0451 | 79 | 2200 | 6000 | 180 | 93.3 | 32* |
| I03A D0466 | D0369 | 99.5 | 2200 | 8000 | 90 | 100 | 16 |

* Partially due to densification.

TABLE 34
PLASMA SPRAYING OF MATERIALS I AND II

| <u>Material Designation</u> | <u>Substrate</u> | <u>Gun to Work Distance</u> inches | <u>Current</u> amps | <u>Results</u> |
|---------------------------------|------------------|---|------------------------|--------------------------------------|
| I02A P009F | Silica Phenolic | 5 | 700 | 12 mil coating, poor self bonding |
| II05 P007 | Silica Phenolic | 5 | 700 | 12 mil coating, poor self bonding |
| I02A P0158F | Stainless Steel | 5 | 700 | 3 mil coating, poor self bonding |
| I02A P0159F | Stainless Steel | 2-3 | 750 | 5 mil coating |
| I02A P0160F | Stainless Steel | 2-3 | 750 | 7 mil coating |
| I02A P0161 | Stainless Steel | 2-3 | 750 | 5 mil coating |
| I02A P0162F | Stainless Steel | 2-3 | 750 | Poor adherence |
| I02A P0175 | Stainless Steel | 2-3 | 750 | 12 mil coating |
| I02A P0176 | Copper | 2-3 | 750 | 11 mil coating |
| I02A P0177 | Aluminum | 2-3 | 750 | 8 mil coating |

TABLE 35

SINTERING CONDITIONS AND RESULTS

| <u>Material Designation</u> | <u>Cold Pressing Pressure</u> 10 ³ psi | <u>Temp.</u> °C | <u>Time</u> min | <u>Atmosphere</u> | <u>Density</u> gm/cc | <u>Wt. Loss</u> % | <u>Laminations</u> |
|-----------------------------|--|--------------------|--------------------|------------------------|-------------------------|----------------------|--------------------|
| V03A B0001* | 70 | 2075 | 60 | 1.5 x 10 ⁻⁵ | 3.68 | 7.27 | No |
| I03A B0002* | 70 | 2075 | 60 | 1.5 x 10 ⁻⁵ | | 2.67 | Yes |
| I03A B0003* | 15 | 2200 | 150 | 1.0 x 10 ⁻⁵ | 5.23 | 28.8 | Yes |
| I03A B0004* | 40 | 2200 | 150 | 1.0 x 10 ⁻⁵ | 5.35 | 27.5 | Yes |
| I03A B0005* | 70 | 2200 | 150 | 1.0 x 10 ⁻⁵ | 5.43 | 28.2 | Yes |
| I02A B0009* | 10 | 2400 | 5 | Argon | 4.50 | 2.7 | No |
| I03A B0010** | 5 | 2000 | 960 | Argon | 3.50 | 1.4 | No |
| V03A B0011** | 20 | 2000-2100 | 990 | Argon | 4.37 | 5.0 | No |
| I05A B0012** | 20 | 2200 | 120 | Argon | 3.48 | 0.5 | One End |

* Samples 1/2 inch diameter x 1/4 inch high.

** Samples 1 inch diameter x 1 inch high.

TABLE 36
REINFORCED COMPOSITES FABRICATION CONDITIONS
AND RESULTS

| <u>Material Designation</u> | <u>Rein- forcing Agent</u> | <u>Temp °C</u> | <u>Pres- sure psi</u> | <u>Time min</u> | <u>Density gm/cc</u> | <u>Remarks</u> |
|---------------------------------|------------------------------------|--------------------|-------------------------------|---------------------|--------------------------|--|
| Vf(5)02A D0566 | SiC Whiskers | 2050 | 4000 | 50 | 5.78 | Whiskers destroyed redistributed |
| Vf(2002A D0567 | SiC Whiskers | 2050 | 4000 | 115 | 3.05 | Whiskers destroyed |
| XHf(5)03A D0572 | Thornel 25 | 2100 | 4000 | 80 | 5.94 | Reaction of Fibers |
| XHf(5)03A D0615 | Thornel 25 | 2060 | 4000 | 103 | 5.89 | Fibers completely disappeared |
| XHf(5)07 D0644 | Thornel 25 | 2060 | 4000 | 102 | 5.83 | Continuous filaments satisfactory dis- tribution |
| XHf(5)02A D0564 | W Filament | 2050 | 4000 | 185 | 5.76 | Filament cluster and slight reaction |

TABLE 37

POSSIBLE DIBORIDE MATRIX FIBER COMBINATIONS*

| <u>Material</u> | <u>Expected Stability Limit</u> | <u>Remarks</u> |
|--|-------------------------------------|--|
| W-ZrB ₂ | 2250°C | Probable cracking due to differences in coefficients of thermal expansion (CTE) but otherwise mechanically and thermally stable. |
| W-HfB ₂ | 2345°C | Same as W-ZrB ₂ . |
| Mo-ZrB ₂ , Mo-HfB ₂ | <1400°C | Possible ternary reaction phase leading to disappearance of fibers. |
| Ta-ZrB ₂ | 2160°C | Liquid formation and possible ternary reaction phase at much lower temperature leading to disappearance of Ta. |
| Ta-HfB ₂ | 2220°C | Same as Ta-ZrB ₂ . |
| B-ZrB ₂ | 2000°C | Eutectic melting, moreover B filaments degrade severely and permanently around 800°C. |
| B-HfB ₂ | 2065°C | Same as B-ZrB ₂ . |
| C-ZrB ₂ | 2390°C | Pseudo binary eutectic melting, also probably cracking due to CTE difference. |
| C-HfB ₂ | 2515°C | Same as C-ZrB ₂ . |
| SiC-ZrB ₂ , SiC-HfB ₂ | 2200°-2300°C | Excellent thermochemical compatibility and increased oxidation resistance of diborides. Cracking found in particulate composites. |
| B ₄ C-ZrB ₂ | 2220°C | Pseudo binary eutectic melting, also probable cracking due to CTE difference. |
| B ₄ C-HfB ₂ | 2330°C | Same as B ₄ C-ZrB ₂ . |
| Al ₂ O ₃ -ZrB ₂ , Al ₂ O ₃ -HfB ₂ | 2049°C | Melting of alumina. Possible long term lower temperature utilization if fabrication can be performed below melting point of oxide. |

TABLE 38
SUMMARY OF THERMAL SCREENING

| <u>Run No. *</u> | <u>Temp °C</u> <u>(optical)</u> | <u>Time-min</u> | <u>Atm</u> | <u>Specimen</u> | <u>Remarks</u> |
|------------------|---|-----------------|--------------------------|---|---|
| 1 | 1830 | 60 | Argon | Carb ZrB ₂ | Thin oxide skin |
| 2 | 1830 | 60 | Argon | Carb ZrB ₂ | |
| 3 | 1830 | 60 | Argon | Norton ZrB ₂ I02A D0283 ² | |
| 4 | 1830 | 60 | Argon | I02A D0291 | |
| 5 | 1830 | 60 | Argon | Carb ZrB ₂ I02A D0305 I03A D0340 | Thin oxide skin Thin oxide skin Thin oxide skin |
| 6 | 1830 | 60 | Argon | I02A D0291 I02A D0326 I02A D0338 I02A D0345 I03A D0309 I03A D0314 I03A D0328 I03A D0360 | |
| 7 | 1830 | 60 | 10 ⁻⁵ Torr | V02 D0372 | ~ 1 mil SiC "recession" |
| 8 | 1800 | 120 | Argon | III05 D0386 | ~ 1 mil SiC "recession" |
| 9 | 2100 | 60 | 10 ⁻⁵ Torr | I02A D0326 I03A D0314 II05 D0348 III05 D0386 IV05 D0410 V02A D0371 V03A D0480 VI05 D0462 | |
| 10 | Furnace failure at 2270°C (optical) in vacuum | | | | |
| 11 | Furnace failure at 2160°C (optical) in vacuum | | | | |

TABLE 38 (CONT)
SUMMARY OF THERMAL SCREENING

| <u>Run No. *</u> | <u>Temp °C</u> <u>(optical)</u> | <u>Time-min</u> | <u>Atm</u> | <u>Specimen</u> | <u>Remarks</u> |
|------------------|------------------------------------|-----------------|------------|--|---|
| 12 | 2300 (color) | 15 | Argon | I02A D0289 I03A D0324 I05A D0590 I07 D0589 II05 D0352 III05 D0538 IV05 D0410 V02A D0372 V03A D0480 V07 D0580K VIII07 D0592 XII02A D0561 | Very large ZrB ₂ grains Peripheral change |
| 13 | 2200 (color) | 15 | Argon | VIII02A D0498 X07 D0596 | Peripheral change Second phase melting |
| 14 | 2200 | 15 | Argon | I07 D0589 | Orange phase |

*Runs No. 13 and 14 were carried out in the oxidation furnaces in flowing argon. Temperatures were determined by a two-color pyrometer.

TABLE 39

MELTING POINTS OF HOT PRESSED STRUCTURES

| <u>Material</u> | <u>Melting Temperature - °C</u> | |
|------------------------------|---------------------------------|-----------------|
| | <u>Incipient</u> | <u>Complete</u> |
| I02A 0289 | 2630 | 3095 |
| I03A 0324 | 2568 | 3075 |
| Norton ZrB ₂ * | 2945 | 3017 |
| Carborundum ZrB ₂ | 2600 | 3085 |
| II05 0315 | 3235 | 3344 |
| II06 0383 | 2697 | 3085 |

* Heavy outgassing at 2540°C.

TABLE 40

BEND STRENGTH AS A FUNCTION OF TEMPERATURE

| Material Designation | Relative Density Grain Intercept μ | Bend Strength, 10^3 psi, at | | | |
|----------------------|--|-------------------------------|--------|--------|------------|
| | | 23°C | 800°C | 1400°C | 1800°C |
| I02A D0305 | 99.3 35 FEM | 42.3* | 72.0* | 21.5 | 19.0 N.B. |
| | | 55.8* | 64.2 | 25.5* | 26.2 |
| | | 51.9 | 68.6 | 27.3* | 29.1 N.B. |
| I02A D0326 | 99.9 40 | 38.5 | 56.6** | 27.5 | 21.1 N.B. |
| | | 36.5 | 56.9 | 25.4 | 20.8 N.B. |
| | | 38.5 | 47.8 | 29.9 | 20.2 S.B. |
| I02A D0345 | 99.2 21 FEM | 50.1* | 49.4* | 30.8 | 27.4 N |
| | | 34.9 | 52.6** | 32.0* | 24.0 N.B. |
| | | 47.7** | 65.3 | 33.3 | 29.5* N.B. |
| I03A D0314 | 99.6 8 | 46.2 | 77.8 | 39.7* | 25.5* S.B. |
| | | 42.3* | 59.7 | 39.5 | 26.8* B |
| | | 48.1 | 57.8 | | 29.2* B |
| I02A D0338 | 97.6 33 | 49.0 | 54.3 | 26.8 | 24.2 S.B. |
| | | 47.8** | 58.7 | 26.6 | 28.3 S.B. |
| | | 40.7* | 46.1 | 23.0 | 37.2 |
| I02A D0291 | 95.9 27 | 44.2* | 54.2** | 17.8 | 13.6 N.B. |
| | | 50.0* | 49.2 | 17.6 | 13.5* N.B. |
| | | 58.6 | 40.9 | | 17.5* S.B. |
| I03A D0360 | 95.6 11 | 59.7 | 36.5 | 35.8 | 29.8* S.B. |
| | | 39.0* | 56.4* | 34.9 | 32.3* S.B. |
| | | 51.7** | 70.2 | | 18.7* B |
| I03A D0328 | 89.1 6 | 30.8 | 67.8 | 33.2 | 33.3 B |
| | | 40.4 | 55.3** | 26.3 | 28.4* S.B. |
| | | 46.2 | 58.0* | | 31.5* B |
| I02A D0343 | 90.0 6 | 40.3 | | | 26.9 |
| | | 25.3 | | | 28.0 S.B. |
| | | 28.2 | | | 28.2* B |
| I05A D0590 | 97 38 | 38.2* | 42.8* | 18.4 | 15.0 N.B. |
| | | 39.2 | 49.0* | 16.1 | 16.8 N.B. |
| | | 32.9* | 42.6* | 15.3 | 17.2 N.B. |

TABLE 40 (CONT)

BEND STRENGTH AS A FUNCTION OF TEMPERATURE

| Material Designation | Relative Density Grain Intercept μ | Bend Strength, 10^3 psi, at | | | |
|----------------------|--|-------------------------------|--------------------------|-------------------------|--|
| | | 23°C | 800°C | 1400°C | 1800°C |
| II05 D0348 | 99.4 34 | 41.4** 36.7 45.9 | | | 9.8* S.B. 10.2* B 9.0 N.B. |
| II05 D0352 | 96.7 15 FEM | 55.7** 63.8** 52.0 | 65.9** 58.4 53.2 | 16.9 14.5* 14.2* | 21.3 S.B. 29.0* S.B. 28.3* N.B. |
| II05 D0349 | 90 11 | 47.5** 44.7** 50.5** | | | 21.3 N.B. 25.8* S.B. 23.0 N.B. |
| II06 D0379 | 96.7 5 | 56.9** 44.8* 50.3** | | 15.1 | 23.3 B 25.8* S.B. 27.4* B |
| III(10)05 D0538 | 98.9 9 | 68.7** 60.9* 63.5* | | | 26.8* B 28.1 B 24.8* B |
| III05 D0386 | 99.7 9 | 54.9** 56.9** 59.2 | | 38.6* 39.0* 38.0* | 35.7* S.B. 41.9* S.B. 42.4* S.B. |
| III05 D0400 | 95.3 9 | 44.3 47.4** 55.3** | 45.6 46.1** 55.9** | 42.0 46.7 45.0* | 42.0* S.B. 53.7 S.B. 48.1 S.B. |
| III05 D0444 | 91.6 6 | 41.7 37.3** 39.9 | | 39.5* 56.6* 28.9 | 26.8* B 32.2 S.B. 37.3 S.B. |
| III05 D0402 | 84.3 6 | 29.9* 22.2 29.9** | | 25.8 22.7 23.1 | 27.9* B 30.0* B 28.0* B |
| IV05 D0410 | 99.4 | 50.4 48.6** 49.0 | 50.9** 54.9 61.3* | 61.7* 61.9 56.4 | 44.9* S.B. 58.9* S.B. 59.6 N.B. |

TABLE 40 (CONT)

BEND STRENGTH AS A FUNCTION OF TEMPERATURE

| Material Designation | Relative Density Grain Intercept μ | Bend Strength, 10^3 psi at | | | |
|----------------------|--|------------------------------|-------------------------------------|-------------------------|--|
| | | 23°C | 800°C | 1400°C | 1800°C |
| IV05 D0449 | 90.2 7 | 41.1** 38.1 34.5* | | 43.0* 34.1* | 20.5*B 30.9*S.B. 40.3*S.B. |
| V02A D0371 | 100 8 | 50.5 50.0* 50.0 | 52.7 50.6 55.0 | 43.0 42.0 39.2 | 38.2*B 44.9 B 41.0 B |
| V02A D0395 | 95.5 7 | 51.2** 52.2 48.2 | 51.5 51.4 46.8 51.2 55.6 45.5 | 23.3 24.3* 19.3* | 34.7*B 32.0 B 39.3 B |
| V02A D0391 | 90.1 7 FEM | 39.7* 48.2** 69.2** | | | 25.5*B 34.9 B 30.4 B |
| V03A D0480 | 100 7 | 39.3** 38.1* 36.4 | 46.3 48.4 34.9 | 41.3* 48.1 48.2** | 43.8*B 35.0*S.B. 40.5*B |
| V(10)02 D0532 | 100 11 | 68.7** 60.9* 63.5* | | | 42.5 B 38.6 B 42.5 B |
| V(35)02 D0541 | 100 6 | 71.8** 62.7** 71.1 | | | 44.9*B 43.3 S.B. 43.8 B |
| VI05 D0461 | 91.2 8 | 55.1* 38.2** 38.5 | | | 42.2**S.B. 34.3* N.B. 34.8* N.B. |
| VII02 D0498 | | 41.2 43.3* 37.8 | | | 47.8 B 48.1 B 45.5**B |
| XII(20)07 D0585 | 100 4.8 | 69.4 63.4 | | | 18.1* B 21.9* B 25.5* B |

*Single fracture at one knife edge.

**Primary fracture within gage length and secondary fracture at one knife edge resulting in three sections.

NB = no bending.

SB = slight plastic bending <1%.

B = plastic bending of <1%.

TABLE 41
PHASE II BEND STRENGTH AS A FUNCTION
OF TEMPERATURE

| <u>Material Designation</u> | <u>Relative Density Grain Intercept</u> % μ | <u>Bend Strength, 10^3 psi at</u> | |
|---------------------------------|--|--|---------------|
| | | <u>23°C</u> | <u>1800°C</u> |
| I03A D0619K | 100 | 52.0** | 20.8* S.B. |
| | 18.4 | 36.1 | 22.8* S.B. |
| | | 49.3 | 25.5* S.B. |
| V07 D0580K | 100 | 57.6* | 37.1* B |
| | 7.0 | 48.2 | 38.3 B |
| | | | 35.2* B |

* Single fracture at one knife edge.

** Primary fracture within gage length and secondary fracture at one knife edge resulting in three sections.

S.B. Slight plastic bending $\ll 1\%$.

B Plastic bending $\ll 1\%$.

TABLE 42

**BEND STRENGTH[†] VERSUS TEST TEMPERATURE FOR
TWO COMMERCIAL LOTS OF HOT PRESSED
ZIRCONIUM DIBORIDE**

| <u>Test Temperature</u> °C | <u>Loading System⁺⁺</u> | <u>Norton ZrB₂[*] Bend Strength</u> 10 ⁴ psi | <u>Carborundum ZrB₂^{**} Bend Strength</u> 10 ³ psi |
|-------------------------------|--|--|--|
| - 196 | 3-point | 35.8 | 48.5 |
| 23 | 3-point | 33.0 | 43.3 |
| 700 | 3-point | 27.7 | |
| 1000 | 3-point | 25.0 | 38.2 |
| 1200 | 3-point | 21.8 | 35.0 |
| 1400 | 3-point | 22.3 | 17.0 |
| | 4-point | 16.2 | 17.2 |
| 1800 | 4-point | 4.7 | 15.6 |

[†]Reported strengths are averages of from 3 to 11 tests per temperature.

⁺⁺3-point tests performed at ManLabs, 4-point tests performed at Avco.

^{*}Norton ZrB₂, 89% dense, 18μ grain intercept, ZrC X-ray second phase (calc. to be 9.0 w/o from chemical analysis), 3.0 w/o metallic impurities (principally Cr, Fe, Al).

^{**}Carborundum ZrB₂, 95% dense, 16μ grain intercept, ZrO₂ X-ray phase (calc. to be 3.8 w/o from chemical analysis), low in metallic impurities.

TABLE 43

BEND STRENGTHS OF PREOXIDIZED COMMERCIAL
HOT PRESSED ZIRCONIUM DIBORIDE

| <u>Material</u> | <u>Test Temperature</u> °C | <u>Unoxidized Matrix</u> 10 ³ psi | <u>Pre-oxidized Matrix</u> 10 ³ psi | <u>Matrix + Oxide</u> 10 ³ psi |
|------------------------------|-----------------------------------|---|---|--|
| Norton ZrB ₂ | 23 | 27-49 | 40.7 | 24.6 |
| | 1000 | 19-31 | 28.0 | 14.4 |
| Carborundum ZrB ₂ | 23 | 30-55 | 38.0 | 23.4 |
| | 1000 | 25-55 | 62.6 | 38.6 |
| | 1000 | 25-55 | 55.3 | 36.1 |

TABLE 44

**EFFECT OF SURFACE FINISH ON BEND STRENGTH OF
BILLET V07 D0576K AT 23°C**

| Surface Preparation Grit Size | 220 | 400 | 500 | 1/4 μ diamond |
|---|---|---|--|---|
| Surface Finish Center Line Average Deviation, Microinches | 13 | 7.5 | 10 | 0.3 |
| Strength Values, 10 ³ psi | 64.7** 76.5** 58.7** 51.3** 45.1* 69.4** | 68.3* 43.0 71.6** 67.9** 64.5 64.1 | 62.0** 62.6** 69.2** 66.8 66.4** 68.1 | 69.9** 72.7** 47.8 60.3 73.8* 76.4 |
| Mean Strength, 10 ³ psi | 60.9 | 63.2 | 65.9 | 66.8 |
| Standard Deviation, 10 ³ psi | 11.6 | 10.3 | 2.9 | 10.8 |

* Single fracture at one knife edge.

** Primary fracture within gage length and secondary fracture at one knife edge resulting in three sections.

TABLE 45
DYNAMIC ELASTIC MODULUS MEASUREMENTS

| Material Designation | Density | | Compress- ional Pulse Velocity V_L | Transverse Pulse Velocity V_T | Poisson Ratio | Young's Modulus E |
|-------------------------|---------|------|---|--|------------------|-------------------------|
| | gm/cc | % | 10^5 cm/sec | 10^5 cm/sec | | 10^6 psi |
| I03A D0313 | 5.99 | 99.4 | 9.30 | 5.85 | 0.17 | 70.5 |
| II05 D0353 | 10.52 | 99.2 | 6.93 | 4.58 | 0.12 | 71.0 |
| II05 D0355B | 10.46 | 98.6 | 7.02 | 4.35 | 0.19 | 68.5 |
| III05 D0385 | 9.25 | 100 | 7.47 | 4.79 | 0.15 | 70.5 |
| III05 D0426 | 9.06 | 98 | 7.25 | 4.78 | 0.12 | 67.2 |
| IV05 D0405 | 9.45 | 100 | 7.35 | 5.03 | 0.06 | 73.0 |
| V02A D0387 | 5.45 | 100 | 9.90 | 5.75 | 0.24 | 66.0 |

TABLE 46

ELASTIC MODULUS AS A FUNCTION OF TEMPERATURE

| Material Designation | Relative Density Grain Intercept % | μ | E at 23°C* | | E at 23°C** | | E at 23°C* | | E at 800°C* | | E at 1400°C* | |
|----------------------|--|-------|------------|---------------------|-------------|---------------------|------------|---------------------|-------------|---------------------|--------------|---------------------|
| | | | Static | 10 ⁶ psi | Static | 10 ⁶ psi | Dynamic | 10 ⁶ psi | Static | 10 ⁶ psi | Static | 10 ⁶ psi |
| I02A D0345F | 99.0 | 21 | 65.7 | | | | | | | | | |
| I03A D0314F | 99.6 | 8 | 57.7 | | | | | | | | | |
| | | | 59.6 | | | | | | | | | |
| | | | 65.6 | | 75.7 | | | | | | | |
| I03A D0457 | 100 | 23 | 68.7 | | | | | | 67.6 | | | |
| I03A D0343 | 90.1 | | 61.8 | | | | | | | | | |
| I03A D0323 | 86.2 | 8 | 55.4 | | | | | | | | | |
| | | | 40.4 | | | | | | | | | |
| V03A D0480 | 100 | 7 | | | | | | | 54.7 | | 37.6 | |
| V02A D0371 | 100 | 8 | 63.3 | | | | | | 71.7 | | 58.5 | |
| V02A D0395 | 94.1 | 7 | 71.0 | | | | 58.5 | | 78.0 | | | |
| V03A D0391F | 90.1 | 7 | 55.1 | | 53.7 | | | | 55.1 | | 37.6 | |
| | | | 54.1 | | | | | | | | | |
| V(10)02A D0532 | 100 | 10 | 69.8 | | | | | | | | | |
| VIII02 D0498 | 100 | 5 | 29.5 | | 34.8 | | | | 35.8 | | 31.4 | |
| | | | 32.4 | | | | | | | | | |

TABLE 46 (CONT)
ELASTIC MODULUS AS A FUNCTION OF TEMPERATURE

| Material Designation | Relative Density Grain Intercept % μ | E at 23°C* Static 10 ⁶ psi | E at 23°C** Static 10 ⁶ psi | E at 23°C* Dynamic 10 ⁶ psi | E at 800°C* Static 10 ⁶ psi | E at 1400°C* Static 10 ⁶ psi |
|----------------------|---|---|--|--|--|---|
| II05 D0348 | 99.4 34 | 69.1 70.4 | | 76.1 | 62.7 70.1 | |
| II05 D0349 | 90.0 11 | 44.1 45.9 | 46.8 | | | |
| III05 D0386 | 99.7 9 | 68.6 69.1 | 79.6 | 72.1 | 75.9 75.0 | 67.0 |
| III05 D0444 | 91.6 6 | 48.5 | | | 50.3 | |
| III(10)02A D0532 | 100 16 | 69.8 | | | | |
| IV05 D0410 | 99.4 6 | 75.9 74.2 | 74.2 | 72.1 | 72.3 75.0 | 69.0 |
| IV05 D0449 | 90.0 7 | 48.1 44.3 45.1 | 48.3 51.2 | | | |

* Performed at AVCO.

** Performed at MANLABS.

TABLE 47
 STATIC AND DYNAMIC MODULUS VALUES FOR
 HOT PRESSED ZrB_2

| <u>Material</u> | <u>Relative Density</u> % | <u>Method</u> | <u>Young's Modulus (E)</u> 10^6 psi |
|-----------------|----------------------------------|---------------|--|
| (13) | 87 | dynamic | 51.9 |
| Norton | 89 | static | 54.5 |
| (13) | 95 | dynamic | 63.8 |
| Carborundum | 95 | static | 65.4 |
| (13) | 98 | dynamic | 73.5 |

TABLE 48

COMPARISON OF POST - 1800°C - TEST FRACTURE GRAIN SIZE
WITH AS-HOT PRESSED GRAIN SIZE

| <u>Material Designation</u> | <u>As-Hot Pressed Grain Intercept</u> | <u>Post - 1800°C - Test Grain Intercept</u> |
|---------------------------------|---|---|
| | μ | μ |
| I02A D0291 | 27 | 36 |
| I02A D0338 | 30 | 27 |
| II05 D0348 | 34 | 36 |
| II05 D0349 | 11 | 14 |
| III05 D0400 | 9 | 7 |
| III05 D0402 | 6 | 9 |
| III05 D0386 | 9 | 12 |
| IV05 D0410 | 6 | 9 |
| IV05 D0449 | 7 | 7 |
| V02A D0371 | 8 | 8 |
| V02 D0391 | 7 | 7 |

TABLE 49
DENSITY MEASUREMENTS ON BEND SPECIMENS
TESTED AT 23°C

| <u>Material Designation</u> | <u>Original Billet Density</u> gm/cm ³ | <u>Specimen Density Displacement Method</u> gm/cm ³ | <u>Specimen Density Geometrical Method</u> gm/cm ³ |
|---------------------------------|--|---|--|
| I02A D0305 | 5.99 | 5.94 | 5.94 |
| I02A D0345 | 5.97 | 6.04 | 5.93 |
| I03A D0314 | 6.00 | 6.06 | 5.96 |
| III05 D0348 | 10.48 | 10.68 | 10.53 |
| III05 D0386 | 9.26 | 9.17 | 9.08 |
| IV05 D0410 | 8.57 | 8.60 | 8.43 |
| V02A D0371 | 5.49 | 5.59 | 5.48 |

TABLE 50

AIR FLOW RATE DEPENDENCE FOR MATERIAL III

(HfB₂ - 20 v/o SiC at 2120°C, 60 Minutes)

(Billet III05D0573, 0.35 in. diameter by 0.35 in. high)

| <u>OX No.</u> | <u>Air Flow Rate</u> ft/sec | <u>Boride Recession</u> | | <u>SiC Recession</u> | |
|---------------|------------------------------------|--|------------------------|--|------------------------|
| | | <u>Height/ Diameter</u> mils/mils | <u>Average</u> mils | <u>Height/ Diameter</u> mils/mils | <u>Average</u> mils |
| 718 | 0.1 | 0/0 | 0 | 3.2/ 4.2 | 3.7 |
| 802 | 0.3 | 9.0/ 9.4 | 9.2 | 103.7/107.2 | 105.5 |
| 814 | 0.3 | 8.7/ 9.7 | 9.2 | 94.5/108.5 | 101.5 |
| 803 | 0.5 | 8.3/ 8.7 | 8.5 | 99.5/ 99.2 | 99.4 |
| 812 | 0.5 | 7.3/ 9.7 | 8.5 | 118.2/103.0 | 110.6 |
| 806 | 0.7 | 8.7/10.0 | 9.4 | 108.6/101.5 | 105.1 |
| 815 | 0.7 | 6.1/ 7.2 | 6.7 | 101.8/ 94.1 | 98.0 |
| 721 | 0.9 | 6.1/10.0 | 8.1 | 87.0/ 94.0 | 90.5 |
| 722 | 0.9 | 7.3/11.1 | 9.2 | 98.4/ 91.9 | 95.2 |
| 724 | 1.8 | 9.4/11.1 | 10.3 | 100.1/ 96.6 | 98.4 |
| 725 | 3.6 | 13.3/12.4 | 12.9 | 119.1/100.0 | 109.6 |

TABLE 51
OXIDATION SCREENING: MATERIAL I (ZrB₂)
(152 Torr O₂ in Air at 0.9 ft/sec - STP)

| Exp. No. | Pressing No. | Temp °C | Time min | Height/Diameter | | Average One Hour Boride Recession mils |
|----------|--------------|------------|-------------|-----------------|---------------------|--|
| | | | | Initial* | Boride Recession | |
| | | | | mils/mils | mils/mils | |
| 440 | I02AD0338 | 1550 | 60 | 300/350 | 12.1/14.2 | 13.2 |
| 559 | I02AD0326 | 1550 | 60 | 290/350 | 8.0/ 8.3 | 8.2 |
| 560 | I03AD0309 | 1600 | 60 | 300/350 | 9.9/10.6 | 10.3 |
| 561 | I03AD0309 | 1660 | 60 | 300/350 | 10.3/11.3 | 10.8 |
| 796 | I02AD0343 | 1690 | 60 | 250/350 | 13.5/13.7 | 13.6 |
| 212 | I02AD0281 | 1700 | 60 | 290/350 | 11.9/16.5 | 14.2 |
| 229 | I03AD0340 | 1700 | 60 | 300/350 | 11.9/13.9 | 12.9 |
| 230 | I03AD0340 | 1700 | 60 | 300/350 | 13.7/13.4 | 13.6 |
| 231 | I03AD0340 | 1700 | 60 | 300/350 | 13.2/15.2 | 14.2 |
| 255 | I03AD0309 | 1700 | 60 | 300/350 | 11.4/10.9 | 11.2 |
| 263 | I02AD0291 | 1700 | 60 | 280/350 | 11.7/15.0 | 13.4 |
| 265 | I02AD0326 | 1700 | 60 | 290/350 | 12.4/14.4 | 13.4 |
| 274 | I03AD0328 | 1700 | 60 | 285/350 | ----/11.6 | 11.6 |
| 285 | I02AD0338 | 1700 | 60 | 300/350 | 13.6/14.4 | 14.0 |
| 286 | I03AD0314 | 1700 | 60 | 300/350 | 11.6/14.4 | 13.0 |
| 287 | I03AD0360 | 1700 | 60 | 270/350 | 13.7/17.8 | 15.8 |
| 295 | I02AD0345 | 1700 | 60 | 300/350 | 12.1/13.9 | 13.0 |
| 304 | I03AD0328 | 1700 | 60 | 265/350 | ----/12.2 | 12.2 |
| 894 | I07D0589 | 1700 | 60 | 300/350 | 12.6/13.1 | 12.9 |
| 899 | I05AD0590 | 1700 | 60 | 300/350 | 12.5/12.9 | 12.7 |
| 1016 | I05AD0590 | 1740 | 60 | 300/350 | 13.6/14.3 | 14.0 |
| 1018 | I03AD0457 | 1740 | 60 | 420/350 | 13.3/14.6 | 14.0 |
| 1014 | I03AD0457 | 1770 | 60 | 420/350 | 17.5/17.4 | 17.4 |
| 1017 | I07D0589 | 1770 | 60 | 360/350 | 15.4/16.4 | 15.9 |
| 1019 | I02AD0305 | 1770 | 60 | 290/350 | 14.9/16.1 | 15.5 |
| 1020 | I05AD0590 | 1770 | 60 | 300/350 | 17.1/17.4 | 17.3 |
| 308 | I03AD0360 | 1800 | 60 | 270/350 | 23.4/22.4 | 22.9 |
| 311 | I03AD0314 | 1800 | 60 | 300/350 | 21.6/20.6 | 21.1 |
| 312 | I02AD0338 | 1800 | 60 | 300/350 | 27.8/21.4 | 24.6 |
| 787 | I02AD0343 | 1800 | 60 | 290/350 | 28.0/32.3 | 30.2 |
| 309 | I03AD0309 | 1810 | 60 | 300/350 | 25.0/27.1 | 26.1 |
| 314 | I02AD0326 | 1810 | 60 | 285/355 | 16.3/22.2 | 19.3 |
| 316 | I03AD0328 | 1810 | 60 | 270/350 | 17.7/17.4 | 17.6 |
| 318 | I02AD0291 | 1810 | 60 | 300/350 | 21.3/22.3 | 21.8 |
| 335 | I02AD0345 | 1810 | 60 | 300/350 | 19.4/20.7 | 20.0 |
| 895 | I07D0589 | 1810 | 60 | 300/350 | 33.8/36.4 | 35.1 |
| 901 | I05AD0590 | 1810 | 60 | 300/350 | 31.5/36.5 | 34.0 |
| 955 | I02AD0343 | 1820 | 60 | 290/350 | 34.9/43.7 | 39.3 |

TABLE 51 (CONT)

OXIDATION SCREENING: MATERIAL 1 (ZrO₂)(152 Torr O₂ in Air at 0.9 ft/sec - STP)

| Exp. No. | Pressing No. | Temp °C | Time min | Height/Diameter | | Average One Hour Boride Recession mils |
|----------|--------------|------------|-------------|-----------------------------------|----------------------------------|--|
| | | | | Initial [*] mils/mils | Boride Recession mils/mils | |
| 253 | I03AD0340 | 1850 | 60 | 300/350 | 28.1/38.1 | 33.1 |
| 288 | I03AD0328 | 1850 | 30 | 300/350 | Severe Oxidation | |
| 332 | I03AD0309 | 1850 | 30 | 300/350 | 31.8/44.1 | (52.9) ⁺ |
| 333 | I02AD0326 | 1850 | 30 | 290/350 | 24.7/31.7 | (40.0) ⁺ |
| 497 | I02AD0345 | 1850 | 30 | 290/350 | 23.2/31.8 | (38.8) ⁺ |
| 504 | I02AD0338 | 1850 | 30 | 300/350 | 41.0/52.8 | (67.0) ⁺ |
| 513 | I03AD0360 | 1850 | 30 | 270/350 | 16.4/22.0 | (25.8) ⁺ |
| 864 | I03AD0457 | 1850 | 60 | 420/350 | 41.5/48.2 | 44.9 |
| 786 | I02AD0343 | 1850 | 30 | 290/350 | 34.5/42.5 | (54.9) ⁺ |
| 897 | I05AD0590 | 1850 | 30 | 300/350 | 29.8/39.8 | (49.2) ⁺ |
| 896 | I07D0589 | 1860 | 30 | 300/350 | 29.6/37.6 | (47.5) ⁺ |
| 473 | I02AD0291 | 1860 | 30 | 280/350 | 29.5/46.6 | (54.0) ⁺ |
| 503 | I03AD0360 | 1860 | 26 | 270/350 | 15.2/16.7 | (24.3) ⁺ |
| 419 | I03AD0360 | 1870 | 30 | 270/350 | 43.6/50.2 | (66.4) ⁺ |
| 420 | I03AD0314 | 1870 | 30 | 300/350 | 29.5/46.6 | (54.0) ⁺ |
| 512 | I02AD0338 | 1890 | 30 | 300/350 | 37.3/---- | (52.7) ⁺ |

^{*} Nominal dimensions.⁺ Assumes parabolic oxidation kinetics.

TABLE 52
OXIDATION OF COMMERCIAL HOT PRESSED
ZIRCONIUM DIBORIDE

(152 Torr O₂ in Air at 0.9 ft/sec - STP)

| Exp. No. | Temp °C | Time min | Height/Diameter | | Average One Hour Boride Recession mils |
|--------------------------------|------------|-------------|-----------------|---------------------|--|
| | | | Initial* | Boride Recession | |
| | | | mils/mils | mils/mils | |
| <u>Carborundum Hot Pressed</u> | | | | | |
| 558 | 1540 | 60 | 400/375 | 11.6/15.5 | 13.6 |
| 638 | 1580 | 60 | 400/375 | 10.0/10.8 | 10.4 |
| 88 | 1610 | 60 | 400/375 | 14.7/21.0 | 17.9 |
| 155 | 1630 | 60 | 400/350 | 10.4/15.8 | 13.1 |
| 129 | 1690 | 60 | 400/350 | 13.0/13.5 | 13.3 |
| 266 | 1700 | 60 | 400/350 | 12.1/12.3 | 12.2 |
| 89 | 1730 | 60 | 400/375 | 16.3/26.5 | 21.4 |
| 130 | 1780 | 60 | 400/350 | 14.4/14.3 | 14.4 |
| 156 | 1810 | 60 | 400/350 | 21.4/20.9 | 21.2 |
| 317 | 1810 | 60 | 400/350 | 21.3/22.3 | 21.8 |
| 90 | 1820 | 60 | 400/375 | 23.0/30.5 | 26.8 |
| 131 | 1850 | 30 | 400/350 | 27.4/30.0 | (40.2) ⁺ |
| 474 | 1860 | 60 | 400/350 | 36.4/50.5 | 43.5 |
| 486 | 1860 | 30 | 400/350 | 16.5/26.5 | (30.5) ⁺ |
| 107 | 1870 | 30 | 400/375 | 38.6/47.5 | (74.6) ⁺ |
| 157 | 1900 | 30 | 400/350 | 36.6/D | (51.8) ⁺ |
| 120 | 1920 | 60 | 400/375 | Complete Oxidation | |
| 124 | 1940 | 30 | 400/375 | 47.9/D | (67.7) ⁺ |
| 121 | 1970 | 60 | 400/375 | Complete Oxidation | |
| 93 | 1980 | 30 | 400/375 | Complete Oxidation | |
| 92 | 1990 | 30 | 400/375 | Complete Oxidation | |
| <u>Norton Hot Pressed</u> | | | | | |
| 639 | 1580 | 60 | 400/390 | 17.5/13.5 | 15.5 |
| 113 | 1620 | 60 | 410/390 | 15.1/13.1 | 14.1 |
| 128 | 1620 | 60 | 400/350 | 13.4/15.3 | 14.4 |
| 267 | 1700 | 60 | 400/400 | 32.0/44.2 | 38.1 |
| 272 | 1700 | 60 | 400/400 | 21.5/21.8 | 21.7 |
| 475 | 1700 | 60 | 400/400 | 26.6/24.5 | 25.6 |
| 114 | 1710 | 60 | 390/340 | 26.3/24.3 | 25.3 |
| 105 | 1820 | 60 | 400/350 | 30.8/31.1 | 31.0 |
| 132 | 1820 | 60 | 400/350 | 43.1/41.8 | 42.5 |
| 421 | 1840 | 60 | 400/400 | 27.6/43.0 | 35.3 |
| 487 | 1860 | 30 | 400/400 | 30.9/32.7 | (45.0) ⁺ |
| 123 | 1870 | 60 | 400/350 | 50.2/D | 50.2 |
| 159 | 1900 | 30 | 400/350 | Complete Oxidation | |
| 112 | 1920 | 60 | 400/340 | Complete Oxidation | |
| 115 | 1960 | 30 | 400/350 | Complete Oxidation | |
| 106 | 2040 | 60 | 400/340 | Complete Oxidation | |

* Nominal dimensions.

⁺ Assumes parabolic oxidation kinetics.

TABLE 53

OXIDATION SCREENING: MATERIAL V ($ZrB_2 + 20\% \text{ SiC}$)
 (152 Torr O_2 in Air at 0.9 ft/sec - STP)

| Exp. No. | Pressing No. | Temp °C | Time min | Initial* mils/mils | Height/Diameter | Average One Hour Boride Recession |
|----------|--------------|------------|-------------|-----------------------|--|--|
| | | | | | Boride Recession (SiC Recession) ⁺ mils/mils | Recession (SiC Recession) mils |
| 388 | V02AD0395 | 1800 | 60 | 300/350 | 1.1/ 0.6 (29.2/ 9.6) | 0.9 (19.4) |
| 441 | V02AD0371 | 1800 | 60 | 300/350 | 4.2/ 2.8 (---/ 7.2) | 3.5 (7.2) |
| 330 | V02D0372 | 1800 | 60 | 295/350 | 1.2/ 1.3 (5.0/---) | 1.2 (5.0) |
| 389 | V02AD0391 | 1810 | 60 | 300/350 | 1.8/ 1.5 (14.8/11.7) | 1.7 (15.5) |
| 918 | V07D0580K | 1810 | 60 | 330/350 | 4.3/ 3.3 (16.6/14.3) | 3.8 (15.5) |
| 631 | V03AD0480 | 1840 | 60 | 350/350 | 1.7/ 2.5 (7.3/ 9.3) | 2.1 (8.3) |
| 433 | V02AD0371 | 1900 | 60 | 300/350 | 7.0/ 6.2 (19.0/25.2) | 6.7 (22.1) |
| 432 | V02AD0395 | 1900 | 60 | 300/350 | 4.2/ 6.7 (32.3/61.9) | 5.5 (47.1) |
| 430 | V02AD0391 | 1910 | 60 | 300/350 | 8.4/ 4.6 (67.6/34.8) | 6.5 (51.1) |
| 391 | V02AD0391 | 1950 | 60 | 300/350 | 6.4/ 6.5 (67.1/31.9) | 6.4 (49.5) |
| 437 | V02AD0371 | 1950 | 60 | 300/350 | 9.7/11.6 (30.3/41.7) | 10.7 (36.0) |
| 343 | V02D0572 | 1960 | 60 | 295/350 | 13.4/18.3 (35.8/31.9) | 15.9 (33.9) |
| 393 | V02AD0395 | 1960 | 60 | 300/350 | 4.5/ 5.2 (76.6/94.8) | 4.9 (86.2) |
| 435 | V02D0372 | 1960 | 120 | 300/350 | 16.1/15.7 (39.3/44.7) | 11.2 ⁺⁺ (29.7) ⁺⁺ |
| 436 | V02D0372 | 1960 | 30 | 300/350 | 10.1/ 9.2 (18.6/30.8) | 13.7 ⁺⁺ (34.9) ⁺⁺ |
| 438 | V02D0372 | 1960 | 60 | 300/350 | 9.9/12.7 (22.0/34.9) | 11.3 (28.5) |
| 903 | V07D0580K | 1970 | 60 | 330/350 | 16.8/ 9.0 (34.3/23.3) | 12.9 (28.8) |
| 634 | V03AD0480 | 2000 | 60 | 350/350 | 3.4/ 2.7 (111.9/93.5) | 3.1 (102.7) |

TABLE 53 (CONT)

OXIDATION SCREENING: MATERIAL V ($ZrB_2 + 20 \text{ v/o SiC}$)
(152 Torr O_2 in Air at 0.9 ft/sec - STP)

| Exp.No. | Pressing No. | Temp °C | Time min | Initial* mils/mils | Height/Diameter | Average One Hour Boride Recession (SiC Recession) |
|---------|--------------|------------|-------------|-----------------------|--|---|
| | | | | | Boride Recession (SiC Recession) ⁺ mils/mils | mils |
| 470 | V02AD0371 | 2010 | 60 | 300/350 | 20.6/---- (73.6/----) | 20.6 (73.6) |
| 471 | V02AD0391 | 2010 | 60 | 300/350 | 21.6/---- (C/----) | 21.6 (C) |
| 472 | V02AD0395 | 2010 | 60 | 300/350 | 7.8/---- (C/----) | 20.6 (C) |
| 398 | V02AD0391 | 2050 | 60 | 300/350 | 56.2/74.5 (C/C) | 65.4 (C) |
| 399 | V02AD0395 | 2060 | 60 | 300/350 | 75.5/65.8 (C/C) | 70.7 (C) |
| 352 | V02D0372 | 2060 | 60 | 295/350 | 22.8/26.4 (C/C) | 24.6 (C) |
| 467 | V02AD0371 | 2110 | 60 | 300/350 | 28.2/---- (127.7/----) | 28.2 (127.7) |
| 913 | V07D0580K | 2130 | 60 | 330/350 | 83.0/121.0 (C/C) | 102.0 (C) |
| 635 | V03AD0480 | 2170 | 60 | 350/350 | 24.3/47.5 (C/C) | 35.9 (C) |
| 906 | V07D0580K | 2220 | 60 | 330/350 | Complete Oxidation | |

*Nominal dimensions.

⁺C designates complete oxidation of the SiC phase.

⁺⁺Assumes parabolic oxidation kinetics for the diboride and SiC phases.

TABLE 54

OXIDATION OF COMMERCIAL HOT PRESSED BORIDE Z
(152 Torr O₂ in Air at 0.9 ft/sec - STP)

| <u>Exp. No.</u> | <u>Temp</u> | <u>Time</u> °C | <u>Height/Diameter</u> | | <u>Average One Hour Material Recession</u> mils |
|-----------------|-------------|-------------------|------------------------------|--|--|
| | | | <u>Initial*</u> mils/mils | <u>Material Recession</u> mils/mils | |
| 636 | 1570 | 60 | 300/350 | 3.6/ 2.8 | 3.2 |
| 444 | 1710 | 60 | 300/350 | 6.3/ 6.7 | 6.5 |
| 445 | 1810 | 60 | 300/350 | 12.6/12.3 | 12.5 |
| 508 | 1850 | 60 | 300/350 | 15.9/15.8 | 17.5 |
| 530 | 1910 | 60 | 300/350 | 16.4/16.8 | 16.6 |
| 531 | 1950 | 60 | 300/350 | 30.3/39.8 | 35.1 |

*Nominal dimensions.

TABLE 55

OXIDATION SCREENING: MATERIAL VIII (ZrB_2 + 30 v/o Graphite + 14 v/o SiC)
 (152 Torr O_2 in Air at 0.9 ft/sec - STF)

| Exp. No. | Pressing No. | Temp °C | Time min | Height/Diameter | | Average |
|----------|---------------|------------|-------------|-----------------|------------------------------|--|
| | | | | Initial* | Boride | One Hour |
| | | | | | Recession (SiC Recession) | Boride Recession (SiC Recession) |
| | | | | mils/mils | mils/mils | mils |
| 1021 | VIII02A D0592 | 1610 | 60 | 290/350 | 8.3/ 9.5 | 8.9 |
| 1022 | VIII02A D0592 | 1770 | 60 | 290/350 | 15.6/ 19.2 | 17.4 |
| | | | | | (20.2/ 22.4) | (21.3) |
| 916 | VIII02A D0592 | 1800 | 60 | 290/350 | 21.0/ 33.3 | 27.2 |
| | | | | | (28.3/ 39.1) | (33.7) |
| 623 | VIII02A D0498 | 1820 | 60 | 300/350 | 3.8/ 11.5) | 7.7 |
| | | | | | (15.1/ 29.0) | (22.1) |
| 915 | VIII02A D0592 | 1970 | 60 | 290/350 | 64.8/ 85.0 | 74.9 |
| | | | | | (75.3/102.2) | (88.8) |
| 627 | VIII02A D0498 | 1980 | 60 | 300/350 | 20.8/ 6.2 | 13.5 |
| | | | | | (34.1/ 48.5) | (41.3) |
| 912 | VIII02A D0592 | 2000 | 60 | 290/350 | Complete Oxidation | |
| 624 | VIII02A D0498 | 2180 | 60 | 300/350 | Complete Oxidation | |

* Nominal dimensions.

TABLE 56

OXIDATION SCREENING: MATERIAL XII (ZrB_2 + 50 v/o Graphite)(152 Torr O_2 in Air at 0.9 ft/sec - STP)

| Exp. No. | Pressing No. | Temp °C | Time min | Height/Diameter | | Average One Hour Boride Recession mils |
|----------|----------------|------------|-------------|-----------------|---------------------|--|
| | | | | Initial* | Boride Recession | |
| | | | | mils/mils | mils/mils | |
| 953 | XII02AD0561 | 1600 | 60 | 290/350 | 41.9/ 70.3 | 56.1 |
| 954 | XII02AD0561 | 1710 | 60 | 290/350 | Complete Oxidation | |
| 844 | XII02AD0561 | 1800 | 60 | 300/350 | 99.3/122.3 | 110.8 |
| 946 | XII(20)07D0585 | 1810 | 60 | 340/350 | 29.0/ 29.6 | 29.3 |
| 947 | XII(5)03AD0572 | 1810 | 60 | 330/350 | 33.6/ 39.8 | 36.7 |
| 843 | XII02AD0561 | 1850 | 60 | 300/350 | 109.8/125.2 | 117.5 |
| 951 | XII(5)03AD0572 | 1860 | 30 | 330/350 | 35.0/ 37.4 | 51.2 ⁺ |
| 950 | XII(20)07D0585 | 1860 | 30 | 340/350 | 26.2/ 30.7 | 40.2 ⁺ |
| 949 | XII(5)03AD0572 | 1910 | 60 | 330/350 | Complete Oxidation | |
| 948 | XII(20)07D0585 | 1910 | 60 | 340/350 | 79.0/ 76.8 | 77.9 |
| 845 | XII02AD0561 | 1980 | 60 | 300/350 | 110.1/132.3 | 121.2 |

* Nominal dimensions.

⁺ Assumes parabolic oxidation kinetics.

TABLE 57

OXIDATION SCREENING: MATERIAL X ($\text{ZrB}_2 + 20 \text{ v/o SiB}_6$)
 (152 Torr O_2 in Air at 0.9 ft/sec - STP)

| <u>Exp. No.</u> | <u>Pressing No.</u> | <u>Temp</u> °C | <u>Time</u> min | <u>Height/Diameter</u> | | <u>Average One Hour Material Recession</u> mils |
|-----------------|---------------------|-------------------|--------------------|--|--|--|
| | | | | <u>Initial</u> [*] mils/mils | <u>Material Recession</u> mils/mils | |
| 925 | X07D0596 | 1700 | 60 | 300/350 | 17.2/14.2 | 15.7 |
| 923 | X07D0596 | 1800 | 60 | 300/350 | 21.6/29.6 | 25.6 |
| 922 | X07D0596 | 1910 | 60 | 300/350 | Complete Oxidation | |

* Nominal dimensions.

TABLE 58

OXIDATION: HIGH PRESSURE HOT PRESSED MATERIALS
(152 Torr O₂ in Air at 0.9 ft/sec - STP)

| Exp. No. | Pressing No. | Temp °C | Time min | Height/Diameter | | Average One Hour Material Recession mils |
|--|--------------|------------|-------------|-----------------|---------------------------|---|
| | | | | Initial* | Material Recession | |
| | | | | mils/mils | mils/mils | |
| <u>Material VI (HfB₂ + 4 v/o Hf-27Ta)</u> | | | | | | |
| 599 | VI05H0585 | 1820 | 60 | 380/310 | 17.8/23.4 | 20.6 |
| 606 | VI05H0586 | 1920 | 60 | 380/330 | 28.9/45.8 | 37.3 |
| 608 | VI05H0585 | 2060 | 60 | 360/310 | 85.9/81.8 | 83.9 |
| <u>Material X (ZrB₂ + 20 v/o SiB₆)</u> | | | | | | |
| 733 | X02AH0649 | 1810 | 60 | 330/330 | 12.1/17.9 (33.6/33.5) | 15.0 (33.6) ⁺ |
| 738 | X02AH0648 | 1910 | 60 | 350/330 | 51.7/50.9 (112.9/95.9) | 51.3 (104.4) ⁺ |
| <u>Material XI (ZrB₂ + 8 v/o Cr)</u> | | | | | | |
| 727 | XI02AH0645 | 1700 | 60 | 350/350 | 18.4/34.3 | 26.4 |
| 598 | XI02AH0583 | 1710 | 60 | 260/340 | 25.1/---- | 25.1 |
| 731 | XI02AH0645 | 1810 | 60 | 350/330 | 38.8/43.6 | 41.2 |
| 729 | XI02AH0645 | 1870 | 30 | 360/310 | 82.2/61.4 | 101.5 ⁺⁺ |

* Nominal dimensions.

⁺ SiB₆ recession.

⁺⁺ Assumes parabolic oxidation kinetics.

TABLE 59

OXIDATION SCREENING: MATERIAL II (HfB_2)
 (152 Torr O_2 in Air at 0.9 ft/sec - STP)

| Exp. No. | Pressing No. | Temp °C | Time min | Height/Diameter | | Average One Hour Boride Recession mils |
|-------------------|--------------|------------|-------------|-----------------|---------------------|--|
| | | | | Initial* | Boride Recession | |
| | | | | mils/mils | mils/mils | |
| 382 | II05D0352 | 1600 | 60-60 | 260/350 | 7.6/ 6.8 | (5.1) ⁺ |
| 401 | II05D0352 | 1600 | 120 | 260/350 | 4.9/ 5.1 | (3.5) ⁺ |
| 349 | II05D0352 | 1700 | 60 | 260/350 | 5.2/ 4.7 | 5.0 |
| 351 | II05D0348 | 1700 | 60 | 265/350 | 4.0/ 5.5 | 4.8 |
| 348 | II05D0349 | 1700 | 35 | 280/350 | 3.7/ 4.5 | (5.4) ⁺ |
| 360 | II05D0349 | 1710 | 60 | 280/350 | 6.4/ 5.7 | 6.1 |
| 327 | II06D0383 | 1800 | 60 | 300/350 | ---/10.9 | 10.9 |
| 363 | II05D0349 | 1800 | 60 | 280/350 | 10.2/12.7 | 11.5 |
| 329 | II05D0315 | 1810 | 60 | 300/350 | 10.7/11.0 | 10.9 |
| 366 | II05D0352 | 1810 | 60 | 260/350 | 11.7/12.2 | 12.0 |
| 321 | II07D0458 | 1810 | 60 | 300/350 | 11.6/11.5 | 11.6 |
| 361 | II05D0348 | 1810 | 60 | 265/350 | 18.9/19.3 | 19.1 |
| 350 | II05D0315 | 1880 | 48 | 300/350 | 54.9/57.5 | (63.0) ⁺ |
| 367 | II05D0348 | 1900 | 60 | 265/350 | 44.1/45.4 | 44.8 |
| 369 | II05D0349 | 1900 | 60 | 280/350 | 40.4/36.6 | 38.5 |
| 375 | II05D0352 | 1900 | 45 | 260/350 | 33.1/33.9 | (38.7) ⁺ |
| 455 | II06D0383 | 1900 | 60 | 300/350 | 28.9/35.2 | 32.0 |
| 456 | II05D0315 | 1900 | 60 | 300/350 | 17.5/26.3 | 21.9 |
| 465 | II07D0458 | 1910 | 60 | 300/350 | 23.2/26.4 | 24.8 |
| 429 ^o | II05D0348 | 1990 | 60 | 265/350 | 31.4/29.8 | 30.6 |
| 428 | II05D0349 | 2020 | 60 | 280/350 | 62.4/81.3 | 71.9 |
| 507 | II06D0383 | 2020 | 60 | 300/350 | 74.6/86.6 | 80.6 |
| 338 | II05D0315 | 2030 | 60 | 300/350 | 67.2/85.8 | 76.5 |
| 386 ^{oo} | II05D0348 | 2030 | 60 | 265/350 | 30.0/24.9 | 27.5 |
| 510 | II07D0458 | 2060 | 60 | 300/350 | 54.4/71.6 | 63.0 |

* Nominal dimensions.

⁺ Assumes parabolic oxidation kinetics.

^o Air flow 0.5 ft/sec.

^{oo} Air flow 0.2 ft/sec.

TABLE 60

OXIDATION SCREENING: MATERIAL III ($\text{HfB}_2 + 20 \text{ v/o SiC}$)
(152 Torr O_2 in Air at 0.9 ft/sec - STP)

| Exp. No. | Pressing No. | Temp °C | Time min | Initial* mils/mils | Height/Diameter | Average One Hour Boride Recession |
|----------|--------------|------------|-------------|-----------------------|--|--|
| | | | | | Boride Recession (SiC Recession) ⁺ mils/mils | (SiC Recession) mils |
| 496 | III05D0386 | 1790 | 60 | 260/350 | 1.1/ 0.7 (3.9/ 4.1) | 0.9 (4.0) |
| 492 | III05D0444 | 1800 | 60 | 300/350 | 0.6/ 0.6 (3.9/ 4.5) | 0.6 (4.2) |
| 493 | III05D0400 | 1800 | 60 | 200/350 | 0.7/ 0.4 (3.2/ 3.8) | 0.6 (3.5) |
| 494 | III05D0402 | 1800 | 60 | 350/350 | 1.5/ 1.0 (4.2/ 5.0) | 1.3 (4.6) |
| 340 | III05D0408 | 1800 | 60 | 300/350 | 0.9/ 1.0 (3.7/ ---) | 1.0 (3.7) |
| 426 | III05D0408 | 1910 | 120 | 300/350 | 2.3/ 8.8 (12.1/19.1) | 4.0 ⁺⁺ (11.0) ⁺⁺ |
| 498 | III05D0402 | 1950 | 60 | 350/350 | 6.4/ 4.2 (68.9/44.6) | 5.3 (56.8) |
| 387 | III05D0400 | 1960 | 60 | 300/350 | 2.3/ 4.7 (34.8/34.0) | 3.8 (44.2) |
| 396 | III05D0386 | 1960 | 60 | 260/350 | 3.6/ 3.5 (32.0/27.0) | 3.6 (29.5) |
| 425 | III05D0408 | 1960 | 30 | 300/350 | 4.7/ 5.7 (29.5/30.9) | 7.4 ⁺⁺ (42.7) ⁺⁺ |
| 427 | III05D0408 | 1970 | 60 | 300/350 | 2.0/ 6.0 (17.3/23.5) | 4.0 (20.4) |
| 442 | III05D0444 | 1980 | 60 | 300/350 | 2.7/ 3.1 (27.5/39.6) | 2.9 (33.6) |
| 464 | III05D0408 | 2020 | 60 | 300/350 | 4.7/ 7.7 (24.6/31.3) | 6.2 (28.0) |
| 384 | III05D0408 | 2050 | 60 | 300/350 | 2.7/ 3.5 (C/C) | 3.1 (C) |
| 500 | III05D0402 | 2060 | 60 | 350/350 | 2.3/ 5.8 (12.8/28.2) | 4.1 (20.5) |
| 525 | III05D0400 | 2100 | 60 | 300/350 | 10.3/13.8 (C/C) | 12.1 (C) |
| 524 | III05D0444 | 2110 | 60 | 300/350 | 15.8/26.6 (C/C) | 21.2 (C) |

* Nominal dimensions.

⁺ C designates complete oxidation of the SiC phase.

⁺⁺ Assumes parabolic oxidation kinetics for the diboride and SiC phases.

TABLE 1

OXIDATION SCREENING: MATERIAL IV ($\text{NiB}_2 + 30 \text{ vol } \text{SiC}$)(152 Torr O_2 in Air at 0.9 ft/sec - STP)

| Exp. No. | Pressing No. | Temp °C | Time min | Initial ^a mils/mils | Height/Diameter | Average One Hour Boride Recession |
|----------|--------------|------------|-------------|-----------------------------------|---|--|
| | | | | | Boride Recession (SiC Recession) mils/mils | (SiC Recession) mils |
| 368 | IV05D0410 | 1800 | 60 | 300/350 | 0.8/ 1.4 (----/ 7.3) | 1.4 (7.3) |
| 484 | IV05D0449 | 1800 | 60 | 300/350 | 2.9/ 2.6 (6.6/ 6.6) | 2.8 (6.6) |
| 383 | IV05D0410 | 1960 | 60 | 300/350 | 6.8/ 0.8 (34.7/48.3) | 3.8 (41.5) |
| 443 | IV05D0449 | 1960 | 60 | 300/350 | 1.4/ 0.6 (77.0/73.1) | 1.0 (75.0) |
| 499 | IV05D0410 | 1980 | 60 | 300/350 | 3.8/ 1.6 (53.8/60.3) | 2.7 (57.1) |
| 502 | IV05D0449 | 2020 | 60 | 300/350 | ---/ 0.9 (59.1/39.6) | 0.9 (49.9) |
| 511 | IV05D0449 | 2070 | 60 | 300/350 | 2.4/ 2.9 (10.3/C) | 2.7 (C) |
| 385 | IV05D0410 | 2100 | 60 | 300/350 | 2.6/ 2.1 (C/C) | 2.4 (C) |
| 431 | IV05D0410 | 2150 | 60 | 300/350 | 8.3/12.8 (C/C) | 10.6 (C) |

^a Nominal dimensions.^{*} C designates complete oxidation of the SiC phase.

TABLE 62

OXIDATION SCREENING: MATERIAL VI (HfB₂ + 4 v o Hf-27Ta)(15% 10.1 P O₂ in Air at 0.4 m/sec - SIPI)

| <u>Exp. No.</u> | <u>Pressing No.</u> | <u>Temp</u> °C | <u>Time</u> min | <u>Height/Diameter</u> | | <u>Average One Hour</u> <u>Material Recession</u> mils |
|-----------------|---------------------|-------------------|--------------------|--|--|--|
| | | | | <u>Initial</u> [*] mils/mils | <u>Material</u> <u>Recession</u> mils/mils | |
| 434 | VI05D0462 | 1760 | 60 | 300/350 | 10.7/10.6 | 12.6 |
| 365 | VI05D0462 | 1800 | 60 | 300/350 | 31.8/17.6 | 24.7 |
| 422 | VI05D0462 | 1875 | 60 | 300/350 | 23.7/27.5 | 25.6 |
| 376 | VI05D0462 | 1960 | 60 | 300/350 | 50.9/64.8 | 57.9 |

^{*} Nominal dimensions.

TABLE 61
EFFECT OF SiC CONTENT ON THE OXIDATION BEHAVIOR
OF MATERIALS III AND V
(152 Torr O₂ in Air at 0.9 ft/sec SiP, 60 Minute Exposure)^a

| OX No. | Pressing | v/o SiC | Temp °C | Boride Recession | | SiC Recession ^b | |
|--------|------------|------------|------------|---------------------|---------|----------------------------|---------|
| | | | | Height/ Diameter | Average | Height/ Diameter | Average |
| | | | | mils/mils | mils | mils/mils | mils |
| 785 | III05D0538 | 10 | 1800 | 1.5/ 1.3 | 2.2 | 2.0/ 2.0 | 3.1 |
| 807 | III05D0538 | 10 | 1794 | 3.1/ 9.1 | 6.1 | 4.0/10.0 | 7.0 |
| 784 | III05D0538 | 10 | 1965 | 7.2/ 6.6 | 6.9 | 18.7/19.3 | 19.0 |
| 783 | III05D0538 | 10 | 2125 | 15.7/23.3 | 19.5 | 70.4/80.5 | 75.9 |
| 764 | V02AD0531 | 5 | 1805 | 12.3/12.9 | 12.6 | C/C | C |
| 763 | V02AD0531 | 5 | 1945 | 33.2/47.5 | 40.4 | C/C | C |
| 762 | V02AD0531 | 5 | 2120 | Complete Oxidation | | | |
| 767 | V02AD0532 | 10 | 1810 | 9.3/ 9.6 | 9.4 | C/C | C |
| 766 | V02AD0532 | 10 | 1950 | 24.2/26.3 | 25.3 | C/C | C |
| 765 | V02AD0532 | 10 | 2105 | 76.2/96.3 | 86.3 | C/C | C |
| 770 | V02AD0534 | 15 | 1805 | 1.6/ 1.1 | 1.4 | 2.6/ 3.8 | 3.3 |
| 769 | V02AD0534 | 15 | 1955 | 14.1/11.4 | 12.8 | ---/23.6 | 23.6 |
| 768 | V02AD0534 | 15 | 2115 | Complete Oxidation | | | |
| 777 | V02AD0534 | 15 | 2115 | Complete Oxidation | | | |
| 773 | V02AD0541 | 35 | 1805 | 3.0/ 1.7 | 2.4 | 9.2/ 9.1 | 9.2 |
| 772 | V02AD0541 | 35 | 1955 | 5.1/ 1.5 | 3.3 | 30.6/15.6 | 23.1 |
| 771 | V02AD0541 | 35 | 2105 | 37.1/29.2 | 33.2 | C/C | C |
| 782 | V02AD0557 | 50 | 1805 | 4.2/ 2.0 | 3.1 | 6.1/ 7.1 | 7.6 |
| 775 | V02AD0557 | 50 | 1955 | 5.9/ | 5.9 | 92.4/ | 92.4 |
| 774 | V02AD0557 | 50 | 2105 | Complete Oxidation | | | |
| 813 | V02AD0557 | 50 | 2120 | Complete Oxidation | | | |

^aOriginal specimen dimensions are 0.35 in. diameter by 0.25 to 0.33 in. length.

^bC is used to indicate complete oxidation of the SiC phase.

^c25 minute exposure, average recessions calculated for 60 minutes assuming parabolic oxidation kinetics.

TABLE 11

SUMMARY OF AVERAGE OXIDE RECESIONS OF OXIDATION SCREENING
MATERIALS AND OF SELECTED COMMERCIAL MATERIALS
AS A FUNCTION OF TEMPERATURE

| Material | Average One Hour Oxide Recessions Mils ^a | | | | | |
|---|---|------------|------------|------------|-------------|---------------|
| | T = 1600°C | 1700°C | 1800°C | 1900°C | 2000°C | 2100°C |
| I(ZrB ₂) | 10 | 13 | 22 | - 100 | | |
| Notexa ZrB ₂ | 14 | 22 | 25 | | | |
| Carborundum ZrB ₂ | 14 | 18 | 20 | - 100 | | |
| V(ZrB ₂ +20 v/o SiC) | | | 2 (7) | 6 (20) | 20 (70) | 60 (>150) |
| Boride Z | 4 | 6 | 12 | 25 | 45 | |
| VIII(ZrB ₂ +30 v/o Graphite) +14 v/o SiC) | | | | | | |
| a) Regal Graphite | | | 7 (20) | 10 (40) | 15 (50) | |
| b) Poco Graphite | 8 (10) | 14 (20) | 25 (35) | 45 (60) | 80 (110) | |
| XII(ZrB ₂ +Graphite) | | | | | | |
| a) 90 v/o Poco Graphite ^{oo} | 55 | 80 | 110 | 120 | 120 | |
| b) 20 v/o Poco Graphite | | | 28 | 70 | | |
| c) 5 v/o Thormal Graphite | | | 35 | | | |
| X(ZrB ₂ +20 v/o SiB ₆) | | 16 | 24 | | | |
| XI(ZrB ₂ + 6 v/o Cr) | | 25 | 40 | 100 | | |
| II(HfB ₂) | 4 | 5 | 12 | 20 | 60 | |
| III(HfB ₂ +20 v/o SiC) | | | 1 (4) | 2 (15) | 4 (55) | 15 (>150) |
| IV(HfB ₂ +35 v/o SiC) | | | 2 (6) | 2 (20) | 2 (40) | 3 (>150) |
| VI(HfB ₂ +4 v/o Hf-27Ta) | | | 15 | 35 | 90 | |

^a Parenthetical numbers are average additive phase recessions, in mils.

^{oo} Probably oxidation is air supply or diffusion limited.

TABLE 65

EXPERIMENTAL VERIFICATION OF PRODUCT RELATION.

$$R_2 = W_{\max} / S$$

| <u>Shape</u> | <u>Material</u> | <u>No. of Specimens</u> | <u>W_{\max}</u> (water/cm) | <u>Ratio</u> (SiC/ Al_2O_3) |
|--------------|-----------------|-------------------------|--|-----------------------------------|
| Circle | Al_2O_3 | 10 | 33.5 ± 0.4 | 4.54 ± 0.13 |
| | SiC | 5 | 152.0 ± 4.0 | 4.54 ± 0.13 |
| Square | Al_2O_3 | 9 | 28.7 ± 0.4 | 4.78 ± 0.07 |
| | SiC | 9 | 137.3 ± 0.7 | 4.78 ± 0.07 |

TABLE 66

SUMMARY OF PRELIMINARY RESULTS OF THERMAL STRESS EVALUATIONS

| Specimen Designation | Shape Factor | Heat Flux (cal/sec cm) | Material Factor, R Calculated Experimental | Outer Wall Temp. °C | Atmosphere | Remarks |
|----------------------|--------------|---------------------------|---|------------------------|------------|--|
| KT 84C | 23.5 | 106-124 | 4.87 | 1350 | Vacuum | Failed |
| KT 84C | 23.5 | 112-115 | 4.87 | 1350 | Vacuum | Failed |
| 102 D0364 | 24 | 196 | --- | 1970 | Vacuum | No failure |
| 103A D0539 | 20.0 | 170 | --- | 1419 | Vacuum | No failure |
| 103A D0439 | 20.0 | 300 | --- | 1629 | Helium | Sample failed while cooling to room temp |
| 103A D0540K | 20.0 | 141 | --- | 1316 | Helium | Sample failed in 1 1/2 min when rapidly heated using a heat flux of 141 cal/cm sec. Failure occurred just before equilibrium temp. was reached |
| V07 D0582K | 15.0 | 142 | --- | 1330 | Vacuum | No failure |
| V07 D0582K | 15.0 | 166 | --- | 1369 | Vacuum | Heat flux changed from 142 to 166 cal/cm sec in 1 in cement. No failure |
| V07 D0586K | 15.0 | 142 | --- | 1236 | Helium | No failure |
| V07 D0586K | 15.0 | 166 | --- | 1326 | Helium | Heat flux changed from 142 to 166 cal/cm sec in 1 in cement. No failure |
| V07 D0586K | 15.0 | 192 | --- | 1386 | Helium | Heat flux changed from 166 to 192 cal/cm sec in 1 in cement. No failure |

TABLE 66 (CONT)

SUMMARY OF PRELIMINARY RESULTS OF THERMAL STRESS EVALUATIONS

| <u>Specimen Designation</u> | <u>Shape Factor</u> | <u>Heat Flux</u> (cal/sec cm ²) | <u>Material Factor, R₂</u> <u>Calculated Experimentally</u> (cal/sec cm) | <u>Outer Wall Temp</u> <u>°C</u> | <u>Atmosphere</u> | <u>Remarks</u> |
|-----------------------------|---------------------|--|---|--|-------------------|--|
| V07 D0471K (cross) | 20.0 | 70 | 3.50 4.61 5.86 6.91 7.46 7.78 8.32 8.70 9.55 12.3 | 1060 1150 1250 1320 1340 1345 1390 1420 1445 1630 | Helium | Heat flux changed in increments to give R ₂ increment shown. R ₂ reduced to 1.50 cal/cm sec between each increment chosen. |
| U05 D0493K U05 D0495K | 15.0 15.0 | 102 166 | 9.50 11.1 | 1235 1320 | Helium Helium | No failure. No failure. Heat flux changed from 142 to 166 cal/cm sec in 1 in increment. No failure. |
| U05 D0493K | 15.0 | 192 | 12.8 | 1385 | Helium | Heat flux changed from 142 to 166 cal/cm sec in 1 in increment. Failed. |

Shape Factor - R₂ values are 21.9 for 1.7 inch o.d., 20.0 for 2.0 inch o.d. circular specimens and 15 for equilateral triangular specimens; all specimens have 1.0 inch i.d.

Graphite Guard Rings - were used for all experiments except for Specimen U05 D0493K for which Material V was employed.

REFERENCES

1. Kaulman, L. and Clougherty, E. V., "Investigation of Boride Compounds for Very High Temperature Applications", RTD-TDR-63-4096, Part I, December (1963).
2. Kaulman, L. and Clougherty, E. V., "Investigation of Boride Compounds for Very High Temperature Applications", RTD-TDR-63-4096, Part II, February (1965).
3. Kaulman, L. and Clougherty, E. V., "Investigation of Boride Compounds for Very High Temperature Applications", RTD-TDR-63-4096, Part III, March (1966).
4. "Nondestructive Methods for The Evaluation of Graphite and Ceramic Type Materials", Contract No. AF33(615)-3942, Avco Corp., Space Systems Division, Lowell, Mass.
5. "Stability Characterization of Refractory Materials Under High Velocity Atmospheric Flight", Contract No. AF33(615)-3859, ManLabs, Inc., Cambridge, Mass.
6. Brühl, C. E., "Ternary Phase Equilibria in Transition Metal-Boron-Carbon-Silicon Systems", AFML-TR-65-2, Part II, Volume X (1966).
7. Rudy, E., Private Communication.
8. Rudy, E., Windisch, St., "Ternary Phase Equilibria in Transition Metal-Boron-Carbon-Silicon Systems", Part II, Volume XIII, December (1966).
9. Krochmal, J. J., "Fiber Reinforced Ceramics: A Review and Assessment of Their Potential", AFML-TR-67-207, October (1967).
10. Kalish, D., Clougherty, E. V. and Ryan, J., "Fabrication of Dense Fine Grained Ceramic Materials", AFML-TR-67-207, November (1966).
11. Vahldek, F. W., Mersel, S. A. and Lynch, C. T., Science (1965) 149, 747.
12. Rhodes, W. H., et al., "Microstructure Studies of Polycrystalline Refractory Oxides", Contract N0W-65-0316-1 (1966).
13. MacKenzie, J. K., Proc. Phys. Soc. (London) (1950) 63B(1) 2.
14. Coble, R. L. and Kingery, W. D., "Effect of Porosity on Physical Properties of Sintered Alumina", J. Am. Ceram. Soc. (1956) 39, 377.
15. Rossi, R. C., Carnahan, R. D. and Janowski, K. R., "A Model for Behavior of Composite Systems at Low Concentrations of Included Phases", SAMSO-TR-68-15, December (1967).

REFERENCES (CONT)

16. Lang, S. M., Properties of High Temperature Ceramics and Cermets
Electricity and Thermal Properties at Room Temperature, National Bureau of
Standards, Monograph No. 6, March (1960)
17. Discussion of Seminar on Structural Ceramics and Testing of Brittle
Materials UTRI, March (1967)
18. Hower, A. H., "The Investigation of The Temperature Dependence of The
Strength of Corundum Crystal", Ph. D. Thesis, University of Leeds,
England (1965)
19. Anthony, F. M., Marcus, L. and Mistretta, A. L., "Selection Techniques
for Brittle Materials - Volume I Evaluation of ZrO_2-MoSi_2 as a Structural
Refractory Ceramic Body", AFML-TR-65-209, September (1965).
20. Hasselman, D. P. H., J. Am. Cer. Soc. (1967) 50, 454.
21. Hasselman, D. P. H., J. Am. Cer. Soc. (1963) 46, 535
22. Kingery, W. D., Introduction to Ceramics, John Wiley and Sons, Inc.,
N. Y., 636 (1960).
23. Manson, S. S., "Thermal Stresses and Thermal Shock", Mechanical Behavior
of Materials at Elevated Temperature, McGraw-Hill Book Co., N. Y.,
John Dorn, Editor, 402 (1961).
24. Baroody, E. M., Duckworth, W. H., Simons, E. M. and Schafeld, H. Z.,
"Effect of Shape and Material on The Thermal Rupture of Ceramics",
AECD-3486 (BMI-70) May (1951).
25. Baroody, E. M., Simons, E. M. and Duckworth, W. H., "Effect of Shape
on Thermal Fracture", J. Am. Cer. Soc. (1953) [1] 30, 38.
26. Smalley, A. K., Baroody, E. M., Simons, E. M. and Duckworth, W. H.,
"The Thermal Fracture of Ceramic Cylinders", BMI-1102, June (1946).
27. Wisbel, E. E., "Thermal Stresses in Cylinders by The Photoelastic Method",
Proceedings of Fifth International Congress for Applied Mechanics, 213-20,
John Wiley and Sons, Inc. (1939)
28. Lynch, J. R. and Raderer, C. G. and Duckworth, W. H., "Engineering
Properties of Selected Ceramic Materials", Am. Cer. Soc., Columbus,
Ohio (1966).

APPENDIX I

CHARACTERIZATION OF DIBORIDE POWDER SHIPMENTS

In addition to the large powder procurements of the diborides, which have been described in Section III, several small quantity shipments have been received for evaluation. These powders were characterized by chemical and X-ray analysis and by powder density measurements. The characterization results are presented in Tables I-1 to I-6.

The ZrB_2 powders 104 and 106 represent small quantity lots. Their chemistries are approximately the same as the 102A powders. Analysis of the 105 powder showed large quantities of metal carbide and oxide impurities. The material was reprocessed with a substantial reduction of phase impurities. The characterization data for the reprocessed powder, identified as 105A, is presented in Table 5.

The HfB_2 powders 1107 and 1108 represent experimental processing lots obtained from the U.S. Borax Research Corporation. Very high hafnium oxide and hafnium carbide contents rejected these materials for further consideration. The 1108 material, which also has a high level of phase impurities, is being reprocessed.

TABLE I-1

CHARACTERIZATION OF ZIRCONIUM DIBORIDE POWDER, 204

Supplier: U. S. Borax Research Corporation

Quantity: 8.5 pound lot

| | |
|---|----------------------------------|
| 1. Qualitative Analysis (weight per cent, w/o) | 4. X-ray Phase Identification |
| Ti 0.01 - 0.1 | ZrB_2 |
| 2. Quantitative Analysis (v/o) | ZrO_2 (impurity) |
| Zr 60.1 | 5. Powder Density |
| B 18.55 | 6.00 g/cc |
| C 0.11 | 6. Phase Assay (volume per cent) |
| O 0.76 | Calculated from Composition |
| Total 99.48 | |
| 3. Atomic Ratio | ZrB_2 ZrO_2 ZrC |
| Over-all B/Zr = 1.91 | 96.1 3.2 0.7 |
| Corrected B/Zr ^a = 2.93 | |

^a Atomic ratio corrected for metal assumed to be present as metal dioxide and metal monocarbide.

TABLE 1-2

CHARACTERIZATION OF ZIRCONIUM DIBORIDE POWDER, 304

Supplier: Shindalloy Corporation (H. C. Starch, Berlin)

Quantity: 5 pound evaluation shipment

| | |
|---|----------------------------------|
| 1. Qualitative Analysis (Weight per cent, w/o) | 4. X-ray Phase Identification |
| Hf 0.1 - 1.0 | ZrB_2 |
| Mo 0.01 - 0.1 | ZrC (impurity) |
| | ZrO_2 (impurity) |
| 2. Quantitative Analysis (w/o) | 5. Powder Density |
| Zr 80.85 | 6.33 g/cc |
| B 15.9 | |
| C 0.48 | 6. Phase Assay (volume per cent) |
| O 1.17 | Calculated from Composition |
| Total 98.40 | |
| 3. Atomic Ratio | ZrB_2 ZrO_2 ZrC |
| Overall B/Zr = 1.66 | 91.7 5.0 2.5 |
| Corrected B/Zr ^a = 1.82 | |

^a Atomic ratio corrected for metal assumed to be present as metal diboride and metal monocarbide.

TABLE L-1

CHARACTERIZATION OF ZIRCONIUM FLUORIDE POWDER, 106

Supplier: U. S. Boron Research Corporation

Quantity: 1 pound evaluation shipment

| | |
|---|---------------------------------------|
| 1. Qualitative Analysis (weight per cent, w/c) | 4. X-ray Phase Identification |
| Fe 0.01 = 0.1 | ZrB ₂ |
| | ZrO ₂ (impurity) |
| 2. Quantitative Analysis (w/c) | 5. Powder Density |
| Zr 79.75 | 5.96 g/cc |
| B 18.75 | |
| C 0.41 | 6. Phase Assay (volume per cent) |
| O 1.18 | Calculated from Composition |
| Total 100.09 | |
| 3. Atomic Ratio | ZrB ₂ ZrO ₂ ZrC |
| Overall B/Zr = 1.96 | 93.2 4.8 2.0 |
| Corrected B/Zr = 2.16 | |

* Atomic ratio corrected for metal assumed to be present as metal dioxide and metal monocarbide.

TABLE I-4

CHARACTERIZATION OF HAFNIUM DEBORIDE POWDER, LB6

Supplier: Shieldalloy Corporation (H. C. Starch, Berlin)

Quantity: 5 pound evaluation shipment

| | |
|--|---------------------------------------|
| 1. Qualitative Analysis (weight per cent w/o) | 4. X-ray Phase Identification |
| Ti 0.1 - 1.0 | HfB ₂ |
| Cr, Co 0.01 - 0.1 | HfC (impurity) |
| | HfO ₂ (impurity) |
| 2. Quantitative Analysis (w/o) | 5. Powder Density |
| Hf + Zr 89.6 | -11.2 g/cc |
| Ti, Cr, Co 0.41 | |
| B 0.66 | 6. Phase Assay (volume per cent) |
| C 0.60 | Calculated from Composition |
| O 0.97 | |
| Total 99.65 | |
| 3. Atomic Ratio | |
| Over-all B/Hf = 1.56 | HfB ₂ HfC ₂ HfC |
| Corrected B/Hf ^a 1.86 | 86.1 7.8 6.1 |

^a Atomic ratio corrected for metal assumed to be present as metal dihydride and metal monocarbide.

TABLE 1-5
CHARACTERIZATION OF MAGNUM DIBORIDE POWDER, 1107

Supplier: U. S. Borax Research Corporation

Quantity: 1 Pound Evaluation Shipment

- | | | | | | | | | | | | | | |
|---|--------------|-----------|----|------------|--|-------|---|------|---|-------------|--------------|--------------|--|
| <p>1. Qualitative Analysis (weight per cent, w/o)</p> <table border="0" style="margin-left: 20px;"> <tr> <td>Ca, Ti</td> <td>0.1 - 1.0</td> </tr> <tr> <td>Cr</td> <td>0.01 - 0.1</td> </tr> </table> | Ca, Ti | 0.1 - 1.0 | Cr | 0.01 - 0.1 | <p>4. X-ray Phase Identification</p> <p style="margin-left: 20px;">MgB_2</p> <p style="margin-left: 20px;">H_2O_2 (impurity)</p> | | | | | | | | |
| Ca, Ti | 0.1 - 1.0 | | | | | | | | | | | | |
| Cr | 0.01 - 0.1 | | | | | | | | | | | | |
| <p>2. Quantitative Analysis (w/o)</p> <table border="0" style="margin-left: 20px;"> <tr> <td>Mg + Zr</td> <td>86.35</td> </tr> <tr> <td>Zr</td> <td>-----</td> </tr> <tr> <td>B</td> <td>11.25</td> </tr> <tr> <td>C</td> <td>0.12</td> </tr> <tr> <td>O</td> <td><u>1.15</u></td> </tr> <tr> <td>Total</td> <td>99.40</td> </tr> </table> | Mg + Zr | 86.35 | Zr | ----- | B | 11.25 | C | 0.12 | O | <u>1.15</u> | Total | 99.40 | <p>5. Powder Density</p> <p style="margin-left: 20px;">19.25 g/cc</p> |
| Mg + Zr | 86.35 | | | | | | | | | | | | |
| Zr | ----- | | | | | | | | | | | | |
| B | 11.25 | | | | | | | | | | | | |
| C | 0.12 | | | | | | | | | | | | |
| O | <u>1.15</u> | | | | | | | | | | | | |
| Total | 99.40 | | | | | | | | | | | | |
- 3. Atomic Ratio**
- Over-all B/Mg = 2.14

TABLE 1-6

CHARACTERIZATION OF HAFNIUM DIBORIDE POWDER, U06

Supplier: U. S. Borax Research Corporation

Quantity 4 Pound Evaluation Shipment

| | |
|---|------------------------------------|
| 1. Qualitative Analysis (weight per cent, w/o) | 4. X-ray Phase Identification |
| Ca, Ti, Cr 0.1 - 1.0 | HfB ₂ HfC (impurity) |
| 2. Quantitative Analysis (w/o) | 5. Powder Density |
| Hf + Zr 84.68 | 9.97 g/cc |
| Zr ----- | |
| B 11.35 | |
| C 1.68 | |
| O <u>0.50</u> | |
| Total 98.13 | |
| 3. Atomic Ratio | |
| Over-all B/Hf = 2.21 | |

BLANK PAGE

APPENDIX II

PROCESSING VARIABLES FOR HOT PRESSING OF DIBORIDES

A Hot Pressing Facility

Fabrication studies were conducted on 2 inch diameter x 5/16 inch high billets. These pressings were conducted in a conventional induction heated graphite mold system which is shown schematically in Figure II-1. Other billets of 3 inch diameter were also made in the same press, but with larger furnaces.

B Diffusion Barriers

Chemical reactions between the graphite furnace and the diboride powder have been frequently observed. The following die liners were tested as reaction limiting diffusion barriers: (a) boron nitride wash on graphite sleeve, (b) tungsten foil, (c) pyrolytic graphite paper, (d) silicon carbide wash and (e) pyrolytic graphite paper with an inner BN wash coating. The results for each barrier system will not be discussed in detail; it is sufficient to report that the pyrolytic graphite paper with an inner boron nitride wash coating is the most effective at temperatures up to 2100°C. Above 2100°C, reaction zones are very apparent and approach the width of those found without a diffusion barrier (about 3/16 inch).

Many billets pressed below 2100°C still showed microstructural evidence, in terms of grain size, porosity level, or phase distribution, of an interaction with the BN layer, but the effects are minor compared with results obtained without such diffusion barriers. The diboride compositions containing SiC, Materials III, IV and V, revealed markedly smaller reaction layers than Materials I and II. In fact, the vast majority of the billets of these additive containing materials exhibited no evidence for a die wall interaction.

C Microstructure Reproducibility

An important aspect of this program is to obtain sufficient process control so that duplicate microstructures and compositions may be fabricated. Experience indicated that density would be the most difficult parameter to reproduce, so this property was utilized as the primary measure of reproducibility.

A number of pressings with comparable temperature-pressure-time cycles are presented in Table II-1. In several cases the degrees of control appears quite good, e.g., D0329 vs. D0390, D0303 vs. D0306 and D0395 vs. D0397. In other comparisons the difference in density can be explained by fabrication time differences, e.g., D0310 vs. D0323 and D0000 vs. D0444. However, some experiments resulted in more than the expected 1 to 2% variations, e.g., D0311 vs. D0314 and D0330 vs. D0335.

Consequently, the hot pressing process was examined in detail in order to determine whether the process control could be improved. Temperature was assumed to be the most difficult parameter to measure. In the temperature range being employed the precision of optical temperature readings is approximately $\pm 20^\circ\text{C}$. Billets prepared in this study with an intentional difference of 20°C in the pressing temperature can give significantly different microstructures. In addition

to the variation introduced by the degree of precision in the temperature measurement, the formation of a deposit within the temperature sight tube makes even the temperature control to $\pm 20^\circ\text{C}$ difficult.

The time of pressing is probably the easiest parameter to control. Some variation in the heating rate is encountered, which could give different effective pressing times if the heating rates were different within 250° to 300°C of the hot pressing temperature.

Pressure is not a difficult parameter to control and an automatic pressure release valve assured a constant pressure during the run. It is somewhat difficult to read the pressure scale accurately since relatively low loads (4 to 6 tons out of a total 75 tons available in the press) are required for the 2 inch diameter billets. A load variation of ± 100 pounds between runs is possible. During the course of this program, data were collected on the effect of pressure on the densification of Material A, Table II-2. It was concluded from these data that a change in pressure from 4000 to 6000 psi produced minor or no variations in density, but some lower pressure between 2000 to 4000 psi acted as a threshold pressure for a uniform densification rate.

During the course of this study, several other parameters were considered for process control. The densification rate was used with limited success as a measure of progress in the densification process. Another technique often employed in hot pressing to obtain a less than fully dense billet is to construct the die so that, for a given quantity of powder, the pressure train comes against a physical stop usually a change in the piston, at the desired density level. However, this technique is not effective for hot pressing the diborides because of the high temperatures required in the fabrication. In the 1800° to 2100°C temperature range, the parts of the graphite furnace creep at a fast rate and this alters the initial geometry which is used to define the stop point.

Another important variable recognized in this program is the hot pressing furnace build. Three furnaces are employed and any variation in their thermal characteristics could manifest itself in the same manner as a variation in hot pressing temperature. The point of temperature measurement (a cavity in the die wall) is approximately 2 inches from the billet; consequently, different rates of heat loss down the pressure train will effect the billet temperature. Carbon blocks are incorporated in the pressure train as thermal insulators. As these blocks graphitize their thermal conductivity changes which probably results in a variation in temperature at the billet relative to the temperature at the die wall.

An experiment was designed to illustrate the importance of furnace construction as a process parameter. Three furnaces were completely rebuilt in as nearly an identical manner as possible. Two pressings were conducted in each furnace with the B3A powder under identical fabrication conditions, the results of which are presented in Table II-3. It appears that, in spite of the precautions, furnace 1A behaves differently from furnace 1B. It is difficult to form any conclusions concerning furnace 1A because of the low density for billet B3A B3145. It is not clear whether errors in the measurement of temperature and pressure, variations in heating rate or, furnace construction led to the variations in density in Table II-3. However, these experiments point out that the expected level of control presently available for hot pressing the diborides is about $\pm 1.7\%$ relative density, although greater variations can occur.

TABLE II-1

**HOT PRESSINGS OF VARIOUS DIBORIDE COMPOSITIONS
SHOWING DEGREE OF PROCESS CONTROL**

| <u>Material Designation</u> | <u>Temp.</u> C | <u>Pressure</u> psi | <u>Time</u> min | <u>Density</u> gm/cc | <u>Relative Density</u> % | <u>Furnace No.</u> |
|---------------------------------|-------------------|------------------------|--------------------|-------------------------|----------------------------------|------------------------|
| 101A D0283 | 2050 | 6000 | 60 | 5.87 | 97.4 | |
| 101A D0304* | 2070 | 6000 | 60 | 5.83 | 96.6 | |
| 101A D0305F | 2075 | 6000 | 60 | 5.99 | 99.3 | |
| 101A D0309 | 2050 | 6000 | 30 | 5.80 | 96.2 | |
| 101A D0290 | 2050 | 6000 | 30 | 5.85 | 96.9 | |
| 101A D0311 | 1800 | 6000 | 120 | 5.56 | 92.0 | |
| 101A D0316 | 1800 | 6000 | 120 | 6.00 | 99.5 | |
| 101A D0324 | 1800 | 6000 | 30 | 5.56 | 92.1 | 1A |
| 101A D0326 | 1800 | 6000 | 25 | 5.37 | 89.1 | 1A |
| 101A D0330 | 1900 | 6000 | 90 | 5.98 | 99.3 | 1A |
| 101A D0339 | 1900 | 6000 | 100 | 5.52 | 91.5 | 1B |
| 1105 D0400 | 2000 | 4000 | 110 | 8.86 | 93.3 | 1B |
| 1105 D0404 | 2000 | 4000 | 100 | 8.52 | 89.9 | 1B |
| 1105 D0385 | 2050 | 4000 | 75 | 9.25 | 98.6 | 2B |
| 1105 D0386 | 2050 | 4000 | 60 | 9.26 | 98.6 | 3B |
| V01A D0195 | 1900 | 4000 | 115 | 5.22 | 94.5 | 1B |
| V01A D0197 | 1900 | 4000 | 110 | 5.28 | 95.1 | 1B |
| V01A D0192F | 2000 | 4000 | 45 | 5.21 | 94.5 | 1B |
| V01A D0193F | 2000 | 4000 | 35 | 5.40 | 97.6 | 2B |
| V01A D0194F | 2000 | 4000 | 50 | 5.47 | 98.0 | 1B |

* Ball milled.

F Fluid energy milled.

TABLE II-2
EFFECT OF PRESSURE ON HOT PRESSING MATERIAL II AT 2200°C

| <u>Material Designation</u> | <u>Pressure psi</u> | <u>Time min</u> | <u>Density gm/cc</u> | <u>Density %</u> | <u>Furnace No.</u> |
|-----------------------------|-------------------------|---------------------|--------------------------|----------------------|------------------------|
| IES D0316 | 6000 | 120 | 10.62 | 99.5 | 1B |
| IES D0348 | 4000 | 200 | 10.58 | 99.0 | 2B |
| IES D0351 | 4000 | 200 | 10.53 | 98.6 | 2B |
| IES D0353 | 4000 | 140 | 10.52 | 98.6 | 2B |
| IES D0355 a and b | 4000 | 120 | 10.46 | 97.9 | 1B |
| IES D0457 | 2500 | 110 | 9.93 | 93.0 | 2B |

TABLE II-3
**BULLET DENSITIES OF MATERIAL 103A HOT PRESSED
AT 2000°C, 4000 PSI FOR 75 MINUTES**

| <u>Bullet Number</u> | <u>Furnace</u> | <u>Relative Density %</u> |
|----------------------|----------------|---------------------------|
| D0360 | 1A | 97.6 |
| D0367 | 1A | 97.0 |
| D0359 | 2A | 98.5 |
| D0368 | 2A | 94.1 |
| D0366 | 1A | 98.1 |
| D0369 | 1A | 99.5 |
| Average | | 97.1 |
| Standard Deviation | | 1.7 |
| Maximum Deviation | | 5.4 |

APPENDIX III

OXIDATION CHARACTERISTICS OF ZIRCONIUM AND HAFNIUM DIBORIDES CONTAINING SELECTED RARE EARTH AND ALKALINE EARTH HEXABORIDE ADDITIVES

The thermal expansion coefficients of vacuum hot pressed ZrB_2 and HfB_2 were determined as part of a coating study for graphite (III-1), to determine the extent of boride coating compatibility. Thermal expansion data were also obtained for ZrB_2 and HfB_2 doped with 20 mole per cent of various alkaline or rare earth hexaborides; these additives were found to alter the expansion coefficients of the diborides and increase the adherence of the coating.

Several of the prepared materials were submitted to Man Labs, Inc. for determination of their high temperature air oxidation behavior. These materials are identified in Table III-1. Oxidation experiments were carried out as described in Section VIII. Briefly, cylinders having nominal dimensions of 0.35 inch diameter by 0.30 inch long were supported on ZrO_2 pads and heated to the test temperature in flowing argon. When the desired temperature was reached, air was admitted at a flow rate of 0.9 ft/sec (STP) for one hour, then argon was readmitted to displace the air and finally the specimen was cooled to room temperature. The ZrB_2 based specimens were oxidized at 1700°C; the HfB_2 and Hf_2B_6 based specimens were oxidized at 1800°C. After oxidation, the quantitative metallographic procedure was employed to measure the extent of conversion to oxide.

A summary of the oxide conversion measurements is given in Table III-1. Representative photomicrographs of the as-received and oxidized specimens are presented in Figures III-1 through III-10. In all cases, the hexaboride additives were observed to oxidize preferentially compared to the diboride phases.

Macrophotographs of the oxidized specimens are presented in Figures III-1 and III-10. The ZrB_2 -base specimens all have rough, pockered outer oxides, whereas the HfB_2 -base specimens are grossly distorted in addition to having pockered, porous outer oxides. In comparison, ZrB_2 and HfB_2 yield smooth, adherent and dense outer oxides after one hour exposures at equivalent temperatures, the appearance of the Hf_2B_6 specimen in Figure III-10 is characteristic of the diborides.

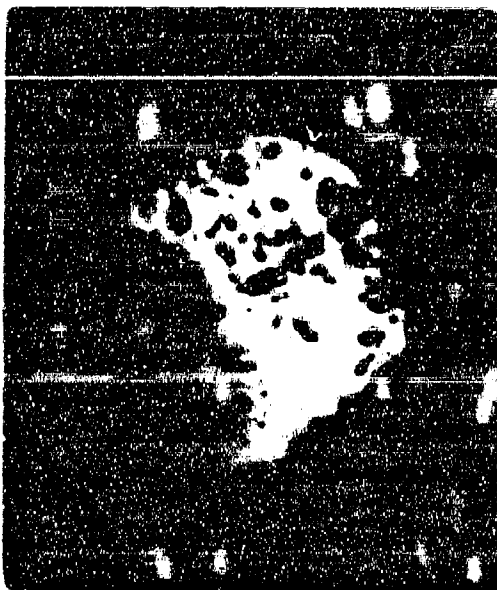
The following features were noted:

- 1) preferential oxidation of the hexaboride phase, as evidenced by a band between the matrix and oxide, this band consists of the bare diboride and voids.
- 2) gross phase distribution (Figure III-12);
- 3) incidence of cracking (Figures III-9 and III-10);
- 4) gross specimen distortion (Figures III-9, III-14 and III-16).

The matrix pictures exhibit comparable microstructures before and after the oxidation exposure. The notable exceptions are the result of excessive second phase present during metallographic preparation (Figures III-2b and III-6b), over-etching (Figures III-6b and III-15b) and lack of a representative initial structure (Figure III-6a).

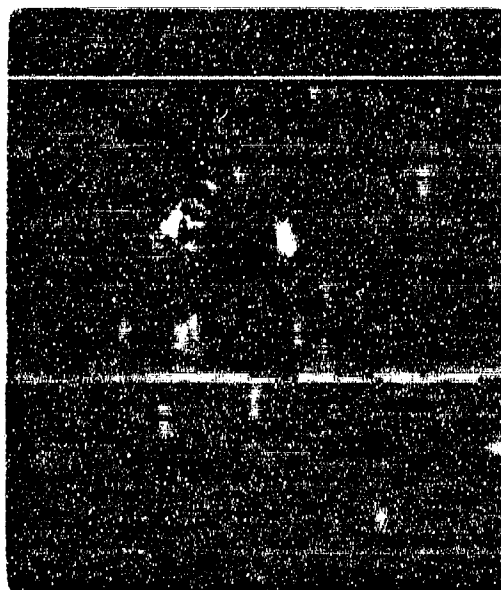
(III-1) Critchlow, J. M., et al., "High Temperature Protective Coatings of Graphite", ML-TDR-64-17, Part IV, November (1964).

The ZrB_2 and HfB_2 without additives exhibit one hour oxide conversions of 12 to 13 mils at the temperatures of 1700° and $1600^\circ C$, respectively. Based upon a limited number of experiments carried out ZrB_2 and HfB_2 -base structures containing selected boraboride additives, it is concluded that the resistance to oxidation in air at temperatures of $1700^\circ C$ (ZrB_2 -based) and $1600^\circ C$ (HfB_2 -based) is reduced by 1.5 to 4 times compared to the unaltered diboride structures.



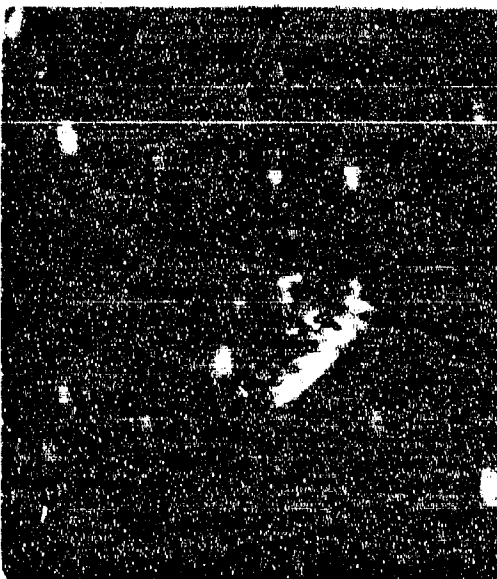
LI-2699

$\text{ZrB}_2 - 10.5 \text{ CaB}_6$



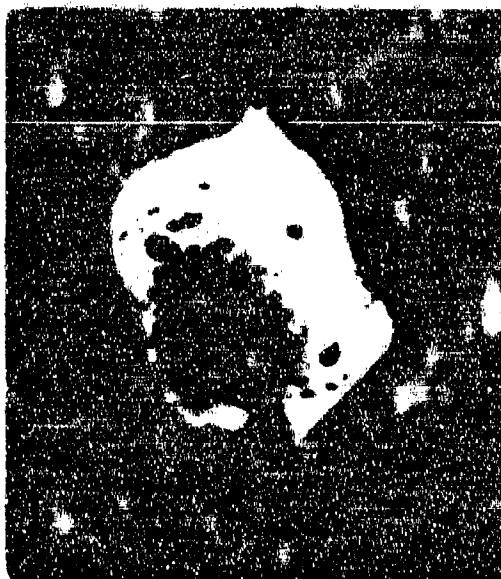
LI-2637

$\text{ZrB}_2 - 15.5 \text{ CaB}_6$



LI-2626

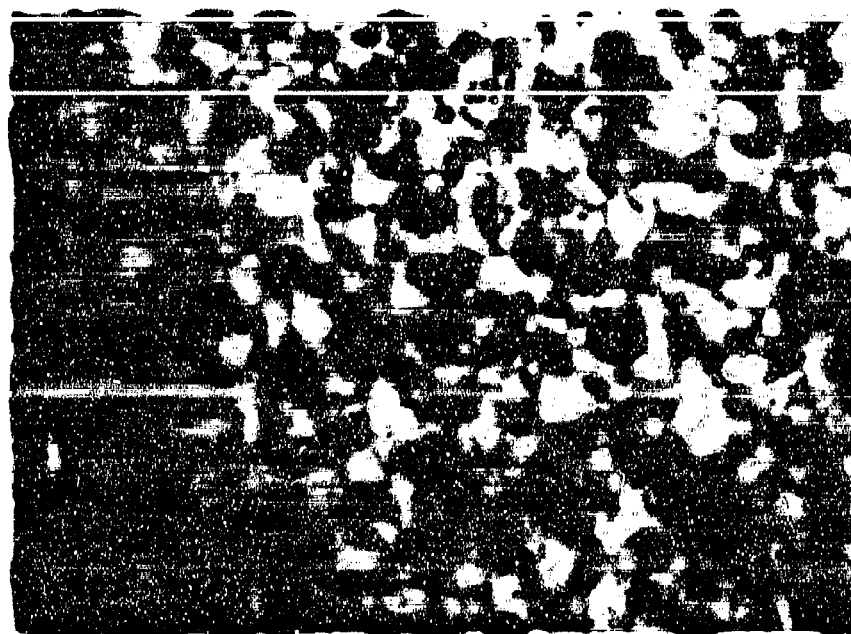
$\text{ZrB}_2 - 22.5 \text{ CaB}_6$



LI-3023

$\text{ZrB}_2 - 20.0 \text{ YB}_6$

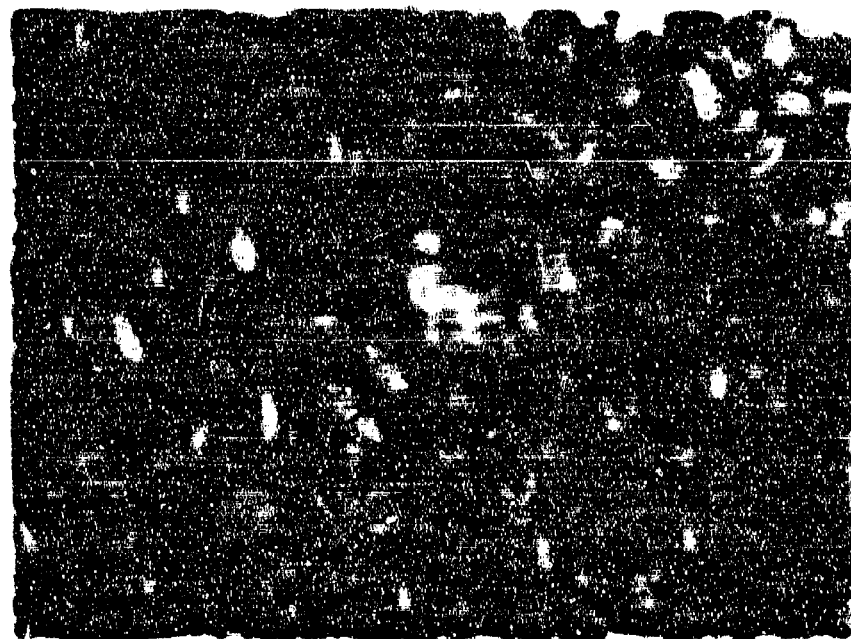
Figure III-1. Macrophotographs of ZrB_2 - MeB_6 Hot Pressed Cylinders after Oxidation in Air for One Hour at 1700°C .



L4630

(a)

500X



L1-1502

(b)

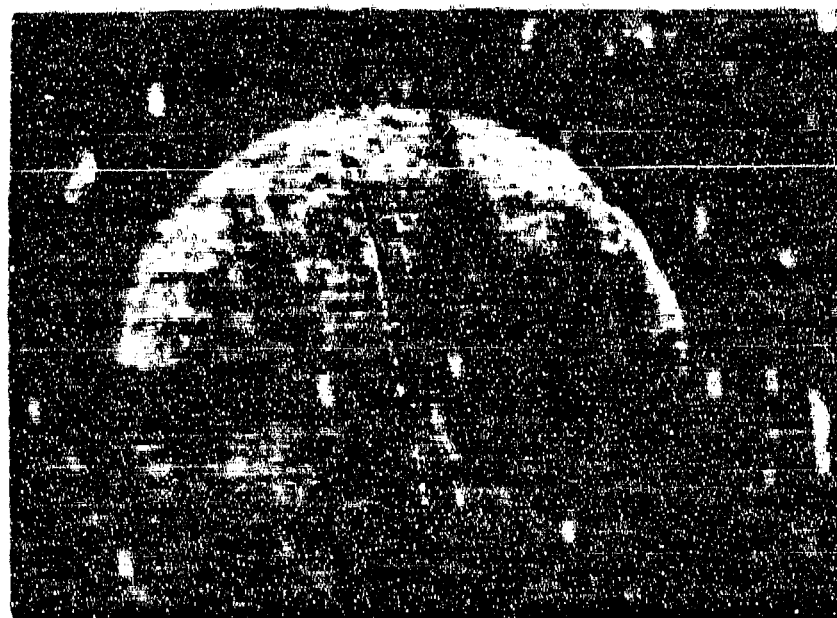
500X

Figure B1-2. Matrix Photomicrographs of Hot Pressed $\text{ErB}_2-10.9\text{CaB}_6$
 a) As Pressed, b) Oxidized in Air for One Hour at 1700°C .



LI-2900

Longitudinal



LI-2903

Transverse

Figure III-3. Retinule Photomicrographs of Hot Pressed $ZrB_2-10.5 CaB_6$. Oxidized in Air for One Hour at $1700^\circ C$ (1 Division = 4.86 Miles).

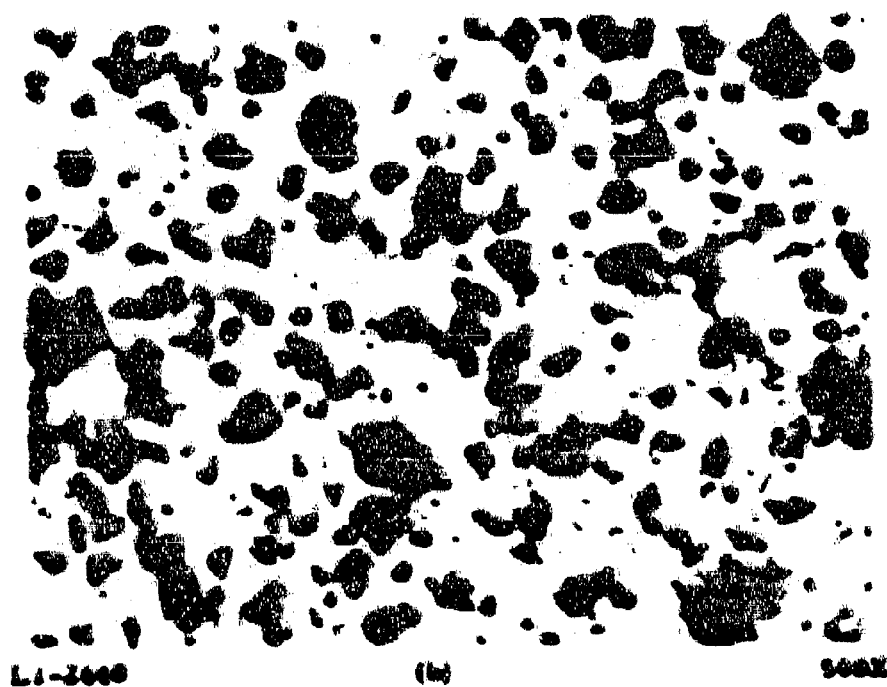
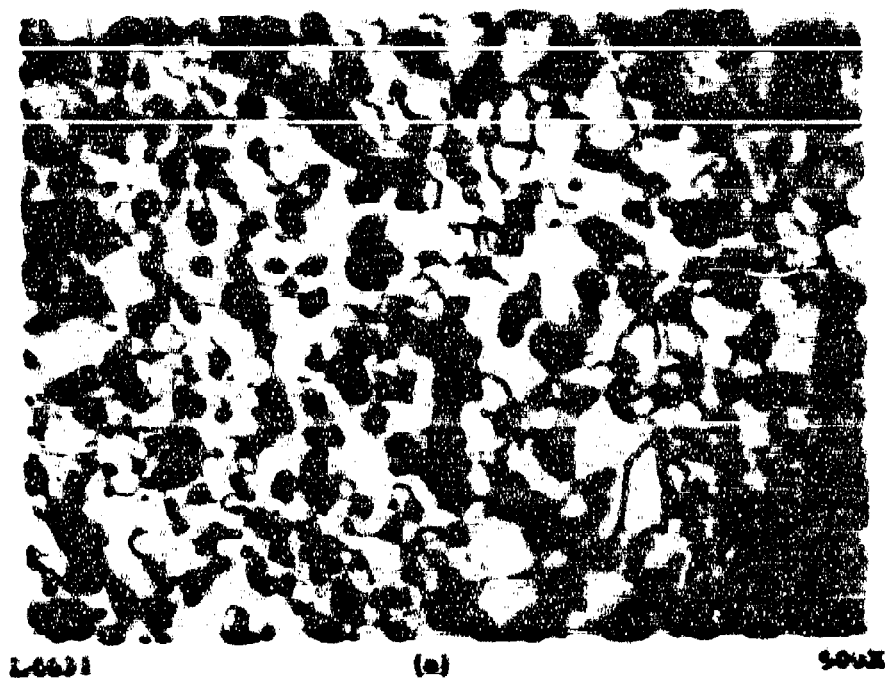
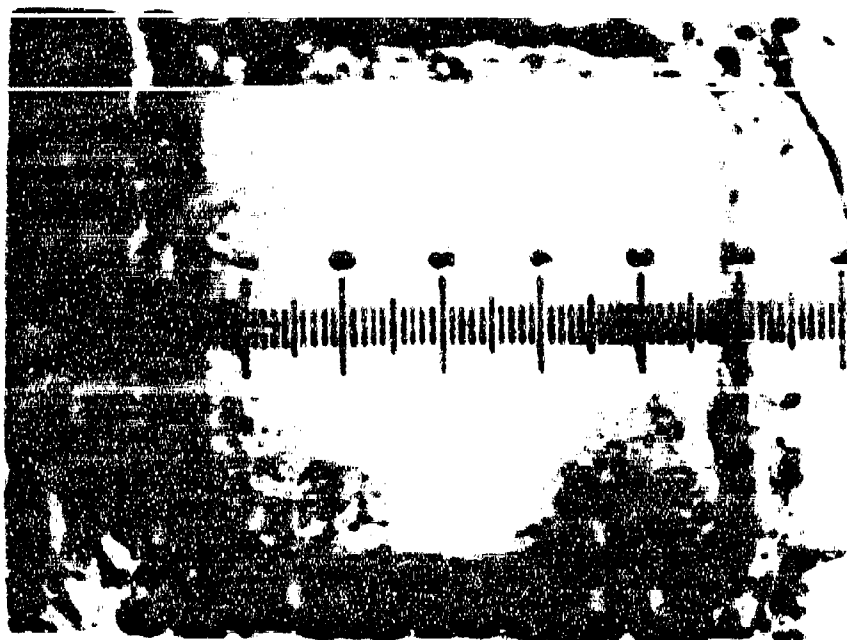
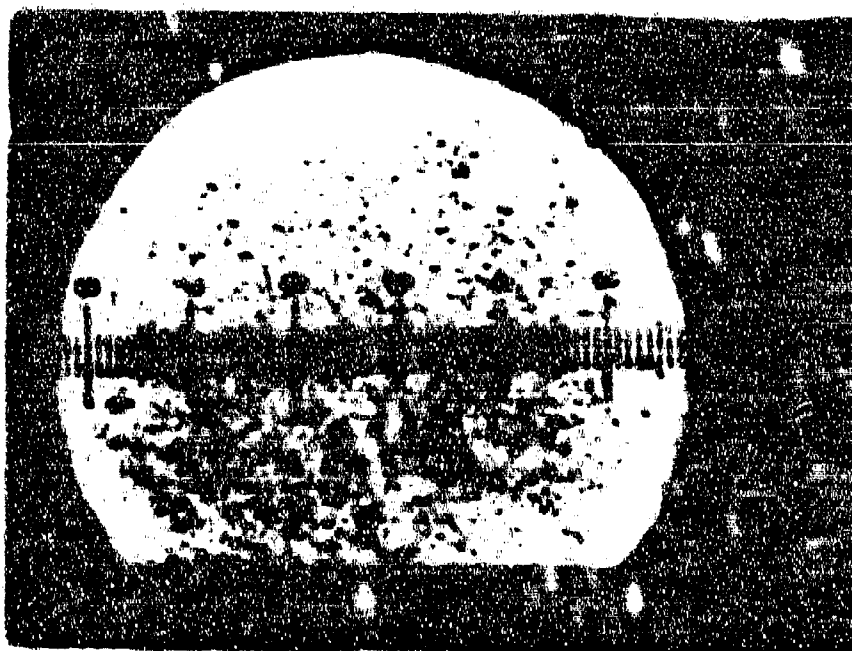


**Figure III-4. Matrix Photomicrographs of Hot Pressed $ZrB_2-15.5 C-4B$,
a) As Pressed, b) Oxidized in Air for One Hour at $1700^\circ C$.**



LI-2638

Longitudinal



LI-2641

Transverse

Figure III-5. Reticula Photomicrographs of Hot Pressed $\text{ZrO}_2\text{-15.5 CaO}$; Oxidized in Air for One Hour at 1700°C (1 Division = 6.86 μm).

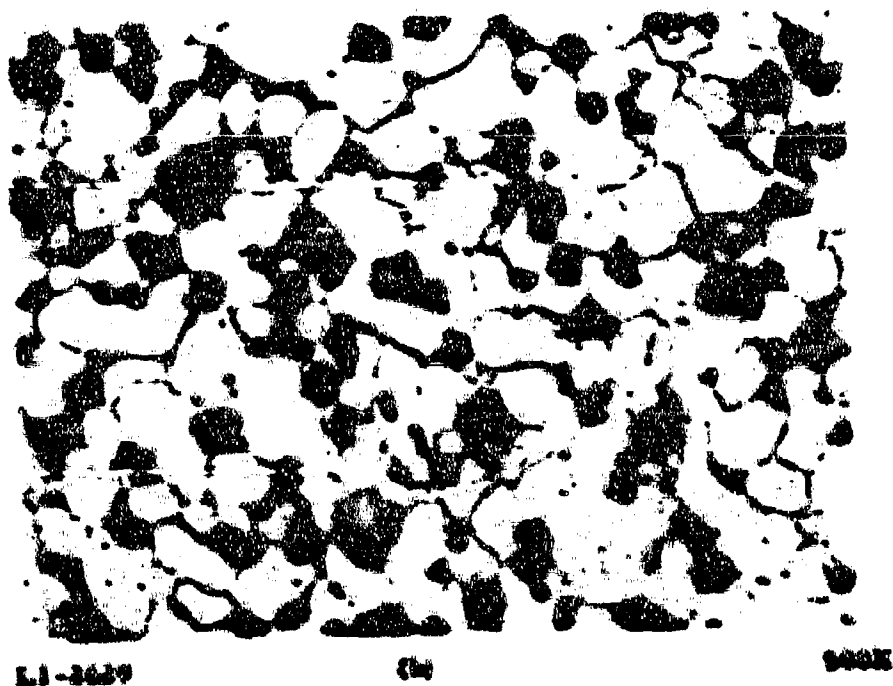
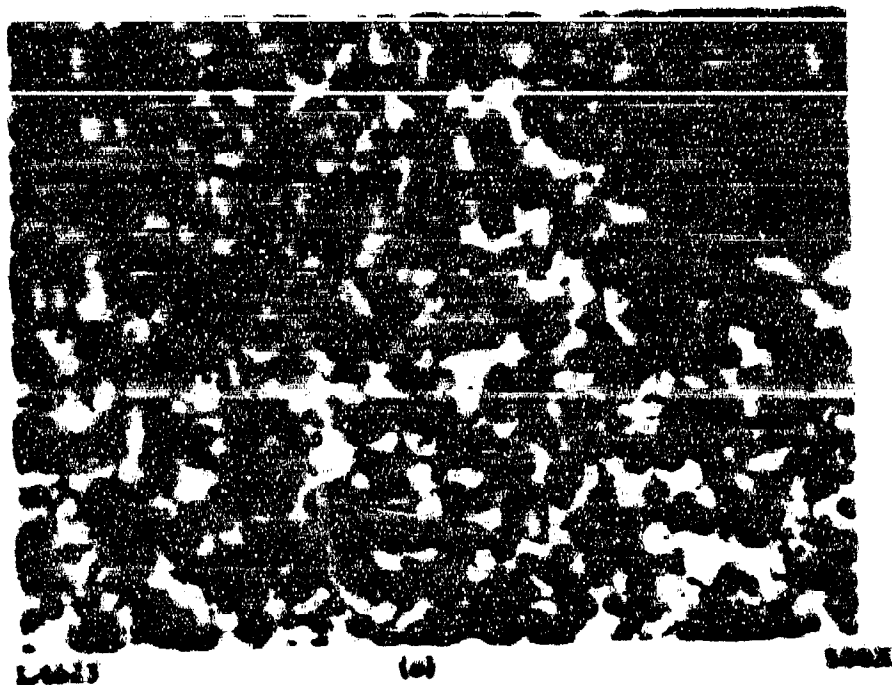


Figure M-6. Micro Photomicrographs of Not Pressed $\text{LaB}_6\text{-21.5 CeO}_2$
a) Thermally cycled, b) Oxidized in Air for One Hour at 1700°C .



LI-2627

Longitudinal



LI-2630

Transverse

Figure III-7. Reticule Photomicrographs of Hot Pressed ZrB_2 -22.5 Cella; Oxidized in Air for One Hour at 1700°C (1 Division = 4.56 μm).

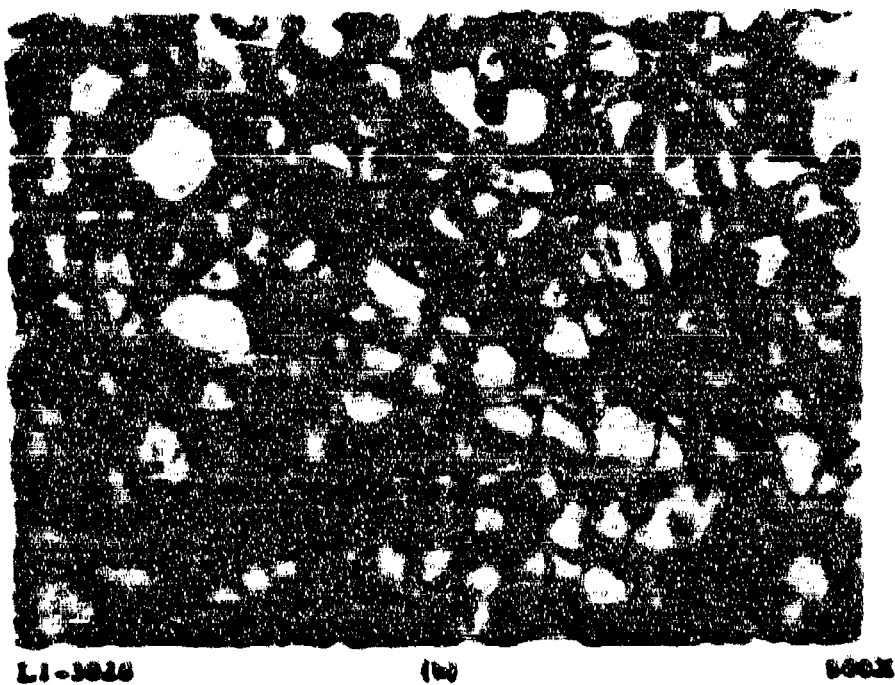
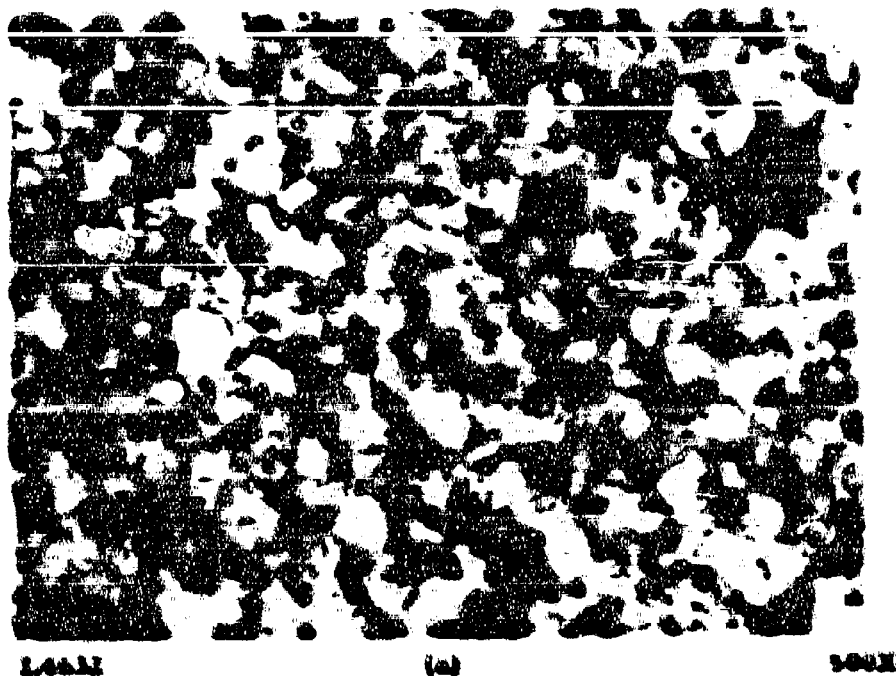
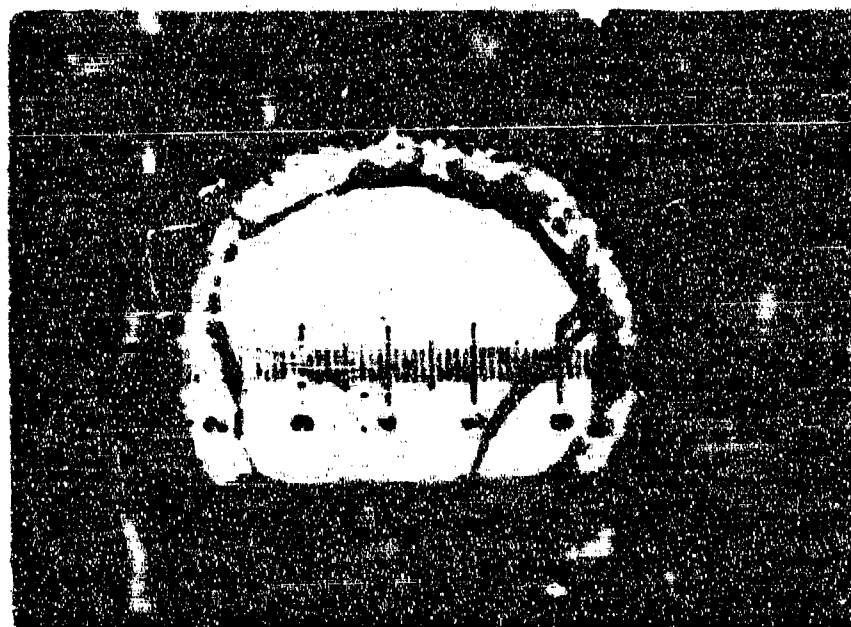


Figure III-6. Matrix Photomicrographs of Hot Pressed ZrB_2 -30.6 YB₂
a) Thermally Cycled, b) Oxidized in Air for One Hour at 1700°C.



LI-1014

Longitudinal



LI-1019

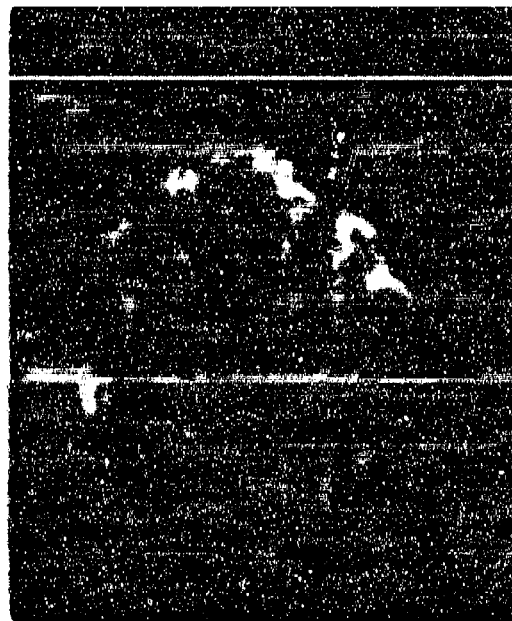
Transverse

Figure III-9. Backscattered Photomicrographs of Hot Pressed $\text{ZrB}_2\text{-30.9 YB}_2\text{O}_3$ Oxidized in Air for One Hour at 1700°C (1 Division = 4.00 μm).



L1-2923

HfB_2



L1-2911

HfB_2 -22.5 LaB_6



L1-2904

HfB_2 -20.0 YB_6



L1-2929

HfB_2 -22.5 CoB_6

Figure III-10. Microphotographs of HfB_2 - MeB_6 Hot Pressed Cylinders after Oxidation in Air for One Hour at 1800°C .

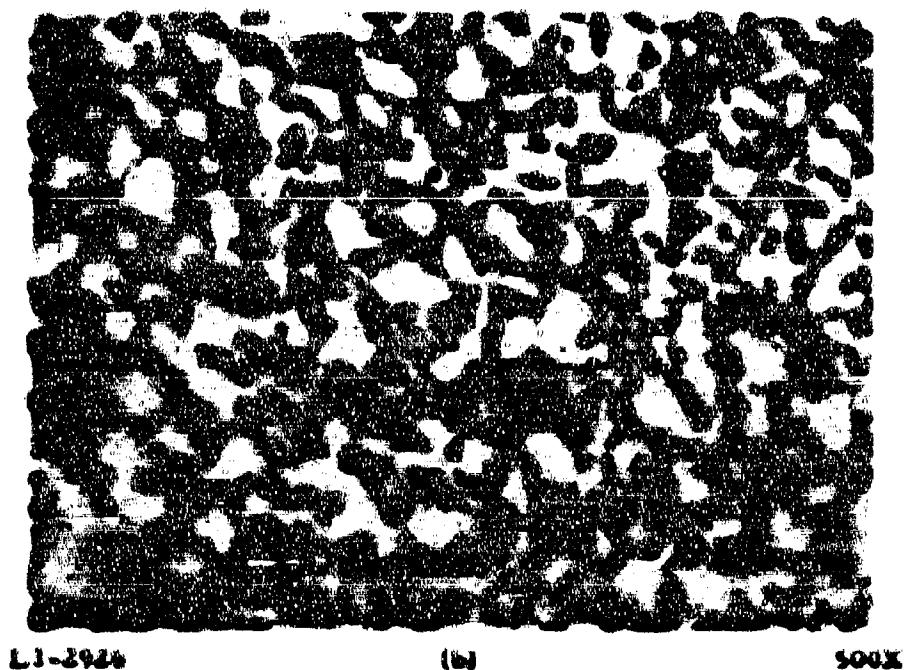
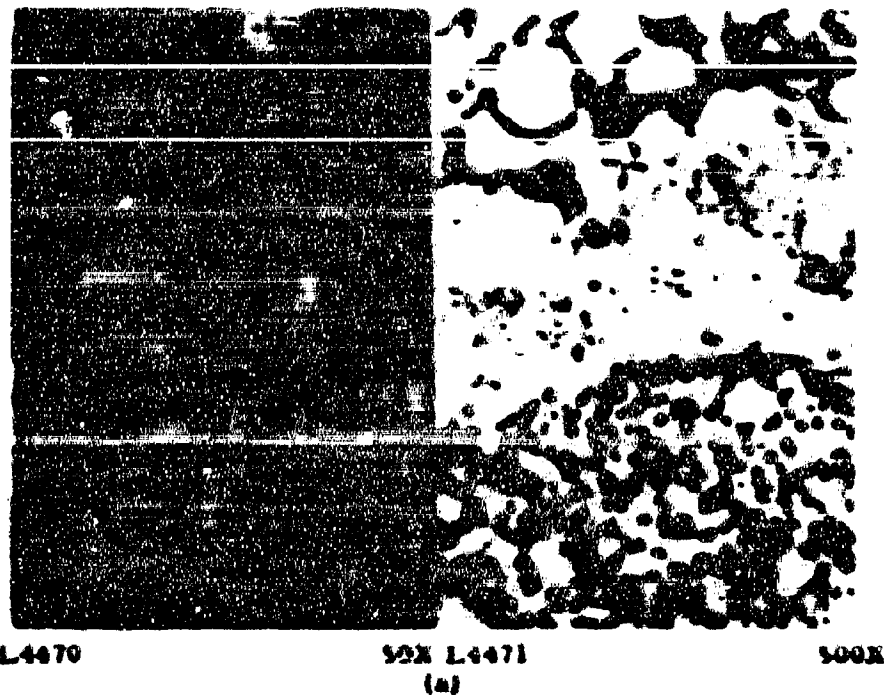
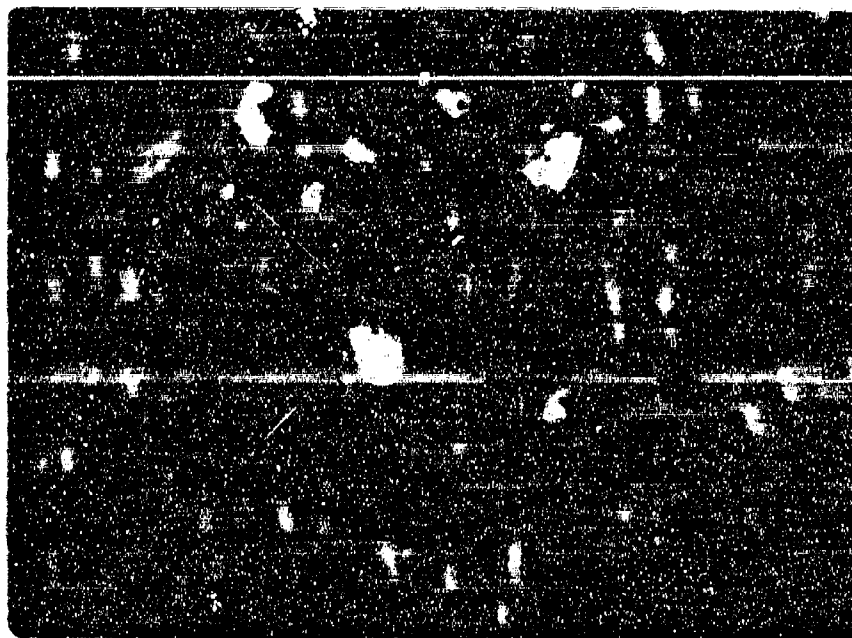
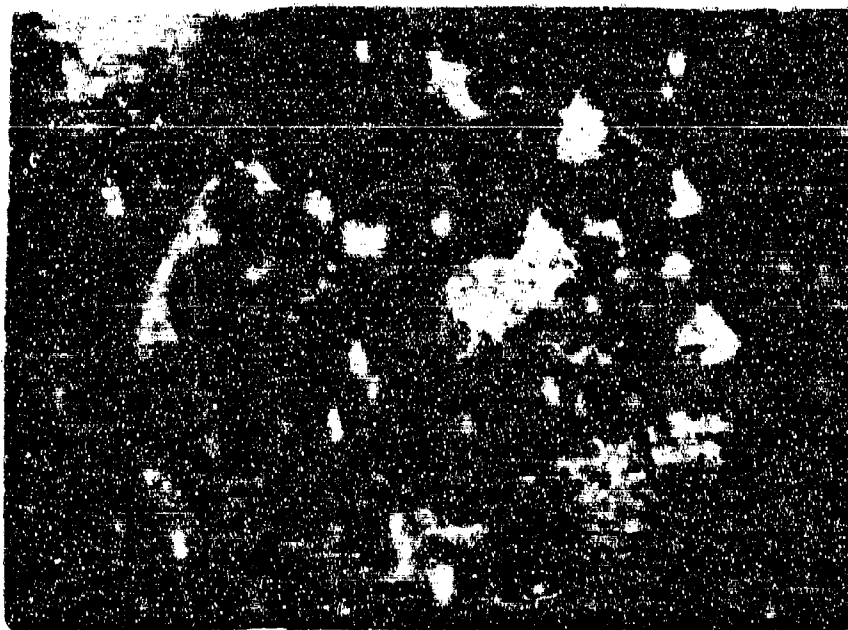


Figure III-11. Matrix Photomicrographs of Hot Pressed HfB₂. a) Thermally Cycled. b) Oxidized in Air for One Hour at 1800°C.



L1-2924

Longitudinal



L1-2927

Transverse

Figure III-12. Reticule Photomicrographs of Hot Pressed $Mg_{1.5}$ Oxidized in Air for One Hour at $1800^{\circ}C$ (1 Deviation = 4.55 Mils).

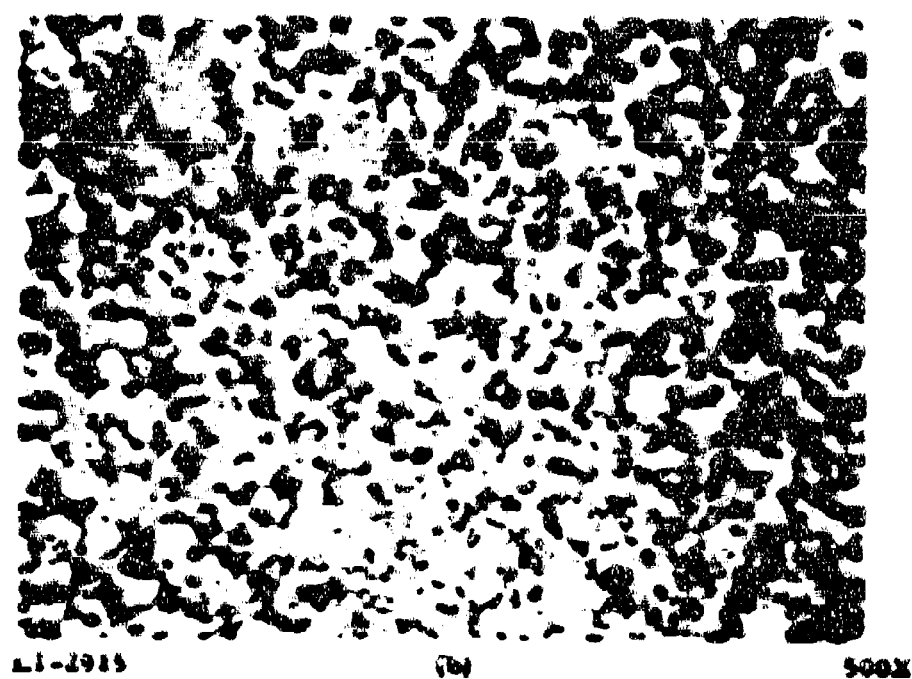
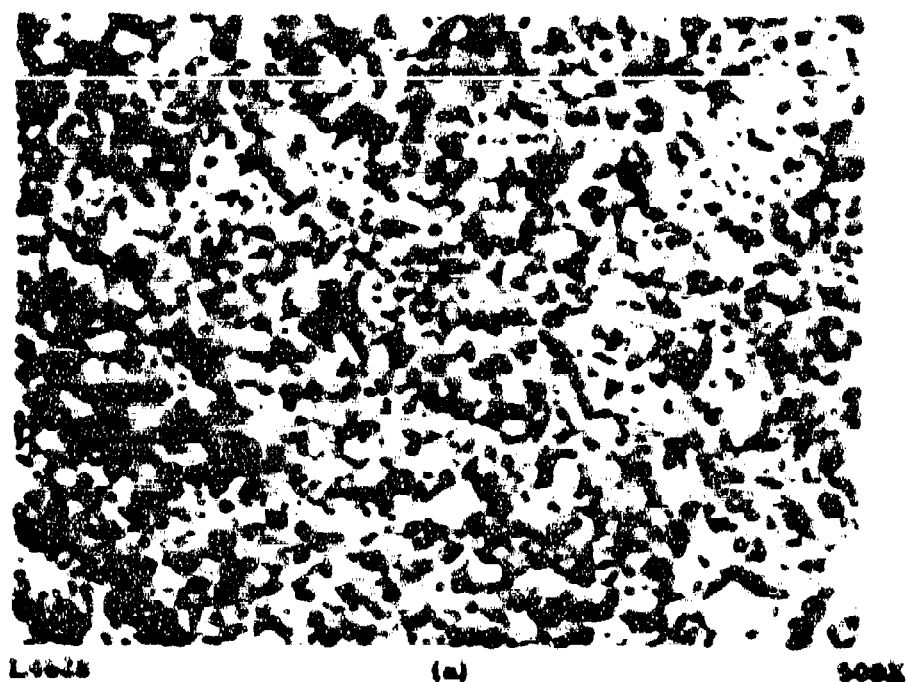


Figure III-13. Matrix Photomicrographs of Hot Pressed MB₂-22.5 LaB₆.
a) Thermally Cycled. b) Oxidized in Air for One Hour at
1800°C.



LI-2912

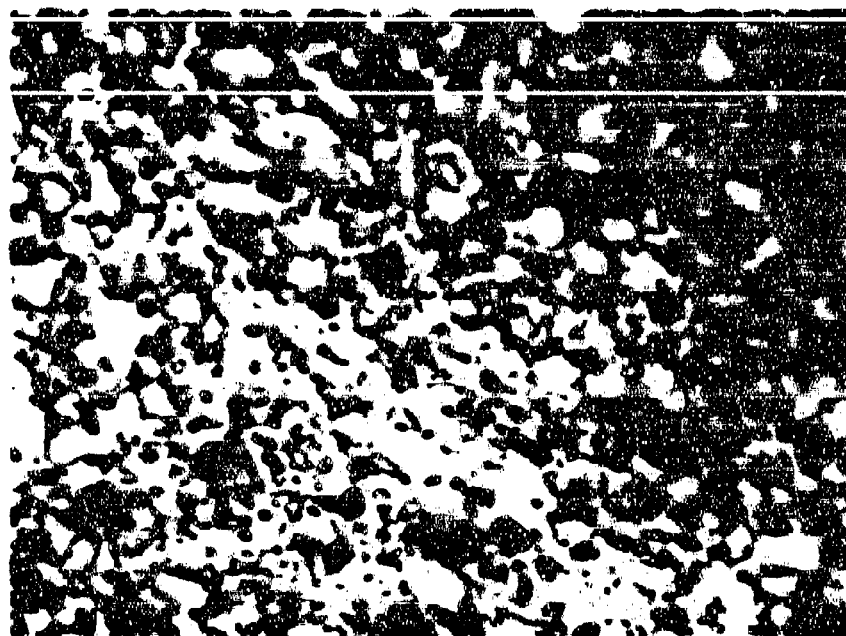
Longitudinal



LI-2916

Transverse

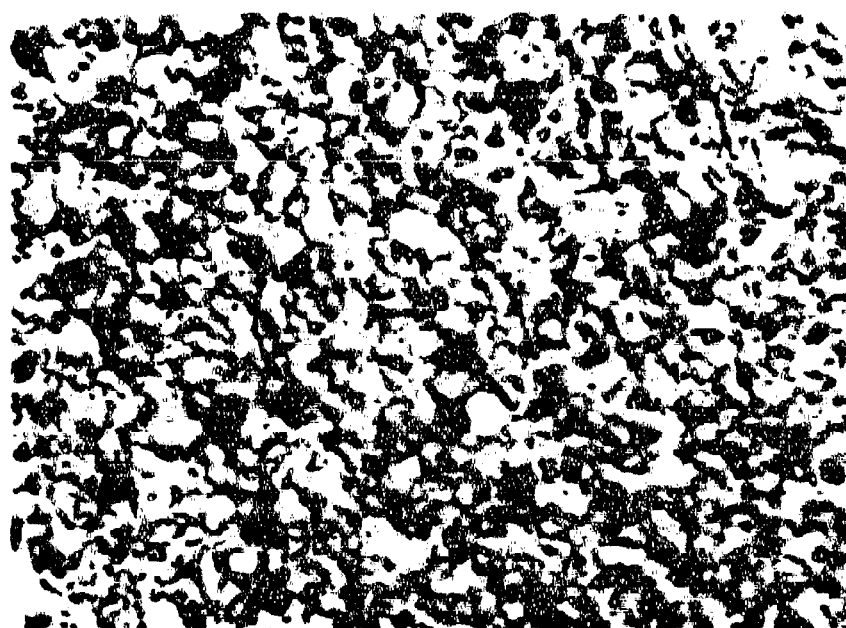
Figure III-14. Retainite Photomicrographs of Hot Pressed $\text{Ni}_3\text{Al}-22.5 \text{ LaAl}_3$, Oxidized in Air for One Hour at 1800°C (1 Division = 6.86 μm).



L4625

(a)

500X

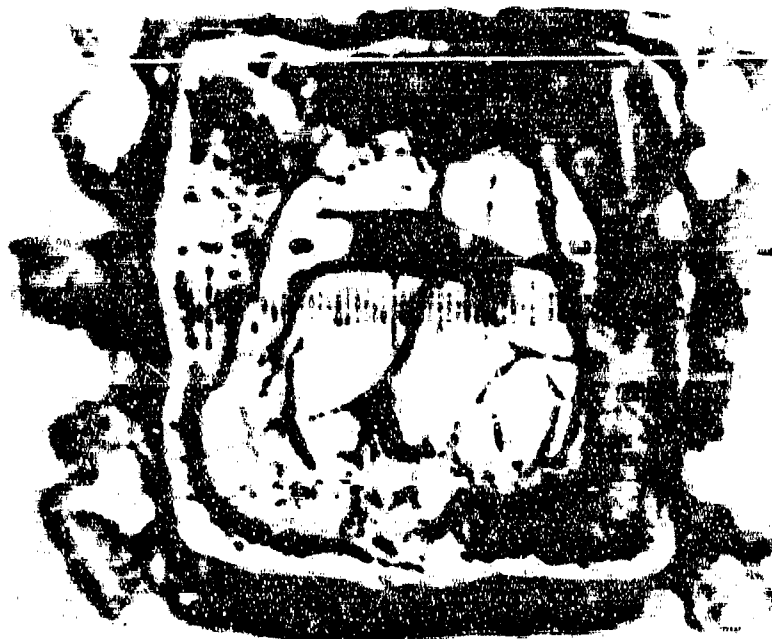


L1-2909

(b)

500X

Figure III-15. Matrix Photomicrographs of Hot Pressed HfB_2 - 20.0 YB₂.
a) Thermally Cycled, b) Oxidized in Air for One Hour at 1800°C.



LI-2905

Longitudinal



LI-2910

Transverse

Figure III-16. Retard Plate Photomicrographs of Hot Pressed $\text{MgO} \cdot 20.0 \text{ Y}_2\text{O}_3$ Quenched in Air for One Hour at 1800°C (1 Division = 4.66 μm).

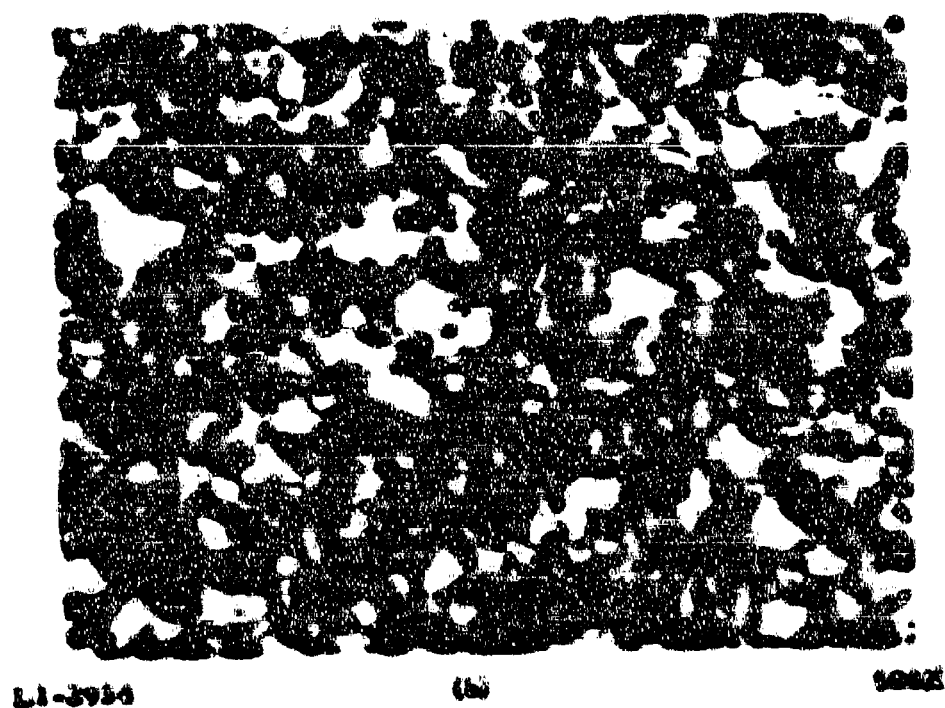
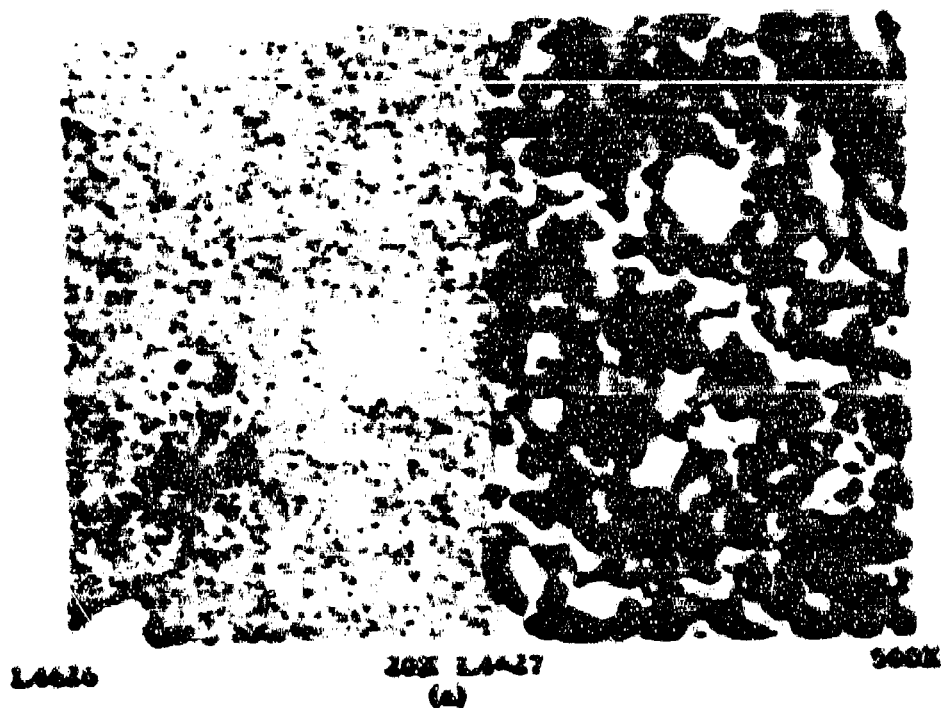


Figure III-17. Matrix Photomicrographs of Hot Pressed NiB₁ - 22.5 Cwt.
 a) Thermally Cycled, b) Oxidized in Air for One Hour at 1800°C.



LI-2910

Longitudinal



LI-2936

Transverse

Figure III-18. Backscattered Photomicrographs of Hot Pressed MgO - 21.5 Cwt. CaO .
Quenched in Air for One Hour at 1650°C (One Division = 4.00 Microns).

TABLE III-1
COMPOSITIONS AND DENSITIES OF HOT PRESSED
LABORITE + NEABORITE SPECIMENS

| <u>Identification No.</u> | <u>Condition^o</u> | <u>Nominal Composition^{oo}</u> | <u>Density</u> | <u>% Theoretical Density</u> |
|---------------------------|------------------------------|---|----------------|------------------------------|
| 292-24-55A | HP | ZrB ₂ -10.5 CaB ₆ | 5.47 g/cc | 100 |
| 292-24-56A | HP | ZrB ₂ -19.5 CaB ₆ | 5.25 | 100 |
| 292-25-1 | TC | ZrB ₂ -22.5 CaB ₆ | 5.50 | 100 |
| 292-25-9 | TC | ZrB ₂ -20.0 YB ₆ | 5.04 | 100 |
| 292-24-91 | TC | MB ₂ | 5.56 | 76 |
| 292-26-41 | TC | MB ₂ -22.5 LaB ₆ | 6.93 | 100 |
| 292-26-51 | TC | MB ₂ -20.0 YB ₆ | 6.46 | 100 |
| 292-26-64 | TC | MB ₂ -22.5 CeB ₆ | 6.66 | 96 |

^oHP-as hot pressed, TC-after a thermal cycle from room temperature to 1800°-2100°C.

^{oo}Compositions in mole per cent.

TABLE III-3

~~CONVERSION OF HOT FORMED DISC~~ + ~~MECHANICAL DEFORMATION~~

(100 Torr O_2 in Air at 0.9 R/sec-STP)

| Material ^a | Oil No. | Temp. °C | Time min | Oil/Gly Conversion mils Range 2225 | Average One Hour Oxidation Conversion-% |
|-----------------------|---------|----------|----------|--|---|
| $3LiH_2-10.5 CoH_6$ | 681 | 1710 | 60 | 27.5/31.4 | 30.4 |
| $3LiH_2-10.5 CoH_6$ | 680 | 1700 | 60 | 22.2/25.8 | 24.0 |
| $3LiH_2-22.5 CoH_6$ | 681 | 1715 | 60 | 16.7/21.1 | 18.9 |
| $3LiH_2-10.0 YH_3$ | 681 | 1700 | 60 | 31.6/34.4 | 45.0 |
| $3LiH_2$ | 681 | 1610 | 60 | 18.6/19.6 | 19.1 |
| $3LiH_2-22.5 LiH_6$ | 680 | 1600 | 60 | 25.3/25.3 | 25.3 |
| $3LiH_2-10.0 YH_3$ | 681 | 1610 | 60 | 16.1/17.9 | 16.0 |
| $3LiH_2-22.5 CoH_6$ | 681 | 1600 | 60 | Specimen severely distorted | |

^aConversions in mole per cent.

UNCLASSIFIED

Security Classification

DOCUMENT CONTROL 374-100

| | | |
|--|--|---|
| 1. Document Title Research and Development of Refractory Oxidation Resistant Diborides | | 2. Document Number 374-100 |
| 3. Author(s) Clougherty, Edward V., Kallish, David and Peters, Edward T. | | 4. Classification UNCLASSIFIED |
| 5. Technical Documentation Report, March 1966 to September 1967 | | 6. Document Date July 1968 |
| 7. Task No. 715D01 | | 8. Document Number AFML-TR-56-100 |
| 9. Summary This document is subject to export controls and each transmittal to foreign governments or foreign nationals may be made only with prior approval of the Military and Chemical Division, Air Force Materials Laboratory (MAMC). | | |
| 10. Classification N/A | | |
| 11. Abstract The oxidation, mechanical and physical properties of zirconium diboride and hafnium diboride and composites prepared from these diborides with appropriate additives, have been determined as a function of composition, microstructure and test temperature. The composites were designed to enhance oxidation resistance, strength and thermal stress resistance without sacrificing high temperature stability, the principal additives were silicon carbide or graphite. Several hundred diboride billets, in sizes from two inches diameter to six inches square, were fabricated by conventional hot pressing. All hot pressed billets were subjected to extensive nondestructive testing correlations and flaw identification criteria. A unique role for ceramic additives has evolved in enhancing the fabricability of diboride materials and producing fine grained crack free billets. All powder materials and hot pressed microstructures subjected to properties evaluations have undergone extensive characterization through qualitative and quantitative chemical analyses, phase analyses and grain size and density measurements. An exploratory fabrication effort was initiated to develop alternate means to hot pressing for producing dense diboride materials; hot forging, plasma spraying and sintering are being studied. In addition, the hot pressing of diboride compositions containing additives such as SiC whiskers, carbon filaments or tungsten filaments is being studied. | | |

374-100

UNCLASSIFIED

Security Classification

UNCLASSIFIED

EXHIBIT C SUBMITTAL GUIDE

4-1-00000

Borides
Hot Processing of Boride Materials
Oxidation Resistant Materials
High Strength Ceramic Materials
Thermal Stress Resistant Borides
Thermal Stress Measurements
Mechanical Properties of Borides
at Elevated Temperatures

1. SUBMITTAL ACTIVITY Show the name and address of the collection, submission, source, Department of Defense activity or other organization responsible for submitting the report.

2a. SECURITY SECURITY CLASSIFICATION Show the overall security classification of the report. Indicate whether "Unclassified" is indicated. Marking is to be an overall one with appropriate security requirements.

2b. GROUP Indicate the group designated in the report as Group 1, 2, 3, 4, 5, 6, 7, 8, 9, 10, 11, 12, 13, 14, 15, 16, 17, 18, 19, 20, 21, 22, 23, 24, 25, 26, 27, 28, 29, 30, 31, 32, 33, 34, 35, 36, 37, 38, 39, 40, 41, 42, 43, 44, 45, 46, 47, 48, 49, 50, 51, 52, 53, 54, 55, 56, 57, 58, 59, 60, 61, 62, 63, 64, 65, 66, 67, 68, 69, 70, 71, 72, 73, 74, 75, 76, 77, 78, 79, 80, 81, 82, 83, 84, 85, 86, 87, 88, 89, 90, 91, 92, 93, 94, 95, 96, 97, 98, 99, 100, 101, 102, 103, 104, 105, 106, 107, 108, 109, 110, 111, 112, 113, 114, 115, 116, 117, 118, 119, 120, 121, 122, 123, 124, 125, 126, 127, 128, 129, 130, 131, 132, 133, 134, 135, 136, 137, 138, 139, 140, 141, 142, 143, 144, 145, 146, 147, 148, 149, 150, 151, 152, 153, 154, 155, 156, 157, 158, 159, 160, 161, 162, 163, 164, 165, 166, 167, 168, 169, 170, 171, 172, 173, 174, 175, 176, 177, 178, 179, 180, 181, 182, 183, 184, 185, 186, 187, 188, 189, 190, 191, 192, 193, 194, 195, 196, 197, 198, 199, 200, 201, 202, 203, 204, 205, 206, 207, 208, 209, 210, 211, 212, 213, 214, 215, 216, 217, 218, 219, 220, 221, 222, 223, 224, 225, 226, 227, 228, 229, 230, 231, 232, 233, 234, 235, 236, 237, 238, 239, 240, 241, 242, 243, 244, 245, 246, 247, 248, 249, 250, 251, 252, 253, 254, 255, 256, 257, 258, 259, 260, 261, 262, 263, 264, 265, 266, 267, 268, 269, 270, 271, 272, 273, 274, 275, 276, 277, 278, 279, 280, 281, 282, 283, 284, 285, 286, 287, 288, 289, 290, 291, 292, 293, 294, 295, 296, 297, 298, 299, 300, 301, 302, 303, 304, 305, 306, 307, 308, 309, 310, 311, 312, 313, 314, 315, 316, 317, 318, 319, 320, 321, 322, 323, 324, 325, 326, 327, 328, 329, 330, 331, 332, 333, 334, 335, 336, 337, 338, 339, 340, 341, 342, 343, 344, 345, 346, 347, 348, 349, 350, 351, 352, 353, 354, 355, 356, 357, 358, 359, 360, 361, 362, 363, 364, 365, 366, 367, 368, 369, 370, 371, 372, 373, 374, 375, 376, 377, 378, 379, 380, 381, 382, 383, 384, 385, 386, 387, 388, 389, 390, 391, 392, 393, 394, 395, 396, 397, 398, 399, 400, 401, 402, 403, 404, 405, 406, 407, 408, 409, 410, 411, 412, 413, 414, 415, 416, 417, 418, 419, 420, 421, 422, 423, 424, 425, 426, 427, 428, 429, 430, 431, 432, 433, 434, 435, 436, 437, 438, 439, 440, 441, 442, 443, 444, 445, 446, 447, 448, 449, 450, 451, 452, 453, 454, 455, 456, 457, 458, 459, 460, 461, 462, 463, 464, 465, 466, 467, 468, 469, 470, 471, 472, 473, 474, 475, 476, 477, 478, 479, 480, 481, 482, 483, 484, 485, 486, 487, 488, 489, 490, 491, 492, 493, 494, 495, 496, 497, 498, 499, 500, 501, 502, 503, 504, 505, 506, 507, 508, 509, 510, 511, 512, 513, 514, 515, 516, 517, 518, 519, 520, 521, 522, 523, 524, 525, 526, 527, 528, 529, 530, 531, 532, 533, 534, 535, 536, 537, 538, 539, 540, 541, 542, 543, 544, 545, 546, 547, 548, 549, 550, 551, 552, 553, 554, 555, 556, 557, 558, 559, 560, 561, 562, 563, 564, 565, 566, 567, 568, 569, 570, 571, 572, 573, 574, 575, 576, 577, 578, 579, 580, 581, 582, 583, 584, 585, 586, 587, 588, 589, 590, 591, 592, 593, 594, 595, 596, 597, 598, 599, 600, 601, 602, 603, 604, 605, 606, 607, 608, 609, 610, 611, 612, 613, 614, 615, 616, 617, 618, 619, 620, 621, 622, 623, 624, 625, 626, 627, 628, 629, 630, 631, 632, 633, 634, 635, 636, 637, 638, 639, 640, 641, 642, 643, 644, 645, 646, 647, 648, 649, 650, 651, 652, 653, 654, 655, 656, 657, 658, 659, 660, 661, 662, 663, 664, 665, 666, 667, 668, 669, 670, 671, 672, 673, 674, 675, 676, 677, 678, 679, 680, 681, 682, 683, 684, 685, 686, 687, 688, 689, 690, 691, 692, 693, 694, 695, 696, 697, 698, 699, 700, 701, 702, 703, 704, 705, 706, 707, 708, 709, 710, 711, 712, 713, 714, 715, 716, 717, 718, 719, 720, 721, 722, 723, 724, 725, 726, 727, 728, 729, 730, 731, 732, 733, 734, 735, 736, 737, 738, 739, 740, 741, 742, 743, 744, 745, 746, 747, 748, 749, 750, 751, 752, 753, 754, 755, 756, 757, 758, 759, 760, 761, 762, 763, 764, 765, 766, 767, 768, 769, 770, 771, 772, 773, 774, 775, 776, 777, 778, 779, 780, 781, 782, 783, 784, 785, 786, 787, 788, 789, 790, 791, 792, 793, 794, 795, 796, 797, 798, 799, 800, 801, 802, 803, 804, 805, 806, 807, 808, 809, 810, 811, 812, 813, 814, 815, 816, 817, 818, 819, 820, 821, 822, 823, 824, 825, 826, 827, 828, 829, 830, 831, 832, 833, 834, 835, 836, 837, 838, 839, 840, 841, 842, 843, 844, 845, 846, 847, 848, 849, 850, 851, 852, 853, 854, 855, 856, 857, 858, 859, 860, 861, 862, 863, 864, 865, 866, 867, 868, 869, 870, 871, 872, 873, 874, 875, 876, 877, 878, 879, 880, 881, 882, 883, 884, 885, 886, 887, 888, 889, 890, 891, 892, 893, 894, 895, 896, 897, 898, 899, 900, 901, 902, 903, 904, 905, 906, 907, 908, 909, 910, 911, 912, 913, 914, 915, 916, 917, 918, 919, 920, 921, 922, 923, 924, 925, 926, 927, 928, 929, 930, 931, 932, 933, 934, 935, 936, 937, 938, 939, 940, 941, 942, 943, 944, 945, 946, 947, 948, 949, 950, 951, 952, 953, 954, 955, 956, 957, 958, 959, 960, 961, 962, 963, 964, 965, 966, 967, 968, 969, 970, 971, 972, 973, 974, 975, 976, 977, 978, 979, 980, 981, 982, 983, 984, 985, 986, 987, 988, 989, 990, 991, 992, 993, 994, 995, 996, 997, 998, 999, 1000, 1001, 1002, 1003, 1004, 1005, 1006, 1007, 1008, 1009, 1010, 1011, 1012, 1013, 1014, 1015, 1016, 1017, 1018, 1019, 1020, 1021, 1022, 1023, 1024, 1025, 1026, 1027, 1028, 1029, 1030, 1031, 1032, 1033, 1034, 1035, 1036, 1037, 1038, 1039, 1040, 1041, 1042, 1043, 1044, 1045, 1046, 1047, 1048, 1049, 1050, 1051, 1052, 1053, 1054, 1055, 1056, 1057, 1058, 1059, 1060, 1061, 1062, 1063, 1064, 1065, 1066, 1067, 1068, 1069, 1070, 1071, 1072, 1073, 1074, 1075, 1076, 1077, 1078, 1079, 1080, 1081, 1082, 1083, 1084, 1085, 1086, 1087, 1088, 1089, 1090, 1091, 1092, 1093, 1094, 1095, 1096, 1097, 1098, 1099, 1100, 1101, 1102, 1103, 1104, 1105, 1106, 1107, 1108, 1109, 1110, 1111, 1112, 1113, 1114, 1115, 1116, 1117, 1118, 1119, 1120, 1121, 1122, 1123, 1124, 1125, 1126, 1127, 1128, 1129, 1130, 1131, 1132, 1133, 1134, 1135, 1136, 1137, 1138, 1139, 1140, 1141, 1142, 1143, 1144, 1145, 1146, 1147, 1148, 1149, 1150, 1151, 1152, 1153, 1154, 1155, 1156, 1157, 1158, 1159, 1160, 1161, 1162, 1163, 1164, 1165, 1166, 1167, 1168, 1169, 1170, 1171, 1172, 1173, 1174, 1175, 1176, 1177, 1178, 1179, 1180, 1181, 1182, 1183, 1184, 1185, 1186, 1187, 1188, 1189, 1190, 1191, 1192, 1193, 1194, 1195, 1196, 1197, 1198, 1199, 1200, 1201, 1202, 1203, 1204, 1205, 1206, 1207, 1208, 1209, 1210, 1211, 1212, 1213, 1214, 1215, 1216, 1217, 1218, 1219, 1220, 1221, 1222, 1223, 1224, 1225, 1226, 1227, 1228, 1229, 1230, 1231, 1232, 1233, 1234, 1235, 1236, 1237, 1238, 1239, 1240, 1241, 1242, 1243, 1244, 1245, 1246, 1247, 1248, 1249, 1250, 1251, 1252, 1253, 1254, 1255, 1256, 1257, 1258, 1259, 1260, 1261, 1262, 1263, 1264, 1265, 1266, 1267, 1268, 1269, 1270, 1271, 1272, 1273, 1274, 1275, 1276, 1277, 1278, 1279, 1280, 1281, 1282, 1283, 1284, 1285, 1286, 1287, 1288, 1289, 1290, 1291, 1292, 1293, 1294, 1295, 1296, 1297, 1298, 1299, 1300, 1301, 1302, 1303, 1304, 1305, 1306, 1307, 1308, 1309, 1310, 1311, 1312, 1313, 1314, 1315, 1316, 1317, 1318, 1319, 1320, 1321, 1322, 1323, 1324, 1325, 1326, 1327, 1328, 1329, 1330, 1331, 1332, 1333, 1334, 1335, 1336, 1337, 1338, 1339, 1340, 1341, 1342, 1343, 1344, 1345, 1346, 1347, 1348, 1349, 1350, 1351, 1352, 1353, 1354, 1355, 1356, 1357, 1358, 1359, 1360, 1361, 1362, 1363, 1364, 1365, 1366, 1367, 1368, 1369, 1370, 1371, 1372, 1373, 1374, 1375, 1376, 1377, 1378, 1379, 1380, 1381, 1382, 1383, 1384, 1385, 1386, 1387, 1388, 1389, 1390, 1391, 1392, 1393, 1394, 1395, 1396, 1397, 1398, 1399, 1400, 1401, 1402, 1403, 1404, 1405, 1406, 1407, 1408, 1409, 1410, 1411, 1412, 1413, 1414, 1415, 1416, 1417, 1418, 1419, 1420, 1421, 1422, 1423, 1424, 1425, 1426, 1427, 1428, 1429, 1430, 1431, 1432, 1433, 1434, 1435, 1436, 1437, 1438, 1439, 1440, 1441, 1442, 1443, 1444, 1445, 1446, 1447, 1448, 1449, 1450, 1451, 1452, 1453, 1454, 1455, 1456, 1457, 1458, 1459, 1460, 1461, 1462, 1463, 1464, 1465, 1466, 1467, 1468, 1469, 1470, 1471, 1472, 1473, 1474, 1475, 1476, 1477, 1478, 1479, 1480, 1481, 1482, 1483, 1484, 1485, 1486, 1487, 1488, 1489, 1490, 1491, 1492, 1493, 1494, 1495, 1496, 1497, 1498, 1499, 1500, 1501, 1502, 1503, 1504, 1505, 1506, 1507, 1508, 1509, 1510, 1511, 1512, 1513, 1514, 1515, 1516, 1517, 1518, 1519, 1520, 1521, 1522, 1523, 1524, 1525, 1526, 1527, 1528, 1529, 1530, 1531, 1532, 1533, 1534, 1535, 1536, 1537, 1538, 1539, 1540, 1541, 1542, 1543, 1544, 1545, 1546, 1547, 1548, 1549, 1550, 1551, 1552, 1553, 1554, 1555, 1556, 1557, 1558, 1559, 1560, 1561, 1562, 1563, 1564, 1565, 1566, 1567, 1568, 1569, 1570, 1571, 1572, 1573, 1574, 1575, 1576, 1577, 1578, 1579, 1580, 1581, 1582, 1583, 1584, 1585, 1586, 1587, 1588, 1589, 1590, 1591, 1592, 1593, 1594, 1595, 1596, 1597, 1598, 1599, 1600, 1601, 1602, 1603, 1604, 1605, 1606, 1607, 1608, 1609, 1610, 1611, 1612, 1613, 1614, 1615, 1616, 1617, 1618, 1619, 1620, 1621, 1622, 1623, 1624, 1625, 1626, 1627, 1628, 1629, 1630, 1631, 1632, 1633, 1634, 1635, 1636, 1637, 1638, 1639, 1640, 1641, 1642, 1643, 1644, 1645, 1646, 1647, 1648, 1649, 1650, 1651, 1652, 1653, 1654, 1655, 1656, 1657, 1658, 1659, 1660, 1661, 1662, 1663, 1664, 1665, 1666, 1667, 1668, 1669, 1670, 1671, 1672, 1673, 1674, 1675, 1676, 1677, 1678, 1679, 1680, 1681, 1682, 1683, 1684, 1685, 1686, 1687, 1688, 1689, 1690, 1691, 1692, 1693, 1694, 1695, 1696, 1697, 1698, 1699, 1700, 1701, 1702, 1703, 1704, 1705, 1706, 1707, 1708, 1709, 1710, 1711, 1712, 1713, 1714, 1715, 1716, 1717, 1718, 1719, 1720, 1721, 1722, 1723, 1724, 1725, 1726, 1727, 1728, 1729, 1730, 1731, 1732, 1733, 1734, 1735, 1736, 1737, 1738, 1739, 1740, 1741, 1742, 1743, 1744, 1745, 1746, 1747, 1748, 1749, 1750, 1751, 1752, 1753, 1754, 1755, 1756, 1757, 1758, 1759, 1760, 1761, 1762, 1763, 1764, 1765, 1766, 1767, 1768, 1769, 1770, 1771, 1772, 1773, 1774, 1775, 1776, 1777, 1778, 1779, 1780, 1781, 1782, 1783, 1784, 1785, 1786, 1787, 1788, 1789, 1790, 1791, 1792, 1793, 1794, 1795, 1796, 1797, 1798, 1799, 1800, 1801, 1802, 1803, 1804, 1805, 1806, 1807, 1808, 1809, 1810, 1811, 1812, 1813, 1814, 1815, 1816, 1817, 1818, 1819, 1820, 1821, 1822, 1823, 1824, 1825, 1826, 1827, 1828, 1829, 1830, 1831, 1832, 1833, 1834, 1835, 1836, 1837, 1838, 1839, 1840, 1841, 1842, 1843, 1844, 1845, 1846, 1847, 1848, 1849, 1850, 1851, 1852, 1853, 1854, 1855, 1856, 1857, 1858, 1859, 1860, 1861, 1862, 1863, 1864, 1865, 1866, 1867, 1868, 1869, 1870, 1871, 1872, 1873, 1874, 1875, 1876, 1877, 1878, 1879, 1880, 1881, 1882, 1883, 1884, 1885, 1886, 1887, 1888, 1889, 1890, 1891, 1892, 1893, 1894, 1895, 1896, 1897, 1898, 1899, 1900, 1901, 1902, 1903, 1904, 1905, 1906, 1907, 1908, 1909, 1910, 1911, 1912, 1913, 1914, 1915, 1916, 1917, 1918, 1919, 1920, 1921, 1922, 1923, 1924, 1925, 1926, 1927, 1928, 1929, 1930, 1931, 1932, 1933, 1934, 1935, 1936, 1937, 1938, 1939, 1940, 1941, 1942, 1943, 1944, 1945, 1946, 1947, 1948, 1949, 1950, 1951, 1952, 1953, 1954, 1955, 1956, 1957, 1958, 1959, 1960, 1961, 1962, 1963, 1964, 1965, 1966, 1967, 1968, 1969, 1970, 1971, 1972, 1973, 1974, 1975, 1976, 1977, 1978, 1979, 1980, 1981, 1982, 1983, 1984, 1985, 1986, 1987, 1988, 1989, 1990, 1991, 1992, 1993, 1994, 1995, 1996, 1997, 1998, 1999, 2000, 2001, 2002, 2003, 2004, 2005, 2006, 2007, 2008, 2009, 2010, 2011, 2012, 2013, 2014, 2015, 2016, 2017, 2018, 2019, 2020, 2021, 2022, 2023, 2024, 2025, 2026, 2027, 2028, 2029, 2030, 2031, 2032, 2033, 2034, 2035, 2036, 2037, 2038, 2039, 2040, 2041, 2042, 2043, 2044, 2045, 2046, 2047, 2048, 2049, 2050, 2051, 2052, 2053, 2054, 2055, 2056, 2057, 2058, 2059, 2060, 2061, 2062, 2063, 2064, 2065, 2066, 2067, 2068, 2069, 2070, 2071, 2072, 2073, 2074, 2075, 2076, 2077, 2078, 2079, 2080, 2081, 2082, 2083, 2084, 2085, 2086, 2087, 2088, 2089, 2090, 2091, 2092, 2093, 2094, 2095, 2096, 2097, 2098, 2099, 2100, 2101, 2102, 2103, 2104, 2105, 2106, 2107, 2108, 2109, 2110, 2111, 2112, 2113, 2114, 2115, 2116, 2117, 2118, 2119, 2120, 2121, 2122, 2123, 2124, 2125, 2126, 2127, 2128, 2129, 2130, 2131, 2132, 2133, 2134, 2135, 2136, 2137, 2138, 2139, 2140, 2141, 2142, 2143, 2144, 2145, 2146, 2147, 2148, 2149, 2150, 2151, 2152, 2153, 2154, 2155, 2156, 2157, 2158, 2159, 2160, 2161, 2162, 2163, 2164, 2165, 2166, 2167, 2168, 2169, 2170, 21